

See discussions, stats, and author profiles for this publication at: <https://www.researchgate.net/publication/369023786>

Modelling railway slab track towards enhanced dynamic performance and reduced track deterioration

Thesis · July 2021

CITATIONS

2

READS

247

1 author:



Samuel Matias

Technical University of Lisbon

11 PUBLICATIONS 104 CITATIONS

SEE PROFILE

UNIVERSIDADE DE LISBOA
INSTITUTO SUPERIOR TÉCNICO



**Modelling railway slab track towards enhanced
dynamic performance and reduced track deterioration**

SAMUEL RIBEIRO MATIAS

Supervisor: Doctor PATRÍCIA ALEXANDRA AFONSO DINIS FERREIRA

Thesis approved in public session to obtain the PhD Degree in
TRANSPORTATION SYSTEMS

Jury final classification: **Pass with Distinction and Honour**

2021

UNIVERSIDADE DE LISBOA
INSTITUTO SUPERIOR TÉCNICO

Modelling railway slab track towards enhanced
dynamic performance and reduced track deterioration

SAMUEL RIBEIRO MATIAS

Supervisor: **Doctor PATRÍCIA ALEXANDRA AFONSO DINIS FERREIRA**

Thesis approved in public session to obtain the PhD Degree in

TRANSPORTATION SYSTEMS

Jury final classification: **Pass with Distinction and Honour**

Chairperson: Doctor LUÍS GUILHERME DE PICADO SANTOS
Instituto Superior Técnico, Universidade de Lisboa

Members of the Committee:

Doctor YANN BEZIN
School of computing and Engineering, University of Huddersfield, UK

Doctor RUI ARTUR BÁRTOLO CALÇADA
Faculdade de Engenharia, Universidade do Porto

Doctor LUÍS GUILHERME DE PICADO SANTOS
Instituto Superior Técnico, Universidade de Lisboa

Doctor PAULO MANUEL DA FONSECA TEIXEIRA
Instituto Superior Técnico, Universidade de Lisboa

Doctor PATRÍCIA ALEXANDRA AFONSO DINIS FERREIRA
Instituto Superior Técnico, Universidade de Lisboa

Doctor PIERRE-ETIENNE GAUTIER
School of Engineering, CentraleSupélec, Paris-Saclay University, France

Funding Institutions

FCT- Fundação para a Ciência e Tecnologia

2021

ABSTRACT

The growing demand for railway traffic in terms of speed and axle load causes an early degradation on the conventional ballasted track, which encourages the development of optimized slab track solutions to minimize maintenance interventions and enhance the structural performance. However, the lack of experience in its application, as well as the cost of initial investment and reparation in case of an accident, discourage their wider use. One of the research gaps thereof is the lack of comprehension in the deterioration phenomena of slab track systems.

Therefore, the main goal of this thesis is to enhance and provide a contribution to railway track modelling, by developing a hybrid and iterative finite element model (HI-Track) capable of predicting instantaneous responses and track deterioration after millions of cycles. A new modelling approach is used through the interaction between two finite element models: a reduced dynamic model (DL-Track) and a nonlinear model (SP-Track) that updates the material properties of the track through empirical formulations. An extensively validated modelling process is thoroughly assessed to study the long-term effects on slab tracks, mainly with real field test campaigns and test rig trials. An additional contribution is to extend the existing work on slab track modelling not only subjected to train loads but also to atmospheric actions. Several weather scenarios (extreme rainfall events and heat/ cold waves) are simulated to study the resiliency and robustness of the track to extreme climates.

Furthermore, several vehicles, weather actions, track configurations, and heterogeneities are assessed to prove the flexibility and the practical utility of the hybrid model to simulate real-world applications and to predict maintenance requirements of the track during its lifetime. With this numerical tool, several new design guidelines are proposed for slab track configurations within the scope of the European railway requisites for the 2030/2050 horizon. These recommendations can be implemented in decision support tools used by infrastructure managers to achieve specific slab track configurations as high performance, resilient and low risk and maintenance solutions.

Keywords: Slab track, finite element modelling, train-track interaction, long-term behaviour, track maintenance, life cycle cost

RESUMO

O aumento de procura por tráfego ferroviário em termos de velocidade e carga por eixo provoca uma degradação precoce na via balastrada convencional, o que encoraja o desenvolvimento de soluções otimizadas de via em laje de betão, a fim de minimizar as intervenções de manutenção e melhorar o desempenho estrutural. Contudo, a falta de experiência na sua aplicação, associada a um custo do investimento inicial e de reparação em caso de acidente, desencorajam a sua utilização mais ampla. Uma das lacunas na investigação em vias em laje de betão é o seu comportamento a longo prazo, nomeadamente os fenómenos de deterioração da via.

Neste sentido, o principal objetivo desta tese doutoral é o desenvolvimento de um modelo híbrido e iterativo de elementos finitos (HI-Track) capaz de calcular respostas instantâneas e deterioração da via em laje de betão após milhões de ciclos. Uma nova abordagem de modelação é utilizada através da interação entre dois modelos de elementos finitos: um modelo dinâmico reduzido (DL-Track) e um modelo de comportamento não-linear (SP-Track) que atualiza as propriedades materiais da via através de formulações empíricas. O processo de modelação é validado e calibrado extensivamente para estudar os efeitos a longo prazo nas vias de laje de betão, principalmente com campanhas experimentais *in situ* e em laboratório. Para além do característico carregamento ferroviário, o modelo numérico tem a capacidade de simular ações atmosféricas. Vários cenários meteorológicos (eventos de chuva extrema e ondas de calor/frio) são simulados para estudar a resiliência e robustez da via a climas extremos.

Vários veículos, ações meteorológicas, configurações da via e heterogeneidades são avaliados para provar a flexibilidade e utilidade prática da ferramenta numérica em simular cenários reais e para prever as necessidades de manutenção da via durante a vida útil. Com o auxílio deste modelo híbrido, diversas diretrizes de dimensionamento são propostas para configurações de vias de laje betão no âmbito dos requisitos ferroviários europeus para o horizonte 2030/2050. Estas recomendações podem ser implementadas em ferramentas de apoio à decisão utilizadas pelos gestores de infraestrutura para alcançar configurações específicas de vias de laje de betão como soluções de alto desempenho, resilientes e de baixo risco e manutenção.

Palavras-Chave: Via em laje de betão, modelação por elementos finitos, interação veículo/via, comportamento a longo prazo, manutenção da via, custo de ciclo de vida.

ACKNOWLEDGEMENTS

The most rewarding aspects of this doctoral path are unequivocally the lessons learned and the joy of researching and contributing to a field that I admire since a young age. This thesis is an important milestone in this path, being the reflection of a journey of personal growth for the last 5 years. Although being an individual endeavour for the majority of the time, research is a team effort. Several people gave important contributions to this final result, for which I would like to leave my most sincere gratitude.

First and foremost, I would like to express my gratitude to Professor Patrícia Ferreira whose guidance and positivity led to the fulfilment of this dissertation with a constructive influence in the final result. Her knowledge and experience in the field of railway engineering, as the extraordinary availability and friendship were invaluable during the development of this research and personal growth. I should also thank her for the support and encouragement in my work to overcome challenges and to pursue my own research ideas. For all the above and the remarkable human care during the most critical moments of the thesis, I am deeply thankful.

To Professor Paulo Teixeira, I would thank him for the share of knowledge and experience of the importance of this industry on the world stage, always with a broad view of the challenges of this area of study and motivated me to pursue this field of research

Also, I would like to express my gratitude to Doctor Tiago Ferreira for the selfless and positive attitude in which he helped to solve theoretical and numerical issues in soil modelling. His notable availability to share his knowledge as his awareness of the common struggles during the development of a doctoral dissertation are sincerely appreciated.

Additionally, to Professor João Pombo from the University of Huddersfield, for whom I acknowledge for sharing his insights and experience in railway technology, and his availability and hospitality in which he kindly received me during my stay in the Railway Institute of Technology in Huddersfield.

Equally, I would like also to thank the several researchers from the research centre that welcomed me, specially Doctor Pedro Antunes and Doctor Hugo Magalhães for promoting a stimulating research environment and to make me feel integrated during my stay.

In addition, Engineer José Saiz-Aja from LADICIM – Laboratorio de la División de Ciencia e Ingeniería de los Materiales (Universidad de Cantabria) who kindly made available test

rig measurements very useful for the long-term validation of the numerical model performed in GRAFT- II in Heriot-Watt University in Edinburgh.

Moreover, a big thanks to SNCF for generously sharing rare and sensitive data from real high speed slab track lines in France for the short-term validation of the model.

Still, in what concerns data availability, an important acknowledgement should be addressed to Doctor José Estaire, from CEDEX Track Box in Madrid for providing crucial experimental measurements that leverage the initial development of the short-term models and his availability to clarify any doubts related to the experimental trials to enhance the modelling process.

I left my recognition to the evaluation board committee of the thesis proposal (Professor Luís Picado Santos and Professor Patrícia Ferreira from Instituto Superior Técnico and Professor Rui Calçada from Faculdade de Engenharia do Porto) for their suggestions and positive influence provided.

This research would not be possible without the financial support by The Portuguese Foundation for Science and Technology (FCT) for the financial support given PD/BD/1137551/2015 and BL302/2019 for Instituto Superior Técnico, and MIT Portugal under the doctoral program in Transportation systems.

It would be of the utmost unfairness not to express sincere gratitude for all the colleagues and friends that helped me along this journey with their shared knowledge and feedback. Especially, the companionship and friendship of Ana, Joana, João, Laura, and Pedro made this journey much more enjoyable. Also, I would like to thank João and Joana for proofreading this document. A profound recognition goes to Inês, for giving me strength when I needed the most and probably more than she'll ever know.

A heartfelt thanks go to my family and close friends, that although not sharing my interest in railways, they shared the struggles that I went through and support me unconditionally, giving me the values, perseverance, and resiliency that makes me what I am today. And that's a good personal reminder that no achievement is good enough if my family and friends aren't there along the way. Hard work, discipline, and sacrifice will get you there, but enjoyment will get you further.

Samuel Matias

Lisbon, Portugal

December 2020

TABLE OF CONTENTS

<i>Abstract</i>	<i>v</i>
<i>Resumo</i>	<i>vii</i>
<i>Acknowledgements</i>	<i>ix</i>
<i>Table of contents</i>	<i>xi</i>
<i>List of figures</i>	<i>xvi</i>
<i>List of tables</i>	<i>xxv</i>
<i>Acronyms</i>	<i>xxvii</i>
<i>Symbols</i>	<i>xxix</i>
1 INTRODUCTION	1
1.1 MOTIVATION	1
1.2 SCOPE OF THE THESIS.....	3
1.3 OUTLINE OF THE THESIS	4
2 STATE-OF-THE-ART ON SLAB TRACK PERFORMANCE	7
2.1 INTRODUCTION	7
2.2 BALLASTLESS SYSTEMS.....	9
2.2.1 Embedded sleeper systems.....	10
2.2.2 Non embedded sleeper systems.....	11
2.2.3 Direct fastening systems.....	12
2.2.4 Embedded rail systems.....	13
2.2.5 Asphalt layer systems.....	14
2.2.6 System benchmarking: pros and cons	15
2.3 STRUCTURAL REQUIREMENTS FOR BALLASTLESS TRACKS	18
2.3.1 Subsoil.....	18
2.3.2 Superstructure	20

2.4	TRACK VIBRATION AND NOISE.....	22
2.4.1	Vibration	22
2.4.2	Noise	25
2.5	TRACK DETERIORATION AND MAINTENANCE	27
2.5.1	Types of track deterioration	28
2.5.2	Slab repair	30
2.5.3	Track monitoring	31
2.6	TRACK MODELLING	31
2.7	SCIENTIFIC FRAMEWORK	36

3 DEVELOPMENT OF SHORT-TERM DYNAMIC AND NONLINEAR SUB-MODELS: DL-TRACK AND SP-TRACK.....39

3.1	INTRODUCTION	39
3.2	DYNAMIC TRAIN/TRACK INTERACTION: DL-TRACK	40
3.2.1	Track and vehicle modelling.....	41
3.2.2	Substructuring formulation	45
3.2.3	Model assembly and calculation phase.....	48
3.2.4	Intermodel validation and calibration.....	51
3.2.5	Comparison between reduced and full 3D models	55
3.3	NONLINEAR CONCRETE BEHAVIOUR: SP-TRACK.....	56
3.3.1	Track modelling	56
3.3.2	Load modelling: transient train loads and temperature variations.	59
3.3.3	Nonlinear material behaviour update	61
3.4	ARCHITECTURE OF THE SUB-MODELS.....	63
3.4.1	Initialization.....	63
3.4.2	Assembly and calculation	64
3.4.3	Post-processing	65
3.5	CONCLUDING REMARKS: HIGHLIGHTS AND LIMITATIONS	66

4 DEVELOPMENT OF A LONG-TERM HYBRID AND ITERATIVE MODEL: HI-TRACK71

4.1	INTRODUCTION	71
------------	---------------------------	-----------

4.2	PERMANENT DEFORMATION OF THE SUBGRADE	72
4.2.1	Factors influencing soil settlement	72
4.2.2	Soil settlement laws	73
4.2.3	Thermo-hydro-mechanical behaviour of the soil.....	74
4.3	CONCRETE SLAB DETERIORATION.....	77
4.3.1	Factors influencing concrete deterioration.....	77
4.3.2	Concrete fatigue laws	79
4.3.3	Crack width evolution.....	81
4.4	HI-TRACK: INTERACTION BETWEEN DL-TRACK AND SP-TRACK	83
4.4.1	Calculation process	83
4.4.2	Soil settlement progression.....	89
4.4.3	Concrete damage progression.....	92
4.5	CONCLUDING REMARKS: HIGHLIGHTS AND LIMITATIONS	95

5 NUMERICAL VALIDATION AND CALIBRATION USING EXPERIMENTAL MEASUREMENTS.....97

5.1	INTRODUCTION	97
5.2	LABORATORIAL SHORT-TERM VALIDATION: CEDEX TRACK Box.....	98
5.2.1	Characterization of the experimental site	98
5.2.2	DL-Track and SP-Track numerical results.....	100
5.2.3	Long-term preliminary results.....	106
5.3	FIELD SHORT-TERM VALIDATION	108
5.3.1	Chauconin case study.....	108
5.3.2	Benicassim case study	112
5.4	LABORATORIAL LONG-TERM VALIDATION: GRAFT-II	116
5.5	FIELD LONG TERM VALIDATION.....	120
5.5.1	Hannover-Berlin high speed line case: concrete slab damage ...	120
5.5.2	Cologne-Frankfurt high speed case: THM behaviour of the soil .	123
5.6	CONCLUDING REMARKS	125

6 SLAB TRACK STRUCTURAL BEHAVIOUR AND GUIDELINES FOR OPTIMIZED DESIGN.....129

6.1	INTRODUCTION	129
6.2	PERFORMANCE INDICATORS	135
6.3	TRAIN OPERATION DURING LIFETIME	138
6.3.1	Train speed.....	138
6.3.2	Vehicle type	141
6.4	EXTREME WEATHER EVENTS.....	144
6.4.1	Temperature	144
6.4.2	Rainfall	147
6.5	STRUCTURAL TRACK DESIGN FOR ENHANCED SHORT- AND LONG-TERM PERFORMANCE	149
6.5.1	Railpad	149
6.5.2	Concrete supportive layer.....	151
6.5.3	Reinforcement	155
6.5.4	Hydraulically bonded layer.....	156
6.6	EFFECT OF TRACK QUALITY CONDITION DURING LIFETIME	157
6.6.1	Geometric quality.....	157
6.6.2	Construction quality	159
6.6.3	Track heterogeneities	164
6.7	OPTIMIZED DESIGN FOCUSING ON LONG-TERM PERFORMANCE.....	168
6.7.1	General assumptions	168
6.7.2	Impact of track design on soft soil platforms	168
6.7.3	Track design resilience under extreme weather events and operation scenarios	170
6.8	PERFORMANCE AND COMPARATIVE ASSESSMENT OF THE SLAB TRACK BEHAVIOUR IN SHORT- AND LONG-TERM	173
6.8.1	Maintenance requirements	173
6.8.2	Scoring and comparative assessment	180
6.9	CRITICAL ANALYSIS OF SLAB TRACK DESIGN AND GUIDELINES.....	184
7	FINAL REMARKS.....	189
7.1	CONCLUSIONS	189
7.2	LIMITATIONS AND PROSPECTIVE WORK.....	194

REFERENCES	197
ANNEXES.....	211

LIST OF FIGURES

Figure 2.1: Relation between the usage of slab track and construction works for several high-speed lines	8
Figure 2.2: Evolution of slab track construction in high speed lines around the globe	8
Figure 2.3: Schematic representation of a ballasted and slab track	9
Figure 2.4: Classification of ballastless systems	10
Figure 2.5: Scheme of the Rheda 2000 (top) and Züblin embedded sleeper systems (bottom) (units in mm)	11
Figure 2.6: Scheme of the Stedef non-embedded sleeper system (units in mm)	12
Figure 2.7: Scheme of the Appitrac cast in situ system (units in mm)	12
Figure 2.8: Scheme of the Bögl (top), Shinkansen (middle) and ÖBB-Porr precast systems (bottom) (units in mm).....	13
Figure 2.9: Scheme of Edilon Corklast embedded rail system (units in mm)	14
Figure 2.10: Scheme of ATD asphalt layer system (units in mm).....	15
Figure 2.11: Schematic representation of the requirements for cuttings (top) and embankments (bottom) of slab tracks according to the German code (SSF Ingenieure GmbH, 2010)	19
Figure 2.12: Schematic representation of soil stabilization alternatives by the usage of piles	19
Figure 2.13: Relationship between train speed, wavelengths and frequency In the train/track system.....	23
Figure 2.14: Relationship between initial investment and frequency attenuation effectiveness of vibration mitigation countermeasures	25
Figure 2.15: Maintenance costs of the ballasted (left) and slab track section (right) on Sanyo Shinkansen (Ando et al., 2001; Takai, 2007).....	27
Figure 2.16: Most common deterioration phenomena of slab tracks: a) rail head checks, b) cracking near the sleepers/ supports, c) track settlement repair, d) rail head squats, e) slab transverse cracks. f) missing fastener. g) systematic wave wear of the rail head (Ripke, 2010; Shanghai Railway Administration, 2017; Vogt et al., 2005)	29
Figure 2.17: Representation of the possible methodologies and techniques for slab track modelling.....	32
Figure 2.18: Spring-damper model developed by Lei et al. (2016): Multibody vehicle model (a) and spring-damper elements for the track (b) and foundation (c) (left). 3D FEM-BEM model developed by Galvín et al. (2010b): Multibody axle model (a), soil boundary element model (b) and track finite element model (c) (right).	35
Figure 2.19: 3D FE slab track fatigue models. (Poveda et al., 2015) (left), (Zhu & Cai, 2014a) (center) and (Matias, 2014) (right)	35

Figure 3.1: Interaction between DL-Track and SP-Track sub-models	40
Figure 3.2: Rail/ railpad modelling in the DL-Track. Rail and railpad (a), 3D Timoshenko beam (b), spring-damper element (c) and integration points for the Timoshenko beam cross section.....	41
Figure 3.3: DL-Track element modelling (left and centre) and damping slice (right).....	42
Figure 3.4: Vehicle representation (left) and DL-Track vehicle model (right).....	42
Figure 3.5: Axle load distribution of the (from top to bottom) TGV Réseau US, CHR ₃ , ICE ₃ Velaro and a common freight train	43
Figure 3.6: Influence of the time step in the wheel/ rail contact force	44
Figure 3.7: Influence of the drop time in the wheel/ rail contact force.....	44
Figure 3.8: Nonlinear contact force and linearization for the 60-120 kN range	45
Figure 3.9: Wheel/ rail contact modelling.....	45
Figure 3.10: Substructuring phases: generation, use and expansion.....	46
Figure 3.11: Superelement and master nodes.....	46
Figure 3.12: Superelement assembly	46
Figure 3.13: Representation of track “slices”	49
Figure 3.14: 2D model version for time efficiency assessment.....	50
Figure 3.15: Different superelement sizes	50
Figure 3.16: Relationship between the module size and the total computing time for a single iteration ..	51
Figure 3.17: Relationship between the module size and the total computing time for multiple iterations ..	51
Figure 3.18: CEDEX track box experimental site (left) and ballasted case study cross section (right) (units in m)	52
Figure 3.19: Dynavoie and DL-Track modelling representation of the ballasted track in the CEDEX Track box	53
Figure 3.20: Rail displacements for the Track box ballasted track simulation at 300 km/h	53
Figure 3.21: Rail acceleration for the Track box ballasted track simulation at 300 km/h	53
Figure 3.22: Ballast displacements for the Track box ballasted track simulation at 300 km/h	54
Figure 3.23: Ballast acceleration for the Track box ballasted track simulation at 300 km/h	54
Figure 3.24: Subballast displacements for the Track box ballasted track simulation at 300 km/h	54
Figure 3.25: Subballast acceleration for the Track box ballasted track simulation at 300 km/h	54
Figure 3.26: Embankment displacements for the Track box ballasted track simulation at 300 km/h.....	54
Figure 3.27: Embankment acceleration for the Track box ballasted track simulation at 300 km/h	54
Figure 3.28: Ballast displacements for different superelement modules.....	56
Figure 3.29: Ballast accelerations for different superelement modules.....	56

Figure 3.30: Multilinear behaviour of a C35/45 concrete for material modelling	57
Figure 3.31: Eight-node structural element with cracking capabilities.....	57
Figure 3.32: Crack modelling on the SP-Track due to train loads on uneven soil support	58
Figure 3.33: Reinforcement modelling on the slab track including longitudinal rebars, stirrups, and prestressed tendons	58
Figure 3.34: Contact modelling between layers for SP-Track.....	58
Figure 3.35: Train load modelling in the SP-Track	59
Figure 3.36: Temperature effects on the track: negative temperature uniform (a), Positive temperature uniform (b), negative temperature gradient (c) and positive temperature gradient (d)	60
Figure 3.37: Hourly stress amplitude spectrum in the longitudinal (xx) direction	61
Figure 3.38: Hourly stress amplitude spectrum in the transversal (zz) direction	61
Figure 3.39: Bundle-chain model for concrete uniaxial loading (adapted from Shan and Yu (2015)).....	61
Figure 3.40: Element damage calculation and initial condition of the track stiffness	62
Figure 3.41: Initialization stage	63
Figure 3.42: Rail profile update by the DL-Track.....	64
Figure 3.43: Assembly and calculation of DL-Track and SP-Track	65
Figure 3.44: Post-processing modules for the DL-Track and SP-Track.....	66
Figure 3.45: Multiple track typologies available for calculation (from left to right: ballasted track, Rheda 2000, Bögl, Stedef and ATD systems)	68
Figure 4.1: Long-term permanent deformation behaviour of the soil	72
Figure 4.2: Atmospheric interactions governing the thermos-hydro-mechanical behaviour of the soil (left) and a 2D FE THM model (right) developed by T. Ferreira (2015).....	75
Figure 4.3: Atmospheric data from 2010 for the city of Barcelona (Mediterranean climate)	76
Figure 4.4: Spatial distribution (top) and temporal evolution of saturation degree granular and bituminous subballast (bottom)	76
Figure 4.5: Wöhler diagram (left); strain – number of cycles diagram (centre); stress-strain diagram (right)	77
Figure 4.6: Long-term calculation process of the HI-Track model	84
Figure 4.7: Concrete damage comparison between adaptive initial update and without of the panel link and sleeper module of a pre-fabricated slab track system after 60 years for an extreme climate scenario	85
Figure 4.8: Effect of temperature and traffic on concrete slab track damage.....	86
Figure 4.9: Influence of the calculation time step for settlement progression for a mixed traffic scenario	87

Figure 4.10: Absolute values of settlement for different calculation time steps for a mixed traffic scenario	87
Figure 4.11: Comparison between a 1 and a 2 year time step in the loss of stiffness of the CSL for 60 years	87
Figure 4.12: Settlement threshold of the HI-Track for the DL-Track calculation	88
Figure 4.13: Damage threshold of the HI-Track for the SP-Track calculation	88
Figure 4.14: Average annual deterioration rate	89
Figure 4.15: Rail levelling calculation process in the HI-Track	90
Figure 4.16 Equivalent traffic approach as a strain hardening method for permanent soil deformation ...	91
Figure 4.17 Concrete semi-empirical (full line) and empirical (dashed line) fatigue models for flexural stress.....	92
Figure 4.18: Cumulative concrete damage (left) in each node of the sleeper module (right).....	94
Figure 5.1: Cross section of the 3MB prototype (left) and the track instrumentation (right) present in the CEDEX track box.....	98
Figure 5.2: 3MB slab track prototype representation	99
Figure 5.3: 3 MB slab track assembly. a) UBP between the blocks and the CSL. b) Block holes to be filled with cement. c) Installation of the fastening system	99
Figure 5.4: SP-Track (left) and DL-Track (right) models of the CEDEX 3MB case study.....	101
Figure 5.5: Numerical, theoretical and experimental results of 3MB static test for a 150 kN wheel load ..	101
Figure 5.6: 3MB static test setup with additional sleepers attached to both ends of the rail	101
Figure 5.7: Rail acceleration comparison between DL-Track and experimental results for the 3MB case study (360 km/h)	102
Figure 5.8: Rail displacement comparison between DL-Track and experimental results for the 3MB case study (360 km/h)	102
Figure 5.9: Block acceleration comparison between DL-Track and experimental results for the 3MB case study (360 km/h)	102
Figure 5.10: Block displacement comparison between DL-Track and experimental results for the 3MB case study (360 km/h)	102
Figure 5.11: CSL acceleration comparison between DL-Track and experimental results for the 3MB case study	103
Figure 5.12: CSL displacement comparison between DL-Track and experimental results for the 3MB case study	103
Figure 5.13: Influence of CSL properties and speed on the 3MB slab track accelerations for high speed trains	104
Figure 5.14: Influence of CSL properties and speed on the 3MB slab track accelerations for freight trains	104

Figure 5.15: Influence of UBP properties and speed on the 3MB slab track accelerations for high speed trains.....	104
Figure 5.16: Influence of UBP properties and speed on the 3MB slab track accelerations for freight trains	104
Figure 5.17: Influence of platform properties and speed on the 3MB slab track accelerations for high speed trains	104
Figure 5.18: Influence of platform properties and speed on the 3MB slab track accelerations for freight trains.....	104
Figure 5.19: Frequency domain of experimental and numerical 3MB rail accelerations for a high speed train circulating at 360 km/h	105
Figure 5.20: Frequency domain of experimental and numerical 3MB block accelerations for a high speed train circulating at 360 km/h.....	105
Figure 5.21: Frequency domain of experimental and numerical 3MB CSL accelerations for a high speed train circulating at 360 km/h.....	105
Figure 5.22: Normalised frequency domain of experimental 3MB block accelerations for a high speed train	105
Figure 5.23: Wavelength sources in the 3MB case	106
Figure 5.24: Longitudinal rail levelling evolution during 60 years of operation	107
Figure 5.25: Maximum settlement of the soil during 60 years of operation	107
Figure 5.26: Cumulative plastic soil settlement for different train speeds and soil types	107
Figure 5.27: Concrete damage on the 3MB slab track (blocks and CSL base) after 60 years of traffic operations for different speeds.....	108
Figure 5.28: LGV-Est high speed line (left) and Chauconin transition site (right)	109
Figure 5.29: Scheme of the Stedef system used in Chauconin case study (units in mm)	109
Figure 5.30: SP-Track and DL-Track sub-models of the Chauconin case study	110
Figure 5.31: Circulation of TGV Réseau trains in the LGV-Est (left), sleeper accelerometers (centre) and potentiometers (right).....	111
Figure 5.32: Comparison between measured and calculated sleeper accelerations in the Chauconin test site for a TGV train at 230 km/h.....	111
Figure 5.33: Comparison between calculated and measured track displacements for a TGV train at 230 km/h (sleeper) and an EMW vehicle (rail).....	111
Figure 5.34: Valencia – Tarragona line (left) with Rheda 2000 system (centre) and Stedef system (right)	112
Figure 5.35: Scheme of the Stedef system used in Benicassim case study (units in mm).....	113
Figure 5.36: SP-Track sub-models representation of the Benicassim case study with the Rheda 2000 system (left) and Stedef system (right).....	113

Figure 5.37: Comparison of calculated and experimental ranges of layer and reinforcement stresses for the Benicassim case study.....	114
Figure 5.38: Comparison between calculated and experimental displacements for the Benicassim case study	115
Figure 5.39: Crack width in the Rheda 2000 of the Benicassim site after 1 year of operation.....	115
Figure 5.40: Calculation of crack width by the HI-Track model for the Rheda 2000 case study	115
Figure 5.41: Bögl slab track system present in the GRAFT-II laboratory.....	116
Figure 5.42: Post-processing settlement data (left) from LVDT sensors installed in the slab (right)	117
Figure 5.43: HI-Track model representation of the GRAFT-II case study with the Bögl system.....	118
Figure 5.44: Comparison between experimental and calculated soil settlement for the Bögl case study in GRAFT-II.....	119
Figure 5.45: Hannover-Berlin high speed line (left) and scheme of the Rheda Classic system used (units in mm)	120
Figure 5.46: Uniform temperature variation during the year used for the Hannover – Berlin case study	121
Figure 5.47: Gradient temperature variation during the year used for the Hannover – Berlin case study	121
Figure 5.48: HBL displacement of the Rheda Classic system present in the Hannover - Berlin high speed line at different times	121
Figure 5.49: Comparison between calculated and experimental HBL displacements at different times ..	121
Figure 5.50: HI-Track model representation of the Hannover – Berlin high speed line case study.....	121
Figure 5.51: CSL and HBL damage for the Rheda classic case study	122
Figure 5.52: Calculation of concrete damage in one CSL sleeper module for the Rheda Classic case study	122
Figure 5.53: Evolution of nodal damage distribution in the CSL	123
Figure 5.54: Cologne-Frankfurt high speed line (left) and soil settlement in the Rheda 2000 system (right)	123
Figure 5.55: Soil settlement after construction in PK. 72.6 in the Cologne – Frankfurt high speed line ..	124
Figure 5.56: Comparison between experimental and numerical soil settlement results for the Cologne-Frankfurt high speed line	124
Figure 6.1: Detailed representation of the Bögl slab track system to be used in the HI-Track.....	130
Figure 6.2: HI-Track representation of the Bögl slab track	130
Figure 6.3: Scenarization scheme divided into actions (vehicle and weather actions) and track properties (design and condition)	131
Figure 6.4: Uniform temperature variation along the day to the proposed scenarios E ₁ , E ₂ and E ₃	132
Figure 6.5: Temperature gradient variation along the day to the proposed scenarios E ₁ , E ₂ and E ₃	132

Figure 6.6: Uniform temperature variation along the year to the scenarios E ₁ , E ₂ and E ₃	133
Figure 6.7: Bending moment/ soft soil scenario (left) and shear force/ transition scenario (right)	134
Figure 6.8: Concrete zones of a Bögl slab track slice (one sleeper)	137
Figure 6.9: Concrete zones of a Bögl slab track link	137
Figure 6.10: Effect of train speed on the longitudinal soil settlement	139
Figure 6.11: Effect of train speed on the progress of the maximum soil settlement	139
Figure 6.12: Effect of train speed on wheel/ rail contact force after 60 years of operation	139
Figure 6.13: Effect of train speed on the rail profile deterioration after 60 years of operation	139
Figure 6.14: Concrete damage level due to flexural stresses caused by vehicles for different speeds	140
Figure 6.15: Effect of train speed on C ₂ node concrete damage after 60 years of operation	140
Figure 6.16: Effect of train speed on the final damage per concrete zone.....	140
Figure 6.17: Comparison between the open module and link damage for different concrete zones after 60 years of operation	141
Figure 6.18: Comparison between concrete damage plots between the open module and link zones after 60 years of operation	141
Figure 6.19: Effect of train speed on maximum crack width on the slab top after 60 years of operation..	141
Figure 6.20: Effect of train speed on maximum crack width on the slab bottom after 60 years of operation	141
Figure 6.21: Effect of vehicle type on overall track settlement profile after 60 years of operation	142
Figure 6.22: Effect of vehicle type on overall track settlement evolution after 60 years of operation	142
Figure 6.23: Effect of vehicle type on the rail profile after 60 years of operation	142
Figure 6.24: Effect of vehicle type on the final damage per concrete zone.....	142
Figure 6.25: Effect of vehicle type on concrete block damage after 60 years of operation	143
Figure 6.26: Effect of vehicle type on the average CSL bottom damage	143
Figure 6.27: Effect of vehicle operation on maximum crack width on the slab top after 60 years of operation	143
Figure 6.28: Effect of vehicle operation on maximum crack width on the slab bottom after 60 years of operation.....	143
Figure 6.29: Loss of concrete stiffness in the CSL and HBL for a) freight scenario at 35 years, b) mixed traffic scenario at 35 years, c) freight scenario at 50 years and d) mixed traffic scenario at 50 years	144
Figure 6.30: Effect temperature scenarios on average concrete damage after 60 years of operation	145
Figure 6.31: Effect of temperature scenarios on the final damage per concrete zone	145
Figure 6.32: Effect of extreme temperature scenarios on concrete damage and loss of stiffness	145
Figure 6.33: Effect of temperature scenarios on maximum crack width on the slab top after 60 years of	

operation.....	146
Figure 6.34: Effect of temperature scenarios on maximum crack width on the slab bottom after 60 years of operation	146
Figure 6.35: Effect of transversal prestressed tendons on the track damage for an E2 scenario	147
Figure 6.36: Effect of rainfall scenarios on the longitudinal soil settlement	147
Figure 6.37: Effect of rainfall scenarios on the progress of the maximum soil settlement.....	147
Figure 6.38: Effect of temperature scenarios on average CSL bottom damage	148
Figure 6.39: Effect of temperature on the final damage per concrete zone	148
Figure 6.40: Effect of rainfall scenarios on maximum crack width on the slab top after 60 years of operation	148
Figure 6.41: Effect of rainfall scenarios on maximum crack width on the slab bottom after 60 years of operation.....	148
Figure 6.42: Effect of railpad stiffness on the longitudinal soil settlement	149
Figure 6.43: Effect of railpad stiffness on the final damage per concrete zone	149
Figure 6.44: Effect of railpad stiffness on maximum crack width on the slab top after 60 years of operation	150
Figure 6.45: Effect of railpad stiffness on maximum crack width on the slab bottom after 60 years of operation.....	150
Figure 6.46: Slab track accelerations under a 300 km/h high speed train for a 100 Hz band pass filter ..	150
Figure 6.47: S-N curve of NAC, RAC and FRC under bending cyclic loading	152
Figure 6.48: S-N curve of NAC, RAC and FRC under uniaxial compressive cyclic loading	152
Figure 6.49: Effect of concrete quality scenarios on average CSL top damage.....	154
Figure 6.50: Effect of concrete quality scenarios on average CSL bottom damage	154
Figure 6.51: Effect of concrete quality on the final damage per concrete zone	154
Figure 6.52: Effect of concrete quality on the final damage plot of the sleeper module	154
Figure 6.53: Effect of concrete type on maximum crack width on the slab top after 60 years of operation	155
Figure 6.54: Effect of concrete type on maximum crack width on the slab bottom after 60 years of operation.....	155
Figure 6.55: Effect of longitudinal rebar size on maximum crack width on the slab top after 60 years of operation.....	155
Figure 6.56: Effect of longitudinal rebar size on maximum crack width on the slab bottom after 60 years of operation	155
Figure 6.57: Effect of HBL thickness on maximum crack width on the slab top after 60 years of operation	156

Figure 6.58: Effect of HBL thickness on the final damage per concrete zone	156
Figure 6.59: Effect of initial rail profile on the progress of the maximum soil settlement.....	157
Figure 6.60: Effect of initial rail profile on the rail profile deterioration after 60 years of operation	157
Figure 6.61: Effect of initial rail profile on concrete damage on the CSL top	158
Figure 6.62: Effect of initial rail profile on concrete damage on the CSL bottom.....	158
Figure 6.63: Effect of initial rail profile on contact force evolution during the lifetime.....	158
Figure 6.64: Effect of initial rail profile on the final damage per concrete zone	158
Figure 6.65: Effect of initial rail profile on maximum crack width on the slab top after 60 years of operation	159
Figure 6.66: Effect of initial rail profile on maximum crack width on the slab bottom after 60 years of operation.....	159
Figure 6.67: Effect of infrastructure design on the progress of the maximum soil settlement	160
Figure 6.68: Effect of infrastructure design on concrete damage on the CSL top	160
Figure 6.69: Effect of infrastructure design on maximum crack width on the slab top after 60 years of operation.....	160
Figure 6.70: Effect of infrastructure design on maximum crack width on the slab bottom after 60 years of operation.....	160
Figure 6.71: Maximum wheel/ rail contact force for different combinations of train speed and number of defective sleepers	162
Figure 6.72: Minimum wheel/ rail contact force for different combinations of train speed and number of defective sleepers	162
Figure 6.73: Effect of module manufacturing on the soil settlement profile deterioration after 60 years of operation.....	162
Figure 6.74: Effect of defective sleepers on wheel/ rail contact force during track's lifetime for scenario 31	162
Figure 6.75: Effect of module manufacturing on concrete damage on the CSL top	163
Figure 6.76: Effect of module manufacturing on the final damage per concrete zone	163
Figure 6.77: Effect of module manufacturing on maximum longitudinal crack width on the slab top after 60 years of operation	163
Figure 6.78: Effect of module manufacturing on maximum transversal crack width on the slab top after 60 years of operation	163
Figure 6.79: Bending moment for different train speeds and number of soft soil sleepers	164
Figure 6.80: Shear force for different train speeds and number of soft soil sleepers.....	164
Figure 6.81: Effect of soft soil scenarios on the progress of the maximum soil settlement	165
Figure 6.82: Effect of transition soil scenarios on the progress of the maximum soil settlement	165

Figure 6.83: Effect of track heterogeneities on maximum contact force evolution	166
Figure 6.84: Effect of soft soil scenarios on the average CSL bottom concrete damage.....	166
Figure 6.85: Effect of transitions scenarios on the average CSL bottom concrete damage.....	166
Figure 6.86: Effect of soft soil scenarios on maximum crack width on the slab top after 60 years of operation.....	167
Figure 6.87: Effect of transition scenarios on maximum crack width on the slab top after 60 years of operation.....	167
Figure 6.88: Effect of design improvements on the average CSL bottom concrete damage for soft soil scenarios	169
Figure 6.89: Effect of design improvements on the average CSL top concrete damage for transition scenarios	169
Figure 6.90: Effect of design improvements on maximum crack width on the slab top for soft soil scenarios after 60 years of operation	170
Figure 6.91: Effect of design improvements on maximum crack width on the slab bottom for transitions scenarios after 60 years of operation	170
Figure 6.92: Effect of design improvements on the average CSL top concrete damage for extreme weather and operation scenarios	172
Figure 6.93: Effect of design improvements on the average CSL bottom concrete damage for extreme weather and operation scenarios	172
Figure 6.94: Effect of design improvements on maximum crack width on the slab top for extreme weather and operation scenarios after 60 years of operation	172
Figure 6.95: Effect of design improvements on maximum crack width on the slab bottom for extreme weather and operation scenarios after 60 years of operation	172
Figure 6.96: Web plot of the speed effect on slab track short-term behaviour.....	180
Figure 6.97: Web plot of the speed effect on slab track long-term behaviour	180

LIST OF TABLES

Table 2.1: Main characteristics of the most commonly used ballastless systems (high speed and heavy rail) (Esveld, 2001; Gautier, 2015; Matias, 2014; Michas, 2012)	16
Table 2.2: Technical comparison between ballastless systems (Matias & Ferreira, 2020).....	17
Table 2.3: International practices for slab track design loads	22

Table 2.4: Topics of slab track dynamics	23
Table 2.5: Slab track components and their elasticity influence on track dynamics (Lei, 2017; Lei et al., 2016)	24
Table 2.6: Main types of slab track degradation (Nielsen & Ekberg, 2005; Ren et al., 2016; Williams et al., 2016; Zhai, Liu, et al., 2015).....	28
Table 2.7: Summary of the most relevant works in slab track modelling found in the literature	34
Table 3.1: Vehicle properties of common high-speed and freight trains (P. A. Ferreira, 2010; Goicolea, 2014; He et al., 2018; Lei, 2017).....	43
Table 3.2: Mechanical properties of the CEDEX track box ballasted track.....	52
Table 3.3: Superelement module size and their performance during calculation.....	55
Table 3.4: Main features of the several versions of the DL-Track	67
Table 3.5: Main features of the several versions of the SP-Track	68
Table 4.1: Empirical models for permanent soil strain behaviour	74
Table 4.2: Semi-empirical fatigue formulations (Smith & Roesler, 2004)	80
Table 4.3: Empirical fatigue formulations (Smith & Roesler, 2004)	81
Table 5.1: Mechanical properties of the CEDEX track box ballasted track	100
Table 5.2: Modal frequencies of the 3MB by the passage of a train	106
Table 5.3: Model parameters for the empirical soil settlement law proposed by Li and Selig (1996)	107
Table 5.4: Geometrical and mechanical properties of the Stedef slab track system present in the Chauconin case study.....	110
Table 5.5: Cyclic test phases performed in the Bögl slab track system in GRAFT-II	117
Table 5.6: Geometrical and mechanical properties of the Bögl slab track system present in the GRAFT-II case study.....	118
Table 5.7: Geometrical and mechanical properties of the Rheda Classic slab track system present in the Hannover – Berlin high speed line	120
Table 5.8: Available experimental data for the validation and calibration of the HI-Track model.....	125
Table 5.9: Reliability level of the numerical model	126
Table 6.1: Traffic conditions of the scenarios to be studied.....	131
Table 6.2: Maximum and minimum variations of uniform and gradient temperature during the year for the temperature scenarios	132
Table 6.3: Scenarization variables	135
Table 6.4: Parametric analysis simulations	135
Table 6.5: Performance indicators.....	136
Table 6.6: Concrete design properties (CEN, 2004b).....	151

Table 6.7: Parametric analysis simulations focusing on slab track optimization for platform heterogeneities	168
Table 6.8: Parametric analysis simulations focusing on slab track optimization for extreme weather and operation scenarios.....	171
Table 6.9: Number of years required to reach rail levelling and settlement maintenance thresholds	174
Table 6.10: Number of years required to reach concrete damage maintenance thresholds for each scenario	175
Table 6.11: Number of years required to reach crack width maintenance thresholds for each scenario ..	176
Table 6.12: Number of years required to reach rail levelling and settlement maintenance thresholds for improved design solutions	178
Table 6.13: Number of years required to reach concrete damage maintenance thresholds for each scenario for improved design solutions	178
Table 6.14: Number of years required to reach crack width maintenance thresholds for each scenario for improved design solutions	179
Table 6.15: Proposed performance score level of each scenario	182
Table 6.16: Proposed performance score level of each improved design scenario	183
Table 6.17: Influence of actions and track condition on slab track long-term performance	185
Table 6.18: Influence of track design optimization on slab track deterioration.....	186

ACRONYMS

ADIF	Administrador de Infraestruturas Ferroviarias
ANSYS	ANalysis SYStems Inc
AVE	Alta Velocidad Española
APDL	Ansys Parametric Design Language
ASL	Asphalt Supportive Layer
ATD	AsphalTragschicht mit Direktauflagerung
BBM	Barcelona Basic Model
BEM	Boundary Element Method
BTD	BetonTragschicht mit Direktauflagerung

CAM	Cement Asphat Mortar
CEDEX	Centro de Estudios y Experimentación de Obras Públicas
CR	Chinese Railways
CRTS	Chinese Railway Track System
CSL	Concrete Supportive Layer
DB	Deutsche Bahn
DOF	Degree of Freedom
EAPA	European Asphalt Pavement Association
EC	Eurocode
FBM	Fibre Bundle Model
FEM	Finite Element Method
FRC	Fibre reinforced concrete
FST	Floating Slab Track
GRAFT-II	Geo-pavement and Railways Accelerated Fatigue Testing Facility
HBL	Hydraulically Bonded Layer
HSL	Hogesnelheidslijn
HSR	High Speed Rail;
ICE	InterCityExpress
ICM	Irreversible Chain Model
IFSTAR	Institut Français des Sciences et Technologies des Transports, de l'Aménagement et des Réseaux
KRNA	Korea Rail Network Authority
LGV	Ligne à Grande Vitesse
LVT	Low Vibration Track
MATLAB	MATRIX LABoratory
MBS	Multibody Systems
MC	Model Code
MTCM	Modified Tension Chord Model
NAC	Natural Aggregate Concrete
ÖBB	Österreichische Bundesbahnen

RAC	Recycled Aggregate Concrete
Renfe	Red Nacional de los Ferrocarriles Españoles
RFF	Réseau Férré de France
SNCF	Société Nationale des Chemins de Fer Français
SR	Stress Ratio
TGV	Train à Grande Vitesse
TIFSA	Tecnología e Investigación Ferroviaria, S.A.
THM	Thermo-Hydro-Mechanical
UBP	Under Block Pad
UIC	Union Internationale de Chemins de Fer
USP	Under Sleeper Pad

SYMBOLS

$[C]$	Damping matrix;
$[\hat{C}]$	Reduced damping matrix;
$\{F\}$	Nodal external forces;
$\{\hat{F}\}$	Reduced nodal external forces;
$[G_{sm}]$	Redundant static constraints matrix.
$[I]$	Identity matrix;
$[K]$	Stiffness matrix;
$[\hat{K}]$	Reduced stiffness matrix;
$[M]$	Mass matrix;
$[\hat{M}]$	Reduced mass matrix;
$[T]$	Transformation matrix;
$\{u\}$	Nodal displacement;
$\{\hat{u}\}$	Reduced nodal displacement;
$\{\dot{u}\}$	Nodal velocity;
$\{\dot{\hat{u}}\}$	Reduced nodal velocity;
$\{\ddot{u}\}$	Nodal acceleration;

$\{\ddot{u}\}$	Reduced nodal acceleration;	
a	Permanent soil deformation material parameter	[-];
a_0	Rayleigh damping constant 0	[-];
a_1	Rayleigh damping constant 1	[-];
A_b	Bogie cross section area	[m ²];
$A_{c,eff}$	Effective area of concrete	[m ²];
A'_p	Area of pre/ post-tensioned tendons within the effective area of concrete	[m ²];
A_s	Reinforcement area	[m ²];
b	Permanent soil deformation material parameter	[-];
acc_i	Acceleration of the element i	[m/s ²];
C_{1b}	Damping coefficient of primary suspension	[N.s/m];
C_{2b}	Damping coefficient of secondary suspension	[N.s/m];
C_H	Hertzian constant	[N/m ^{3/2}];
c_p	Longitudinal compression wave velocity	[m/s];
C_t	Factor that redirects any loss of tensile capacity of the concrete to the reinforcement	[-];
D	Damage level of concrete	[-];
D_{avg}	Average damage in the effective area of concrete in tension	[-];
D_{CAM}	CAM average damage	[-];
D_{CAM_L}	CAM link average damage	[-];
$D_{CSL\ BOT}$	Slab bottom average damage	[-];
$D_{CSL\ L\ BOT}$	Slab link bottom average damage	[-];
$D_{CSL\ L\ TOP}$	Slab link top average damage	[-];
$D_{CSL\ SLEEPER}$	Sleeper average damage	[-];
$D_{CSL\ TOP}$	Slab top average damage	[-];
$D_{HBL\ BOT}$	HBL bottom average damage	[-];
$D_{HBL\ L\ BOT}$	HBL link top average damage	[-];
$D_{HBL\ L\ TOP}$	HBL link top average damage	[-];
$D_{HBL\ TOP}$	HBL top average damage	[-];
e	Void ratio	[-];
el_i	Maximum element size of the material i	[m];
E_0	Initial Young modulus of concrete	[N/m ²];
E_d	Reduced Young modulus of damaged concrete	[N/m ²];

E_i	Young modulus of the material i	[N/m ²];
E_{v2}	Second Young modulus of the soil	[N/m ²];
f	Receptance frequency	[m];
F_c	Wheel/ rail contact force	[N];
f_c	Compressive stress of concrete	[N/m ²];
f'_c	Ultimate compressive stress of concrete	[N/m ²];
f_{cd}	Compressive design strength of concrete	[N/m ²];
$f_{cd,fat}$	Compressive design fatigue strength of concrete	[N/m ²];
f_{cm}	Average compressive strength of concrete	[N/m ²];
$f_{ct,f}$	Flexural concrete stress strength	[N/m ²];
f_{ctm}	Average tensile strength of concrete	[N/m ²];
f_{ck}	Characteristic compressive strength of concrete	[N/m ²];
f_{cko}	Reference characteristic strength of 10 MPa concrete	[N/m ²];
$f_{td,fat}$	Tensile design fatigue strength	[N/m ²];
$f_{ctk,005}$	Characteristic tensile strength of concrete	[N/m ²];
f_{yd}	Tensile design strength of steel	[N/m ²];
F_t	Tensile force in the effective area of concrete in tension	[N];
G_i	Shear modulus of the material i	[N/m ²];
G_s	Specific gravity of the soil solid	[‐];
$h_{c,eff}$	Effective height of the concrete slab	[m];
I_b	Rotational inertia of half bogie	[m ⁴];
L_a	Length of acceleration equivalent force	[m];
l_b	Bogie spacing	[m];
L_b	Length of braking equivalent force	[m];
L_x	Domain of the numerical model in the xx direction - Length	[m];
l_w	Axle spacing	[m];
L_y	Domain of the numerical model in the yy direction - Depth	[m];
L_z	Domain of the numerical model in the zz direction - Width	[m];
LT_{CSL}	Long-term performance score index – CSL deterioration	[‐];
LT_{GEO}	Long-term performance score index – Geometry	[‐];
LT_{HBL}	Long-term performance score index – HBL deterioration	[‐];
K_{1b}	Stiffness of primary suspension	[N/m];
k_1	Reinforcement bond coefficient	[‐];
K_{2b}	Stiffness of secondary suspension	[N/m];
k_2	Load distribution coefficient	[‐];
k_c	Contact stiffness	[N/m];

K_p	Railpad vertical stiffness	[N/m];
k_t	Load duration factor	[-];
m	Permanent soil deformation material parameter	[-];
M_b	Mass of half bogie	[kg];
M_c	Mass of quarter carbox	[kg];
M_w	Mass of wheelset	[kg];
N	Number of cycles	[-];
n_b	Number of bogies	[-];
Q_{lak}	Longitudinal acceleration equivalent force	[kN/m];
Q_{lbk}	Longitudinal braking equivalent force	[kN/m];
q_{soil}	Deviatoric stress	[N/m ²];
R_v	Track vertical radius	[m];
SC	Overall performance score index	[-];
S_{cro}	Crack width spacing	[m];
$SR_{cd,min}$	Minimum concrete compressive stress ratio	[-];
$SR_{cd,max}$	Maximum concrete compressive stress ratio	[-];
$SR_{td,max}$	Maximum tensile stress ratio	[-];
S_r	Saturation degree of the soil	[-];
SC	Short-term performance score index	[-];
V	Vehicle operational speed	[m/s];
u_z	Node displacement in the zz direction	[m];
u_x	Node displacement in the xx direction	[m];
u_y	Node displacement in the yy direction	[m];
x_i	Starting point of the dynamic simulation	[m];
x_f	Ending point of the dynamic simulation	[m];
w	Rayleigh frequency spectrum	[-];
W_c	Soil water content	[-];
w_{cr}	Crack width	[m];
$w_{k bot}$	Longitudinal crack width on slab bottom	[m];
$w_{k top}$	Longitudinal crack width on slab top	[m];
$w_{k trs}$	Transversal crack width on slab top	[m];
y_{rail}	Vertical rail profile	[m];
y_{soil}	Vertical overall soil settlement	[m];

α_e	Steel – concrete stiffness ratio	[-];
β	Permanent soil deformation material parameter	[-];
β_c	Shear coefficient for closed cracks	[-];
β_{cc}	Variable dependent on the age of concrete	[-];
β_{SG}	Calibration factor for the subgrade permanent deformation	[-];
β_t	Shear coefficient for open cracks	[-];
$\gamma_{c,fat}$	Partial safety coefficient	[-];
$\Delta\sigma_p$	Stress variation in the prestress tendons for the state of zero strain of the concrete at the same level	[N/m ²];
δ_c	Contact deflection	[m];
δ_i	Displacement of the element i	[m];
ε	Concrete strain	[-];
ε_0	Ultimate concrete strain	[-];
$\varepsilon_0/\varepsilon_r$	Permanent soil deformation material parameter	[-];
ε_{cm}	Average concrete strain	[-];
ε_p	Permanent deformation of the soil	[-];
ε_{sm}	Average steel rebar strain	[-];
ε_{di}	Irreversible concrete damage strain	[-];
ε_v	Average vertical resilient strain of the soil	[-];
ξ_1	Adjusted ratio of bond strength	[-];
ξ_n	Rayleigh damping coefficient	[-];
η_c	Averaging factor for concrete stresses in the compression zone considering the stress gradient	[-];
θ_p	Diameter of prestressing steel	[m];
θ_s	Diameter of reinforcing steel	[m];
θ_x	Node rotation in the xx direction	[-];
θ_y	Node rotation in the yy direction	[-];
θ_z	Node rotation in the zz direction	[-];
ρ	Permanent soil deformation material parameter	[-];
ρ_i	Density of the material i	[kg/m ³];
$\rho_{p,eff}$	Mechanical percentage of reinforcement	[-];
σ_I	First principal stress	[N/m ²];
σ_{II}	Second principal stress	[N/m ²];
σ_{III}	Third principal stress	[N/m ²];

σ_c	Compressive concrete stress	[N/m ²];
σ_{cs}	Compressive strength of the soil	[N/m ²];
σ_t	Tensile concrete stress	[N/m ²];
σ_d	Deviatoric stress	[N/m ²];
σ_s	Reinforcement stress at the crack section	[N/m ²];
σ_θ	Bulk stress	[N/m ²];
v_i	Poisson coefficient of the material i	[-];
ϕ_d	Dynamic amplification factor	[-];

1 INTRODUCTION

1.1 MOTIVATION

Railways have been a transportation mode that is under constant improvement and always raising the bar in terms of capacity and operational efficiency, mainly by increasing the speed, frequency, or weight of the trains. Therefore, the track is subjected to higher and more frequent loads, which leads to faster deterioration rates and consequently rising maintenance interventions. These maintenance needs brought numerous improvements to railway engineering, as well as new solutions for vehicle and track to remain a competitive high capacity transportation mode.

For this reason and the interest of the European network for very high-speed (>350 km/h) and high axle load corridors, the current ballasted tracks are reaching, and will soon overpass, their performance limits given the growing mobility demands (Esveld, 2001). Therefore, the scientific community and railway infrastructure managers are directing efforts to modernize the railway track and promote its technical innovation, improving safety, operability, and life cycle cost efficiency. Hence, several solutions of ballastless tracks, namely concrete slab tracks, were developed over the past 50 years, mostly in Japan and recently in China. These solutions present numerous advantages, such as greater vehicle stability, reduced height, and weight of the superstructure enhanced dynamic behaviour, and predominantly low maintenance (Bilow & Randich, 2000). The ballastless track is already a viable and competitive solution for high-speed, whose main focuses of research are: (i) capacity increase; (ii) operational speed increase; (iii) reduced number of maintenance operations and (iv) increased security level (Fumey et al., 2002).

However, ballastless tracks are not particularly popular in Europe. Typically, European countries have a strong tradition in ballasted track construction due to the initial investment cost, the lack of experience, and the uncertainty about the serviceability life of slab track systems.

Notwithstanding, clear signs of ballast wear began to be reported, leading the European railway institutions towards new slab track solutions.

An example of recent European developments is the ongoing slab track project HS2 in the United Kingdom with a desired running speed of 360 km/h. In addition to the interest in faster circulations, the current maximum operating speed in the world is 350 km/h in the Shanghai-Beijing high-speed railway line in China, with some 400 km/h corridors planned since there are multiple examples of rolling stock capable of circulating above these speeds. Higher speed is inevitably reflected in growing operation costs, yet they are advantageous if demand is time/cargo sensitive. The growing capacity in the railway sector becomes a more competitive feature in short/ medium distances and possibly can take a market share portion to the aeroplane in medium distances cities. The construction of ballasted high-speed lines in Paris-Lyon (500 km in 2 hours) or Madrid-Barcelona (600 km in 2 hours and 30 minutes) has captured a big portion of the air market share (97% and 65% respectively) (Crozet, 2013; Pita et al., 2012). In 2012, and with slab track usage, the travel between Beijing-Shanghai takes 4 hours and 40 minutes to complete the 1200 km between the two cities, which is the same time spent by air travel. Thereby, the use of a more robust infrastructure, as when slab tracks are used, can leverage this advantage and allow an increasing number of city pairs to be in a feasible and commercially-competitive distance of each other. Also, these city pairs can create high-speed rail and airline cooperation hubs as a decarbonisation strategy (Sato & Chen, 2018).

Furthermore, railways are the only transportation mode whose carbon emissions have been systematically decreasing since 1990. The European Commission wants railway infrastructure to have a major role in the European mobility future. This leads to favourable environments (e.g. increasing carbon taxes for airliners) for the rising of cost-competitive high speed trains as the HSR OUIGO by SNCF and Avlo by Renfe (Delaplace & Dobruszkes, 2015).

Yet transport systems that depend on high speed trains entails resilient and robust track infrastructure, requiring further testing and research to homologate any track specification.

Since slab track solutions are relatively new in operation, the information about their performance is commercially sensitive, which arises issues related to the lack of published technical literature:

- Few published studies about the dynamic and long-term behaviour of train-track interaction with real field measurements validation.
- Due to the long-term investment nature of slab tracks and the implementation of non-modular older systems, design issues are not promptly addressed, avoiding the development of innovative ideas related to crack propagation, construction time, noise, maintenance and drainage.
- Lack of information available about the real cost-effectiveness of existing slab tracks.

Thus, the research of new slab track solutions as viable alternatives for high demand lines are of

great interest to railway infrastructure managers. The main problems related to the design, construction, and operation require a comprehensive and critical study to achieve a resilient and robust infrastructure to avoid economic repercussions.

1.2 SCOPE OF THE THESIS

The lack of effort and required resources for the development, production, and installation of slab track systems, is justified by the existence of a strong competitor with lower investment costs, i.e. the ballasted track. However, the ballasted track presents a presumed higher life cycle cost than the slab track when the speed and axle load increase. As a result, different slab track solutions are available and since there are some specific issues and flexibility on their configuration, these aspects trigger further optimization.

The demanding scenario of the European railways for the near future calls for the development of slab track solutions and all its technical feasibility, thus requiring intense research to assure the proper performance in the short- and long-term run. These new requirements in addition to extreme weather incidents, demands for very high proficiency (low risk and vulnerability) from modern railway tracks. Slab tracks arise as adequate solutions in this framework.

Since ballastless tracks are high investment solutions designed for longer life spans than the traditional ballasted tracks, it is essential to maintain their deterioration levels at reasonable levels. These issues are related to high requirements regarding track geometry, which is hard to maintain, and non-standardized repair and maintenance procedures and equipment. These features establish the main problem with ballastless solutions in Europe, i.e. a lack of design information and experience.

Although slab tracks are labelled as “maintenance free”, this is not observed during operation and larger-than-expected maintenance investments are common (Andrés et al., 2015). The track degradation of ballastless systems is still poorly understood due to the lack of long-term records and research. The most common maintenance operations are crack repair in the grout mix layer under the slab (pre-fabricated solutions), fastening system adjustment, rail alignment due to long wave defects and rail grinding due to short wave defects, and, in rare cases, the slab renewal as a result of freeze-thaw cycles (Takai, 2007).

Furthermore, according to research, damage of concrete (Poveda et al., 2015; Tarifa et al., 2015) and differential settlements (Chiou et al., 2016; Zhu & Cai, 2011) are significant deterioration phenomena mainly caused by the effects of mixed traffic (Ren et al., 2019) and weather actions (T. Ferreira, 2015; Pingrui et al., 2014) - this thesis contributes to the state-of-the-art concerning these matters. The degradation of concrete will worsen the slab structural integrity which in turn will amplify dynamic forces of the track and therefore increase the track settlement rate. Higher settlement leads to higher dynamic forces and higher concrete degradation and so on.

This thesis develops a novel hybrid model that enables the dual interaction between the calculation of the train/track system dynamic interaction and the nonlinear track deterioration (concrete damage and track settlement) subjected to vehicle loads, temperature variations, and rainfall events. The interactive and iterative approach between dynamic and nonlinear sub-models makes it possible to emulate long-term behaviour with millions of train passages and thousands of weather daily cycles.

The thesis main objectives are as follows:

- Development of a numerical tool capable of accurate predictions of the short- and long-term behaviour of railway slab tracks.
- Improvement of slab track design for the European requisites for 2030/2050 railways.
- Decision assistance for the technical feasibility of slab track solutions focusing on longer life cycle and extended lifetime.

1.3 OUTLINE OF THE THESIS

The structure of the thesis comprises 8 chapters that divide the different types of work that support the envisaged goals.

In this first **Chapter 1 – Introduction**, a brief introductory explanation on the motivation of the research of slab track performance, the aim and structure of the thesis are presented.

Chapter 2 – State-of-the-art on slab track performance describes the most important achievements in slab track engineering, mainly the available commercial systems and their highlights and limitations, the structural and dynamic performance. Topics like track dynamics and deterioration are also addressed in this chapter focusing on design and maintenance issues for railway engineering. Moreover, track modelling is comprehensively evaluated with a critical review of the most relevant models developed in the last 20 years. As a result, this review aids to the model choice to be implemented in the thesis methodology concerning the aim of the thesis. For instance, hybrid models that encompass dynamic train/track interaction and nonlinear cumulative damage on the track during lifetime are non-existent at the moment.

Chapter 3 – Development of short-term dynamic and nonlinear models: DL-Track and SP-Track address the conception and development of two fast computing sub-models to study the slab track behaviour. A reduced 3D dynamic train/track model (DL-Track) and a nonlinear 3D pseudo-static model (SP-Track) that can operate independently and interactively are presented. The DL-Track model features a full bogie-vehicle model with settling soil longitudinal levelling and the SP-Track contains nonlinear material and geometric modelling for both track and temperature loads. Each sub-model is successively and simultaneously improved in each version with comparative assessments with analytical and numerical models to validate preliminary track results.

Following **Chapter 4 – Development of a long-term hybrid model: HI-Track**, the hybrid model that controls the interaction between DL-Track and the SP-Track is presented. Furthermore, the hybrid model features the update of track properties (concrete damage and soil settlement) in each iteration. To fulfil this purpose, mechanistic-empirical formulations are studied and incorporated in the model architecture for cumulative permanent damage. To enhance the meteorological influence on track deterioration, the hybrid model is coupled with a thermo-hydro-mechanical model of the soil (T. M. Ferreira, 2015) making possible the modelling of atmospheric actions as heavy rainfall events.

Chapter 5 – Validation of the numerical model with experimental measurements describes several experimental campaigns conducted in laboratory test rigs and from instrumented tracks sections in various high-speed tracks in Europe. Various track responses (short- and long-term) were collected and later statistically interpreted for particular data sets, including sensor miscalibration and frequency filtering. Each case study was thoroughly characterized to ensure a precise comparison between the experimental and numerical results - this required the meticulous modelling of the slab track systems used. This extensive validation and calibration process was undertaken simultaneously with the development of the models (Chapter 3 and 4) to guarantee a strong reliance on the calculated results.

Chapter 6 – Slab track performance and guidelines for optimized design during lifetime represents the applicability of the numerical tool for design recommendations. Multiple parametrized simulation scenarios are presented to cover as many track conditions as possible, with some extreme cases to test the design limits of ballastless systems. The effect of vehicle operation, extreme weather scenarios, element properties, and soil support conditions are studied to assess track resiliency and maintenance requirements. Moreover, optimized design solutions are presented with a performance assessment. Every scenario is ranked by a proposed performance scoring system that enables the comparison between different scenarios.

Finally, **Chapter 7 - Final remarks** summarize the main conclusions of the previous chapters regarding slab track modelling and design and, taking those into account, prospective work is suggested for further research on slab track performance.

2 STATE-OF-THE-ART ON SLAB TRACK PERFORMANCE

2.1 INTRODUCTION

The commercial exploration of high-speed rail transport put forward numerous improvements, as well as new solutions for vehicle and track to remain a competitive transportation mode in comparison with air and road transport. The circulation demands of high-speed trains cause significant changes in the track geometry due to the non-linear behaviour of the ballasted track, which in turn require more stringent geometric requirements. This brings forth a greater need for maintenance operations, which is reflected in significant economic consequences for the infrastructure manager. If these operations are inefficient, more serious problems may occur, such as reduced traffic or speed, and, in more severe cases, accidents. In some railways in Europe, the daily maintenance period is less than 5 hours (Esveld, 2001). In these high demand scenarios, the railway infrastructure manager cannot afford the non-availability of the track. For this reason, and given the interest of multiple infrastructure managers in very high speed (> 350 km/h) and high axle load corridors, the current ballasted tracks are now reaching their performance limits and are increasingly unable to meet the growing demands of mobility (Tzanakakis, 2013).

The scientific community gained interest in developing alternative technical solutions aimed at the modernization of the railway infrastructure and promoting technology innovation to improve safety, operability, and life cycle cost reductions, hence the rise of ballastless systems.

A good example of this preferred type of solution for high speed operation is the Japanese National Railways, which for 50 years has shown considerable interest in slab track implementation on new high-speed lines. The rapid proliferation of slab tracks in Japan is mainly

driven by the country's complex topography that calls for a large number of bridges, viaducts, and tunnels, where slab track application is economically more attractive than ballasted solutions (Figure 2.1). In Europe, Germany has been the biggest driver in slab construction since 1972, developing numerous successful systems that are used worldwide. More recently, the construction boom in the Chinese high-speed network has relied heavily on slab track technology. In less than 10 years, China has built almost 29 000 km of ballastless systems, which currently account for more than 80% of all slab tracks worldwide. Figure 2.2 illustrates the evolution of slab track use in high speed lines worldwide.

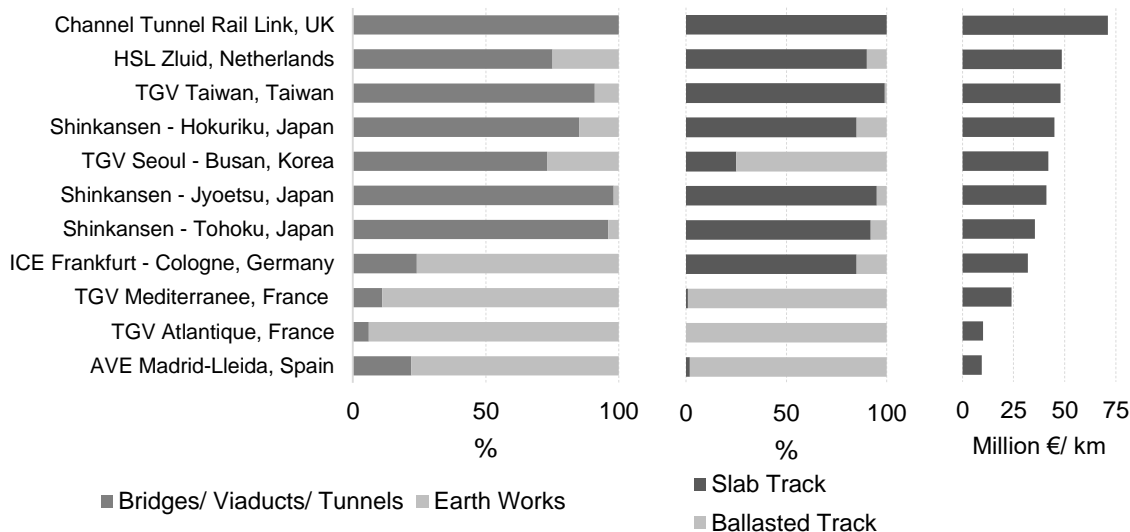


Figure 2.1: Relation between the usage of slab track and construction works for several high-speed lines

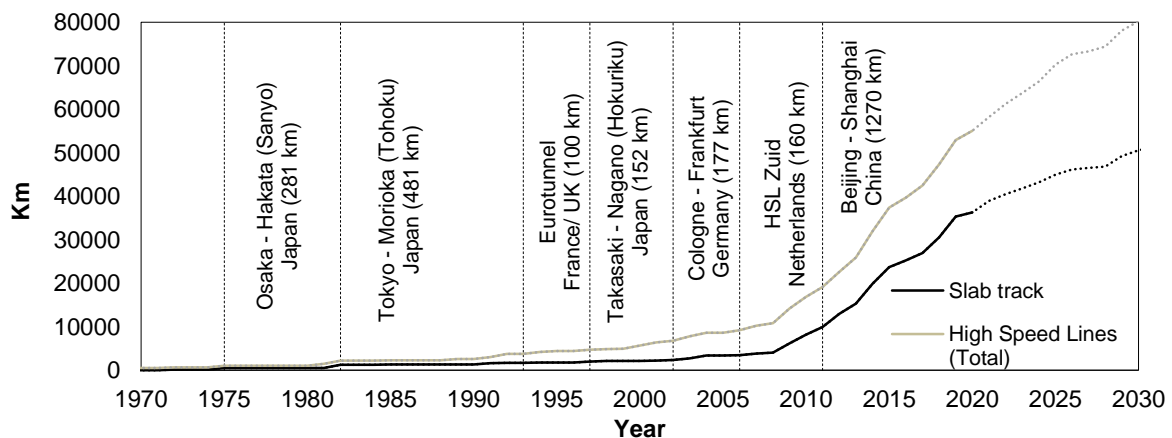


Figure 2.2: Evolution of slab track construction in high speed lines around the globe

However, the initial investment cost, the required specialized equipment, and the need for noise and vibration mitigation are drawbacks. Thence, this trend was not matched in Europe (except for Germany), which continued a strong tradition in ballasted track construction due to lower initial investment cost, and the lack of experience with and uncertainty as to the lifetime in service of ballastless tracks. Yet clear signs of ballast wear have become evident, leading European railway administrations to show a more positive attitude towards the new slab track.

Nowadays, with the technological limits to high-speed rail travel on ballasted tracks at around 360 km/h, slab track systems are of great interest to railway stakeholders. Still, the main issues related to design, construction and operation of slab tracks require a comprehensive and critical review. Hereafter, this chapter will address the research potentials, pointing out the main strengths and limitations of each design expertise of ballastless systems.

2.2 BALLASTLESS SYSTEMS

Similarly, to the ballasted track, the ballastless track has to assure the appropriate degradation of the loads from the upper to the underlying layers, so that the platform can withstand the soil stresses without significant settlements. Both ballasted and ballastless tracks are grouped in two categories that can be subdivided according to the functionality of each element: the superstructure and infrastructure illustrated in Figure 2.3.

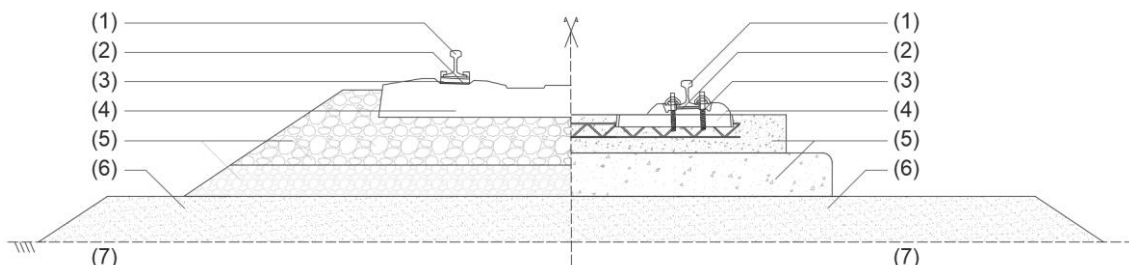


Figure 2.3: Schematic representation of a ballasted and slab track

The superstructure is conventionally composed of the track grid, i.e. the rails (1), the fastening system (2), railpads (3), and sleepers/ blocks (4), which can be optional in slab track systems, and a multilayer system (5). This multilayer system is usually referred as the ballast and subballast layer (some authors consider the subballast layer as infrastructure) in the case of ballasted tracks and the concrete supportive layer (CSL) and hydraulically bonded layer (HBL) in the case of slab tracks. The infrastructure (7) is commonly comprised of a set of soil sublayers that encompass the formlayer and the embankment soil.

The ballastless track constitution may take many forms, being the result of the improved mechanical, construction, and operational characteristics, aiming to a desired overall performance. Given the scenario, there is a variety of non-ballasted track systems, each one having its own characteristics, whether in its structural behaviour or either in its construction process.

The UIC suggests seven categories of ballastless tracks, grouping them by principles and technologies used, particularly in components (fastening systems and sleepers), the construction method (top/ down or bottom/ up), and the elasticity level (embedded rail, railpads, or under sleeper pads) and the supporting layer (concrete slab or asphalt mix) (Fumey et al., 2002).

Alternatively, a simpler characterization of different ballastless tracks may be made through the nature of the support layer (concrete or asphalt), the support conditions (discrete or continuum) and the fastening system. The main categories and a few examples of patented systems with a complete review are outlined in the work of several authors (Esveld, 2001; Fumey et al., 2002; Gautier, 2015; Lichtberger, 2005; Michas, 2012) and schematically shown in Figure 2.4.

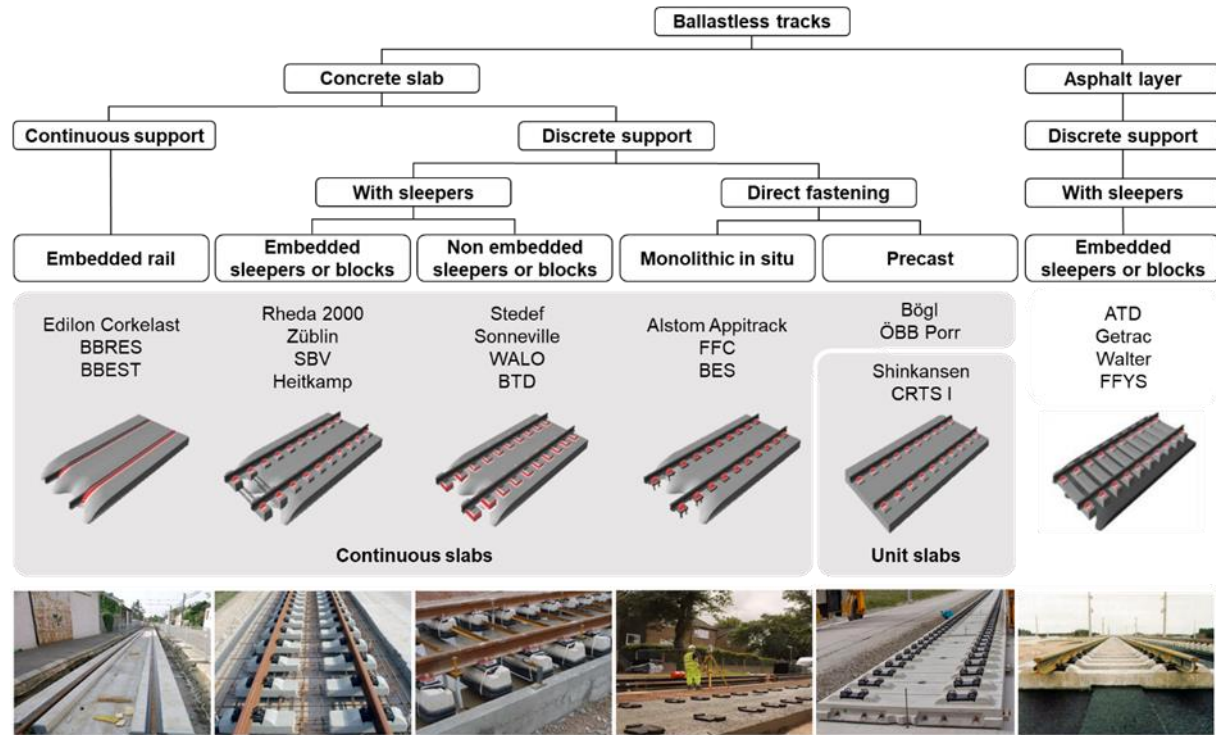


Figure 2.4: Classification of ballastless systems

2.2.1 EMBEDDED SLEEPER SYSTEMS

The embedded sleeper systems are the initial design of slab tracks, with the closest analogy to ballasted tracks, where the ballast is replaced by a concrete supportive layer. The sleepers are used to adjust the track grid through which, after the geometry adjustment, are cast together with the concrete slab (top / down approach). As is easily understood, changes in track geometry after the concrete hardening are only possible through the fasteners, and if the geometry adjustment is not sufficient, changing the geometry becomes significantly onerous. This approach is used in slab track systems as Rheda 2000 (twin blocks cast with top/ down approach) and Züblin (twin blocks placed in fresh concrete through vibration with a bottom/ up method) and illustrated in Figure 2.5.

The Rheda 2000 is one of the most widely used slab track around the world (3500 km) due to its optimization over the years by the early development of Rheda Classic, Rheda Sengenberg, and Rheda Berlin concepts and specialization for high speed (300 km/h) and high axle loads (22.5 t/ axle) (Michas, 2012).

Although being the system category that is the most efficient in terms of construction time and being driven by a high degree of automation (500 m/day for the Rheda 2000 system), the repair

and renewal of the track are costly and time-consuming procedures owing to their “compact” structure.

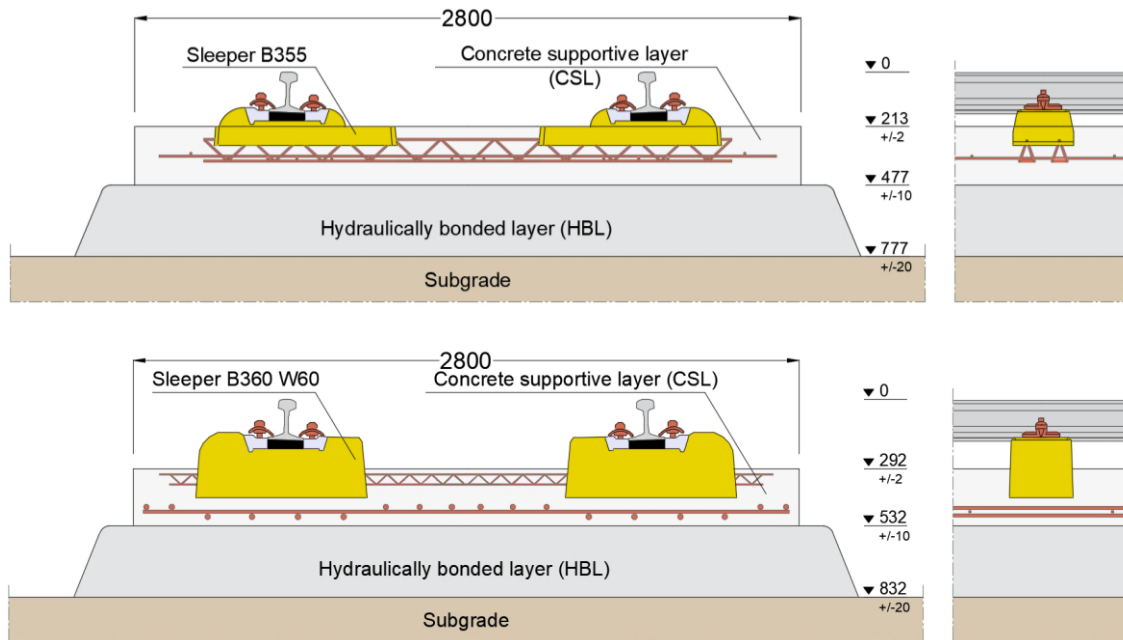


Figure 2.5: Scheme of the Rheda 2000 (top) and Züblin embedded sleeper systems (bottom) (units in mm)

2.2.2 NON EMBEDDED SLEEPER SYSTEMS

This slab track family involves the sleepers in a hull with an under sleeper pad, that is inserted into the concrete slab in most systems, except for the BTD system which uses monoblock sleepers simply laid on the concrete slab (Fumey et al., 2002). This solution achieves an enhanced vibratory performance due to the second level of elasticity provided by the under sleeper pad (a system with two-mass springs), which makes it an attractive alternative for railway tunnels. It also has the advantage that the track grid can be easily removed and replaced, and adjusting the track geometric quality can be performed after casting through the fastening systems or by repositioning the hull (Bilow & Randich, 2000).

One example is the Stedef system, with several applications, mainly in conventional lines in tunnels, in Spain, France, and Switzerland. High-speed applications are found on the Marseille tunnel in the LGV-Méditerranée and on a 2 km experimental section near Meaux in the LGV-East (both 230 km/h) (Dieleman et al., 2008). Another system, as the Sonneville that is very similar to the Stedef system (Figure 2.6), was the design applied in the Eurotunnel (160 km/h).

Even though, these solutions present an enhanced vibratory performance and a wide spectrum of stiffness flexibility with a small level of modularity, they are very expensive and require additional maintenance in the hull and under sleeper pads due to water infiltration. In order to become financial competitive solutions for plain track, further efforts are required to reduce the investment cost.

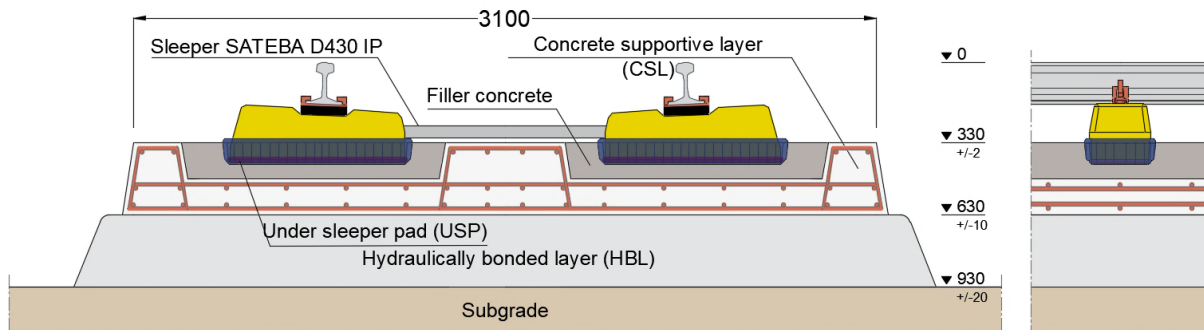


Figure 2.6: Scheme of the Stedef non-embedded sleeper system (units in mm)

2.2.3 DIRECT FASTENING SYSTEMS

The systems that make use of direct fastenings follow a bottom/ up construction method that requires the assurance of the gauge and cant during the fabrication. This adjustment requires utmost precision if the slab is cast in situ. Direct fastening systems that are cast in situ are not common solutions for slab track due to the complex geometric adjustment only allowing conventional speeds.

Recently, the result of a 5-year development of various French administrations was a new ballastless track form called Appitrac (Figure 2.7) that are cast in situ with no sleepers, for very high-speed (360 km/h) and mixed traffic (25 t/ axle) (Robertson et al., 2014). One of the principal features of the prototype built by Alstom in the French network is the automated construction method through a paver (1000 m/ day) that is similar to the construction programme used for ballasted track, in order to reduce the investment costs.

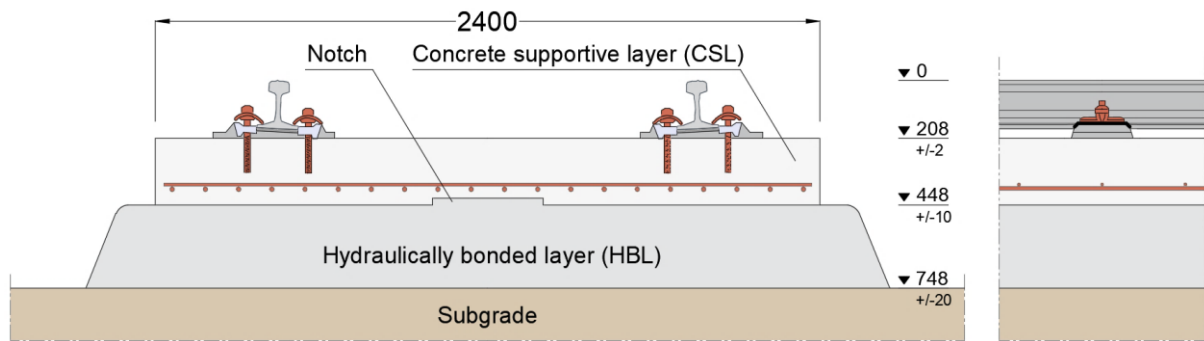


Figure 2.7: Scheme of the Appitrac cast in situ system (units in mm)

The slab tracks cast in situ are the most common of ballastless tracks, however, they have some disadvantages including the quality control and concrete curing time. When these aspects are the key to fulfil the criteria for a new high-speed line, a precast slab track is the best solution. This solution of slab tracks has the advantages of optimum quality control, low construction time due to the mechanization of the assembly process (which is reflected in the lower cost of manual labour), and ease of removal and repair of the slab panels. Still, the implementation of this type of solution is very expensive with respect to logistics, which makes it prohibitive to construct far from the manufacturing site (Lichtberger, 2005). Prefabricated slab tracks are the

most common ballastless category nowadays with more than 85% of the total number of built slab tracks. The Bögl, CRTS series, and the Shinkansen J-slab systems are the most representative precast systems with more than 30 000 km built around the globe respectively. The Bögl and Shinkansen J-slab systems consist of a hydraulically stabilized sub-layer where are laid the slab panels. The geometry is adjusted with the injection of a cement asphalt mortar between the slab panel and the sub-layer. Other solutions, as the ÖBB-Porr, uses an elastomer layer underneath the slab panel which has a filling layer between for self-compacting concrete injection. These systems are represented in Figure 2.8.

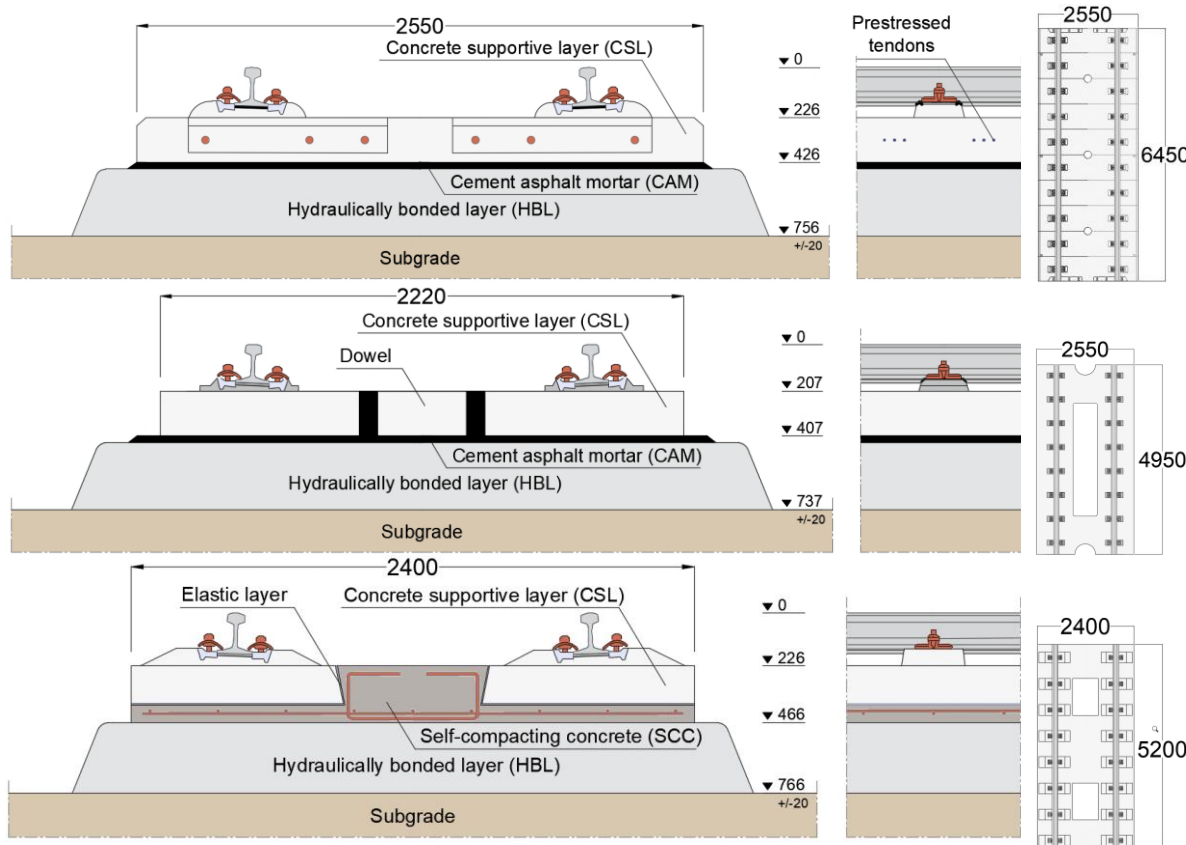


Figure 2.8: Scheme of the Bögl (top), Shinkansen (middle) and ÖBB-Porr precast systems (bottom) (units in mm)

Notwithstanding the possible complex geometries and reinforcements, anchoring problems, and the higher risk of derailment (the slab moves as a rigid body), these precast solutions are the most common trend of slab track construction. The actual tendency is to follow the concept of modularity towards an easy and fast replacement, as well as a standardization of the track components. Therefore, characteristics of the precast solutions, as modular assembly and plug & play design are important pre-requisites for future developments in slab track systems, mainly ladder tracks to reduce weight and the initial investment cost.

2.2.4 EMBEDDED RAIL SYSTEMS

Embedded rail systems are distinguished by the continuous support of the rail along its length,

so standard sleepers and fastening systems are not required. The rail gauge is obtained through notches in the concrete slab and the rail is embedded into an elastomeric resin, usually polyurethane or cork based resin (Esveld, 2001). The notch width is limited to reduce the amount of resin needed and limit the transverse rigidity (Fumey et al., 2002). Within this category, there are several systems, however, they are intended mainly to light traffic (metros and trams) and will not be covered in this document.

The construction of this type of system can be automated through the equipment of pavement engineering with high geometrical precision. By placing the resin, it is possible to position the rail for the desired track geometry. Nevertheless, repositioning the rail can cause stiffness variations, which may result in bending problems given the continued support of this type of system, so geometry repairs are expensive and longstanding. One of the main patented systems is the Edilon Corklast (Figure 2.9), mainly applied in conventional lines in the Netherlands.

This solution reveals good levels of stability and load distribution due to continuous support of the rail, which drastically reduces fatigue stresses in the rail. The embedded rail is a feature that works as an efficient noise absorber and is attractive for metropolitan areas with stricter noise level restrictions. Even though their enhanced vibratory and acoustic behaviour, embedded systems are commonly used for urban and conventional lines, instead of high-speed operations.

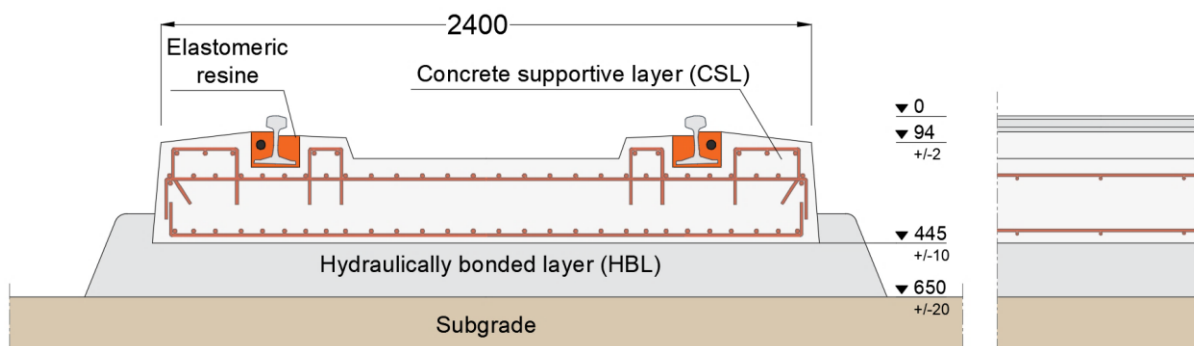


Figure 2.9: Scheme of Edilon Corklast embedded rail system (units in mm)

2.2.5 ASPHALT LAYER SYSTEMS

The use of bituminous mixtures proved to be an interesting hypothesis given the asphalt capability to ensure a good track elasticity independently from the foundation stiffness. Asphalt is a competitive solution due to the variety of possible bitumen compositions, making it possible to adapt the bituminous mixture to a range of several scenarios, giving this solution a large versatility. Unlike concrete slabs, these solutions adopt a bottom / up approach, namely the alignment of the rails is carried out after the pouring of the asphalt layer.

The advantages of this type are centred on the ease of correction of the track geometry as the high productivity since it can be loaded immediately after installation. The non-ballasted tracks which use asphalt layers (ATD, Getrac and Walter) simply lay the sleepers that may be laterally fixed through stoppers or studs. The ATD system is illustrated in Figure 2.10. A more detailed

review is presented in Fumey et al. (2002) and by the European Asphalt Pavement Association (EAPA) (2014).

However, these solutions are not very widespread, with some applications in Germany (Fumey et al., 2002), since asphalt is used in special conditions due to high investment cost, favouring concrete as the preferable material.

Nevertheless, the use of asphalt in railway tracks has potential to be applied as substructure instead of the superstructure, bringing benefits to the reduction of maintenance requirements already studied for ballasted tracks with improved dynamic stress distribution and lower vibration (Fang et al., 2011; S.-H. Lee et al., 2014; Teixeira et al., 2009).

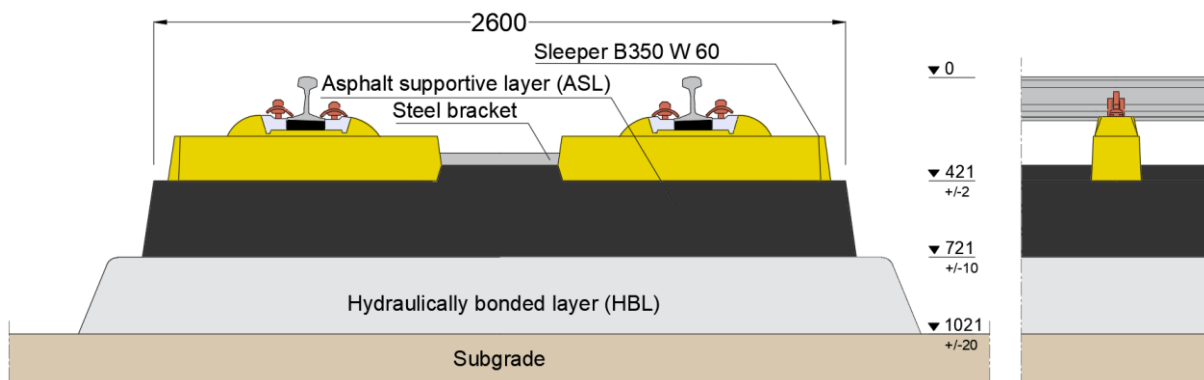


Figure 2.10: Scheme of ATD asphalt layer system (units in mm)

2.2.6 SYSTEM BENCHMARKING: PROS AND CONS

There is an open debate about the functional, technological, and economic constraints of ballastless systems. Each system shows conceptual evolution towards an optimized performance for a specific purpose. A comprehensive study of the main ballastless track systems currently in commercial operation around the globe is most important, to assess the viability of these solutions in high demand corridors. The main weaknesses of non-ballasted tracks should guide as to further optimization, and as to which systems are more likely to be competitive in the near future. Taking this into consideration, a summary of the main characteristics and technical advantages/disadvantages of the leading existing ballastless systems as found in the literature is presented in Table 2.1.

As far as the characteristics of each system are concerned, the key issue that affects the economic viability of ballastless tracks is their realization, i.e. the high costs and low efficiency of its construction. The high level of precision, in terms of the assembly of the track in its final position, together with the need for highly qualified manpower, gives rise to an undesirable increase in the initial investment. Also, the construction rate for most systems (200 m/day on average) is not competitive when compared to ballasted tracks (1000 m/day on average). If they are to be a viable solution, ballastless systems must achieve construction costs and rates similar to ballasted track systems, as well as similar levels of ease in adjusting the geometry of the track.

Table 2.1: Main characteristics of the most commonly used ballastless systems (high speed and heavy rail) (Esveld, 2001; Gautier, 2015; Matias, 2014; Michas, 2012)

Family	System	First-year/ Total km*	Example	Pros	Cons
Embedded sleepers or blocks (e.g. Rheda 2000, Züblin, Heitkamp, SBV)	Rheda 2000 (Germany)	Germany (1972) 3485 km	Wuhan - Guangzhou (China, 2010, 980 km)	Widespread system; Optimized for high-speed (V>300 km/h); Simple assembly.	Costly reparation and renewal; Noise and vibration.
	Züblin (Germany)	(1988) 606 km	Zhengzhou - Xi'an (China, 2005, 430 km)	Automated and precise construction; Low construction costs; Certified for high-speed (V>300 km/h).	Specialized pavement equipment; Complex embedment for sleepers with cant superior to 150 mm; Noise and vibration.
Non embedded sleepers or blocks (e.g. LVT - Sonneville, Stedef, WALO, EBS)	LVT Sonneville (Switzerland)	(1960) 516 km	Eurotunnel (France/ UK, 1994, 100 km)	Noise and vibratory behaviour; Track grid replacement; Accumulated experience in tunnels.	Water infiltration in the hull; High investment cost.
	Stedef (France)	(1966) 177 km	Marseille tunnel (France, 2001, 16 km)	Waterproof hull; Vibratory behaviour; Easy replacement of the track grid.	High investment; Steel bars are sensitive to thermal variations when assembled.
Cast in situ (e.g. Appitrack, Hotchief, FFC)	Appitrack (France)	(2013) 1 km	Gisoy (France, 2013, 1 km)	Low investment costs; Low construction time due to specialized equipment; Removable slab panels after casting.	Limited post-adjustment; Low representability; High precision equipment.
	Bögl (Germany)	(1977) 4400 km	Beijing - Shanghai (China, 2011, 1270 km)	Accumulated experience in high-speed (V>350 km/h); Low construction times; Specialized turnouts and crossings systems.	Prohibitive slab logistics; High risk of derailment; Time-consuming intervention for slab replacement.
Pre-cast (e.g. Bögl, ÖBB-Porr, Shinkansen, IPA)	ÖBB-Porr (Austria)	(1989) 640 km	Erfurt - Leipzig/ Halle (Germany, 2013, 179 km)	Noise and vibratory behaviour; Low construction times; High geometry precision;	Fatigue strength of components;
	Shinkansen J-slab (Japan)	(1972) 2517 km	Tokyo - Morioka (Japan, 1982, 451 km)	Vast experience in Japan (V>300 km/h); Easy replacement of rails and fasteners. Low construction time.	Prone to systematic failures; Low workability of the cement asphalt mortar.
Embedded rail (e.g. Infundo- Edilon, BBRES, BBEST)	Infundo- Edilon (Netherlands)	(1974) 211 km	Atocha station (Spain, 1992 - 8 km)	Road vehicle circulation; Low investment cost and maintenance interventions; Low structure-borne noise; Low rail fatigue.	Very expensive geometrical adjustment; Rail failure inspection; Turnouts and crossings.
Asphalt layer (e.g. ATD, Getrac, Walter, SATO, FFYS)	ATD (Germany)	(1993) 28 km	Nantenbach (Germany, 1993 - 14 km)	Easy geometry correction; Low construction time; Noise and vibratory behaviour;	Longitudinal resistance; Not suitable for temperatures over 50°C.
	Getrac (Germany)	(1995) 17 km	Westkreuz - Ruhleben (Germany, 1995 - 7 km)	Short construction time; Conventional equipment; Noise and vibratory behaviour.	Not suitable for temperatures over 50°C; Turnouts and crossings.

*Since 2015

A significant and extensive literature review is given in Table 2, where justified scientific opinions on some of the technical features of the various systems, including a qualitative assessment of their performance levels, are presented. Classification of performance is ranked from 1 (weak) to 3 (strong) and covers aspects such as construction cost, maintenance, noise and vibration, and turnouts and crossings. Concerning maintenance, three factors are taken into account, namely: preventive maintenance as an illustration of maintenance frequency; corrective maintenance as an illustration of how easy it is to intervene if required; and finally, the geometry adjustment as an illustration of the systems' capability to adjust the track levelling. About noise and vibration, the solutions are ranked from low to high vibration/noise radiation (impedance), and turnouts and crossings are classified per how flexible a system is in implementing them. By way of example, the Infundo-Edilon system receives a high score in preventive maintenance and noise and vibration, due to the absence of rail supports and embedment of the rail. On the other hand, there is no possibility of turnouts and crossings, and if some geometric correction is needed, this may require the demolition or reconstruction of the track section.

Table 2.2: Technical comparison between ballastless systems (Matias & Ferreira, 2020)

		Qualitative evaluation of different systems													
		<table border="1" style="margin-left: auto; margin-right: auto;"> <tr> <td>1 (weak)</td><td>2 (average)</td><td>3 (strong)</td></tr> </table>											1 (weak)	2 (average)	3 (strong)
1 (weak)	2 (average)	3 (strong)													
		Total height [*] (mm)	Reduced height in tunnels (mm)	Dimensions Thickness x Width (mm)	Max. speed (km/h)	Construction rate (m/day)	Initial Cost (1.0 = ballast) (-)	Preventive Maintenance	Corrective Maintenance	Geometry Adjustment	Noise & Vibrations	Crossings			
Embedded sleepers	Rheda 2000	780	472	240 2800	320	500	1.5-3	2	1	2	1	3			
	Züblin	775	600	240 2800	350	200	1.25-1.5	2	1	2	2	2			
Non embedded sleepers	LVT Sonneville	805	500	216 3080	230	-	2-3	2	1	2	3	2			
	Stedef	931	452	300 3030	270	-	1.5-3	2	1	2	3	2			
Direct fastening systems	Cast in situ	Appitrac	792	-	240 2400 4800**	-	1000	1-1.2	1	1	1	1			
	Bögl	752	454	200 2550 6450**	350	-	1.5-1.8	2	2	3	1	3			
	ÖBB-Porr	792	500	240 2400 5160**	300	-	1.5-2	2	2	3	2	3			
	Shinkansen J-slab	715	415	190 2220 4900**	320	350	1.3-1.7	2	2	3	1	3			

Table 2.2: Technical comparison between ballastless systems (Matias & Ferreira, 2020) (Continued)

Family	System	Qualitative evaluation of different systems										
		Total height [*] (mm)	Reduced height in tunnels (mm)	Dimensions Thickness x Width (mm)	Max. speed (km/h)	Construction rate (m/day)	Initial Cost (1.0 = ballast) (-)	Preventive Maintenance	Corrective Maintenance	Geometry Adjustment	Noise & Vibrations	
Embedded rail	Infundo-Edilon	650	400	400 2450	300	200	1.2-1.5	3	1	1	3	1
Asphalt layer	ATD	1021	721	300 2800	300	200	1.4-1.7	2	2	3	2	1
	Getrac	1008	721	300 2900	300	270	1.4-1.7	2	2	3	2	1

*Total height of the plain track from the top of the subbase to the rolling surface of the rail.

**Slab length (direct fastening solutions).

2.3 STRUCTURAL REQUIREMENTS FOR BALLASTLESS TRACKS

Ballastless solutions can achieve a broader spectrum in terms of mechanical performance requirements, as their construction can be adapted to optimize certain features. The following subchapters will focus on the specificities and requirements of ballastless systems about any noteworthy structural and geotechnical issues.

2.3.1 SUBSOIL

An important component for slab track design that is less controllable than other components is the foundation soil and the inherent high requirements for non-settling soil (high precision is required to keep it stable during operation lifetime). One of the main arguments against the use of slab tracks is the complexity introduced by the need for a non-setting soil, due to limited post-construction adjustments. A controlled settlement environment soil may require considerable improvements, which increases the construction costs. A good review of railway geotechnics with a focus on the design, construction, and maintenance of railway substructure can be found in the work carried out by Selig and Waters (1994), and more recently by D. Li et al (2015).

Differential settlements can occur in soft soils. In such a case there is the need to continuously control the permissible level of a settlement, which affects ride safety, track durability, and passenger comfort. About admissible tolerance levels, the Japanese guidelines for slab track design advise a maximum settlement of 12.5 mm for a 20 m chord (Zhou, 2011). The Chinese code TB10621 (Professional Standard of the People's Republic of China, 2009) suggests a 15 mm threshold settlement, and if the settlement is regular, the limit is 30 mm with a track vertical radius $R_v \geq 0.4V^2$, being V the operating speed (km/h) in the line.

Several studies have been carried out using numerical models to predict the train-track system response (Duan et al., 2018). To minimize differential settlements and respect safety and comfort criteria, the majority of the studies suggest a maximum of 15 mm settlement in a 20 m chord (X. Zhang et al., 2015). The authors found that, at speeds around 200 and 300 km/h, for an amplitude of 20 mm, the wavelength between 8 and 15 m chords would result in prejudicial car body accelerations. In the case of shorter wavelengths, the slab acts as a “bridge” over the defect, and for longer wavelengths, the settlement behaves as a vertical transition curve, reducing dynamic effects. These results suggest that certain specific settlements are insignificant enough to be negligible.

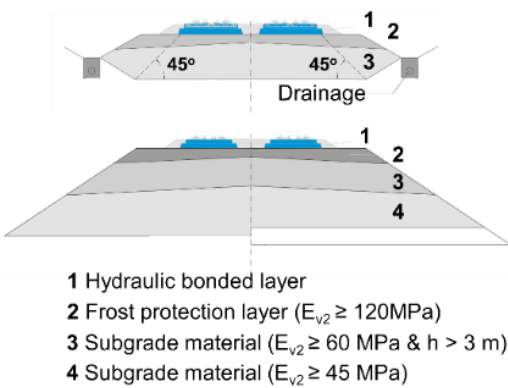


Figure 2.11: Schematic representation of the requirements for cuttings (top) and embankments (bottom) of slab tracks according to the German code (SSF Ingenieure GmbH, 2010)

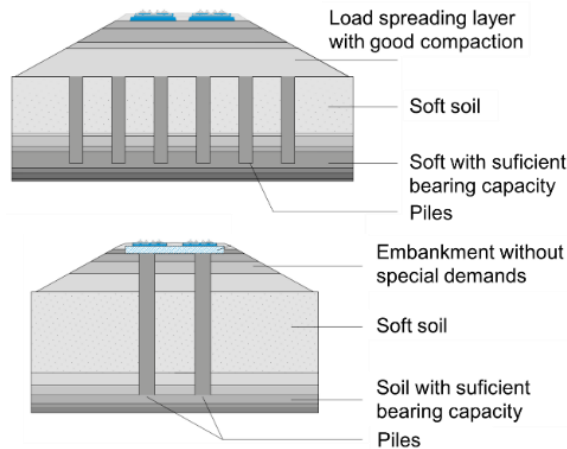


Figure 2.12: Schematic representation of soil stabilization alternatives by the usage of piles

However, most of the slab track construction around the globe apply the German standards for soil requirements. The settlement criteria for newly constructed tracks are indirectly controlled by the quality requirements for the substructure (Figure 2.11), with the frost protection layer with a requirement of $E_{v2} \geq 120$ MN/m² and an embankment of $E_{v2} \geq 60$ MN/m². For existing tracks, the corresponding value for the required deformation modulus drops to $E_{v2} \geq 100$ MN/m² and $E_{v2} \geq 45$ MN/m², for the frost protection layer and embankment, respectively (Darr & Fiebig, 2006). The Chinese standards use a similar approach composed of a 0.4 m deep upper formation layer and a 2.3 m deep lower formation layer, with a $E_{v2} \geq 120$ MN/m² and $E_{v2} \geq 80$ MN/m² respectively. Both the Chinese and German specifications set a limit of $E_{v2} \geq 45$ MN/m² for the subgrade soil. Where soil requirements are not verified, as in the case of cohesive and organic soils, strengthening techniques should be applied. In such cases, it is recommended to remove the affected soils from the upper edge of the track and replace them by improved soils (Lichtberger, 2005). However, soft soil replacement can be a very expensive procedure and can be avoided with alternative solutions, such as mechanical compaction, hydraulic stabilization, or building structures to increase the bearing capacity and stiffness of the subgrade (Khabbaz & Fatahi, 2014) as illustrated in Figure 2.12. More complex and expensive soil stabilization can be carried out with pile systems, on which the slab track is founded. One example is the

construction of the Dutch high-speed line HSL Zuid, for which the consortium responsible for the project chose a ballastless track (Rheda 2000) despite the poor subgrade.

Although many studies on the cumulative settlement have been conducted (Zongqi et al., 2018), their accuracy is low, due to the uncertainty of the soil parameters, e.g. as saturation in the soil-climate interaction. Thermo-hydro-geological conditions and moisture effects have a major influence on soil settlements and are usually taken into consideration in road pavements (ARA, 2004). The doctoral thesis of T. Ferreira (2015) gave rise to very important research in this field, with a two dimensional numerical model of the thermo-hydro-mechanical behaviour of the soil and an innovative constitutive model being developed. Obtained results show that, compared to a ballasted track, a slab track reduces the risk of instability (with regard to rainwater infiltration) due to the additional protection given to the embankment. The impact caused by the coupled effect of cyclic train loading and atmospheric actions on subgrade settlements requires further studies in order to improve slab track-soil interaction predictions for extreme weather scenarios.

2.3.2 SUPERSTRUCTURE

The slab track superstructure can be divided into 2 subsystems: railway track components; and supporting structure. The key element in the supporting structure is the monolithic concrete (or asphalt) structure, which is commonly built with concrete of at least the C35/45 strength class.

The concrete must also have good frost-resistance (important for cold-weather countries), with a cement content between 350 and 370 kg/m³ and a typical overall height of around 200 mm (Lichtberger, 2005). Also, the hydraulically bonded layer is part of the supporting structure and should be approximately 300 mm thick with crack joints every 5/6 m, and with a cement content of 110 kg/m³. Recommendations for a design methodology for slab track solutions are explored by Giannakos & Tsoukantas (2009).

The structural configuration of ballastless systems may vary for different regions due to different development backgrounds. The most important design schools of slab tracks are Japanese and German. The Japanese school uses unit slab tracks, i.e. modular slabs without load distribution between them, while the German school uses continuous slab tracks that consist of mechanically linked panels or a monolithically cast structure. The Japanese Shinkansen slab track (unit slab track) was first introduced in bridges and tunnels and then gradually migrated to open plain track. On the other hand, German ballastless tracks (continuous slab tracks) took the opposite route, with the technology being adopted from road pavement engineering. With regard to unit slab tracks, the major concern is the train load, rather than the temperature loads and concrete contraction. Notwithstanding this fact, Japanese guidelines take into consideration the temperature indirectly through slab warping and the consequent uneven support of the slab (Satoshi, 1989).

As mentioned above, due to their very nature, the major issue in the design of continuous slab tracks is the imposed deformations (that can be modelled as a temperature variation). The reinforcement ratio applied is around 0.8%-0.9%, usually for crack control due to thermal dilatations (X. Liu et al., 2011). These values are usually adopted to limit the crack width to 0.2 - 0.5 mm. In most cases, the reinforcement is placed in the neutral axis of the slab, since a controlled settlement concept is adopted, but it can be mounted eccentrically if a higher bending stiffness is envisaged (Steenbergen et al., 2007). The effects of the number of steel bars and their size in temperature-induced actions were studied by Cho et al. (2014) on CRTS-II slab tracks in the Chinese rail network. As expected, the results show that an increase in steel bar size does not increase the crack width and stress patterns. On the contrary, an increase in the number of steel bars reduces directly the crack width. The current design standards use plain unreinforced concrete for controlled environments in which cracking is not expectable (e.g., tunnels), and reinforced concrete is used mainly in open plain track to limit cracking. Prestressed concrete is used in very weak foundations as it is more economically viable, and also in severe cold areas with high-temperature gradients. The reinforcement configuration plays a major role in the cracking pattern and stress distribution, which have considerable influence on the serviceability performance of the track (X. Liu et al., 2011). However, it must be said that, currently, reinforcement configurations subjected to the effects of temperature-induced stresses coupled with cyclic train loads is an area of study and research still waiting to be further explored.

Another important railway component for slab track design is the fastening system, which has a direct effect on vibratory performance and riding comfort. Slab tracks feature lower fastening stiffness (≈ 22.5 kN/mm) to replace the ballast elasticity, which causes a higher extra deflection between rail supports. If the difference between deflections is more than 3-4% of the global rail displacement, problems such as structure/airborne noises and corrugation will be increased (Vossloh Fastening Systems GmbH, 2009). The fastening system should also be able to assure ride safety at very high speeds, mainly for longitudinal and lateral loads, caused by acceleration, braking, yaw movement of the train, and centrifugal forces on curves. Table 2.3 presents a review of the most important standard design loads for ballastless systems (CEN, 2004a; X. Liu et al., 2011; Professional Standard of the People's Republic of China, 2009).

Table 2.3 shows the German influence on the design, which places greater emphasis on temperature action than the Japanese school. On the other hand, Japanese guidelines focus mainly on train loads, essentially not taking into account temperature loads, as seen in the modular nature of the Shinkansen design. Chinese standards set the vertical temperature gradient as $45^{\circ}\text{C}/\text{m}$, nevertheless, given the extreme climate conditions in certain regions of the country, temperature gradients can be greater than $70^{\circ}\text{C}/\text{m}$. With that said, Liu et al. (2011) suggest a maximum positive gradient of $80\text{-}95^{\circ}\text{C}/\text{m}$, depending on the climate severity, and approximately half that for a negative temperature gradient.

Table 2.3: International practices for slab track design loads

	Europe (EN 1991-2)	Japan	China
Vertical Loads	$\phi_d \times LM_{71}$ ϕ_d – Dynamic amplification factor; LM_{71} – UIC Load model 71: 4 x 250 kN axles // 1.6m (locomotive) + 80 kN/m (carriages)	$\phi \times$ static wheel tread $\phi = 3$ for dynamic checking $\phi = 1.45$ for fatigue checking	$\phi \times$ static train load $\phi = 3$ for only train load $\phi = 1.5$ for load combination
Lateral Loads	100 kN (yaw movements) or Y/Q limit	Y/Q limit	Y/Q limit
Longitudinal Loads	$Q_{lak} = 33$ [kN/m] $L_{a,b} \leq 30$ [m] (acceleration)	$Q_{lbk} = 20$ [kN/m] $L_{a,b} \leq 300$ [m] (braking)	-
Uniform Temperature	+/- 35°C	-	According to local weather conditions
Temperature Gradient	50°C/m (Germany)	-	45°C/m

2.4 TRACK VIBRATION AND NOISE

Ballastless systems, as with ballasted tracks, are a set of interacting subsystems that can be understood as a periodic structure with infinite extension subjected to a set of moving masses. Accordingly, the structure has a distinct modal behaviour, with a wide range of frequencies – from ground vibrations to high pitch noises. Induced vibrations are caused by wheel/rail interaction, and it is widely accepted by the scientific community that these phenomena are strongly correlated with track degradation, which will be discussed in section 2.5.

2.4.1 VIBRATION

The corresponding vibration modes and natural frequencies of ballastless systems are characterized by the properties of several components of the track, in particular by the track's elasticity and damping since both have a major impact on track receptance.

Nonetheless, typical ballastless systems exhibit the following approximate common natural modes (M. Wang et al., 2016): full system resonance (60-90 Hz); slab resonance (100-200 Hz); rail movement relative to the sleeper (400-1000 Hz); pinned-pinned rail resonance (1000-2000 Hz). Possible resonance may arise on a track, depending on the train speed and the geometries at state (wheelbases, train configuration, sleepers distance, corrugation wavelength, OOR wheels order, etc.) due to the receptance frequency $f = V/d$, in which V is the train velocity and d the receptance wavelength. Figure 2.13 presents a comprehensive representation of the relationship between wavelength and frequency sources of the train/track system, but also the possible resonance phenomena that could arise on the track.

Many approaches to reducing structure-borne vibration and noise have been proposed, the clear majority of which have been for ballasted tracks. The inherent high stiffness of ballastless systems gives rise to different dynamic responses than those observed in ballasted tracks. In recent years, the scientific community's efforts have been focused on the effects of surface

irregularities, track alignment, and running train speed on the vibration of the train/track system (Balendra et al., 1989; Cox et al., 2006; Galvín et al., 2010b; Hussein & Hunt, 2006; Lombaert, Degrande, Vanhauwere, et al., 2006; Steenbergen et al., 2007; Van Lier, 2000). More research work that has been carried out on slab track vibration is described in Table 2.4.

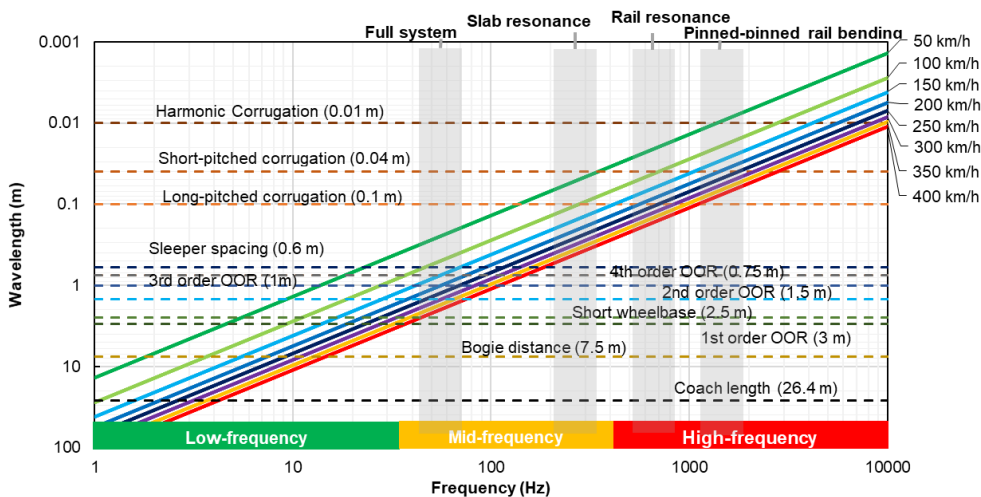


Figure 2.13: Relationship between train speed, wavelengths and frequency In the train/track system

Table 2.4: Topics of slab track dynamics

Topic	Focus	Reference	
		Numerical	Experimental
Vibration design	Soil improvement	(Steenbergen et al., 2007)	-
	Influence of elastic elements (rail pad and/ or CAM layer)	(Feng et al., 2017; Lei & Zhang, 2011; Zhu et al., 2015)	(Cox et al., 2006; Guigou-Carter et al., 2006)
Vibration properties of the track	Structure-borne vibration	(Aggestam et al., 2018; Cui & Chew, 2000; Kuo et al., 2008)	(M. Wang et al., 2016; Yue et al., 2017)
	Groundborne vibration	(Xuecheng Bian et al., 2011)	(Xuecheng Bian et al., 2014; Zhai, Wei, et al., 2015)
Vibration mitigation measures	Airborne vibration	(Sheng et al., 2017)	-
	Track vibration isolation	(Kaewunruen & Remennikov, 2016)	
	Vibration transmission to the bridge deck	(Dai et al., 2016; L. Shi et al., 2016; Xin & Gao, 2011)	(Zhai et al., 2013)
	Vibration isolation in tunnels	(Gupta & Degrande, 2010; Hussein & Hunt, 2006)	(Verbraken et al., 2012)

However, only a small number of studies have been conducted on the influence of the track on overall system vibratory behaviour, and those have mainly examined slab track component optimization aimed at reducing track deterioration and increase track service life (Esveld & De Man, 2003). X. Lei (2017) developed a finite element train-track-subgrade model that seeks to represent the dynamic behaviour of a Bögl slab track system used in the Chinese high-speed network. In his study, the author conducted several parametric analyses of the properties of different track components and their influence on track response. Table 2.5 presents the elasticity influence of some components on the track response. It is noted that these results are merely suggestive since they are subjected to the track configuration, vehicle characterization, and other factors.

The study indicates that rail pad properties have a low level of influence on track displacements (except for rail displacement), as do the CA mortar characteristics. On the other hand, subgrade stiffness has a very high impact in terms of track displacements. Conversely, track accelerations are sensitive to the elastic components, whereby the rail pad is responsible for the largest deflections in CSL and HBL, while CA mortar has a moderate impact. A stiffer rail pad leads to higher track accelerations, due to a more centralized force. Thus, more energy is transferred to the track and subgrade, resulting in their deterioration. However, softer rail pads increase rail vibration, making the rail prone to rail wear phenomena. Besides the fastening system, the most significant source of structure-borne vibration is, unquestionably, train speed. Increasing the speed from 200 km/h to 350 km/h results in a more than 200% increase in rail vibration and an almost 90% increase in slab acceleration. It should be taken into account that these results are merely indicative since they are influenced by the track configuration, vehicle characterization, and other issues.

Table 2.5: Slab track components and their elasticity influence on track dynamics (Lei, 2017; Lei et al., 2016)

	Railpad Stiffness [kN/mm] $20 \rightarrow 120$	Railpad Damping [10^4 N.s/m] $5 \rightarrow 100$	CA Mortar Stiffness [10^4 N/m] $3 \rightarrow 30$	CA Mortar Damping [10^4 N.s/m] $2 \rightarrow 32$	Subgrade Stiffness [10^7 N/m] $2 \rightarrow 12$	Speed [km/h] 200 - 350	
δ_{rail}	--				--	++	{ $\pm 10\%$ }
acc_{rail}	-	--			---	++++	{ $\pm 10\%, \pm 25\%$ }
δ_{CSL}			-		---	++	{ $\pm 25\%, \pm 50\%$ }
acc_{CSL}	+++	++++	-	-	--	+++	{ $\pm 50\%, \pm 100\%$ }
δ_{HBL}					---	++	{ $>\pm 100\%$ }
acc_{HBL}	+	++++	--	-	--	+++	

Another important issue for railway engineering related to ground-borne vibration and propagation is the concept of critical speed. Critical speed occurs when the train speed matches the Rayleigh wave speed of the subgrade soil, giving rise to a resonance phenomenon (Connolly et al., 2015; Madshus & Kaynia, 2000). This is a common issue in high-speed railway tracks built on soft soils (Khabbaz & Fatahi, 2014). However, slab track systems are usually laid on rigid foundations and their superstructure is generally stiffer, which means that the Rayleigh wave speed is higher (Nsabimana & Jung, 2015), thus avoiding this problem. Notwithstanding this fact, the ongoing increase in train speeds means that this particular possible issue for slab tracks must be brought under control in the near future.

A common countermeasure for reducing ground-borne vibrations in ballastless systems is the inclusion of an elastomeric mat under the slab, i.e. a floating slab track (FST). This solution is effective in isolating the slab for frequencies above 10 Hz (Kuo et al., 2008). As far as lower frequencies (<10 Hz) are concerned, floating slab tracks have shown weaker performance levels when compared with directly fastened tracks (Balendra et al., 1989). If not designed and built properly, floating slab tracks may result in higher maintenance costs and raise concerns regarding quality and track damage (Kuo et al., 2008). With the use of stiffer rubber mats, the purpose of floating slab tracks is reduced, as this would mean higher wheel/rail contact forces. If soft mats are used, outgoing vibrations are reduced. However, vibrations in the slab and rail

components are increased, resulting invariably in higher wear rates and maintenance interventions (Kuo et al., 2008).

Apart from floating slab tracks, other track vibration mitigation techniques can be implemented in ballastless systems. Each vibration countermeasure has a distinct vibratory behaviour that enables it to effectively reduce vibrations for a certain range, and thus to reduce life cycle costs. Kaewunruen and Remennikov (2016) compiled and summarized a set of vibration attenuation techniques for slab track systems, including rail dampers, resilient rail pads, booted sleepers, and floating slab tracks. Recently, the collaborative European project RIVAS (Bongini et al., 2013) developed vibration mitigation measures for slab tracks, namely for the Getrac system, where an under sleeper pad was added, as well as wider and heavier sleepers. Additionally, as part of the same project, several field tests were conducted to study vibration countermeasures in the Infundo-Edilon, LVT, and Züblin systems (Deutsche Bahn AG & Terno, 2011). Based on the literature and the interpretation of the main vibration mitigation techniques and their initial investment costs and frequency reduction effectiveness, i.e. in which frequency range said solutions effectively reduce vibration, is summarized in schematic form in Figure 2.14. Also, one should note that track drainage also plays a crucial role in vibration behaviour, since deficient drainage and the presence of water may worsen the performance of attenuation measures and also increase wave propagation.

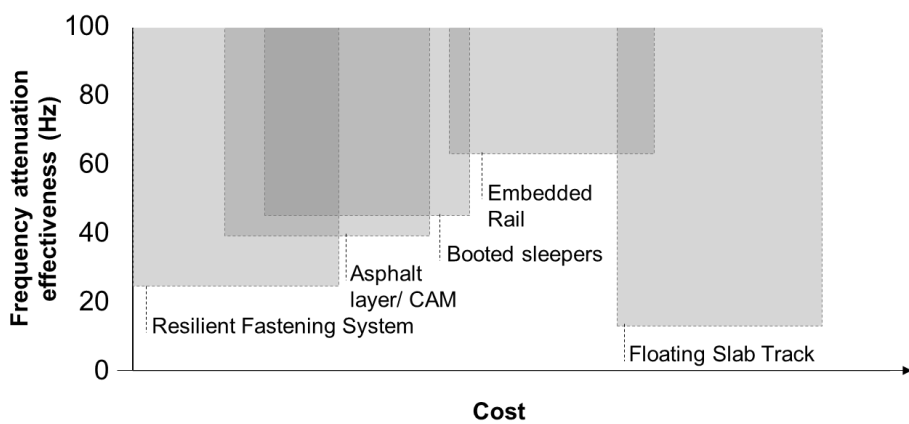


Figure 2.14: Relationship between initial investment and frequency attenuation effectiveness of vibration mitigation countermeasures

2.4.2 NOISE

Besides its higher investment cost, another major disadvantage of the slab track is its acoustic performance. Slab tracks are, generally speaking, 2-4 dB noisier than ballasted tracks (Thompson & Gautier, 2006). As opposed to the absorber effect of the ballasted track, slab track solutions function as noise reflectors on account of the smaller difference in stiffness when compared to rail, which guarantees it has high mechanical impedance. Given the demanding lower noise limits set by the European Union rail noise standards (De Vos, 2016), several noise mitigation measures have been studied.

Regarding airborne noise, the typically softer rail pads of slab tracks (rail pad stiffness ranging from 20 to 60 kN/mm) enable a higher amplitude of rail vibration, thus contributing to greater noise (Thompson, 2009). Nevertheless, different combinations of rail pads and under sleeper pads (without affecting the overall track stiffness) can achieve a better airborne noise isolation performance (Thompson, 2009). Other mitigation procedures can also be performed using acoustic barriers (sound mitigation of roughly 6 dB), absorption panels on tracks (2-3 dB), wheel dampers (4 dB) and wheel skirts (1 dB) (Thompson & Gautier, 2006). As a further matter, structure-borne noise is mitigated by track designs for vibration isolation, such as booted sleepers with under sleeper pads and floating slabs (noise in tunnels), to ensure low noise emission.

The development of the embedded rail with continuous support has been a major achievement, as it has led to a targeted reduction in rail vibration, although it remains 2-3 dB louder than the ballasted track. This solution is particularly effective for high frequencies, however, given the high damping factor of the elastomer, it vibrates with the rail at low frequencies, propagating the sound waves faster.

Preliminary studies were carried out by the Dutch ICES “Stiller Treinverkeer” project in a multi-partner project in the Netherlands in 1998, aimed at mitigating noise levels produced by freight traffic. The study developed low noise concepts using theoretical modelling and an experimental slab track (Van Lier, 2000). Acoustic treatments and improvements have been carried out on slab tracks in Germany in 2000, but they were not sufficient to achieve performance levels similar to those of ballasted tracks (Diehl et al., 2000). Similar European projects, such as the STAIRSS project (STAIRRS, 2003), presented mitigation measures to reduce noise radiation from vehicles or tracks that could also be applied to slab tracks. Furthermore, and more recently, the Quiet-Track (Venghaus & Petz, 2014), studied and tested low noise radiation solutions as a new embedded rail system for trams (also applicable to conventional tracks) that were capable of achieving a 6 dB noise reduction in comparison to standard tracks.

Moreover, noise from railway viaducts/bridges is of greater significance than noise on open plain tracks, be they ballasted or ballastless, due to the higher mechanical impedance of the underlying structure. It results in increased airborne and structure-borne sound radiation to buildings nearby. This extra noise radiation is heightened in the case of slab track systems. The use of soft resilient rail pads will reduce structure-borne noise radiation, but will also increase airborne noise, so an optimal rail pad stiffness could be achieved. Cooper and Harrison (2002), described the development of an alternative design for viaducts by West Rail in Hong Kong. The elevated double-track viaduct has an exigent limit of 64 dB noise level at the 25 m point in the track from the passage of a nine-car train at 130 km/h, which is 20 dB lower in comparison to the standard viaduct. Floating slab tracks were applied with soft rail fasteners, sound-absorbing barriers installed under the walkways and parapets and even the box girder of the viaduct was designed to limit the structure-based noise to meet the noise targets.

2.5 TRACK DETERIORATION AND MAINTENANCE

Railway tracks are subjected to demanding operation conditions, whereby proper maintenance procedures for each component must be assured to guarantee the enhanced performance of a high-speed track during its lifetime. Whilst they are often referred to as “maintenance free”, slab tracks require a moderate level of maintenance that is estimated to be between 40% and 60% of the level required for ballasted solutions, according to Ripke (2010). Although some data shows almost a 90% reduction in track geometry maintenance (Andrés et al., 2015), other common maintenance operations, such as logistics, supply, and maintenance of materials and equipment, rail grinding, switches and crossings availability, inspection, management operations, and surveillance staff, achieve smaller reductions. In Figure 2.15, it can be observed the comparison of the evolution of maintenance costs for the ballasted section and the non-ballasted section for the Sanyo Shinkansen. The ratio of maintenance costs between the ballasted and the slab track section was close to ten until the early nineties, four until 2006, and more recently towards an asymptotic ratio of two representing design improvements in ballasted track design. Although significantly less than the ballasted track, track levelling and lining corresponded to 70% of the maintenance costs in that slab track section.

Taking this into consideration, a comprehensive evaluation of the track deterioration (combined with advanced diagnostic and monitoring systems) would support condition-based maintenance, making it possible to reduce costs, periodical track possession, and further deterioration. The presumed causes of track degradation will be explained further below, focusing on ballastless systems.

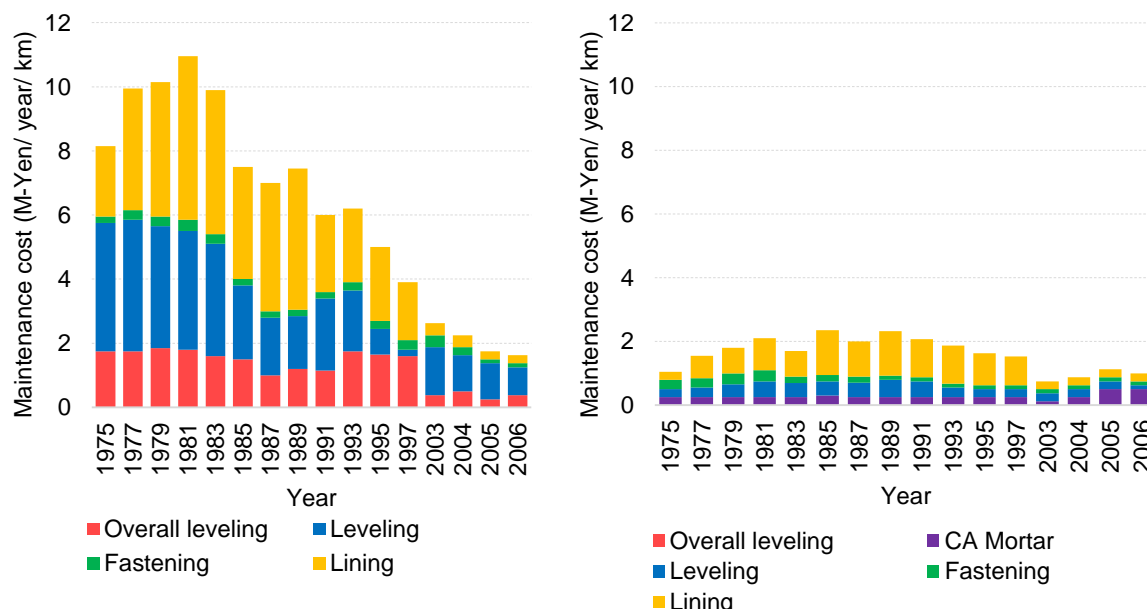


Figure 2.15: Maintenance costs of the ballasted (left) and slab track section (right) on Sanyo Shinkansen (Ando et al., 2001; Takai, 2007)

2.5.1 TYPES OF TRACK DETERIORATION

Concerning structural deterioration, fatigue phenomena in railway components are mainly determined by the evolution of a track's physical deficiencies. Due to their relatively short period in operation (except in Japan), slab track systems are lacking in systematic research focusing on degradation phenomena. Such phenomena may have the most diverse origins: e.g., soil settlement, concrete slab damage, fastening system fatigue, and rail wear and corrugation, to name just a few (see Table 2.6 and Figure 2.16).

Table 2.6: Main types of slab track degradation (Nielsen & Ekberg, 2005; Ren et al., 2016; Williams et al., 2016; Zhai, Liu, et al., 2015)

Deterioration type	Main origin	Damage mechanisms	Maintenance operations
Rail wear: Rail plastic flow/ Rail corrugation/ Rolling contact fatigue	Rail superficial defects; Vertical stiffness; Geometric quality; Out-of-round wheels; Hardness/ yield limit	Delamination and oxidation wear; Rolling contact fatigue; Plastic flow; Rutting	Ultrasonic/ eddy current inspection; Grinding; Replacement
Fastening systems fatigue	Broken/ worn insulator; Broken/ worn shoulder; Groundborne vibrations; Excessive lateral forces	Loss of insulator contact adhesion; Rail seat deterioration	Clamp fixing; Replacement
Concrete slab damage	Extreme temperatures; Subgrade settlement; Alkali aggregate reaction; Reinforcement corrosion	Loss of rebar adhesion; Crack width growth; Uneven support conditions	Grout injection of crack; Adjustment of the slab by injection
Cement asphalt mortar (CAM) cracking	Rainwater infiltration; Insufficient lateral resistance; Insufficient bonding between slab and cement asphalt mortar to resist slab warping	Delamination and spalling due to hydrological pressure; Uneven support of the slab	Grout injection of the crack; Replacement of the damaged area
Track settlements (track geometry quality)	Lack of soil bearing support capacity due to train loads or hydrological phenomena	Volume reduction (particle rearrangement); Permanent deformation (inelastic recovery)	Drainage improvements; Soil replacement; Soil reinforcement; Insertion of geotextiles; Track rebuilt (large interventions)

Rail-related deterioration, in particular, rolling contact fatigue and rail wear, is one of the common damage processes resulting from increasing axle loads and speeds that require frequent maintenance (Grassie, 2012). These phenomena are strongly influenced by vertical pinned-pinned resonance (1000Hz) (Nielsen et al., 2003). The frequency difference between track resonance and pinned-pinned resonance in ballastless tracks is smaller when compared to ballasted tracks. Said that, and due to the usually higher loads that slab tracks are subjected, rail corrugation and rolling contact fatigue (head checks and squats) occurs at a faster rate for slab tracks, giving rise to rail pad deterioration and concrete slab cracking. Solutions such as embedded rail systems can avoid these problems.

Fastening systems, as well as the concrete sleepers beneath, have been shown to have a wide range of service life when subjected to high axle loads in various study reports. One identified

fatigue problem for fastening systems is rail seat deterioration, i.e. the degradation of the concrete underneath the rail, something that is reported in high axle load lines in the United States (Williams et al., 2016). Also, shoulder and fastener wear are significant issues that reduce the lifespan of the fastening system.

Certain pre-fabricated systems use cement-emulsified asphalt mortar (CAM) between the CSL and the HBL. Studies have shown that deterioration of this element, which plays a major role in track supporting and damping, increases slab track vibrations, leading to fatigue in other track components. Cement asphalt mortar, when subjected to high demand traffic and severe climate/weather conditions, is prone to the formation of voids, which reduces the bearing capacity of the track (Ren et al., 2016). Also, the damaged interface between the CAM layer and the slab under thermal and train loads causes cracking and delamination (Zhu & Cai, 2014a).

Finally, one of the most important long-term mechanical processes for slab tracks is the differential settlements that may occur along the track. The literature is almost completely lacking in track settlement laws that apply specifically to ballastless tracks. Whenever soil foundation is of moderate or bad quality, settlements are most likely to arise over the track's lifetime. Also, due to the abrupt changes in vertical stiffness, railway transitions are intensive maintenance zones due to repeated amplified dynamic solicitations (Sañudo et al., 2016).

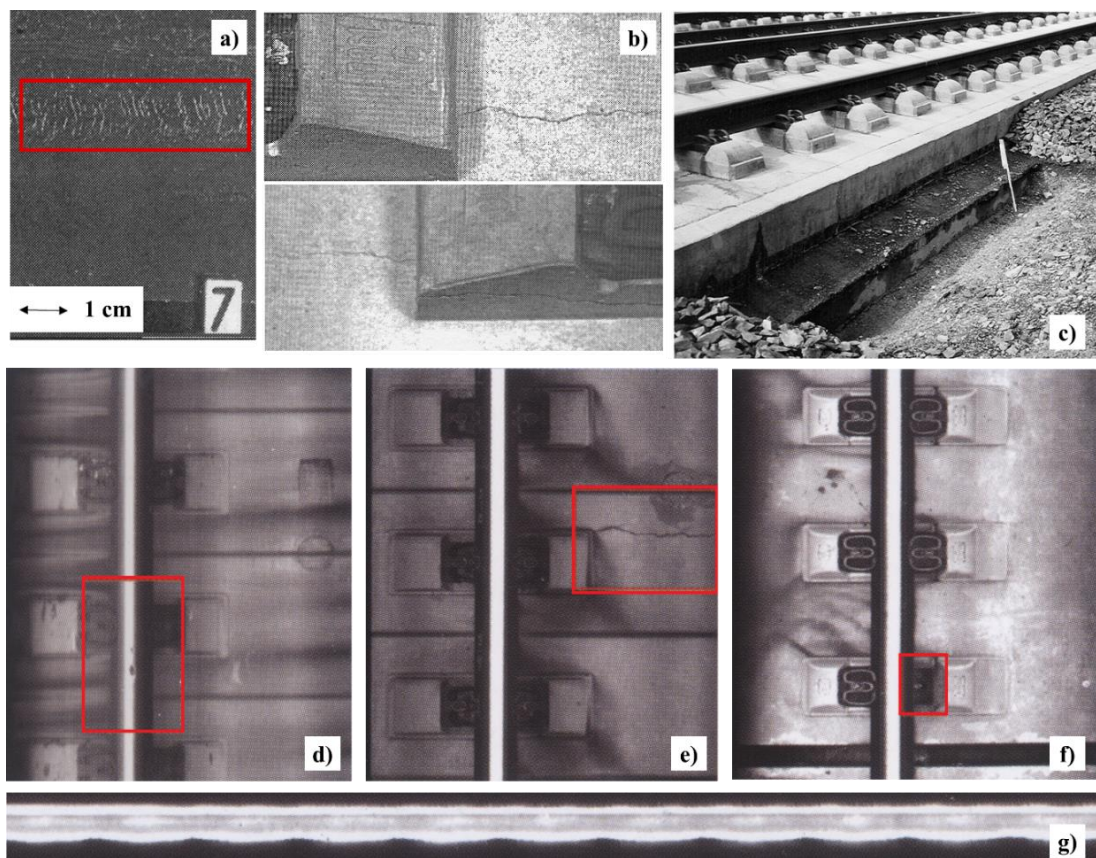


Figure 2.16: Most common deterioration phenomena of slab tracks: a) rail head checks, b) cracking near the sleepers/supports, c) track settlement repair, d) rail head squats, e) slab transverse cracks. f) missing fastener. g) systematic wave wear of the rail head (Ripke, 2010; Shanghai Railway Administration, 2017; Vogt et al., 2005)

2.5.2 SLAB REPAIR

Whilst there is a multitude of maintenance issues concerning slab tracks, this section will focus on assessing the maintenance interventions related to concrete cracking, putting all the other existing types of slab track deterioration identified in Table 2.6 to one side.

Concrete cracking in slab tracks reduces the durability of the overall structure. Concrete cracks and the expansion of the reinforcement due to corrosion accelerates water infiltration into the foundation, which in turn affects the normal stability of the track. To overcome cracking-related issues, some solutions use fibre-reinforced polymers (Y. Yang et al., 2015). However, the technological development of concrete rigid pavements for road and airport engineering, as described by Ioannides (2006), has not yet been transferred to railway engineering, and there is a distinct lack of study references in relation to this matter.

In the early days of their implementation, slab tracks were applied mainly in tunnels, i.e. in a controlled environment, meaning that crack control was a minor problem. Today, however, their implementation in open plain track, associated with high fatigue loads and short maintenance window, has made the control of concrete cracking a challenging maintenance issue. The Japanese repair guidelines for the Shinkansen slab track structure define the maintenance needs according to the crack width in three categories A, B, and C, determined by visual inspection. Category A ($w_k \geq 0.2$ mm) requires immediate and rapid repair, B ($0.1 \text{ mm} < w_k < 0.2 \text{ mm}$) calls for preparation of a repair process, whilst class C ($w_k \leq 0.1$ mm) cracks are merely registered to assess the crack progress (Yongjiang et al., 2009). The German specifications limit crack width to 0.5 mm and require that no crack should appear near the fastening system to avoid potential disintegration of the sleeper/slab interface, as there may be a risk of the fastening becoming loose (Lichtberger, 2005).

Yongjiang et al. (2009) differentiated between cracks in the slab and the hydraulically bonded layer (HBL). In the slab, the authors reported crack formation on the inner side of frame tracks used in Japan, the main cause of which is an alkali-aggregate reaction, which results in the substitution of some panels. With regard to cast in situ slab tracks, several cracks appear around the interface between the sleeper and the cast slab. Transversal cracks are concentrated in the expansion joints. As for the HBL, the same authors reported the occurrence of transversal cracks that sometimes ran the total depth of the HBL.

A common countermeasure for concrete cracking is crack sealing at an early stage, as newly formed cracks have more fracture energy. The most significant factors for crack assessment control are also the main parameters related to drying shrinkage – cement content, elastic Young's modulus, reinforcement configuration, and possible concrete adjuvants. Temperature variations are also responsible for crack propagation. This is an important parameter in countries with high-temperature variations that may reach $70^\circ\text{C}/\text{m}$, as has been recorded in China (Gautier, 2015). Here, expansion joint spacing is also an important influencing factor. High temperatures together with low environmental moisture result in large cracks. This is not so

important for standard concrete buildings, but it is crucial for slab tracks, as they are subjected to cyclic train loads that will repeatedly open and close the cracks, increasing their propagation. The requirements for repairing the cracks in concrete slabs are defined essentially by the fatigue condition, the available time window, and the repair technology, among other factors.

2.5.3 TRACK MONITORING

Real-time monitoring techniques and tools applied to ballastless tracks are crucial for detecting early-stage deterioration, making this issue an important field of investigation for slab tracks. The most common structural monitoring technique is the application of strain gauges in the concrete slab or the reinforcement. Most recently, in the collaborative project C4R (ACCIONA, 2017), RFID sensor technology coupled with strain gauges was installed in the reinforcement bars. The sensors can be used to collect live data on the structural health condition of the slab track, so track malfunctions can be detected and repaired in advance.

The most recent trend is the use of fibre optic sensors embedded in the concrete slabs as a monitoring system for structural integrity evaluation and to facilitate identification of potential failure points at an early stage, which is a key factor for efficient maintenance. The refraction properties of the fibre depend on temperature and strain, so optical fibre sensors are a recent technology that complements the traditional electric strain gauges. A real-scale mock-up slab track built by IFFSTAR (Chapeleau et al., 2013), was subjected to mechanical and thermal fatigue tests, as well as mechanical and chemical resistance tests of the fibres. A validation procedure was performed with traditional electrical strain gauges for 10 million cycles. The technology can monitor the location and evolution of cracks during the fatigue test. It allows for the effective monitoring of the thermo-mechanical behaviour of the slab in real-time and proves to be very useful for scheduling maintenance operations and validating numerical models. The main drawback is that high-frequency data cannot be gathered using this technology (passage of high-speed train). A similar study was conducted by Crail et al. (2002), with a Bögl full-scale test example in Berlin, as well as measurements in a real German high-speed track. With this technology, it was possible to measure extremely small strains in the order of 10^{-8} m/m.

2.6 TRACK MODELLING

Today, given the demands for higher performance and enhanced reliability requirements, extensive experiments and scientific research work has been carried out to study the dynamic behaviour and deterioration processes of railway tracks. This investment is reflected, on one hand, in the construction of experimental trials, and on the other, by the development of efficient numerical models at the required performance.

In what regards experimental measurements, despite their importance, data from laboratory tests or instrumented track sections are not easily gathered or available. As for laboratory

experiments, a small number of researchers have tested full-scale models, mainly focused on the dynamic response of slab track systems (Xuecheng Bian et al., 2014; Cox et al., 2006; Guigou-Carter et al., 2006; M. Wang et al., 2016), and more recently on fatigue behaviour (Gautier, 2017; Tarifa et al., 2015). Instrumented track sections are usually performed in collaboration with railway infrastructure administrations and the tests are expensive. Unfortunately, the information gathered from these experiments is stored with a high level of confidentiality. Few examples of experimental slab track studies were conducted by SNCF (Dieleman et al., 2008) (France), DB (Ripke, 2010) (Germany), CR (Zhai, Liu, et al., 2015; Zhai, Wei, et al., 2015) (China) and KRNA (Jang et al., 2008) (South Korea).

On the other hand, numerical simulation is a powerful tool to assess the challenging task of railway system modelling, since its space and time domain have very broad spectrums. The real track performance could stretch for several kilometres long with millimetric geometry tolerances as well as short-term responses up to 200–300 Hz (slab resonance) and several years of long-term fatigue.

Numerical models can be as detailed as needed, starting from a static load on a Winkler foundation to models of the vehicle itself, track geometry irregularities (rail corrugation, soil longitudinal heterogeneity, etc.), wheel-rail and soil-structure interaction, non-linear behaviour of the rail components, among others. The modelling architecture and methodology have evolved as the necessity to solve new and different problems. The main approaches to railway modelling for each specific element and common modelling strategies for different railway problems are presented in Figure 2.17.

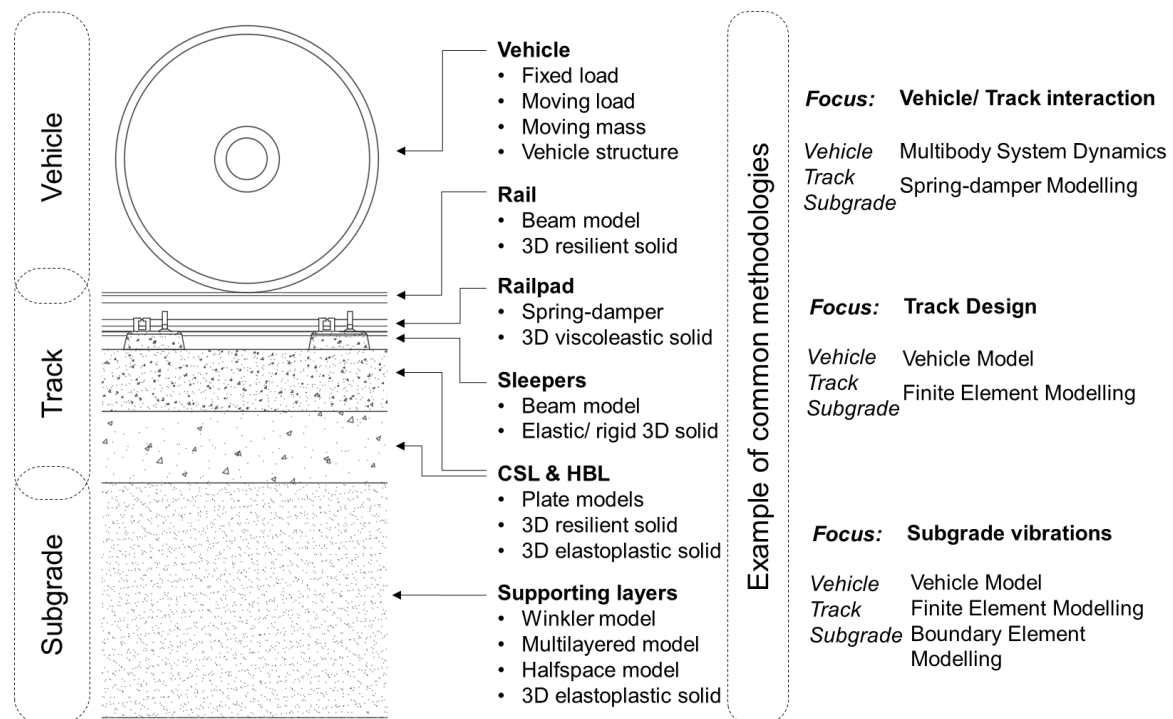


Figure 2.17: Representation of the possible methodologies and techniques for slab track modelling

Given the increase in computing power, the most commonly used approaches to simulating

large domains subjected to moving loads are the finite element method (FEM), and the boundary element method (BEM) (Andersen et al., 2007).

In more recent years, to overcome the shortcomings of 2D (less representative of the real phenomena) and 3D models (computationally more onerous), a common approach has been the use of 2.5D FEM-BEM models. This kind of reduced model uses the finite element method (FEM) and the boundary element method (BEM) to model the track superstructure and the underlying soil respectively. The boundary element method assumes the invariability and linearity of the longitudinal domain through the discretization of the cross-section of the railway, based on Fourier expansions for the soil as a layered full or half-space, which is mostly homogeneous in the track direction. This methodology allows the model to obtain a 3D solution without the track discretization along with the longitudinal domain. Several authors have adopted this approach in ballasted track models in the frequency domain with reduced computational effort (Alves Costa et al., 2012; Araujo, 2010; Freitas da Cunha, 2013; Gao et al., 2012; Lombaert, Degrande, Kogut, et al., 2006; Sheng et al., 2006). More recently Galvín et al. (2010a) developed a fully 3D FEM-BEM multibody model in the time domain to study vibrations on the track and the surroundings due to train passage.

Despite the advances in ballasted railway track modelling, the aforementioned models, whilst helpful, cannot be directly applied to slab track systems, since the vibration and mechanical behaviours of the two systems are considerably distinct. The major studies carried out in slab track modelling, in each research topic, are summarized in Table 2.7. The studies are categorised according to their focus, author(s), modelling methodology for each subsystem (foundation, track, and vehicle), loads, and simulated systems. For example, Galvín et al. (2010a) developed a fully three-dimensional MBS-FEM-BEM model, i.e. where the vehicle is modelled as a multibody system (vehicle: MBS), the track uses the finite element method (track: FEM), the soil is modelled using the boundary element method (foundation: Half-space/ BEM), and only the train load is modelled (load: Train).

The literature review reveals that there are few 2D-based approaches to studying slab track dynamic behaviour, although studies using more advanced models, such as the 2.5D FEM-BEM models, do exist. Auersch conducted several studies on ground vibrations, mainly for ballasted tracks, and more recently, he has directed his interest in studying floating slab track vibrations and resonance using coupled finite-element boundary-element methods (Auersch, 2005, 2012). Other studies related to floating slab track are presented in the work of Li & Wu (2008) and Hussein & Hunt (2009). Galvín et al. (2010b) have presented a 3D multibody system for the vehicle, a finite element model for the track, with the soil represented using boundary elements, in an effort to evaluate the vibration performance of floating slab tracks. The aforementioned models have mainly used the FEM to model the track structure and other structural elements, coupled with an MBS system for accurate wheel-rail interaction, in order to study the dynamic behaviour and wave propagation, which can be very significant at very high speeds. Further

examples relating to the direct effects on slab track characteristics and vehicle-track interaction can be found in the work of Bezin et al. (2010) and Blanco-Lorenzo (2011). An example of how the models can be distinguished according to their purpose is illustrated in Figure 7. On the left, is presented a detailed model of the vehicle for the study of the train/track interaction (Lei et al., 2016). However, this model is not suitable, for instance for the research of the effect of ground-borne vibrations as the 3D FEM-BEM model developed by Galvín et al. (2010b) presented on the right hand of Figure 2.18.

Table 2.7: Summary of the most relevant works in slab track modelling found in the literature

		Author	Foundation		Track		Vehicle	Load	System
Purpose			Winkler	Half-space/BEM	2D Multibeam	Nonlinear behaviour			
				FEM	FEM	Moving Load	MBS	Train	Temperature
Vibration	Acoustic	Markine et al. (2000)	•		•		•	•	Edilon
	Ground-borne vibrations	Lombaert et al. (2006)	•	•				•	FST
		Galvín et al. (2010a, 2010b)	•		•		•	•	FST
	Vibration isolation	Gupta & Degrande (2010b)	•		•		•	•	FST
	FST	Auersch (2012)	•	•	•		•	•	FST
Train-Track interaction		Zhu et. al (2017)			•		•	•	FST
	Dynamic performance	Lei et al. (2016)	•		•		•	•	CRTS-II
		Blanco-Lorenzo (2011)	•		•		•	•	Rheda Stedef FST
	Track irregularity	Bezin et al. (2010)			•		•	•	BBEST
		Yang et al. (2015)	•		•		•	•	CRTS-I
Deterioration	Transition zones	Shahraki et al. (2015)		•	•	•		•	Rheda
	CSL/ HBL Interface damage	Zhu & Cai (2014a)		•	•	•	•	•	CRTS-II
		Zhu & Cai (2014b)		•	•	•	•	•	CRTS-II
	Slab track life	Poveda et al. (2015)		•	•			•	Shinkansen
		Zhu & Cai (2011)		•	•		•	•	CRTS-I
Design	Damaged slabs	Auersch & Said (2017)		•	•	•		•	Rheda
	Uneven settlement evolution	Shan et al. (2017)		•	•		•	•	CRTS-II
	Temperature	Song et al. (2014)		•	•			•	CRTS-II
		Cho et al. (2014)		•	•			•	Rheda
	Track configuration	Matias(2014)		•	•	•		•	Rheda Bögl Stedef

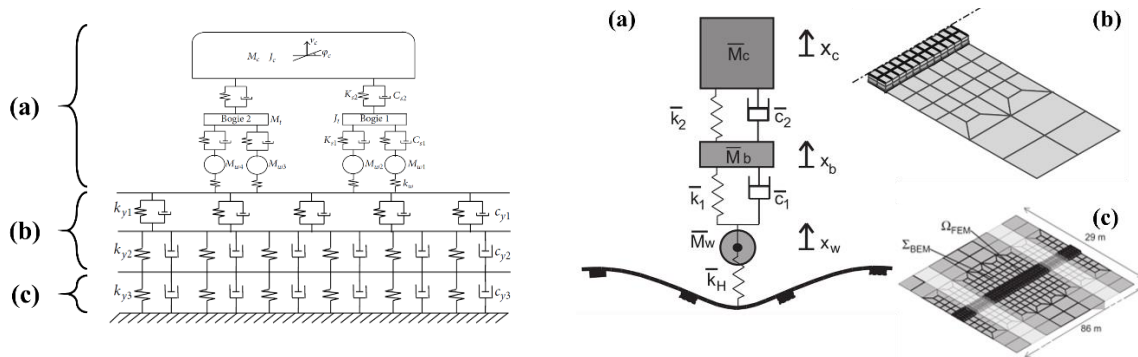


Figure 2.18: Spring-damper model developed by Lei et al. (2016): Multibody vehicle model (a) and spring-damper elements for the track (b) and foundation (c) (left). 3D FEM-BEM model developed by Galván et al. (2010b): Multibody axle model (a), soil boundary element model (b) and track finite element model (c) (right).

Another major concern that recently gained the increasing attention of engineers and researchers is the deterioration of slab tracks, one of the main areas that require further investigation (Auersch & Said, 2017; X. Liu et al., 2011). Poveda et al. (2015) used a 3D FEM model, which enabled the extraction of the principal vibration modes, and transient analysis under time-dependent loads validated with full-scale experiments on slabs (Figure 2.19). The concrete slab is modelled applying a stress amplitude fatigue criterion. As mentioned above in Section 5.1, S. Zhu et al. (2014a) studied the evolution of fatigue and damage in the cement asphalt mortar layer on floating slab tracks (Figure 2.19), whereby the cement asphalt layer was modelled with a non-linear constitutive behaviour and the damage it suffers due to temperature and vehicle dynamic loads were studied. Also, S. Zhu & Cai (2011) predicted the fatigue life of the concrete slab due to differential settlements in the subgrade using a FEM model in an ANSYS (APDL) environment. The fatigue life of the concrete slab track was assessed by S-N empirical curves. Shan et al. (2017) developed an iterative train/track model to evaluate the evolution of differential settlements in high-speed railway transition zones. The cumulative soil plastic strain is based on an empirical model derived from triaxial tests that are based on the deviatoric stress level in the soil. Also, aiming to long-term predictions regarding the track settlement, some authors adopted a shakedown theory (Zhuang & Wang, 2017) to simulate the elastic-plastic behaviour of the soil when subjected to cyclic loads. Some examples of this approach in slab track applications can be found in the work of Alves Costa et al. (2018) and Liu et al. (2018).

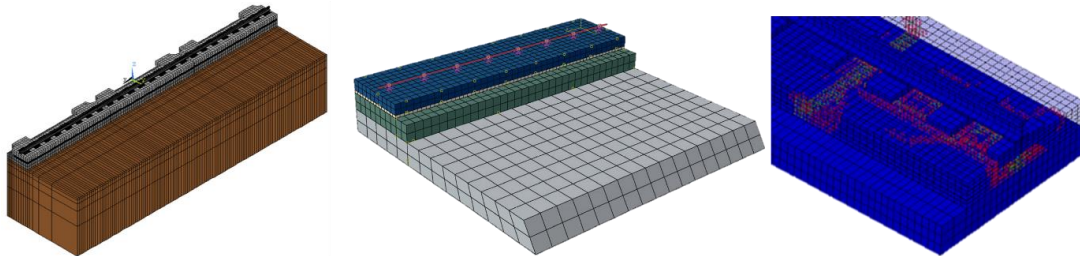


Figure 2.19: 3D FE slab track fatigue models. (Poveda et al., 2015) (left), (Zhu & Cai, 2014a) (center) and (Matias, 2014) (right)

About the evolution of cracking and reinforcement behaviour, there is also an almost complete lack of published research. Cho et al. (2014) performed a steel ratio study and its effects on the slab track behaviour due to temperature loads. Matias (2014) developed 3D FEM models of several slab track systems to study cracking patterns and reinforcement stresses when subjected to longitudinal heterogeneities (Figure 2.19). The prevention of early cracking in concrete is one of the main challenges for concrete structures. Nevertheless, the majority of formulations assume certain indirect simplifications such as linear damage accumulation implied by Miner's rule, non-consideration of load sequence, and non-probabilistic nature of the damage (Springenschmid, 1998). This is the basis of the mechanistic-empirical models that evaluate the fatigue behaviour of concrete based on Wöhler diagrams. As far as cracking prediction is concerned, some studies based on structural credibility theory have been carried out, with the models for the early cracking of concrete structures taking into consideration the randomness of the main cracking factors (Yongjiang et al., 2009). A review of probabilistic crack growth models can be found in the work of Cross et al. (2006). These models present stochastic predictions for maintenance and inspection of concrete structures, thus playing a significant role in structural risk assessment analysis (Straub & Faber, 2005). Nevertheless, there has still been no reporting in this area for ballastless tracks. The cost of maintaining a track is directly related to its condition, which depends upon a variable number of uncertainties that are inherent in the respective models. Accordingly, these models could be used to optimize track maintenance activity, meaning that the field will continue to receive further attention from the scientific community.

In summary, as already mentioned, research into slab track fatigue caused by the joint action of the train loading, temperature, and differential settlements, to evaluate the real life span and track durability, is almost non-existent. Long-term vehicle/slab track interaction modelling is a highly sophisticated undertaking if one is to achieve a meaningful and accurate output. Nevertheless, as shown here, this matter requires further investigation in the coming years.

2.7 SCIENTIFIC FRAMEWORK

This chapter aims to provide insight into and summarize the state of the art in terms of the modelling, design, construction, and maintenance research for slab track systems. A literature review was undertaken to provide a scientific basis as support for the thesis goals. The following remarks are considered important for future research:

- The design and construction requirements follow a trend of fewer construction steps towards automation, making construction faster, simpler, and cheaper. Another important feature of the slab track of the future is modularity, which leads to standardized systems. They can be easily upgraded by plug & play design modules according to the corridor necessities over time or the emergence of newer technology;
- Slab track systems must be resilient with rapid recovery to **natural hazards**. Heavy

rainfall, persistent drought (dry and wet cycles), and extreme low and high temperatures coupled with long-term dynamic loading all lead to performance issues in the form of excessive settlements, slab cracks, and large voids under the slab. The thermo-hydro-mechanical behaviour of the soil is very important in evaluating long-term settlements, revealing the need for future researchers to focus on the soil-water characteristics and water movement under extreme weather conditions;

- Regardless of the installation precision, potential **settling soil** is currently a major challenge for slab track operation. If the settlement exceeds the adjustment capacity of the fastening system, additional adjustment levels would be desired features of a future slab track design; these would include modularity and fast recovery. Today, prefabricated slab tracks come with an intermediate mortar layer for post-construction adjustments;
- **Modelling techniques** are fundamental for assessing the most influential variables that affect the structural performance of slab tracks, particularly the dynamic and long-term behaviour. Currently, the main gap in the track modelling literature is related to research on fatigue analysis over a determined life period;
- New designs of slab tracks should be examined in extensive **life cycle cost assessment** studies, using RAMS methodology, in order to compare and assess system performance. However, the complexity of the sub-systems and the relations among them, together with the lack of available data for slab tracks, have restricted the number of published works.

Enhanced dynamic performance, low-risk vulnerability, rapid recovery, low construction, and maintenance costs are coveted features for slab tracks that will be the focus of research for future designs.

3 DEVELOPMENT OF SHORT-TERM DYNAMIC AND NONLINEAR SUB-MODELS: DL-TRACK AND SP-TRACK

3.1 INTRODUCTION

This chapter is dedicated to the design, development, and calibration of two sub-models: a 3D FE train/track interaction model by using numerical reducing techniques to achieve faster calculation times and a 3D nonlinear finite element model that receives the train/track response of the DL-Track (Figure 3.1). These two sub-models are developed to work independently as well as to cooperate interactively (this topic is explained in Chapter 4).

In Chapter 2, several numerical models were presented. Each model fits a particular purpose, which shaped its development and architecture. The most used modelling methodology to study the vibratory and deterioration behaviour of the railway track is the finite element method. This is going to be the methodology of choice for both models.

Taking into consideration the proposed goals of the thesis, the DL-Track (dynamic & linear) envisages a fast-computation dynamic numerical model that is required to encompass the train/track interaction with an increasingly deteriorated track. Thus, a linear material behaviour modelling is adopted to allow the use of numerical reduction techniques. At first glance, a linear approach of the track-soil system could be oversimplified to elements as in the typically nonlinear behaviour in ballasted tracks, mainly in the ballast layer and sleeper/ ballast contact (Varandas, 2013). Nonetheless, the main purpose of the DL-Track model is dedicated to slab track systems, in which the train/track interaction is less influenced by sleeper contact and soil nonlinear response. On the one hand, soil quality requirements are significantly higher in slab

track systems (Lichtberger, 2005) and on the other hand, the construction quality of CSL and HBL are less prone to uncertainty related to material properties and the higher stiffness leads to low soil stresses on the top of the platform. Hence, the linear material modelling could deliver realistically accurate results with a lower computational cost. The implementation of a more detailed and sophisticated nonlinear model would possibly require a large dataset of nonlinear properties that are not easy to reliably obtain and therefore the trade-off between the precision of the results and the higher computational cost could be counterproductive.

Regarding the second model, the full purpose of the SP-Track (static & plastic) is to narrow the precision of stress and damage calculation that could easily be overlooked by the DL-Track. This approach is fundamental for the proposed goals and this subdivision can enrich the knowledge of track deterioration subjected to train and weather loads. Additionally, one of the main features of the SP-Track is the ability to start the simulation with a pre-defined structural condition that provides insights on how the slab track system responds to train and temperature loads during the lifespan of the track. The SP-Track is the resuming work developed by Matias (2014), therefore a proof of concept or an intermodal validation is not presented in this chapter.

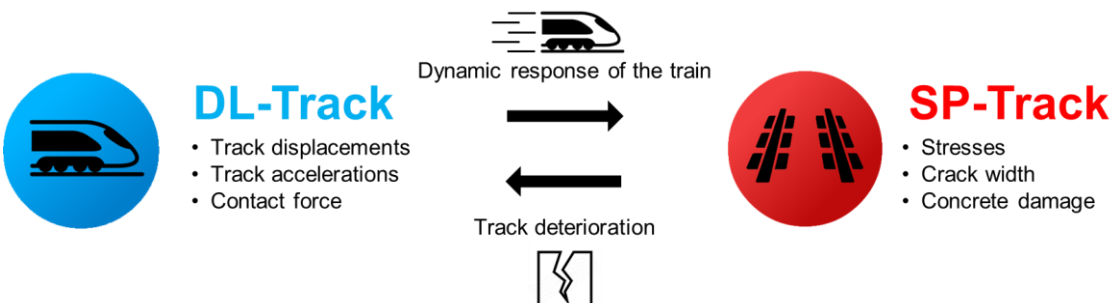


Figure 3.1: Interaction between DL-Track and SP-Track sub-models

Both numerical models will be developed in an ANSYS/APDL environment since this is a powerful FEM software with a high level of parametrization and is widely flexible and reliable to study most dynamic and structural engineering problems, thus being the preferred choice for railway modelling. The already vast library of built-in modules and the inherent platform stability acquired over years of development and improvement enable nonlinear and dynamic analysis, otherwise, time and effort consuming.

3.2 DYNAMIC TRAIN/TRACK INTERACTION: DL-TRACK

The following section describes the adopted track and vehicle modelling strategy, to comply with the goal of a fast computation of slab track long-term performance. As a starting point, the herein developed numerical model is represented by a ballasted track configuration due to the higher availability of literature for comparison and validation. Special emphasis is going to be applied to the development of the substructuring technique. The modelling process and architecture is mainly concerned with the slab track behaviour in the long run by trying to address the problem of track response subjected to rail geometry deterioration.

3.2.1 TRACK AND VEHICLE MODELLING

The 3D model of the track entails the common railway elements of a ballasted track, usually composed of a rail, fastening system, sleeper, ballast, subballast and platform underlayers.

The rail-railpad frame is modelled as a beam-spring-damper system, with the rail being modelled as a two-noded Timoshenko beam that uses thick beam theory (Timoshenko, 1926) that includes shear deformation, and in each node, there are six degrees of freedom (three translations and three rotations). An Euler –Bernoulli theory could also be used, but this element has a larger spectrum of applications, hence it is usually used for rail beam modelling. The simplified rail section is a typical I-shaped UIC60 rail with an equivalent z-axis inertia, flange width, and rail height to the real rail profile, to allow the proper modelling of rail bending phenomena. The 2D rail elements are provided with cross sections that feature integration areas, position derivative functions, etc., that are automatically associated with several section points. Each section is a set of nine nodes with four integration points (Figure 3.2).

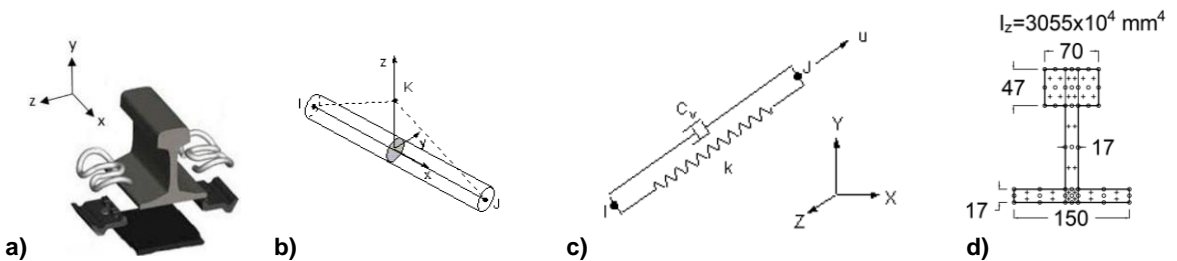


Figure 3.2: Rail/ railpad modelling in the DL-Track. Rail and railpad (a), 3D Timoshenko beam (b), spring-damper element (c) and integration points for the Timoshenko beam cross section

The railpad is modelled as a 2-noded spring-damper element with uniaxial tensile-compression, 3 degrees of freedom (three translations), and no bending effects considered. Also, the spring element has an intentionally higher height (15 cm) to avoid numerical problems. The remaining elements (sleeper, superstructure, and infrastructure layers) are modelled as 8-noded prismatic solid elements with 3 degrees of freedom per node (3 translations). The material behaviour is elastic isotropic mainly characterized by the Young modulus, Poisson ratio, mass density, and damping factor. Furthermore, in materials with isotropic behaviour, wave propagation can be decomposed in longitudinal compression waves (c_p) and transversal shear waves (c_s), the latter being the most constraining for soil design. The wave speed and propagation can be a limiting factor for soil mesh size, since an accurate wave propagation modelling requires a mesh size no longer than 1/6 of the shear waves wavelength, as represented by the following expression:

$$el_j \leq \frac{1}{6} \min_{j \in layers} \left(\frac{c_s^j}{f_{max}} \right) = \frac{1}{6} \min_{j \in layers} \left(\sqrt{\frac{G_j}{\rho_j}} \cdot \frac{1}{f_{max}} \right) \quad (3.1)$$

Where G_j and ρ_j are the shear modulus and elastic density of the soil layer j . The variable f_{max} is the maximum range of frequency to be used for the DL-Track, which is by default 100Hz.

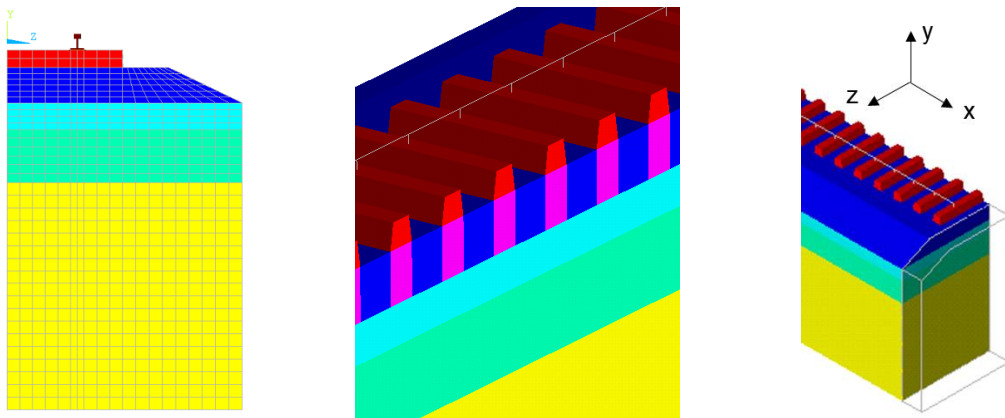


Figure 3.3: DL-Track element modelling (left and centre) and damping slice (right)

Concerning the boundary conditions, the movements out of the frontier plans are constrained ($u_x = 0$ for $x = -L_x$ & $x = L_x$, $u_y = 0$ for $y = -L_y$ and $u_z = 0$ for $z = L_z$) and since transversal loads are not intended as a study subject, a symmetry simplification is adopted to reduce the size of the numerical simulations ($u_z = 0$ & $\theta_x = 0$ for $z = 0$).

At both longitudinal ends of the model, there is a track “slice” composed of one lengthwise sleeper (Figure 3.3) with a significant high damping factor to act as a dampener for outgoing track vibrations. Previous versions of the DL-Track that lacked these “slices” would produce resonance effects on track accelerations on reflecting waves at the model boundaries. Every variant of the model undergoes a mesh and domain size analysis to achieve an efficient trade-off between result accuracy and computational cost.

The vehicle model is a vital element in the DL-Track model. It is represented by a single bogie with two axles or, in some cases, a set of bogies, since if bogies are too close and the second wheel may have an influence on track accelerations when combined with the first wheel.

The vehicle model is represented as a set of 2D mass-spring-damper FEM elements connected by a beam element (bogie) that represents the axle, primary and secondary suspensions, and a carbox. Figure 3.4 illustrates the vehicle and the main variables.

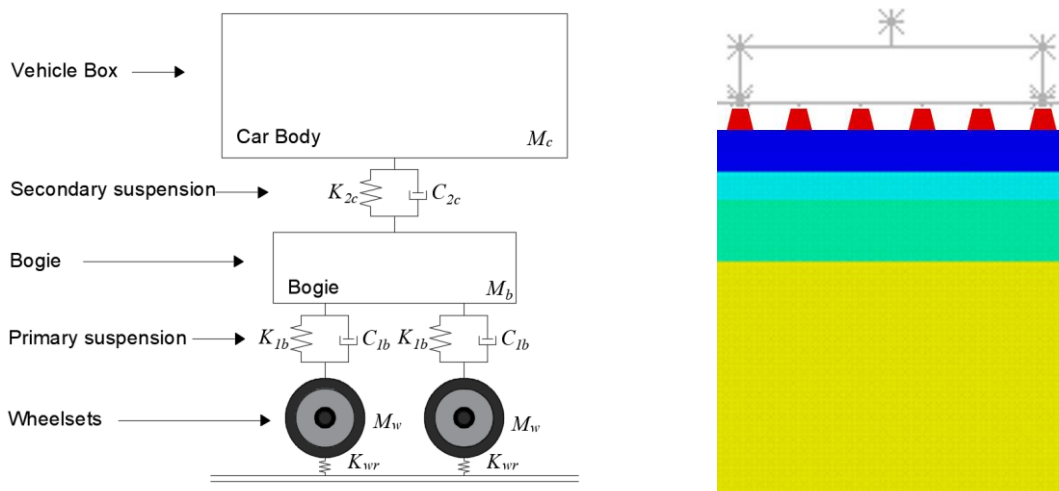


Figure 3.4: Vehicle representation (left) and DL-Track vehicle model (right)

The model scheme can represent most of the high speed trains that circulate in Europe (Thalys, TGV, ICE, AVE, etc.) and Asia (CHR3, N700 Shinkansen series, etc.), but also freight trains locomotives and wagons. In Table 3.1 and Figure 3.5, the modelling properties of high-speed and freight trains used in this thesis are presented.

Table 3.1: Vehicle properties of common high-speed and freight trains (P. A. Ferreira, 2010; Goicolea, 2014; He et al., 2018; Lei, 2017)

Item	ID	TGV	ICE	CRH3	Freight	Units
Wheelsets mass	M_w	1024	900	1200	1580	[kg]
Stiffness of primary suspension	K_{lb}	1.23×10^6	1.2×10^6	2.08×10^6	1.3×10^6	[N/m]
Damping coefficient of primary suspension	C_{lb}	1.0×10^4	1.0×10^4	1.0×10^5	2.2×10^4	[N.s/m]
Stiffness of secondary suspension	K_{lc}	1.23×10^6	0.35×10^6	0.8×10^6	0.69×10^6	[N/m]
Damping coefficient of secondary suspension	C_{2b}	2.0×10^4	2.0×10^4	1.2×10^5	3.7×10^4	[N.s/m]
Mass of half bogie	M_b	1191	1400	1600	1191	[kg]
Rotational inertia of half bogie	I_b	1344	6800	6800	1344	[m ⁴]
Mass of quarter carbox	M_c	1.36×10^4	1×10^4	1×10^4	2.12×10^4	[kg]
Bogie cross section area	A_b	7.7×10^{-3}	7.7×10^{-3}	7.7×10^{-3}	7.7×10^{-3}	[m ²]
Axle spacing	l_w	3	2.5	2.5	2	[m]
Bogie spacing	l_b	4.8	5	5	3	[m]
Number of bogies	n_b	20	16	16	22	[\cdot]

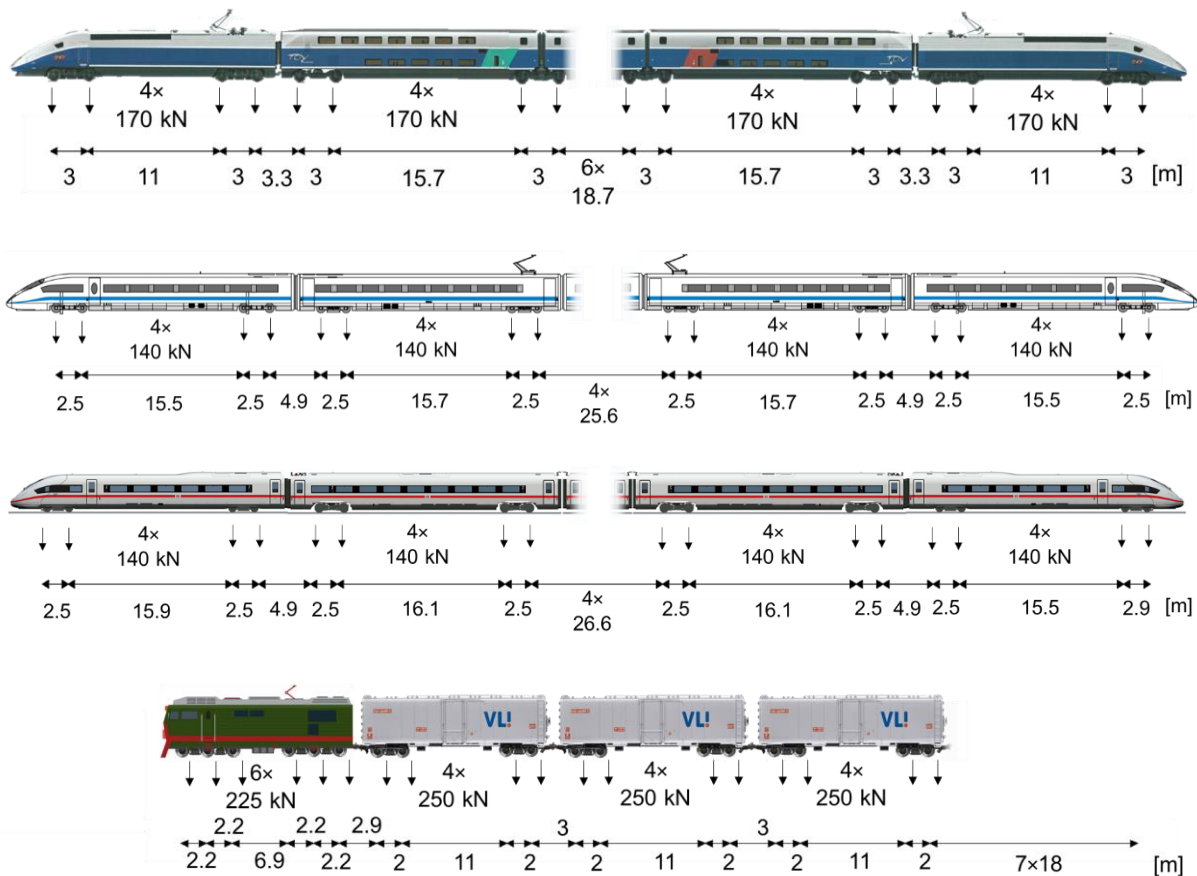


Figure 3.5: Axle load distribution of the (from top to bottom) TGV Réseau US, CHR3, ICE3 Velaro and a common freight train

Aside from the physical properties of the elements (masses, suspensions, and geometry), certain modelling features are included as input, notably the train circulation velocity (V) (m/s), the starting (x_i) and ending point (x_f) to avoid the influence of boundary conditions and speed up the steady-state regime and a time step variable. This time step variable has an important effect on the contact force calculation during the simulation. In Figure 3.6, it can be verified that the smaller the time step, the lower the contact variation, and the smoother the dynamic calculation are. The time step here adopted was carefully studied to monitor the trade-off between dynamic results accuracy and computational cost, as previously presented. A time step lower than $\frac{1}{20f_{max}} \approx 0.0005$ s is desired in order not to miss dynamic interaction content for the relevant frequency.

Additionally, the train passage calculation has two main phases: in the first one, the vehicle is “dropped” onto the track to preload the suspensions, and the rail track is defined by a drop time t_{drop} (s) before the second phase, which is running time of the train, usually around 0.1 s. This preliminary loading by the gravity of the track, before the dynamic simulations, helps to achieve a faster and smoother stabilization of the rail contact force without compromising computational time (Figure 3.7).

The vehicle suspensions, as the railpad, follow a simple modelling strategy that uses a Kelvin-Voigt model, which is unreliable for high speed frequencies (loss factor tends to infinite). Nevertheless, the scope of this thesis is for frequencies below 200 Hz, which is considered low frequency. The same is valid for the interaction model between the vehicle and the track, which adopts an overall simple structure instead of more complex models, such as multibody system dynamics. Yet for track response, this simple model can achieve a satisfactory level of reliability.

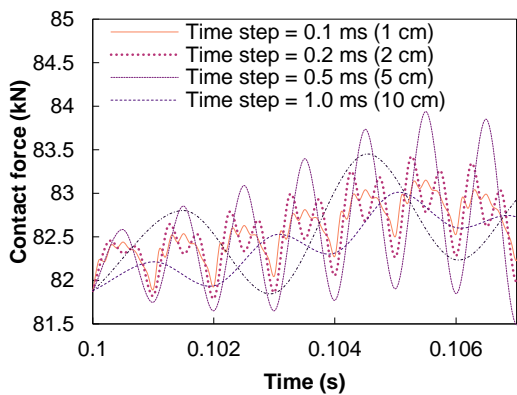


Figure 3.6: Influence of the time step in the wheel/ rail contact force

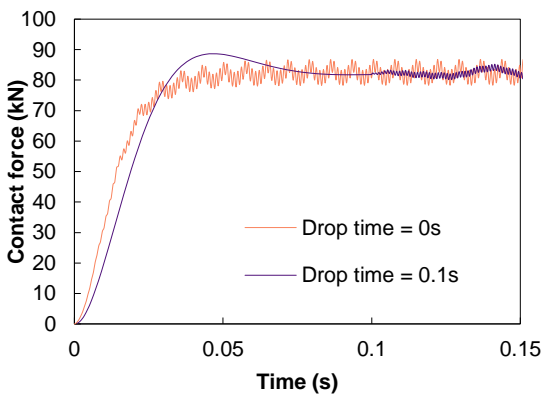


Figure 3.7: Influence of the drop time in the wheel/ rail contact force

Moreover, the contact between the wheel and the rail is modelled as a spring using the Hertzian theory, with the assumed hypotheses of non-deformable wheels and perfect paraboloid contact surface. Contact between rail and wheel is highly nonlinear since higher forces cause a higher surface area, and therefore a stiffer contact spring. With these assumptions, the contact force F_c can be related to the spring deflection δ_c as:

$$F_c = \begin{cases} C_H \cdot \delta_c^{\frac{3}{2}}, & \text{if } \delta_c > 0 \\ 0, & \text{otherwise} \end{cases} \quad (3.2)$$

$$C_H = \frac{2}{3} \cdot \frac{E}{1 - \nu^2} \cdot \sqrt{\left(\frac{1}{r}\right)^3 \cdot \frac{1}{A + B}} \quad (3.3)$$

Where C_H is the Hertzian constant that can be calculated through the mechanical properties of the contact (Young modulus E and Poisson ratio ν), surface curvatures (A and B), and equivalent radius of curvature r . For common rail-wheel contact, A , B , and r are 1.08 m^{-1} , 1.66 m^{-1} , and 0.986 , respectively (Thompson et al., 2003), which results in a Hertzian constant $C_H = 92.1 \text{ GN/m}^{3/2}$. To simplify the contact stiffness, a linear stiffness with a value of $k_c = 1.3 \text{ GN/m}$ can be assumed for the 60-120 kN range, as observed in Figure 3.8.

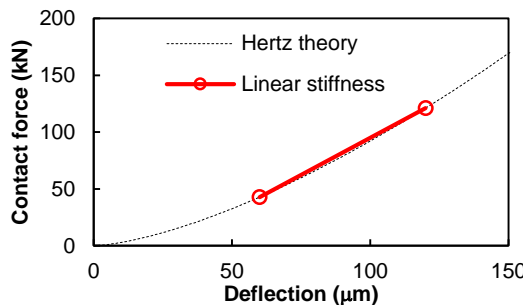


Figure 3.8: Nonlinear contact force and linearization for the 60-120 kN range

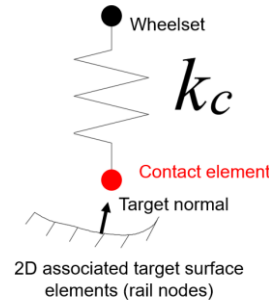


Figure 3.9: Wheel/ rail contact modelling

According to Thompson et al. (2003), linear contact stiffness values for wheel/ rail contact vary from 1.0 to 1.5 GN/m, and, the higher the value, the more rigid the contact between the rail and wheel, which leads to high contact forces and, thus, more wheel/ rail wear. Said that, for the proposed track deterioration phenomena that this model is intended to aid, higher contact stiffness results in higher contact forces, and therefore a more conservative approach; nevertheless, it has more numerical issues regarding convergence. On the other hand, lower contact stiffness does not present numerical issues, but it can filter out track defects that are important for the long-term soil permanent deformation, thence the adoption of an intermediate value (1.3 GN/m).

In addition, this contact spring has an augmented Lagrangian method contact algorithm that calculates the actual forces on the spring when the contact elements penetrate the target elements (rail nodes that created a target surface) as illustrated in Figure 3.9. The contact is frictionless and enables studying the loss of contact by the rail vehicle when circulating on the track with heterogeneities.

3.2.2 SUBSTRUCTURING FORMULATION

A commonly used approach to overcome large domain models, as in the case of railway tracks, is the substructuring procedure, which compresses several elements into a group called “superelement”. The substructuring analysis uses a matrix reduction technique to decrease the system’s matrices into smaller reduced matrices, and consequently lower the degrees of freedom.

Recently, P. Ferreira (2010) and Arlaud (2017) used this periodic substructuring approach in railway engineering for ballasted tracks.

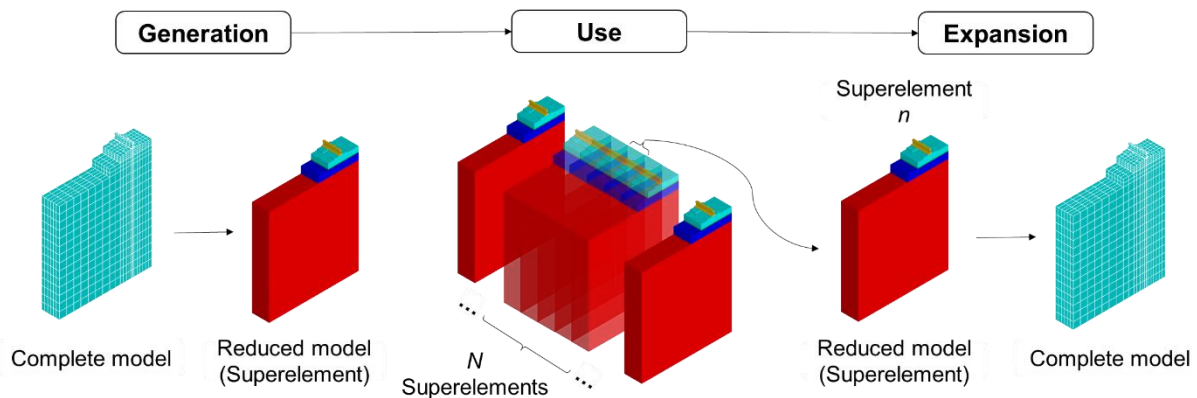


Figure 3.10: Substructuring phases: generation, use and expansion

Two possible approaches are possible with this technique. The most common method is the bottom-up substructuring, in which each element is created individually and compatible in the use phase. In a top-down approach, the entire model is built, and the superelements are created thereafter. Both strategies have advantages and disadvantages according to the number of repetitions and the size of the model. Bottom-up approaches are more suitable for smaller models and the superelement can be easily assembled by replication along the track. The substructuring method can be divided into three distinct phases: generation, use, and expansion (Figure 3.10).

The first phase is the generation of the superelement through the grouping of previously meshed elements of a track slice, as explained in the previous subchapter, using 3D FEM techniques. The rail and the railpad are excluded from the generation phase, and only sleeper downward elements are generated.

After the slice modelling and meshing, the substructuring analysis is performed by selecting master nodes of freedom (leaving the remaining as slave degrees of freedom), usually on interface nodes with other superelements or elements, and loads/ constraints are applied (Figure 3.11). Mathematically speaking, the equations are divided into two groups, the master (m) and the inherent slave (s) DOF's.

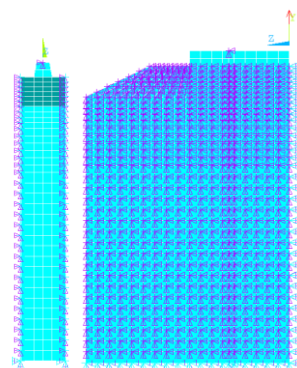


Figure 3.11: Superelement and master nodes

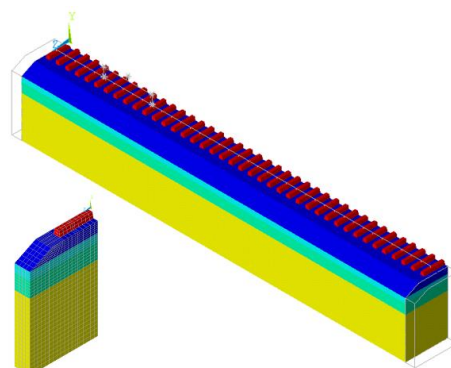


Figure 3.12: Superelement assembly

With this in mind, the time integration scheme for linear systems can be expressed as:

$$[M]\{\ddot{u}\} + [C]\{\dot{u}\} + [K]\{u\} = \{F\} \quad (3.4)$$

In which the $[M]$, $[C]$, and $[K]$ are the mass, damping, and stiffness matrices, and $\{\ddot{u}\}$, $\{\dot{u}\}$, $\{u\}$, and $\{F\}$ are accelerations, velocities, displacements, and external forces, respectively. With a substructuring approach, the equation is simply transformed into:

$$[\hat{M}]\{\ddot{\hat{u}}\} + [\hat{C}]\{\dot{\hat{u}}\} + [\hat{K}]\{\hat{u}\} = \{\hat{F}\} \quad (3.5)$$

Then the structural stiffness matrix $[\hat{K}]$ for the reduced superelement, takes the form:

$$\begin{bmatrix} K_{mm} & K_{ms} \\ K_{sm} & k_{ss} \end{bmatrix} \begin{bmatrix} u_m \\ u_s \end{bmatrix} = \begin{bmatrix} F_m \\ F_s \end{bmatrix} \quad (3.6)$$

By expanding 3.5, the two following equations are obtained:

$$[K_{mm}]\{u_m\} + [K_{ms}]\{u_s\} = \{F_m\} \quad (3.7)$$

$$[K_{sm}]\{u_m\} + [K_{ss}]\{u_s\} = \{F_s\} \quad (3.8)$$

Solving equation 3.6 for u_s :

$$\{u_s\} = [K_{ss}]^{-1}\{F_s\} - [K_{ss}]^{-1}[K_{sm}]\{u_m\} \quad (3.9)$$

By substituting $\{u_s\}$ in equation 3.6, the new equation can be expressed as:

$$[[K_{mm}] - [K_{ms}][K_{ss}]^{-1}[K_{sm}]]\{u_m\} = \{F_m\} - [K_{sm}][K_{ss}]^{-1}\{F_s\} \quad (3.10)$$

Which can be translated to:

$$[\hat{K}]\{\hat{u}\} = \{\hat{F}\} \quad (3.11)$$

Matrices $[\hat{K}]$ and $\{\hat{F}\}$ are the superelement component (e.g. stiffness, mass, damping, etc.) and the load vector. The whole process is similar to reducing the nodal displacement:

$$\{u\} = \begin{Bmatrix} \{u_m\} \\ \{u_s\} \end{Bmatrix} [T] \{\hat{u}\} \quad (3.12)$$

$[T]$ is the transformation matrix, which is also known as static constraint nodes (Craig & Bampton, 1968) and can be expressed as:

$$[T] = \begin{bmatrix} [I] \\ [G_{sm}] \end{bmatrix} \quad (3.13)$$

Where $[I]$ is the identity matrix, and $[G_{sm}]$ is a redundant static constraints mode. It follows:

$$[G_{sm}] = -[K_{ss}]^{-1}[K_{sm}] \quad (3.14)$$

With this in mind, the reduced stiffness matrix and the reduced load vector take the form:

$$[\hat{K}] = [T]^T[K][T] \quad (3.15) \qquad \qquad \qquad \{\hat{F}\} = [T]^T\{F\} \quad (3.16)$$

In this mathematical development, the load vector for the superelement can be subdivided in any existing independent load vector, which may be scaled in the use phase. Expanding 3.1:

$$\{F_m\} = \sum_{i=1}^N \{F_{mi}\} \quad (3.17) \quad \{\mathbf{F}_s\} = \sum_{i=1}^N \{\mathbf{F}_{si}\} \quad (3.18)$$

N is the independent load vector, and by substituting these equations in 3.16:

$$\{\hat{F}\} = \sum_{i=1}^N \{F_{mi}\} - [K_{ms}][K_{ss}]^{-1} \sum_{i=1}^N \{F_{si}\} \quad (3.19)$$

In order to have independently scaled vectors in the use pass, the left-hand side of the equation 3.19 must be expanded:

$$\{\hat{F}\} = \sum_{i=1}^N \{\hat{F}_i\} \quad (3.20)$$

Substituting 3.20 in 3.19:

$$\{\hat{F}_i\} = \{F_{mi}\} - [K_{ms}][K_{ss}]^{-1}\{F_{si}\} \quad (3.21)$$

If the load vector is scaled in the use phase, $\{\hat{F}\}$ is expressed as:

$$\{\hat{F}\} = \sum_{i=1}^N b_i \{\hat{F}_i\} \quad (3.22)$$

Where b_i is the scaling factor, and therefore equation 3.9 takes the form:

$$\{u_s\} = [K_{ss}]^{-1} \sum_{i=1}^N b_i \{\hat{F}_i\} - [K_{ss}]^{-1} [K_{sm}] \{u_m\} \quad (3.23)$$

Equation 3.23 is used in the expansion phase to obtain all the model DOF's values. Said that, $\{u_s\}$ are calculated as the internally prescribed displacement boundaries, since $\{u_m\}$ are known in the expansion phase.

Similarly, the computation of the reduced mass matrix $[\hat{M}]$ is described by Guyan (1965) as:

$$[\hat{M}] = [M_{mm}] + [M_{ms}][G_{sm}] + [G_{ms}]([M_{sm}] + [M_{ss}][G_{sm}]) \quad (3.24)$$

Where $[G_{ms}] = [G_{sm}]^T$. The damping matrix is likewise calculated as:

$$[\hat{C}] = [C_{mm}] + [C_{ms}][C_{sm}] + [C_{ms}]([C_{sm}] + [C_{ss}][C_{sm}]) \quad (3.25)$$

This matrix reduction technique (used in the modelling of the sleepers and subjacent layers) can achieve an outstanding reduction in computation times. A full 60-meter railway track with 0.25 million nodes after the generation phase is transformed into a superelement assembly of just 35 thousand nodes (Figure 3.12). The reduction in the number of DOF plays a key role in having a fast computation calculation and is an essential feature for multiple runs to emulate the long-term behaviour of the railway track.

3.2.3 MODEL ASSEMBLY AND CALCULATION PHASE

After having generated a superelement with all the required dynamic information gathered, it

can be replicated along the track length to a determined number of N track slices that comprise the full length of the track, as illustrated in Figure 3.13.

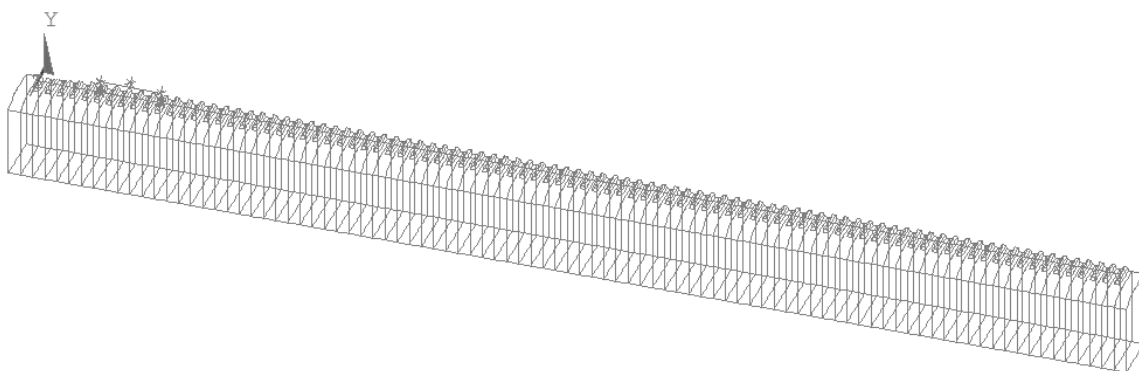


Figure 3.13: Representation of track “slices”

The global model is comprised of a series of (possibly different) superelements that are periodically repeated. The assembly of the track can be divided into the following phases:

- 1. 3D modelling and generation of the track slice**

As previously stated, the reduction technique is selected and the slice model (sleeper, ballast/ CSL, subballast/HBL, and platform layers) is generated with every relevant mechanical property characterized, and boundary conditions defined. Different superelements can be generated to simulate longitudinally heterogeneous tracks (e.g. transitions, soft soil sections, culverts, etc.), but in most cases, the additionally created superelements are the damping slices at both ends of the assembled model. After all model properties are defined (material properties, geometry, boundary conditions, etc.), the superelement is created by the substructuring analysis through a full Newton-Raphson and the transform matrix $[T]$ is calculated.

- 2. Use phase and model assembly**

In this phase, all the superelements are inserted in the global track model, where static and kinematic inter-slice conditions should be admissible. Rail, railpad, and vehicle are modelled separately, and coupled to the already implemented group of superelements, again with static and cinematic continuity.

- 3. Model calculation**

With the complete model assembled, the calculation phase is proceeded by calculating the dynamic equation 3.4 of the global track. In each matrix, the reduced and full elements are included and assembled in the computation. Then the implicit Newmark integration scheme is used to solve the differential equations.

The expansion phase is not used in the simulation since key sensor master nodes are priorly selected to make the cinematic DOF's for generation, which turns the model more time-efficient.

Additionally, on most dynamic models, the damping matrix $[C]$ can be obtained as a linear combination of stiffness and mass matrices (Chopra, 1995):

$$[C] = a_0[M] + a_1[K] \quad (3.26)$$

Where a_0 and a_1 are the Rayleigh damping constants, that can be calculated as:

$$a_0 = \xi_n \frac{2w_i w_j}{w_i + w_j} \quad (3.27) \qquad \qquad a_1 = \xi_n \frac{2}{w_i + w_j} \quad (3.28)$$

w_i and w_j are the left and right end of the frequency spectrum of interest for the dynamic simulation, which in the proposed model are 5 and 100 Hz, and the Rayleigh damping coefficient $\xi_n = 2\%$, that is a common value used for railway modelling literature (Chopra, 1995).

The main point of this substructuring approach is to reduce computation times and to test the efficiency of the trade-off between the generation phase time and the calculation use phase time. A 2D model was developed to assess the equilibrium and evaluate multiple comparisons regarding the trade-off (Figure 3.14). The 2D model is composed of an Euler-Bernoulli beam element for the rail, spring-damper elements for railpads and the remaining elements use 4-noded plain elements for solid structures in-plane stress. A detailed modelling procedure and calibration can be consulted in Matias (2014).

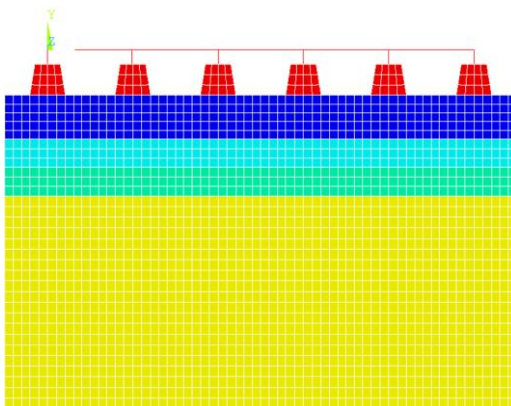


Figure 3.14: 2D model version for time efficiency assessment

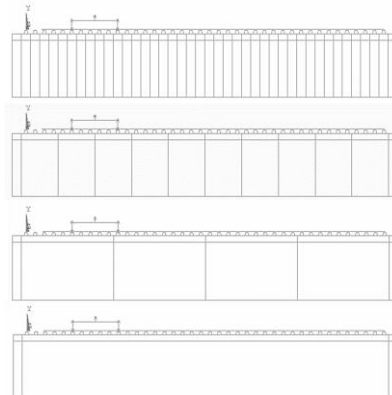


Figure 3.15: Different superelement sizes

Larger track slices (Figure 3.15) would consume more computational resources, yet they lead to a faster calculation in the use phase, which indicates a balance between the size of the track and calculation efficiency. In Figure 3.16, the generation and use phase calculation times can be observed, for a static response of a train over a 50 sleeper track. For this bi-dimensional model, a track slice between 5 and 10 sleepers is the most time-efficient for one single short-term calculation. Nonetheless, since multiple runs are envisaged, longer track slices become more advantageous, and, ultimately, an infinite number of repetitions would require the largest track slice possible for the available computer memory (Figure 3.17).

Compared to full models, the variation in computation time is astonishing, with an 80 m long track being calculated in 9h37m, while a reduced superelement was calculated in under 3

minutes. If a full 3D model with 80 m is used, the dynamic calculation would require a 150h simulation; meanwhile, a reduced model can achieve this under 15 min, with a 30-minute generation superelement file (almost 600 times faster) with a size over 6Gb. All of these computations were performed with an Intel Core i7-7700k CPU at 4.2 Ghz.

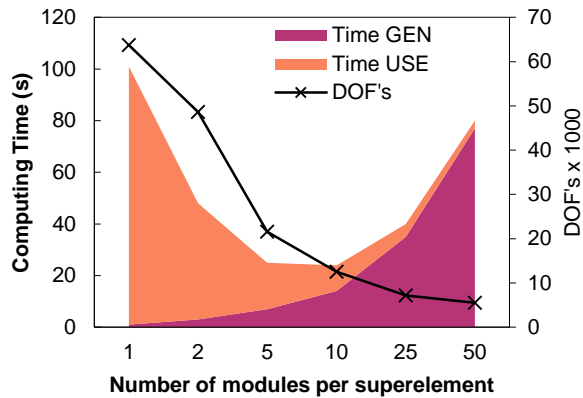


Figure 3.16: Relationship between the module size and the total computing time for a single iteration

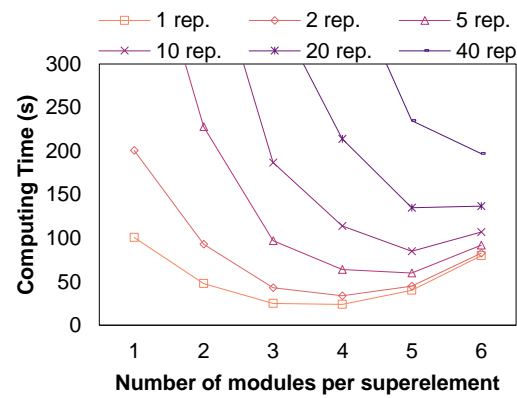


Figure 3.17: Relationship between the module size and the total computing time for multiple iterations

It should be noted that superelement DOF's equations take 3 to 4 times longer to be solved, due to the time taken accessing files, and could lead to a far longer time for the superelement to be solved if only a small reduction in DOF's is achieved.

3.2.4 INTERMODEL VALIDATION AND CALIBRATION

In what regards the reliability and correctness of the DL-Track model as a dynamic train/track interaction numerical tool, a comparison may be carried out with already validated numeric models, preferably models that also use matrix reduction techniques. The intermodel validation will be done by comparing the results of the Dynavoie model, developed by SD Tools at the request of the French railway administrator SNCF, and later improved and upgraded by Ferreira (2010) and Ferreira and López-Pita (2015).

The validation case is a ballasted track configuration present in the Track Box laboratory at CEDEX, Madrid, that intends to reproduce a section of the high speed line track between Madrid and Barcelona, in the Guadalajara site. The construction materials are transported from the actual track site (ballast, subballast, formlayer, and embankment), and rails, railpads, and sleepers were provided by the same manufacturer.

The Track Box was extensively instrumented with displacement transducers, extensometers, pressure cells, geophones, and accelerometers. Nevertheless, for the validation, only displacement transducers and accelerometers were used. The passage of trains was simulated through hydraulic actuators that apply phased loads on the rails with a maximum force of 250 kN, and at frequencies under 50 Hz.

Concerning the Dynavoie model, a similar approach was used as the DL-Track model, except for the use of solid elements for the rail and railpad. The remaining elements are modelled quite similar to equivalent boundary conditions (off plane movement restriction and damping slices). In both models, DL-Track and Dynavoie, only one track slice representing one sleeper distance (0.6 m) are used, and the vehicles are modelled similarly also.

The ballasted track typology is illustrated in Figure 3.18. The track grid uses UIC60 rails, 7mm thick railpads, and monoblock concrete prestressed B90.2 sleepers. The modelling properties are presented in Table 3.2. The geometrical data and material data were provided by CEDEX, which in turn were given by the manufacturers, or obtained with in situ geotechnical tests.

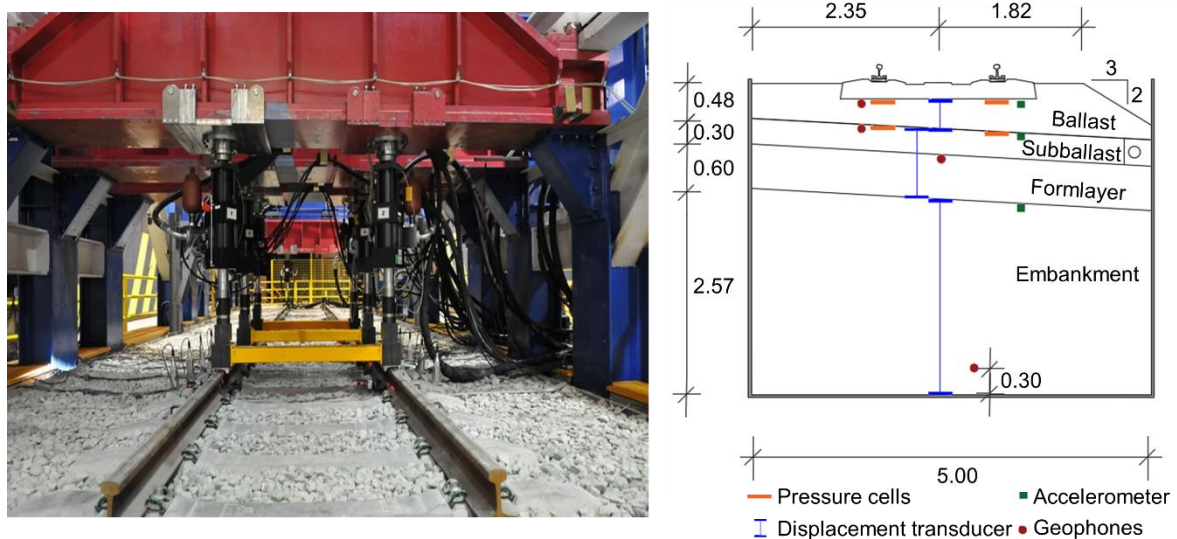


Figure 3.18: CEDEX track box experimental site (left) and ballasted case study cross section (right) (units in m)

Table 3.2: Mechanical properties of the CEDEX track box ballasted track

Element	Mechanical properties	Geometry
Rail	$E_r=200 \text{ GPa}$; $v_r=0.3$; $\rho_r=78.5 \text{ kN/m}^3$; $\xi_r=0.01$	UIC60
Railpad	$k_p=100 \text{ kN/mm}$; $c_p=60 \text{ kN}\cdot\text{s/m}$	-
Sleeper	$E_s=43 \text{ GPa}$; $v_s=0.2$; $\rho_s=25 \text{ kN/m}^3$; $\xi_s=0.05$	B90.2
Ballast	$E_b=230-400 \text{ MPa}$; $v_b=0.2$; $\rho_b=22 \text{ kN/m}^3$; $\xi_b=0.08$	$h_b=0.48 \text{ m}$
Ballast (consolidated)	$E_{bc}=230-400 \text{ MPa}$; $v_{bc}=0.2$; $\rho_{bc}=22 \text{ kN/m}^3$; $\xi_{bc}=0.08$	-
Subballast	$E_{sb}=170-440 \text{ MPa}$; $v_{sb}=0.3$; $\rho_{sb}=22 \text{ kN/m}^3$; $\xi_{sb}=0.01$	$h_{sb}=0.30 \text{ m}$
Formlayer	$E_{fr}=165-400 \text{ MPa}$; $v_{fr}=0.3$; $\rho_{fr}=21.5 \text{ kN/m}^3$; $\xi_{fr}=0.01$	$h_{fr}=0.60 \text{ m}$
Embankment	$E_{e1}=165-385 \text{ MPa}$; $v_{e1}=0.4$; $\rho_{e1}=20.2 \text{ kN/m}^3$; $\xi_{e1}=0.01$	$h_{e1}=2.57 \text{ m}$

Both the experimental and numerical results from the previously described Dynavoie model were used to validate the DL-Track model in a preliminary stage. The location of the data sensors is matched as close as possible to the experimental campaign in each model (Figure 3.19) and is mainly focused on track displacements and accelerations. For each model, a parametric analysis was performed in what regards the uncertainty related to mainly granular layers and their stiffness.

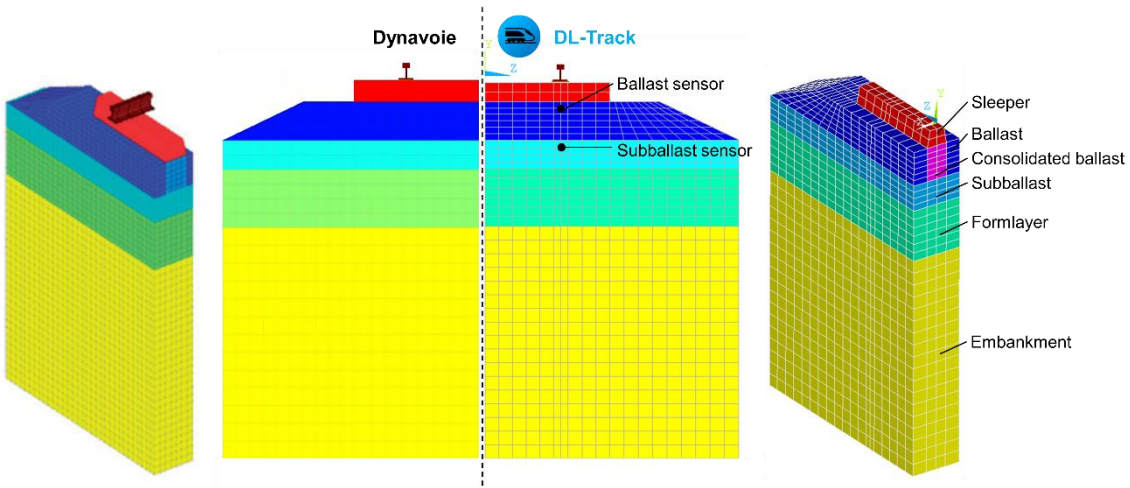


Figure 3.19: Dynavoie and DL-Track modelling representation of the ballasted track in the CEDEX Track box

A total of 12 bogie passages were simulated in the CEDEX Track Box, with the main focus on the 4-10 bogie, which excludes the locomotive wagons of a TGV Réseau vehicle running at a speed of 300 km/h.

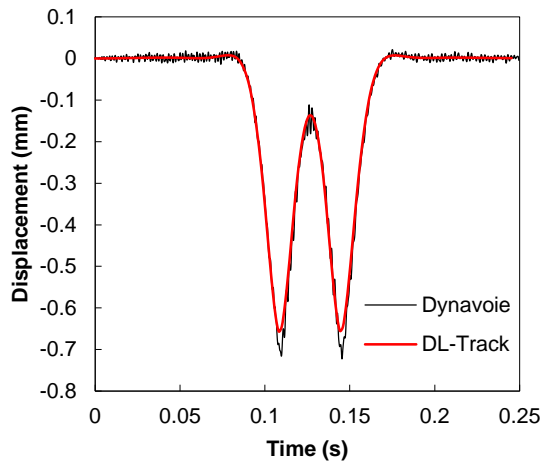


Figure 3.20: Rail displacements for the Track box ballasted track simulation at 300 km/h

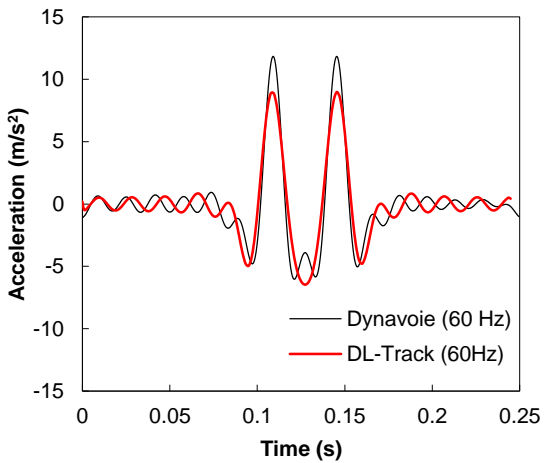


Figure 3.21: Rail acceleration for the Track box ballasted track simulation at 300 km/h

Figure 3.20 and Figure 3.21 show the vertical displacements and accelerations, respectively, on the rail for both DL-Track and Dynavoie. Track accelerations are filtered by a 60Hz low-pass filter. An apparent small difference between the two models can be justified by the use of different modelling strategies (3D elements for the rail and railpad for Dynavoie). For both cases (displacements and accelerations), the DL-Track slightly underestimates the track response when compared with Dynavoie; notwithstanding, rail modelling is not the main concern in any of the models.

From Figure 3.20, it is possible to notice that the frequency spectrum in the case of the DL-Track is less detailed than the Dynavoie. Furthermore, Figure 3.22 to 3.25 illustrate the comparison between DL-Track results, Dynavoie, and the experimental data for the CEDEX Track Box for

the track displacements and accelerations (with a low bandpass filter at 60 Hz for subballast and ballast).

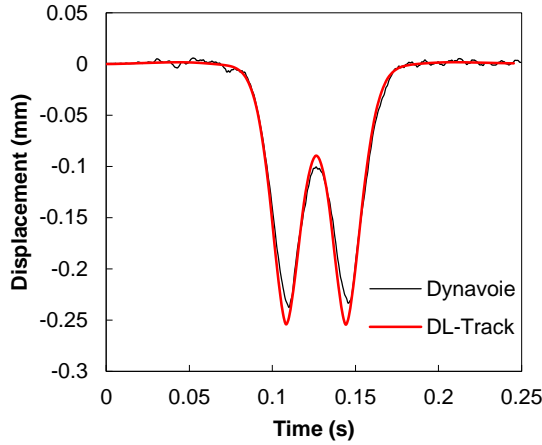


Figure 3.22: Ballast displacements for the Track box ballasted track simulation at 300 km/h

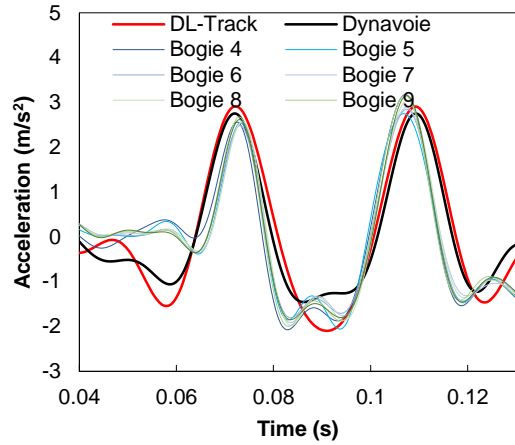


Figure 3.23: Ballast acceleration for the Track box ballasted track simulation at 300 km/h

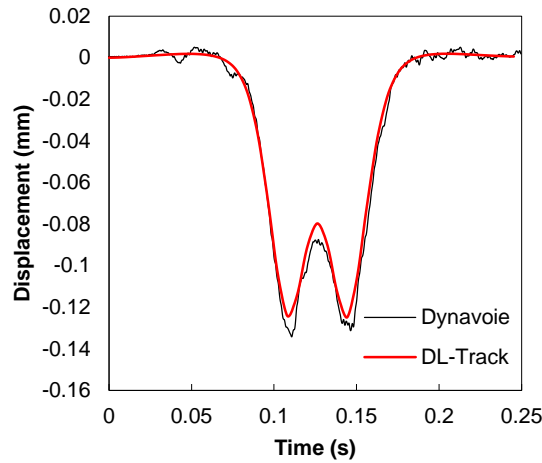


Figure 3.24: Subballast displacements for the Track box ballasted track simulation at 300 km/h

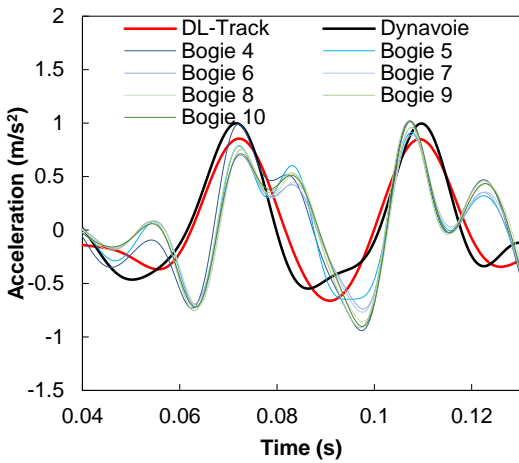


Figure 3.25: Subballast acceleration for the Track box ballasted track simulation at 300 km/h

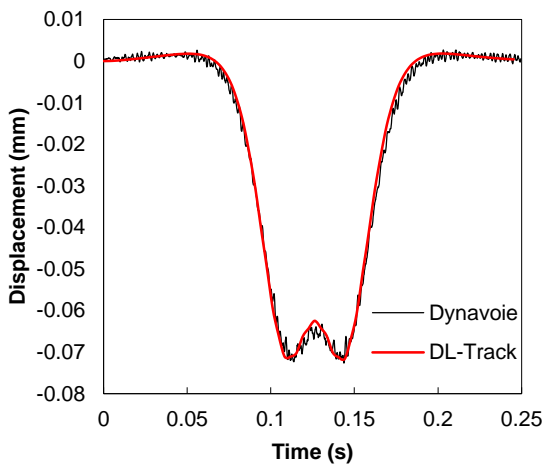


Figure 3.26: Embankment displacements for the Track box ballasted track simulation at 300 km/h

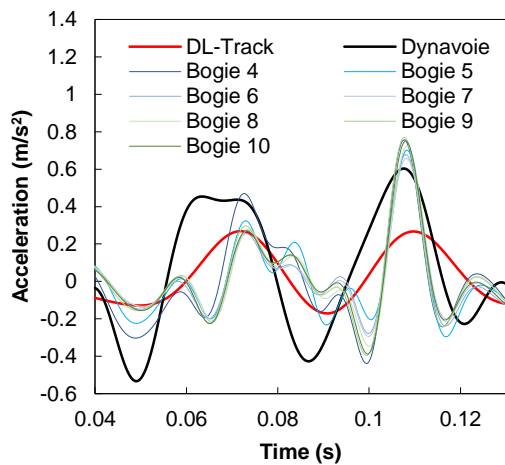


Figure 3.27: Embankment acceleration for the Track box ballasted track simulation at 300 km/h

As the main goal of the DL-Track is a fast but reliable track response for the main layers of the superstructure (ballast/ CSL and subballast/ HBL), a good correspondence with the results is desirable, and in Figure 3.22 to 3.26 a very good correlation may be noticed for the ballast acceleration and displacement. Acceleration amplitudes match with little deviation, and most model shape vibrations are present in both the DL-Track and Dynavoie. Subballast accelerations also present similar amplitudes to the Dynavoie and experimental data, yet some frequencies are not considered by the DL-Track, a deviation that increases in depth as shown in Figure 3.27. Further, a good correlation is observed in the track stiffness (track displacements).

These preliminary results are in good agreement with the intended goals of the DL-Track, which is mainly focused on the superstructure behaviour. Greater improvements may be implemented to enhance the model's reliability in predicting rail and substructure dynamic response, nevertheless, this would affect the computational efficiency, and, therefore, not be aligned with the thesis's goals regarding track damage.

3.2.5 COMPARISON BETWEEN REDUCED AND FULL 3D MODELS

An important test to verify the reliability of the substructuring technique is the comparison with the full 3D version, as well as different combinations of superelement modules, to gain confidence for reproducing the DL-Track for different conditions.

With this in mind, eight model variants of the DL-Track were conceived, where seven comprise alternative superelement sizes (1,2,4,5,10,20 and 40 sleepers), each of which was repeated to form a 40 sleeper track. The numerical data for the parametric analysis is presented in Table 3.3. The generation and calculation times grow almost linearly compared to the number of DOF's.

Table 3.3: Superelement module size and their performance during calculation

Superelement size	Number of module repetitions	DOF's (thousands)	Run time (hh:mm:ss)	Gen time (mm:ss)
1	40	24.4	00:34:08	00:01
2	20	13.2	00:18:34	00:03
4	10	7.6	00:10:58	00:05
5	8	6.5	00:09:30	00:06
10	4	4.3	00:06:02	00:15
20	2	3.17	00:04:05	00:33
40	1	2.7	00:03:20	01:15
Full model	-	332	06:35:56	-

As expected, the obtained results, in Figure 3.28 and 3.29, display almost no difference among the various versions with acceleration deviation under 0.08% and displacements under 0.18%, being this difference the result of numerical approximations during the calculation. Such findings foster the confidence to compress the track slice to the desired size to reach a particular goal since virtually no difference is obtained. In the following chapters, a track slice would be used at a certain number of sleepers to meet the model geometries and reduce the overall computational cost for the available running memory.

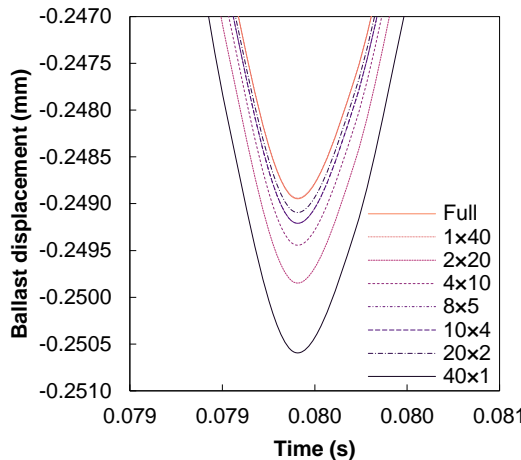


Figure 3.28: Ballast displacements for different superelement modules

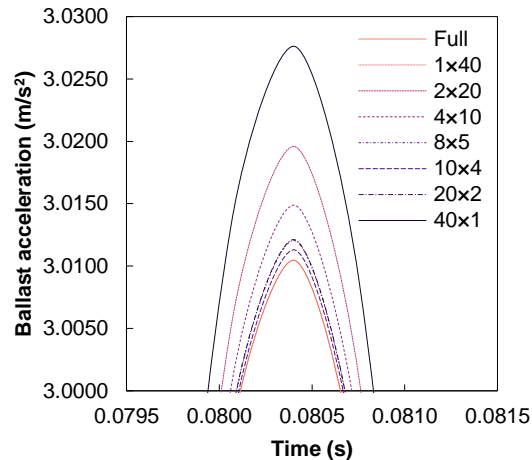


Figure 3.29: Ballast accelerations for different superelement modules

3.3 NONLINEAR CONCRETE BEHAVIOUR: SP-TRACK

The SP-Track is the nonlinear counterpart of the DL-Track. In this section, the modelling strategy of track deterioration and the update of track properties is presented. The main focus of this sub-model is dedicated to the calculation of the track stresses, particularly concrete and soil stresses, under train and temperature loads to be later used for deterioration calculation.

3.3.1 TRACK MODELLING

The track modelling employed in the SP-Track is at a smaller scale, reproducing the proper functioning of the slab track mechanics. This sub-model, unlike the macroscopic DL-Track model, is specialized for ballastless systems, as will be discussed in this subchapter. Most modelling choices are derived from the study performed by Matias (2014).

The rail-railpad system is modelled with eight-noded solid elements with 3 DOF in each node, with geometry as close as possible with the real track (taking in mind the mesh required for an adequate time computation). In the case of the rail, as explained previously, the flange width and the yy inertia are the priority variables to keep constant for an adequate load transmission to the lower elements in the track section in the first and most elastic level of the track (Figure 3.2). The railpad is also modelled with 3D solid elements, and thus the vertical stiffness of the railpad is recalculated with a specific elastic modulus, which takes into consideration the dimensions, and the Poisson effect on the overall vertical deformation. The railpad modulus of elasticity E_p can be calculated through the following expression:

$$E_p = K_p \cdot \frac{h}{l \cdot c} \cdot \frac{(1 + v) \cdot (1 - 2v)}{(1 + v)} \quad (3.29)$$

Where K_p is the vertical stiffness of the railpad, v is the Poisson coefficient and h , l , and c are the height, length, and width of the railpad, respectively. In order to avoid numerical problems

in the stiffness matrix due to slender elements ($h: b \geq 3$), as is the case of railpads, the height can be greater (and the elastic modulus artificially corrected).

All the remaining possible elements are modelled with the same 8-noded structural solid elements, excepting the concrete slab (CSL) that also uses the same element, but is capable of representing phenomena such as cracking in tension and crushing in compression (Figure 3.30 and 3.31). This feature enables load distribution after a strength threshold is reached, and the load stresses are more realistically redirected to other parts of the structure, hence a stiffness loss map can be created.

This element requires linear and multilinear properties. Besides the elastic properties (Young modulus, Poisson effect, and material's density) it uses a multilinear concrete constitutive relationship by the following expressions:

$$f_c = \frac{E_c \varepsilon}{1 + (\frac{\varepsilon}{\varepsilon_0})^2} \quad (3.30)$$

$$\varepsilon_0 = \frac{2f'_c}{E_c} \quad (3.31)$$

Where f_c is the (compressive) stress of concrete for a strain ε , and ε_0 is the ultimate concrete strain. The f - ε curve is for a commonly used concrete (C35/45 or any other concrete) in slab tracks, and is represented in Figure 3.30, in which: point 1 is defined as 30% of the ultimate stress, points 2,3 and 4 are calculated by 4.30 and 4.31 and point 5 represents the concrete's failure by compression. Typical material parameters to the William-Warnke yield criterion are the compressive (f_{cm}) and tensile (f_{ctm}) strength, and the shear coefficients for open (β_t) and closed cracks (β_c).

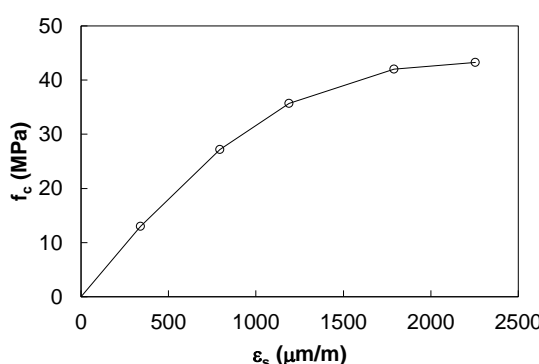


Figure 3.30: Multilinear behaviour of a C35/45 concrete for material modelling

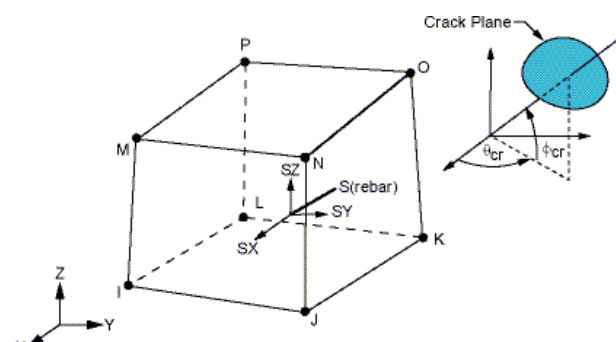


Figure 3.31: Eight-node structural element with cracking capabilities

These shear coefficients represent the roughness of the crack interface that varies from 0 (with no shear transmission) to 1 (full shear transmission). To avoid convergence problems, this shear coefficient should be higher than 0.4. Nevertheless, this value does not have a major influence on the final results in what concerns track displacement and stress distributions.

Although possible to be accounted for, creep effects of the concrete are not considered for this simulation in order to avoid further unnecessary complexity in the model.

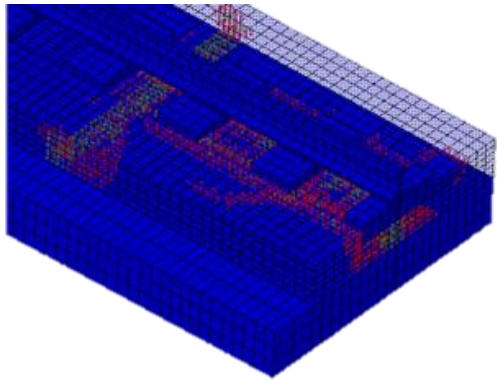


Figure 3.32: Crack modelling on the SP-Track due to train loads on uneven soil support

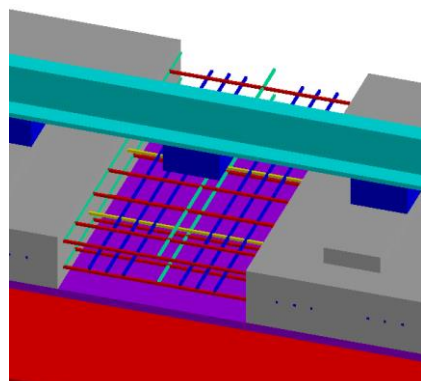


Figure 3.33: Reinforcement modelling on the slab track including longitudinal rebars, stirrups, and prestressed tendons

Another important element in the SP-Track model is the detailed reinforcement scheme that is critical to estimate the tensile stress of the reinforcement, and, therefore, perform an indirect calculation of the crack width (Figure 3.32 and 3.33). The reinforcement rebars use the bilinear elastoplastic model that yields at the steel strength stress with a hardening modulus $E_s' = 0.01 \cdot E_s$, in which E_s is the steel Young modulus. This hardening modulus smooths the nonlinear numerical integration when the tensile strength is reached, and avoid convergence problems.

At last, another prominent feature present in the SP-Track model is the incorporation of contact elements between the CSL and HBL to enables the slab warping due to temperature differentials and uniform temperature (Figure 3.34). Also, contact elements, similarly to the wheel/ rail contact, are contact (slab) – target (HBL) surfaces that enable the slab to warp and slide over the HBL, otherwise constraint stresses would occur in the slab and HBL. This feature also allows evaluating peak corner stresses more accurately.

The contact algorithm used is a Lagrangian augmented method with a frictionless surface, to keep the model simple. Finally, since SP-Track is intended for nonlinear analysis, in each step the stiffness matrix is updated according to the contact development. This is due to the fact that, in most real-life cases, the load magnitude does not reach the concrete's, nor the reinforcement's, yield thresholds. This would only occur under specific extreme scenarios for which the modified Newton-Raphson algorithm is a more efficient choice, as it does not mandatorily update the stiffness matrix in each substep.

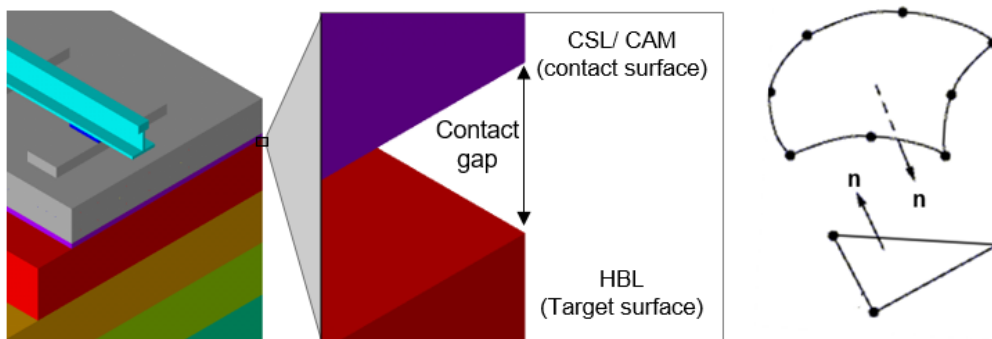


Figure 3.34: Contact modelling between layers for SP-Track

3.3.2 LOAD MODELLING: TRANSIENT TRAIN LOADS AND TEMPERATURE VARIATIONS

The inclusion of a full dynamic train/track interaction in the SP-Track model would result in unaffordable computational costs due to the material nonlinearity and train speed step in the time integration scheme. To overcome this issue, the train/track interaction is calculated in the DL-Track, and each rail support/ sleeper is recorded during the train passage. At the end of the simulation, each rail support has its maximum contact force for each wheel of the bogie. In the presence of track heterogeneities, each sleeper can have a significant variation on the level of loading and that can be represented in the SP-Track.

After the DL-Track simulation, the vector with the highest sleeper load values is chosen a track length that corresponds to the SP-Track length (usually the most conditioning section) and then each sleeper is loaded by a static load as illustrated in Figure 3.35.

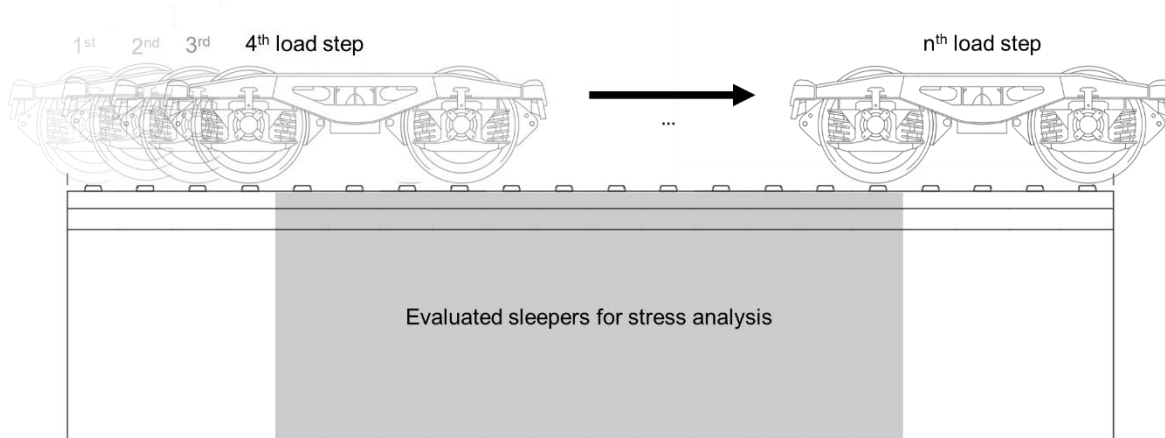


Figure 3.35: Train load modelling in the SP-Track

In this approach, the SP-Track is simulated several times (number of evaluated sleepers in the model) and in each time, every stress amplitude in each direction is recorded into a matrix. When the transient load simulation is over, the maximum/ minimum stress in each direction for each node is saved.

A big limitation of this method is the loss of dynamic information for smaller frequency-dependent stress amplitudes due to the passage of high speed trains. Nonetheless, the purpose of this stress calculation is related to fatigue calculation, in which the overall maximum stress amplitude is the most important feature and the one with the greater contribution to cumulative fatigue. Once again, the trade-off between an accurate transient analysis load with different frequencies would result in high computational cost, without a significant gain in result reliability. Besides, due to the uncertainty related to concrete fatigue damage, it was not worth to invest in a detailed load transient algorithm.

Regarding temperature variation, this action is an important external factor that has a striking impact on long continuous concrete structures, due to thermal expansion and contraction, and

is usually overlooked in slab track modelling. In cases of continuous slab track, e.g. the Rheda 2000 or the Züblin systems, expansion joints are mandatory to control the thermal expansion of the track, otherwise, the concrete slab will experience failure due to extreme cracking. In modular solutions, this is usually not an issue, since the mortar between the panels acts as an expansion joint since it can easily crack before the slab panel itself. Also, some solutions can present transversal cuts on the top surface of the slab to avoid uncontrolled cracking, such as the Bögl system.

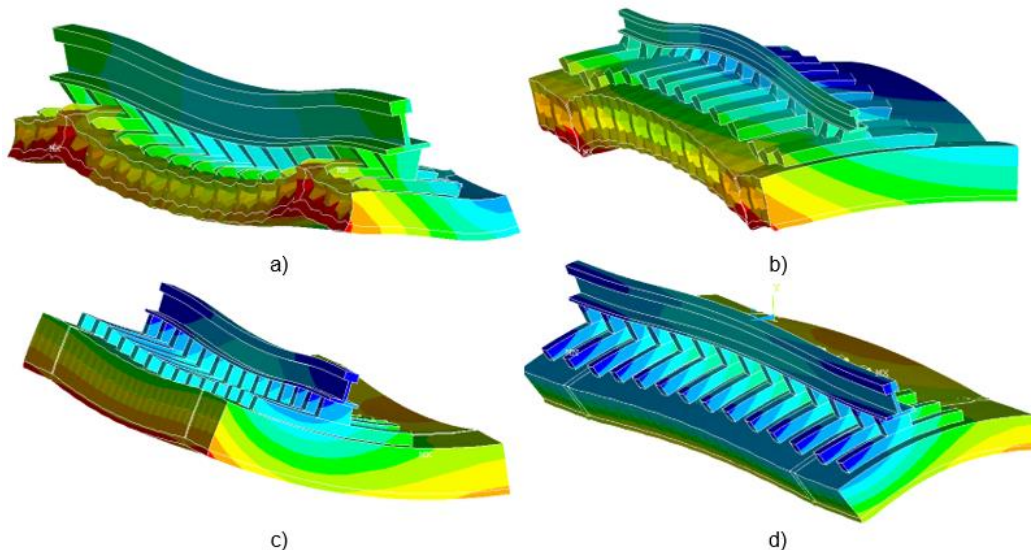


Figure 3.36: Temperature effects on the track: negative temperature uniform (a), Positive temperature uniform (b), negative temperature gradient (c) and positive temperature gradient (d)

Another temperature-relevant phenomenon is the vertical temperature gradient (X. Liu et al., 2011) that can cause the slab to warp as illustrated in Figure 3.36. This bending effect inflicted by the temperature gradients can cause extra damage, specially the negative gradient, since the top surface of the slab is more vulnerable than the bottom one, which leads to higher tensile stresses. The temperature loads are directly applied independently in every node on the track slab, according to a certain uniform temperature and gradient from a scenario case study. In Figure 3.37 and 3.38, the impact on temperature loads on the overall stress peaks on the track can be observed. The example is a mid-section node at the top of the slab for a standard climate ocean climate (0°C minimum during the Winter and a 30°C maximum during the Summer for a typical Cfb Klöppen climate that will be explained in detail in Chapter 5). In the xx direction, the influence of the temperature is controlled by the existence of expansion joints, being the vehicle the main source of stress variation in a daily basis. In the zz direction, the temperature gradients play a larger influence and higher daily temperature occurs as well as seasonal disparities. The winter months are responsible for larger tensile stresses due to concrete shrinkage caused by low temperatures, while in summer, higher compressive stresses are formed due to concrete expansion. On the contrary, summer months tend to expand the concrete slab track and therefore, compression stresses are more common. It is noteworthy to mention that these are nodes in which the temperature has a larger impact as the block support or the slab edges.

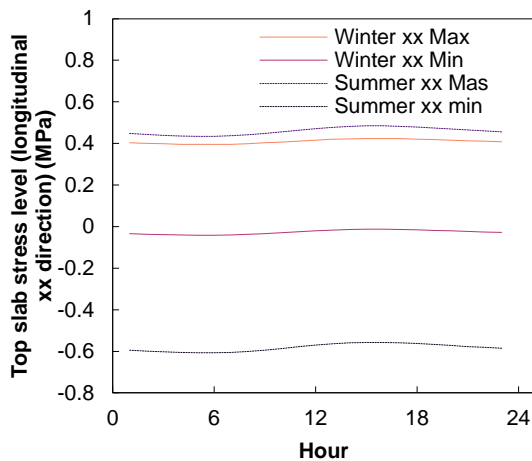


Figure 3.37: Hourly stress amplitude spectrum in the longitudinal (xx) direction

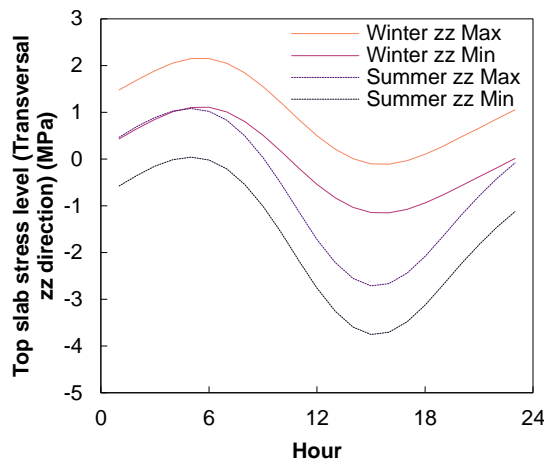


Figure 3.38: Hourly stress amplitude spectrum in the transversal (zz) direction

The temperature is modelled as an imposed deformation in each node, instead of a more complex convection, radiation, or conduction thermal model. Nevertheless, the properties required to model this phenomenon would become unreasonable due to the lack of certainty and reliability on such parameters.

3.3.3 NONLINEAR MATERIAL BEHAVIOUR UPDATE

From the mesoscopic scale, concrete is a highly heterogeneous material, which leads to a nonlinear stress-strain relationship during the load process. In ultimate limit states, this is observed in macroscopic cracks and can be modelled with the previously applied William and Warnke yield criterion. On the other hand, slab tracks are normally under serviceability design conditions, and in this regime, there are pre-existing micro-cracks caused by initial damage when subjected to external loads. As a proposal to model the micro-mechanical behaviour of the concrete, the fibre model is used by several authors (Le & Bažant, 2011; Le et al., 2011; Wu et al., 2006) to simulate the evolution and propagation of micro-cracks during the lifetime of the concrete elements, thus having an impact on the model's stiffness.

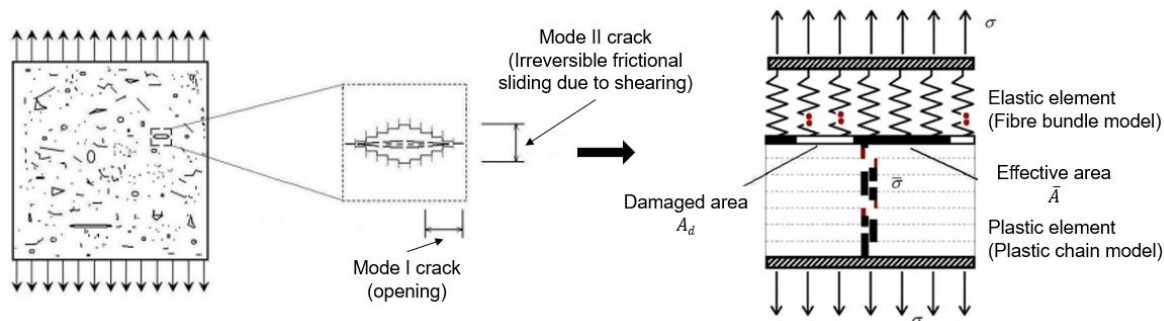


Figure 3.39: Bundle-chain model for concrete uniaxial loading (adapted from Shan and Yu (2015))

Fibre bundle models (FBM) can provide the representation of the anisotropic characteristics of concrete from a probabilistic point of view, but only characterize normal elastic elements, and

lack the irreversible micro-elements present in irreversible chain models (ICM). To solve this, Shan and Yu (2015) developed a mixed bundle-chain model that combines irreversible strains due to micro-cracks and the normal elastic component as illustrated in Figure 3.39.

In this model, when a strain exceeds the yield criterion (and a micro-crack is formed), it does not break as in the normal ICM and results in the occurrence of irreversible strains.

According to Mazars (1986) and Shan and Yu (2015), the scalar constitutive damage model can be expressed as:

$$\sigma_i = (I - D_i) \cdot E_0 \cdot \varepsilon_i \quad (3.32)$$

$$\varepsilon_{di} = D_i \cdot \varepsilon_i \quad (3.33)$$

Where I is the identity matrix, E_0 is the initial Young modulus, ε is the strain level calculated in the numerical model, D is the damage level, i is the fatigue load cycle, and ε_{di} is the irreversible damage strain. Taking this into consideration, the loss of stiffness and the updated Young modulus E_d can be calculated as follows:

$$E_d = (I - D_i) \cdot E_0 \quad (3.34)$$

The loss of stiffness will be a key role feature to calculate stress redistribution and crack width evolution during the track's lifetime.

Despite having a nonlinear characterization of the concrete material behaviour, the main advantage of this feature in SP-Track is the stress redistribution during a singular load cycle, instead of millions of train load cycles and thousands of temperature cycles. Although possible, it is not computationally feasible yet. With this in mind, the SP-Track requires an initial slab condition at the beginning of each iteration that simulates the track damage at a certain point of the slab track's life.

After the computation of each node's damage level (later explained in Chapter 4), which will be highly dependent on the stress level in each principal direction, the module script in the SP-Track model calculates the damage in each element by the average of each node's damage. Said that, before the track calculation, an initial condition of track stiffness is attributed to each cementitious material, i.e. CSL, HBL, fibrous concrete, sleepers, CAM, etc.

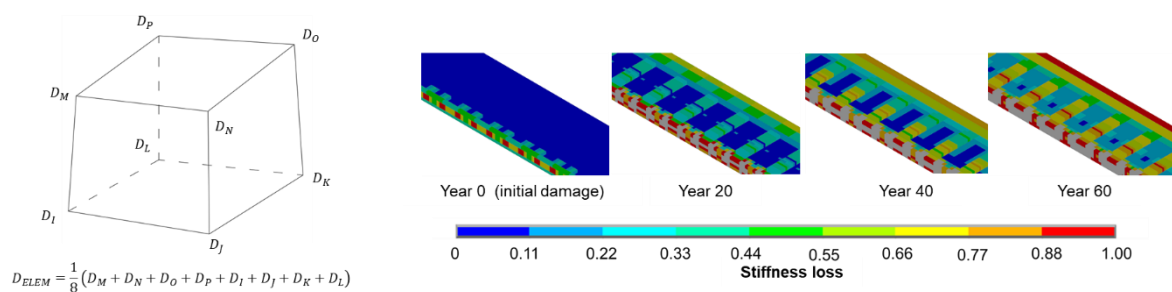


Figure 3.40: Element damage calculation and initial condition of the track stiffness

The loss of track stiffness is directly calculated by equation 3.32 and enables a detailed heterogeneous loss of stiffness in different areas of the track. Figure 3.40 presents the initial state

that is installed in the short-term calculation in each cycle of the slab track, taking into consideration the load stress path. With this approach, crack width can be predicted in multiple areas with progress plateaus or sharp increases due to the level of stress accommodated by the reinforcement.

3.4 ARCHITECTURE OF THE SUB-MODELS

In this section, the model architecture will be explained and structured to multiple phases to simulate the long-term effect on the track, which will be discussed in Chapter 4.

Both DL-Track and SP-Track models are divided into three distinct phases: Initialization, model assembly and calculation, and post-processing. The presented model structure is the result of an iterative process conducted in course of this thesis, comprised of entirely original code, and designed to allow high parametrization flexibility.

3.4.1 INITIALIZATION

The first stage is responsible for the definition of all geometry and material properties of the track system in question (slab track or ballasted track). Figure 3.41 illustrates the stage architecture that is initiated with two main external modules alluding to model controls and track geometry that are intrinsic and exclusive to each particular track type. The model control routine has every detail about the track layout (track size, rail defects, track heterogeneities, etc.), vehicle (vehicle type, speed, etc.), and track properties (geometry and material characteristics). The track geometry routine is the geometric definition of the entire model with two different modules for the DL-Track and SP-Track for the envisaged track typology.

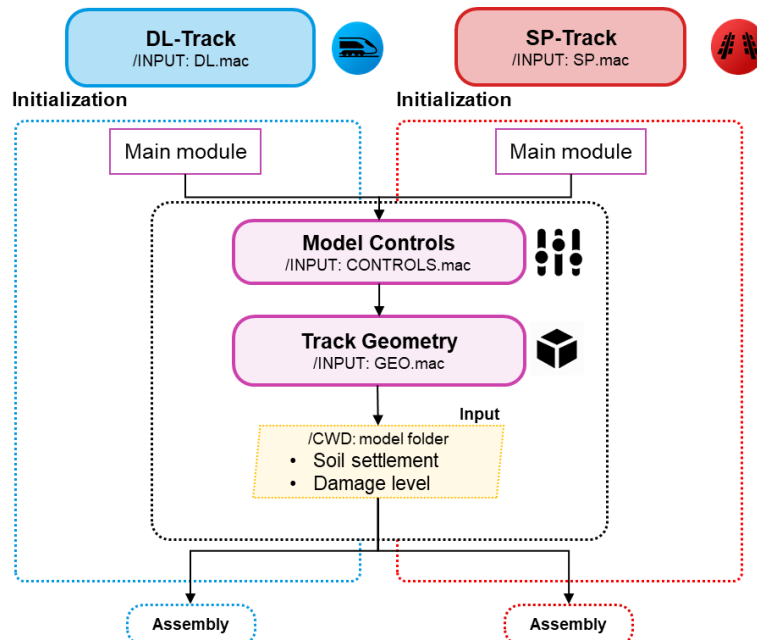


Figure 3.41: Initialization stage

Next, each model checks for the update of the properties, namely the soil settlement and the slab damage level. In the case of the SP-Track, only the concrete damage level, i.e. the loss of stiffness is of interest for the model generation. For the DL-Track, the main deterioration phenomena to be addressed is the progressive soil settlement, however, the concrete-like materials are also updated with an average loss of stiffness for the entire element.

3.4.2 ASSEMBLY AND CALCULATION

After the initialization stage, the next step is the model assembly that in the case of the SP-Track model is straightforward, with the meshing of the previously defined geometry followed by a routine that updates the track stiffness. On the contrary, the DL-Track requires a much more detailed assembly.

Subsequently, the DL-Track enters the generation phase, in which the geometry modelling and slice generation are performed. In this phase, multiple superelements can be created taking into account the specifications of the intended scenario. All modelling strategies are constructed to be as efficient and optimized as possible to minimize simulation times. Said that, and since the DL-Track and SP-Track models will be implemented in multiple repetitions: if the long-term simulation does not require updating the model geometry and superelement library after their initial definition, bypasses were created in the geometry and model generation stages to avoid needlessly repeating the superelement generation. The same bypass routines are applied to the SP-Track model assembly that requires an even larger amount of computational time.

Regarding the DL-Track, an important issue is the capability to perform a static analysis under imposed settlements, in order to compute the rail profile subjected to a particular soil settlement. This feature implies that the main generation module is different according to the intended analysis (DL_GEN and DL_GENS for dynamic and static analysis respectively) since different master nodes are required to compute a tridimensional soil settlement, as illustrated in Figure 3.42. Next, track assembly and boundary conditions are implemented, and the analysis is selected according to the required calculation (later explained in chapter 4).

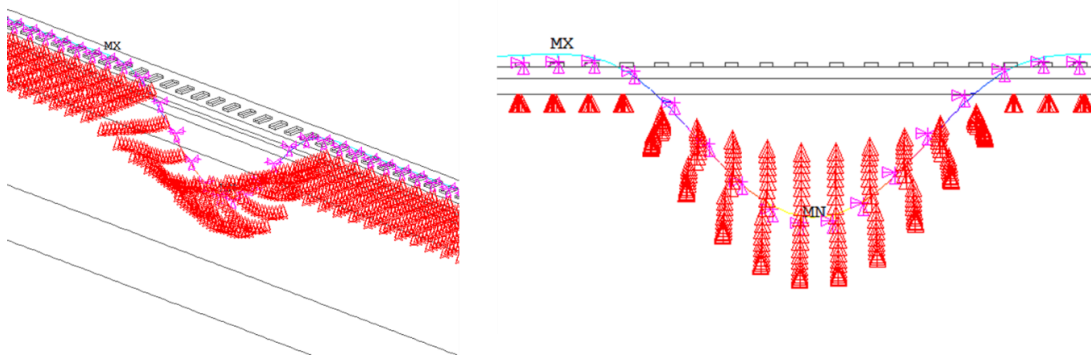


Figure 3.42: Rail profile update by the DL-Track

In a similar mode, after track modelling, SP-Track runs a subroutine to update the concrete stiffness of each element to emulate the concrete cracking during its lifetime. Subsequently, a

different structural analysis is performed depending on whether it is intended a one-time short-term analysis, or it is inserted in a long-term simulation (most common application of the model) in which every action is modelled independently as it will be explained in the next section. A summary of the assembly and generation of each model is illustrated in Figure 3.43.



Figure 3.43: Assembly and calculation of DL-Track and SP-Track

3.4.3 POST-PROCESSING

Although using substructuring techniques in the DL-Track and reducing the material nonlinearity to the essential in the SP-Track, the amount of information calculated in each reaches 20 Gb. Thus, a dedicated submodule to post-processing the results is built as depicted in Figure 3.44. This macro file extracts the nodal data to be stored in track sensors previously stated as track response variables, concrete stress cells, soil pressure cells, and vehicle sensors.

In what concerns the DL-Track, the results depend on the selected analysis. If the static settlement analysis is selected, only the rail settlement profile is extracted; otherwise, common cinematic variables are extracted. Also in this file, important filtering and data post-processing tasks are implemented with a built-in Matlab module, mainly to calculate fast Fourier transform

to compute the frequency domain results and low-pass filters to the aimed spectra of frequencies.

Likewise, the post-processing module of the SP-Track is only run if a long-term analysis is selected. Several SP-Track calculations are performed during the post-processing phase to individually calculate the effect of each action (prestressed loading, gravity, uniform temperature, gradient temperature, train loading, etc.) on the track, to be later combined for damage calculation. The main reason for this relates to the possible number of combinations of coupled actions: it is unfeasible to compute all track responses for the entire lifetime of the track. A significant simplification was assumed in the non-joint action effect on nonlinear short-term behaviour and load distribution. However, it is believed that this simplification does not significantly affect the result, since the slab load stresses are usually under control and far from resistance thresholds. Thus, only in extreme load and temperature scenarios would the model be likely to lose accuracy. Finally, a vast amount of data is delivered regarding concrete, reinforcement stresses, and soil stresses, as well as tailored built modules, to compute shear and bending moments from solid element stresses.

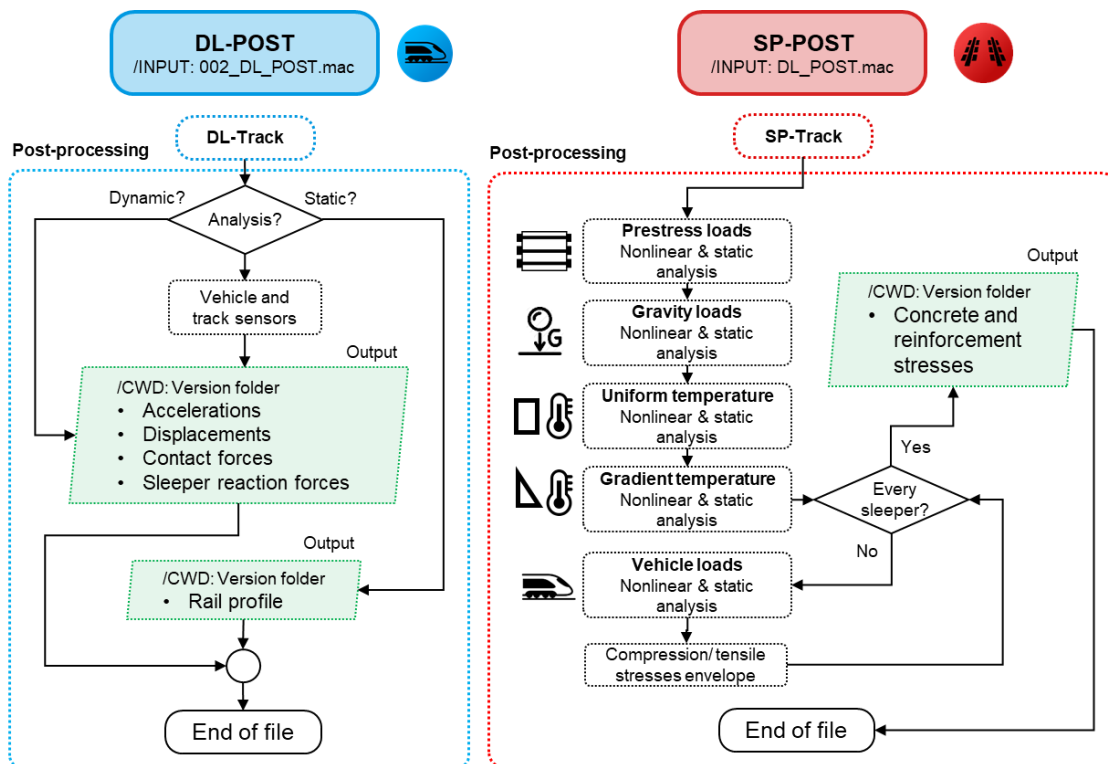


Figure 3.44: Post-processing modules for the DL-Track and SP-Track

3.5 CONCLUDING REMARKS: HIGHLIGHTS AND LIMITATIONS

The DL-Track and SP-Track were subjected to several stages of development that followed a stepwise approach to issues that arose during the conception stage. The final versions of these models present long-term features and update modules whose details will be explained hereafter in this document. Table 3.4 presents the major improvements to the DL-Track model.

Table 3.4: Main features of the several versions of the DL-Track

Version	1	2	3	4
Rail	Euler-Bernoulli beam (2D elastic)	Euler-Bernoulli beam (3D elastic)	Timoshenko beam	≡
Railpad	Kelvin-Voigt Spring-damper	≡	≡	≡
Sleeper	2D plane 4-noded elements	3D solid 8-noded elements	Undersleeper pads and biblock/monoblock sleepers	≡
Underlayers (e.g. ballast/ CSL, etc.)	2D plane 4-noded elements	3D solid 8-noded elements	Mesh refinement due to shear waves; Multiple slab track systems and ballast configurations	Update of superstructure properties
Contact	Hertzian spring	Specific contact and target elements with penalty stiffness factor.	≡	≡
Train-vehicle	Moving mass	Multiple axle MBS	≡	Multiple vehicles available (TGV, ICE, CHR ₃ , Freight)
Boundary conditions	Track end, side and bottom with fixed displacements	≡	Damping “slices”	≡

Although some improvements were made in the rail element, the rail-railpad system is modelled in simplistically by a punctual connection to the sleeper, which leads to less accurate results than more complex and detailed models. Nonetheless, rail-related results are not the main priority for the thesis' goals: a balance between the accuracy of the main superstructure layers results and computational cost is preferred at this stage of the DL-Track. These shortcomings are attenuated by the SP-Track model, which will be explained in the next chapter.

Superstructure-wise, the main layers (ballast, subballast, CSL, HBL) are modelled as continuous elastic solids, which is one of the main limitations of the use of substructuring techniques. For instance, in order to model contact elements between the sleeper and ballast, full elements for the contact are required, even if the sleeper and ballast are modelled with superelements. In this situation, it is more advantageous to model the intervening elements (sleeper and ballast) as full finite element solids, since the number of required master DOF will reduce the efficiency of the substructuring technique, with high access times to the superelement library.

Despite this limitation, the preliminary results show a good correlation with the ballast and subballast displacement and accelerations under 100Hz frequency. These promising results indicate that the train load is being effectively transmitted to the superstructure. This is a strong feature of the DL-Track model, along with its high flexibility to model multiple track configurations (Figure 3.45) as desired.

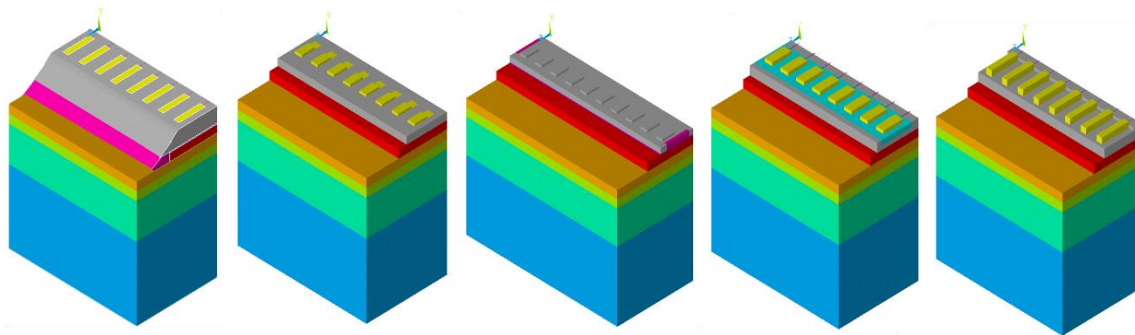


Figure 3.45: Multiple track typologies available for calculation (from left to right: ballasted track, Rheda 2000, Bögl, Stedef and ATD systems)

The inclusion of an improved contact algorithm is justified and linked to the need for a more realistic wheel/ load contact, which should be able to simulate contact force variations upon different sets of longitudinal defects. For this reason, the vehicle model architecture includes the suspended and non-suspended masses (primary and secondary suspensions) that, although a simple model for the study of vehicle dynamics, shows a reasonable amount of accuracy in modelling the load transmitted to the track.

The substructuring method did not change throughout the versions of the DL-Track, since the envisaged results were almost indistinguishable from the full model (Figure 3.28 and 3.29) although the validity is restricted to the low-frequency range.

In terms of the second sub-model, the 3D nonlinear SP-Track is a detailed FEM model that had a starting point in the work of Matias (2014) and was further developed to meet the thesis goals. The main features of each version are represented in Table 3.5.

Table 3.5: Main features of the several versions of the SP-Track

Version	1	2	3
Rail	3D elastic solid	≡	≡
Railpad	3D elastic solid	≡	≡
Sleeper	3D elastic solid	3D elastic solid with contact element (if necessary)	Stiffness update
Underlayers (e.g. ballast/ CSL, etc.)	3D elastic solid	3D elastic solid with nonlinear concrete behaviour and reinforcement	Stiffness update
Actions	Train load (rail pressure)	Maximum sleeper reaction per axle	Temperature loads and prestress tendons
Boundary conditions	Track end, side and bottom with fixed displacements and one longitudinal plane of symmetry	≡	≡

The major highlights of the SP-Track model are concentrated in 2 main elements: superstructure layer modelling, and external actions. The remaining elements had none, or little, improvement.

The superstructure received great enhancements in geometric details, with a meticulous representation of reinforcement bars and prestressed cables. This implementation of detailed reinforcement elements, together with the stiffness update for each element, can deliver more accurate crack width predictions in the long-term perspective. The loss of stiffness and the

geometric deterioration will inevitably cause larger stress redirection to the reinforcement, and therefore higher crack width and slab deterioration.

Additionally, the stiffness update of the track is an important feature that enables the SP-Track model to start the simulation with initial damage on the track and to predict the influence of short-term actions on a deteriorated track. Also, this feature can represent the loss of bearing capacity of the superstructure, which increases the soil stress and, consequently, the permanent deformation of the soil. The faster deterioration of the geometric quality increases the train loads, therefore increasing the damage in a vicious cycle, i.e., deteriorated tracks deteriorate faster.

In what regards the load modelling, the SP-Track has a complete set of different permanent loads, such as gravitational and prestress forces (the latter if the slab track features prestress tendons), temperature loads (only applied in the track slab, and assuming that the underlying layers are protected from temperature variations), and train loads.

The train load is transferred to the SP-Track in a simple methodology that does not account for the dynamic frequency content of loading. In this methodology, fatigue is mainly caused by the large amplitude of the load transmitted to the track. This does not take into account smaller load frequencies that add damage to the track, notwithstanding, their influence is rather small, and this simplification complies with the intended goals of the thesis.

Due to the train-track interaction computed by the DL-Track and later implemented in the SP-Track, the track can no longer be longitudinally symmetrical since different track responses would rise when subjected to track longitudinal heterogeneities. As an example, the train approach to a differential settlement precedes a loss of contact force and can be reproduced in the SP-Track with non-symmetrical forces.

To sum up, the DL-Track is a powerful tool specifically designed for very fast computations of long sections of railway tracks, with strong reliability for predicting the loads transmitted to the superstructure. To complement the structural behaviour of slab track systems, SP-Track is a numerical model capable of delivering concrete damage patterns and reinforcement stresses subjected to train and environmental loads.

Also due to the modular nature of the model architecture, several modelling blocks can be added for studying specific scenarios. The intermodal validation delivered confidence on the modelling technique in a preliminary phase. Chapter 5 concerns the validation of the model by multiple experimental campaigns for short- and long-term responses.

4 DEVELOPMENT OF A LONG-TERM HYBRID AND ITERATIVE MODEL: HI-TRACK

4.1 INTRODUCTION

Long-term analysis is a desired feature for slab track engineers and a vital part of the thesis goals. Important factors, such as infrastructure deterioration, are going to be carefully addressed in this chapter. The previous chapters focused on the short-term response of the track, with special attention to train/track interaction to track defects heterogeneities (DL-Track) and concrete and soil stresses (SP-Track). The main idea of the model architecture and purpose is for the results of the DL-Track to be implemented as inputs for the SP-Track model, which delivers stress and strain loads on the track.

These results largely affect the track deterioration, which in turn affects the short-term performance. The correlation between the obtained track results and deterioration is currently done by empirical laws that update the track conditions under a mechanistic-empirical design. The long-term effect is achieved through simulation of millions of cycles, emulating several years of track lifetime, and, in each cycle, several parameters are updated. The deterioration of the track is assessed mainly by two parameters: longitudinal rail levelling, and concrete loss of stiffness. Other deterioration phenomena that are likely to occur, such as rail contact fatigue or CAM delamination, will not be addressed in the final version of the model; yet, they can easily be implemented in future versions, if a more comprehensive empirical law is developed. Taking this into consideration, a hybrid model (HI-Track – Hybrid & Iterative) will be explained as a dual approach between short- and long-term calculations.

Running a finite element method analysis to determine the deterioration of the track structure can be very wasteful and expensive to do each cycle, especially if the nominal response of the track is almost elastic linear between cycles. Said that the hybrid model will entail adaptive time steps to calculate the track deterioration and properties update as efficiently as possible.

4.2 PERMANENT DEFORMATION OF THE SUBGRADE

4.2.1 FACTORS INFLUENCING SOIL SETTLEMENT

In regards to soil design, two main considerations emerge as the bearing capacity and soil settlement, being the latter a more critical design parameter to take into account in railway applications.

Regardless of the soil type used for the foundation platform, long-term soil deformation can be divided into three different stages illustrated in Figure 4.1, and can be summarized as follows:

- The primary stage has an elevated level of permanent deformation with a decreasing rate of plastic deformations, associated with volumetric change, i.e. a compaction stage.
- The secondary stage is characterized by a stabilization of the settlement rate still associated mainly with volumetric changes but with growing participation of shear deformation.
- The tertiary phase represents the shear failure of the soil with no volume changes

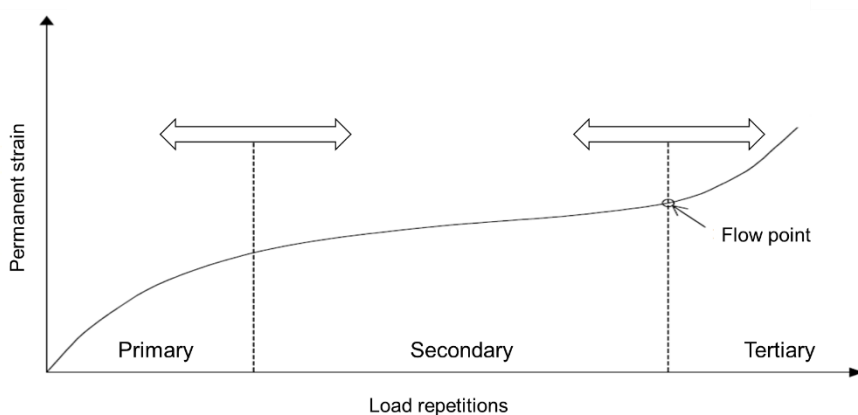


Figure 4.1: Long-term permanent deformation behaviour of the soil

Numerous factors can affect soil response under cyclic loads and therefore influence the overall long-term behaviour. Among them, the most relevant factors are the soil stiffness, the applied level of load pressure and frequency (mainly shear deformation), the consolidation level, temperature, the composition of the grains, and soil structure (Kucharczyk et al., 2018). Usually, the temperature can be neglected (aside from the effect of evapotranspiration that changes the water content of the soil). Additionally, soil structures and the composition of the grains are usually parameters to fit the settlement curves.

Frequency-dependent loads on soil permanent deformation are limited, but usually, the general effect of the load frequency tends to dissipate with the increasing number of cycles (Kumar et al., 2018). Also, when lower frequency loads are applied, larger shear strains occur and larger pore pressure is generated (Konrad & Wagg, 1993; Kumar et al., 2018; Vucetic, 1988). These fatigue tests were conducted for 500 repetitions and a frequency range below 2 Hz. Under these conditions, soil loading for a long-term permanent strain is usually considered as a quasi-static load in which the frequency-dependent forces are not considered.

Aside from the unequivocal impact of the strain level imposed on the soil, the consolidation state, which is governed by pore water pressure and water content present in the soil voids, has a major role on the overall settlement (T. M. Ferreira et al., 2011). The hydraulic behaviour of the soil depends on parameters such as soil suction, capillarity, water level rising plus atmospheric actions as precipitation that cause water changes between the multiphasic status of porous materials, i.e. unsaturated soils. Due to the presence of water, the interlocking shear resistance between soil grains is reduced and overall settlement can be duplicated in the presence of partially saturated soils.

The amount of water that is infiltrated and stored in unsaturated soils depends on the hydraulic properties of the soil as the soil water infiltration retention behaviour, i.e. the coefficient of permeability. This coefficient represents the water movement inside the soil, and the higher the coefficient, the faster the water infiltrates. Moreover, higher coefficients of permeability are associated with higher suction recovery after the rainfall (Tsaparas et al., 2002). If the rainfall intensity surpasses the saturated coefficient of permeability, i.e. the infiltration capacity of the soil, the consequence is a superficial runoff.

Additionally, the rainfall characteristics (intensity, duration, and frequency) play an important role in the hydrological behaviour of the soil. The primary factor that affects the level of water infiltration in the soil is the rainfall intensity. There is a threshold rainfall intensity for a given duration and soil type that maximizes infiltration in the soil. For low permeability soils, the most conditioning factor becomes the rainfall duration (Rahimi et al., 2011).

Furthermore, another issue that has a major impact on the water content of the embankment soil is the groundwater table that extremely affects the pore water pressure distribution, usually associated with antecedent rainfall (Rahardjo et al., 2007).

4.2.2 SOIL SETTLEMENT LAWS

Track settlement is an important design parameter for slab track construction, and usually, a maintenance-free condition is linked to a zero-settlement requirement, instead of the ballasted track that a significant part of the maintenance is allocated to ballast tamping, mostly caused by ballast (80%) and the remaining by the soil (20%). Nonetheless, soil settlement is inevitable, yet manageable and an accurate prediction for long-term permanent deformation on the soil layer

is of interest. Usually, the permanent deformation accumulation in the soil settlement laws is a function of the number of load applications and stress conditions of the soil. (Selig & Waters, 1994). Usually, the application of soil mechanics plasticity theories to numerical models has a reduced application for railway purposes focusing on long-term performance, due to high computational costs. An alternative approach to predict track settlement in fine-grained soils (the case of unbound granular materials) is analytical mechanistic-empirical formulations. This is the most common methodology to evaluate cumulative permanent deformation of the soil that associates the excessive deformation of the soil to a permanent strain.

The vast majority of the model follows a power expression usual to simulate the growing consolidation of the soil, as follows:

$$\varepsilon_p = a \cdot f(\sigma, \varepsilon) \cdot N^b \quad (4.1)$$

Where ε_p is the accumulated permanent deformation of the soil for a determined number of cycle N , a soil response $f(\sigma, \varepsilon)$ dependent of soil stresses and strains, and a and b are regression parameters. Table 4.1 summarizes the main works regarding soil permanent deformation:

Table 4.1: Empirical models for permanent soil strain behaviour

Expression	Author	Parameters
$\varepsilon_p = a + b \cdot \log(N)$	(4.2) (Barksdale, 1972)	
$\varepsilon_p = a \cdot \varepsilon_r \cdot N^b$	(4.3) (Veverka, 1979)	ε_p - Accumulated permanent strain after N load repetitions; ε_r - Resilient strain;
$\varepsilon_p = A \cdot \frac{\sqrt{N}}{\sqrt{N} + D}$	(4.4) (Paute et al., 1988)	σ_d - Deviatoric stress;
$\varepsilon_p = \varepsilon_0 \cdot e^{(\frac{\rho}{N})^\beta}$	(4.5) (Tseng & Lytton, 1989)	σ_s - Compressive strength of the soil;
$\varepsilon_p = a \cdot N^b$	(4.6) (Sweere, 1990)	a, b, A, D, B - Regression parameters
$\varepsilon_p = a \cdot \left(\frac{\sigma_d}{\sigma_s} \right) \cdot N^b$	(4.7) (D. Li et al., 1996)	$\varepsilon_0, \rho, \beta, C$ - Material parameters
$\varepsilon_p = A \cdot \left(1 - \left(\frac{N}{100} \right)^{-B} \right)$	(4.8) (Hornych & Paute, 1998)	$R = \frac{q}{q_f}$ - Ratio between the deviatoric stress q and the failure deviatoric stress q_f
$\varepsilon_p = C \cdot N^b \cdot \left(\frac{R}{A - R} \right)$	(4.9) (Korkiala-Tanttu, 2008)	

Usually, the mechanistic-empirical formulations address the two first stages and do not consider the tertiary stage of settlement. Although being important, the tertiary stage is currently a challenging task to model accurately due to the time-consuming and difficult implementation of laboratory tests. While shear deformation failure can be modelled numerically at the expense of a large amount of computing power, plastic shear deformation is only modelled in a few, if any, mechanistic-empirical deformation prediction models. This is not a relevant limitation since this deformation phase is substantially lower than common design tolerances in actual practice.

4.2.3 THERMO-HYDRO-MECHANICAL BEHAVIOUR OF THE SOIL

The soil behaviour is not only influenced by the response of traffic loads since unsaturated soils are subjected to atmospheric actions that can cause significant influence on soil behaviour. -

such as precipitation, infiltration, evapotranspiration, and groundwater table variations.

This hydraulic mechanism is mainly affected by the osmosis phenomena of soil suction and retention characteristics that depend on the thermo-hydro-mechanical behaviour of the soil. The water movement inside the embankment soils causes the deterioration of the railway substructure by changes in water pressure.

In his Ph.D. thesis, T. Ferreira (2015) developed a thermo-hydro-mechanical (THM) model that can calculate multiple parameters of the soil as water pore pressure and saturation degree (ratio between the liquid phase and the total void volume in the soil) when subjected to traffic and environmental loads (see Figure 4.2)

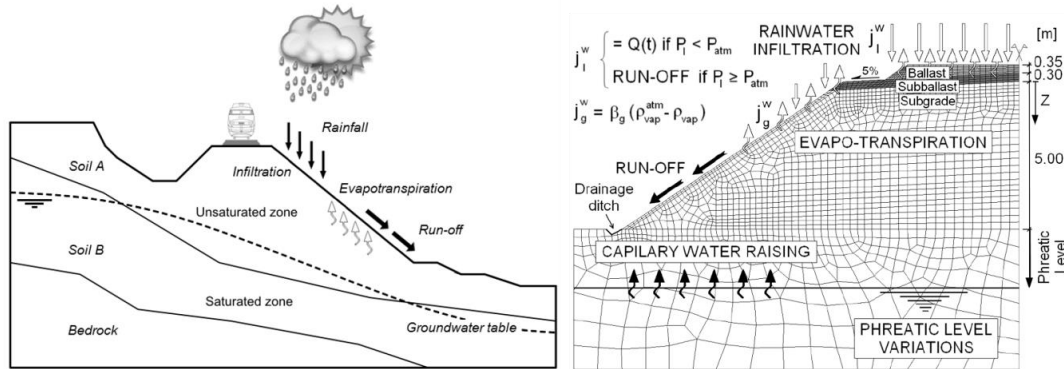


Figure 4.2: Atmospheric interactions governing the thermo-hydro-mechanical behaviour of the soil (left) and a 2D FE THM model (right) developed by T. Ferreira (2015)

The hydraulic behaviour of this model is studied with a new constitutive law entitled bubble-BBM model, that uses the original bubble theory developed by Al-Tabbaa and Wood (1989) that is a kinematic hardening model based on the modified cam clay model, i.e. an elastic-viscoplastic constitutive model (BBM) with kinematic hardening smaller inner yield surface (bubble) defining the limits of the elastic region.

This method is capable of cyclic loading under the vehicle and environmental actions, namely percolation, infiltration, and runoff of rainwater, properties of rainfall, soil hydraulics properties, embankment geometry, evapotranspiration, and drainage systems.

Such a powerful THM model can predict the specific stresses and hydraulic condition of the embankment soil during the track's lifetime. This is used to model extreme precipitation cases that can change the phreatic level and the deficiency of the drainage system. The hydraulic behaviour of the soil will affect the geomechanics of the soil spatially and temporally by variation of suction gradients. These suction gradients are caused by pore water pressure variations that are closely linked to soil deformations. The main controller is the rainfall that affects the transient hydraulics, yet rain infiltration and surface run-off are mainly controlled by hydraulic properties of the soil, as well as pore water pressure conditions due to water level rising and antecedent precipitation. Also, processes as temperature, relative humidity, wind, and radiation affect the variations of soil saturation degree.

With this in mind, atmospheric data from Barcelona (Mediterranean climate) from 2010 is considered in the finite element thermo-hydro-mechanical model and demonstrated in Figure 4.3. The saturation level of the soil is then calculated with the defined soil characteristics (typical embankment $E_{v2} \approx 80$ MPa for high speed lines) with the aggregation of multiyear atmospheric annual data. Moreover, the groundwater table can be variable which has a considerable impact on the water present in the soil. An example of the obtained results of the saturation degree in the soil for a period of 3 years is represented in Figure 4.4.

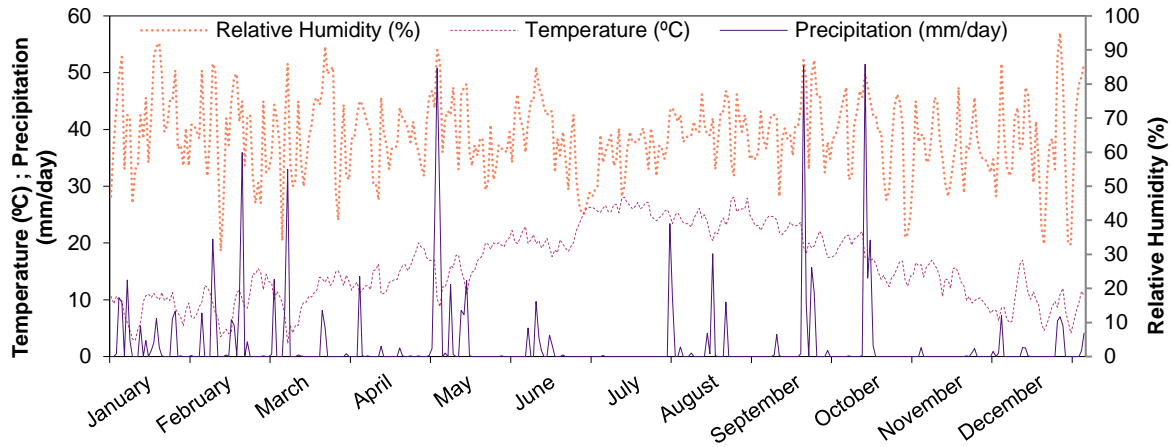


Figure 4.3: Atmospheric data from 2010 for the city of Barcelona (Mediterranean climate)

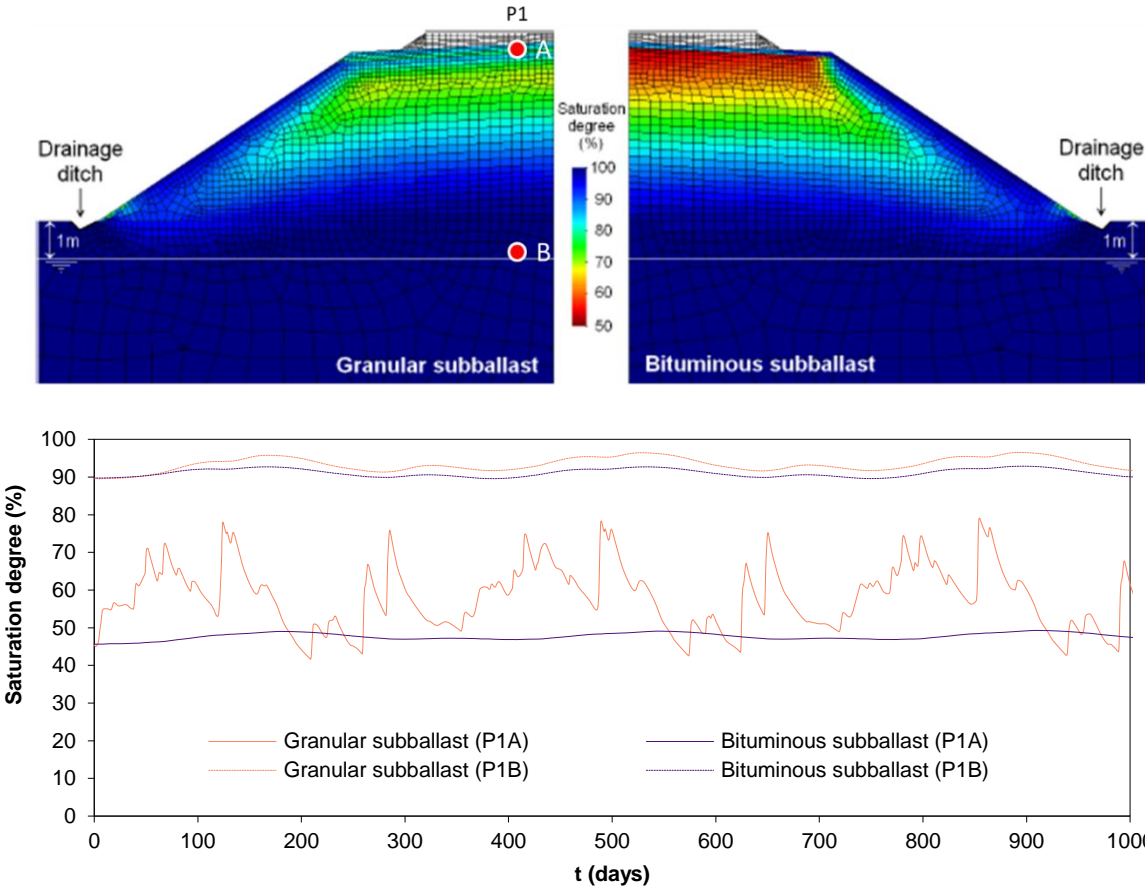


Figure 4.4: Spatial distribution (top) and temporal evolution of saturation degree granular and bituminous subballast (bottom)

4.3 CONCRETE SLAB DETERIORATION

4.3.1 FACTORS INFLUENCING CONCRETE DETERIORATION

The deterioration process of the concrete by fatigue occurs due to a degradation process, where a cyclic load generates lower stresses than the concrete modulus of rupture. Yet, microstructure degradation occurs due to the presence of air voids and flaw areas between the aggregate and the binder that causes microcracks, which later develops to a macro scale with inherent stiffness loss of the structure (ACI, 1992). Nevertheless, during the hardening of concrete, microcracks are formed due to shrinkage and temperature differentials in the concrete pavement, before any load application, which accelerates the fatigue phenomena.

The fatigue life assessment of concrete pavements is focused on high cycle fatigue (between 10^3 and 10^7 cycles) and the process can be classified into three stages (Figure 4.5):

- Stage 1: Crack initiation with a stress concentration due to discontinuities or flaws in the concrete, e.g. microcracks (0%-15% of the pavement lifetime);
- Stage 2: Crack propagation that evolves with certain stress cycle increments that exceed the fatigue limit of the concrete for a determined scenario (15%-85% of the pavement life);
- Stage 3: Failure precedence (flow point), which occurs very rapidly with a decrease in stiffness (85%-100% of the pavement life).

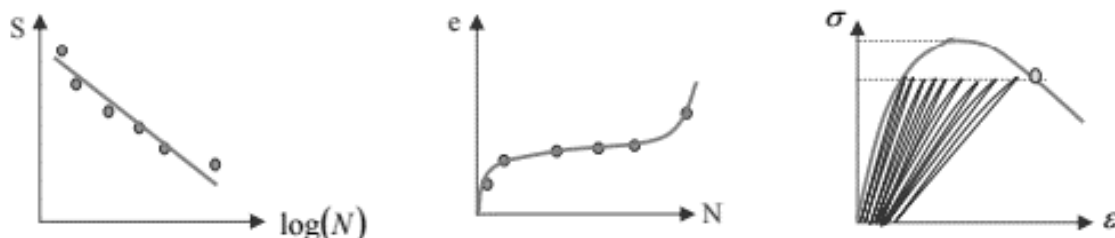


Figure 4.5: Wöhler diagram (left); strain – number of cycles diagram (centre); stress-strain diagram (right)

In Figure 4.5, the common fatigue behaviour of concrete pavements is presented. Serviceability life in several cycles depending on the stress ratio is shown in the left, the three stages of fatigue life are shown in the centre and the loss of stiffness is presented in the right.

The fatigue of concrete pavements is mainly controlled by the flexural strength of the concrete slab, nonetheless, several other factors have an influential potential in concrete pavement fatigue, as the type, duration and frequency of the load, concrete heterogeneity, environmental loads among others.

In concrete pavements, the applied loads can be grouped in vehicular loads with or without thermally induced actions being the most well-known model for concrete pavement analysis is the model developed by Westergaard in 1926 with important guidelines for the horizontal stress

and deflection of elastically supported slabs (Westergaard, 1926). More recently, the most significant work without temperature differential is the work performed by Packard & Tayabji (1985). These authors found out that the maximum induced tensile stress without temperature differentials occurs when the vehicle load is applied at the middle of the longitudinal joints between transversal joints. Hiller & Roesler (2005) take similar conclusions regarding the bottom of the middle slab edge as the critical location of fatigue damage in the absence of thermal loads.

The temperature differentials interpret an important factor in the design of concrete pavements. These curling of the slab is constrained by its self-weight, so in a case of positive temperature differential ($T_{top} > T_{bottom}$) the tensile stress is greater at the top of the slab and vice versa in case of a negative temperature differential ($T_{top} < T_{bottom}$). Preliminary studies only consider a linear temperature distribution in the slab depth, however, Choubane and Tia (1995) claim that temperature distribution is nonlinear, and later, Mohamed and Hansen (1997) developed an analytical method to study the tensile stress in concrete pavements to induced nonlinear temperature gradients. Results indicate that nonlinear temperature stress distributions along the depth of the pavement result in tensile stresses that are lower than the ones caused by a linear temperature with a positive differential. Nevertheless, when there is a negative temperature differential, the nonlinear distribution produces greater tensile stresses than the linearized temperature gradient.

An important aspect to take into consideration the fatigue design of concrete pavements is the superimposed action of temperature and traffic that can accelerate the effect of fatigue. Rodofo and Balbo (2001) performed numerical simulations in a finite element model, and conclude that the temperature-induced stresses are almost 100% of the stress when compared with the stress induced by traffic, performing an important parcel to account for the design. Houben (1994) also developed a finite element model for the evaluation of temperature gradients in concrete pavements and concluded that the superposition effect of both traffic and thermal loads, conducts to lower stresses than the combined stress calculated from individual loading (thermal or traffic). In this note, a detailed consideration of temperature gradients is a relevant factor to take into account in the fatigue life assessment of concrete pavements. However, for the fatigue design of slab tracks, the temperature influence may have a lower (but non-negligible) participation than in the case of road and airport pavements.

The stresses generated by the action of the traffic are the principal sources of damage in concrete pavements, and these actions could have a wide range of characteristics, yet, the principal factor to take into account for fatigue analysis on concrete pavements is the ratio between the maximum induced flexural stress and the static strength of the concrete.

Despite the amplitude, other factors as load frequency and sequence could be relevant to the concrete fatigue behaviour. Regarding the magnitude of the load, it is unanimous that higher levels lead to a lower number of supported cycles by the slab. Oh (1991) conducted a study about the concrete fatigue behaviour, where it was applied three levels of maximum induced stress –

SR, (65%, 75% and 85%) and it was found that the $SR = 65\%$ produces 93% more cycles than $SR = 75\%$, and this last 93% more cycles than $SR = 85\%$.

Concerning the sequence of the loads, Zhang *et al.* (1996) performed various trials combined with alternating maximum stress levels from 50% to 97,5% and frequencies of 1 Hz (until 10^3 cycles), 5 Hz (between 10^3 and 10^5 cycles) and 20 Hz (over 10^5 cycles). The results of this work indicated that the alternating stress causes a reduction in fatigue strength, yet, had little influence in tensile, compression and flexural trials. Other studies, as the one performed by Cervo (2004) verified that the ascending alternating stresses present a longer fatigue life than constant stresses, however, for descending alternating stresses, the fatigue strength is reduced. This alternating stresses could be rather important for mixed traffic scenarios.

Concerning the load frequency, this is a relevant factor to review, especially in the high speed rail context, due to the associated high-frequency loading. Cervo (2004) conducted several trials on concrete pavements, with a stress ratio of 83% and concluded for frequencies of 1 Hz, 5 Hz, and 10 Hz, the latter achieve a fatigue resistance of approximately 95% greater when compared to the 1 Hz and 5 Hz frequencies. Other studies, like the one performed by Stet and Frénay (1998) and Keerthana and Kishen (2019) suggest that, if the stress level is relatively high, the reduction of the load frequency diminishes the fatigue life.

It is worth to note that these findings concern flexural tests only. Notwithstanding flexural tests being the most accurate to evaluate the fatigue of concrete pavements, validation of findings with traction and/or compression tests is lacking.

4.3.2 CONCRETE FATIGUE LAWS

The fatigue life prediction of concrete elements is performed by cracking propagation and energy of fracture governed by fracture mechanics theory, however, due to a practical necessity for a simple evaluation method, it is used Wöhler diagrams, i.e. S-N curves (Stress – Number of cycles) with semi-logarithmic representations (CEB, 1988). This representation can be obtained experimentally from fatigue tests, and is usually expressed as:

$$\frac{\sigma_t}{f_{ctm}} = a + b \times \log N \quad (4.10)$$

Where σ_t represents the maximum induced flexural stress (most relevant stress for pavement analysis), f_{ctm} stands for the concrete modulus of rupture, N is the number of cycles and a and b are constants empirically determined. The vast majority of the proposed fatigue models about concrete pavements follows the principle of equation (4.14).

From observed fatigue tests of concrete pavements, it can evidence two types of S-N behaviour: the greater the magnitude of the stress, the lower the number of cycles the concrete pavement can resist before fatigue failure and there is a stress ratio limit below which no fatigue accumulation is noticed.

The conception of concrete pavements comes inevitably with the development of cracks that during the lifetime of the pavement will cause several deterioration processes. These deterioration processes on a highly heterogeneous material as concrete results in a wide results dispersion.

The following models are common in the literature regarding concrete pavements fatigue design, with highlighting of their principal features, hypotheses and limitations. The summary presented can be useful for conducting performance fatigue verification on concrete pavement fatigue and evaluate the main factors that influence fatigue behaviour.

The models apply mechanistic-empirical design methods to calculate the slab thickness, determining the critical stresses, usually flexural stresses at the bottom of the slab under an edge loading condition (bottom-up cracking). The mechanical behaviour of the fatigue phenomena is based on the Miner's rule (Miner, 1945) that assumes a linear increase in accumulated damage for a certain number of load applications, expressed as:

$$D = \sum_{i=1}^k \frac{n_i}{N_i} \quad (4.11)$$

Where D represents the accumulated damage caused by a number of single load application with a determined stress level (n_i) in relation to a maximum allowable number of load applications at that stress level with defined failure criteria (N_i). The accumulated damage D , for design purposes, is usually 1, notwithstanding it could vary in function of the load characterization (nature, magnitude and sequence) and material properties.

To determine the number of allowable load cycles is required to define a performance index, particularly the stress ratio (SR), that is the quotient between critical stress induced in the slab (σ_s) and the concrete modulus of rupture, or flexural strength ($f_{ct,f}$).

The most common fatigue models for concrete pavements are based on mechanistic-empirical design concepts and can be divided into empirical (laboratory) and semi-empirical (field measurements).

Table 4.2: Semi-empirical fatigue formulations (Smith & Roesler, 2004)

Fatigue model	Expression	
PCA (1973)	$\log N = 11.810 - 12.165 \times SR \text{ for } 0.5 < SR < 1.0$	(4.12)
Foxworthy (1985)	$\log N = 1.323 \times 1/SR + 0.588$	(4.13)
Darter (1990)	$\log N = 2.13 \times (1/SR)^{1.2}$	(4.14)
NCHRP 1-26 (1992)	$\log N = -1.7136 \times SR + 4.284 \text{ for } SR > 1.25$	(4.15)
	$\log N = 2.8127(SR)^{-1.2214} \text{ for } SR < 1.25$	(4.16)
FAA (1995)	$SR = (0.75 \times \sigma_s)/MR = 1.3B^{-2}$	(4.17)
	$B = \begin{cases} 1 + 0.07058 \times [\log(C/5000)], & \text{if } C < 5000 \\ 1 + 0.15603 \times [\log(C/5000)], & \text{if } C > 5000 \end{cases}$	(4.18)
LEDFAA (1995)	$SCI = \frac{0.535(1/SR) - 0.297 - (0.388 + 0.000039 \times SCI)\log C}{0.002269}$	(4.19)

The semi-empirical models (Table 4.2) are developed through the attainment of data by

monitoring pavements with real-world traffic circulation throughout their serviceability life, according to the theory already developed. These models present limitations due to the conditions of the realized trial, with extrapolation for other scenarios being more narrowed.

The empirical models (Table 4.3) are obtained with controllable conditions from laboratory tests with built specimens or with samples extracted from field measurements and are subjected to cyclic loading, usually with high frequency and without resting times. The experimental models do not consider the load position and usually are placed in the most unfavourable condition with magnitude fluctuation, which makes them conservative models.

Table 4.3: Empirical fatigue formulations (Smith & Roesler, 2004)

Author(s)	Description	Fatigue model
Tepfers & Kutti (1979)	Minimum and maximum stress ratios between 0.2-0.4;	$SR_{max} = 1 - 0.0685(1 - \sigma_{min}/\sigma_{max})\log N$ (4.20)
Cornelissen (1984)	Maximum Stress level between 40-90% and minimum stress level between 0% and 40% for alternating bending;	$\log N = 9.19 - 1.931 \left(SR_{min} \times \frac{f_{ct,f}}{f_{ck}} \right) - 7.45(SR_{max})$ (4.21)
Peterson (1990)	Consideration of vehicular and thermal loads;	$\log N = 11 \times ((1 - SR_{max})/(1 - SR_{min}))$ (4.22)
Yao (1990)	Consideration of vehicular and thermal loads with a failure probability of 50%;	$\log SR = 0.0162 - 0.042(1 - \sigma_{min}/\sigma_{max})\log N$ (4.23)

4.3.3 CRACK WIDTH EVOLUTION

Crack prediction in reinforced concrete structures is mainly important for serviceability limit states, which larger cracks can reduce the functionality and lifespan of the structure. Slab tracks are subjected to environmental actions that may include extremely harsh weather conditions and at the same time, these structures are designed for 60 or more years of operation. So, accurate predictions of crack width limits are an important design criterion for slab track systems, since cracking accelerates the penetration of deleterious agents that cause the steel reinforcement corrosion (Tan, 2019).

In the last decades, several authors developed empirical formulations (Smith & Roesler, 2004) and fracture mechanics theories (Aure & Ioannides, 2010; Denneman et al., 2009; Gaedicke & Roesler, 2009; Sancho et al., 2007), based on the concept of induced stresses ratio and the energy dissipation for propagation (W_j). The theoretical complexity and computational cost associated dismiss the use of fracture mechanics theory for the proposed goals of the thesis.

Generally speaking, the crack width can be obtained as the difference between the steel and concrete strains over a crack spacing as follows:

$$w_{cr} = S_{cr0} \cdot (\varepsilon_{sm} - \varepsilon_{cm}) \quad (4.24)$$

Where S_{cr0} is the crack spacing, ε_{sm} is the maximum principal strain of the reinforcement and

ε_{cm} is the maximum principle strain for concrete. The concept can be applied to reinforced concrete ties, beams and one-way bearing slabs, i.e. slab tracks subjected to traffic, temperature, shrinkage, creep amongst others.

Nevertheless, the accurate prediction of crack width is quite complex (Cervenka et al., 2018) and a large portion of uncertainty is directly linked to the phenomena itself in a highly nonlinear regime. This mechanical behaviour can be simplified by assuming steel and concrete as elastic materials disregarding the internal cracking at the crack interface (Russo & Romano, 1992). This approach is followed in design codes and guidelines such as EC2 and MC2010, MTCM. Tan et al. (2018) compared these models by their accuracy on predicting the crack width for several rebar diameters and covers and conclude that the MTCM delivers more accurate results with a maximum cracking spacing prediction/measured ratios of 2, and 2.2 and 3.2 respectively for MC2010 and EC2. Also, the standard deviation was larger for the EC2 and MC2010 than the MTCM. These results are worsened for larger rebar sizes which in turn lead to over-conservative results for EC2 and MC2010. For smaller diameters (8-12 mm longitudinal rebar size), which are typically for slab tracks, the deviation between the design guidelines and the experimental results reduces but is still conservative. Along these lines, the chosen methodology to predict the concrete crack width on slab tracks is the one presented by EC2. This option was taken due to familiarity with European concrete design practices and by conducting to slightly more conservative predictions. According to the EC2, crack width extension can be calculated as:

$$S_{cro} \cdot (\varepsilon_{sm} - \varepsilon_{cm}) = \frac{3.4 \cdot c + k_1 \cdot k_2}{\rho_{p,eff}} \cdot \left(\sigma_s - \frac{k_t \cdot \frac{f_{ct,eff}}{\rho_{p,eff}} \cdot (1 + \alpha_e \cdot \rho_{p,eff})}{E_s} \right) \geq 0.6 \cdot \frac{\sigma_s}{E_s} \quad (4.25)$$

In which σ_s is the reinforcement stress at the crack section (if the slab track presents prestressed tendons, σ_s is replaced by $\Delta\sigma_p$, as the stress variation in the tendons for the state of zero strain of the concrete at the same level. These reinforcement stresses are directly obtained from the SP-Track model and adjusted by a factor $C_t = \frac{F_t \times D_{avg}}{A_s}$ that redirects any loss of tensile capacity of the concrete to the reinforcement being F_t the tensile force in the effective area of concrete in tension, D_{avg} the average damage in the same zone and A_s the reinforcement area in the perpendicular direction in that zone. The coefficient α_e is the $\frac{E_s}{E_{cm}}$ ratio, $\rho_{p,eff}$ is the mechanical percentage of reinforcement expressed as $\rho_{p,eff} = \frac{A_s + \xi_1 \cdot A'_p}{A_{c,eff}}$.

A'_p is the area of pre/post-tensioned tendons within $A_{c,eff}$, that is the effective area of concrete in tension surrounding by the reinforcement on prestressed tendons of depth $h_{c,eff}$ as $\min\left(2.5 \cdot (h - d), \frac{h-x}{3}, \frac{h}{2}\right)$. ξ_1 is the adjusted ratio of bond strength taking into account the different diameter of prestressing (θ_p) and reinforcing steel (θ_s) $\xi_1 = \sqrt{\frac{\theta_s}{\theta_p}}$. Finally k_t is a load duration factor ($k_t=0.6$ for short-term and 0.4 for long-term duration).

In what concerns the crack spacing S_{cro} , c represents the longitudinal reinforcement cover, k_1

is a coefficient that takes into account the bond properties (0.8 for high bond bars and 1.6 for plain surface), and k_2 considers the distribution of the strain (0.5 for bending and 1.0 for pure tension). In the case of eccentric tension, k_2 values can be interpolated.

All the response parameters are calculated by the SP-Track model. Afterwards, crack widths are computed for several locations in the slab. Although this simplified empirical approach lacks the probabilistic complexity of fracture analysis, it makes possible to deliver crack width predictions with an accurate order of magnitude that will be important to compare track deterioration scenarios later in this document.

4.4 HI-TRACK: INTERACTION BETWEEN DL-TRACK AND SP-TRACK

4.4.1 CALCULATION PROCESS

The HI-Track model is the core contribution of this thesis and allows the emulation of long-term behaviour on slab tracks by creating a dual approach between the DL-Track and SP-Track sub-models and using their outputs as input variables for track update properties.

This interaction remains a challenging task with little examples in the literature, and in this sense, the model architecture is code-intensive with multiple modules that interact with each other. The model can be subdivided into 3 main phases: **Initialization**, **long-term calculation** and **adaptive adjustment**. The model architecture is illustrated in Figure 4.6.

The first **initialization** stage is dedicated to defining all variables that are going to be implemented in the hybrid model, particularly long-term controls: external actions and incremental characteristics.

External actions are implemented in the model as input files that have all data relative to a certain number of years of track operation. As an example, the traffic scenario includes a daily train schedule (high speed and/or freight trains) that is replicated over a determined amount of time. Although not considered in this work, the expected evolution of operational speeds and traffic volume can be introduced in this file. Environmental input files are divided in temperature (uniform temperature variations and temperature gradients), and rainfall data (precipitation, temperature and relative humidity). This data is relative to an entire year and then aggregated as a multi-year set. As the traffic progression, yearly changes in weather to simulate climate change can also be introduced. Regarding incremental properties, these are time-related variables that the HI-Track use to control the duration of the simulation and the time step in each iteration as the number of day/ year distinct divisions and the deterioration tolerances to avoid wasteful computation if the nominal response of the track is almost linear.

Track and vehicle properties are in the model controls routine, which are required for the complete definition of the DL-Track and SP-Track mechanical and geometrical properties of the track to be studied.

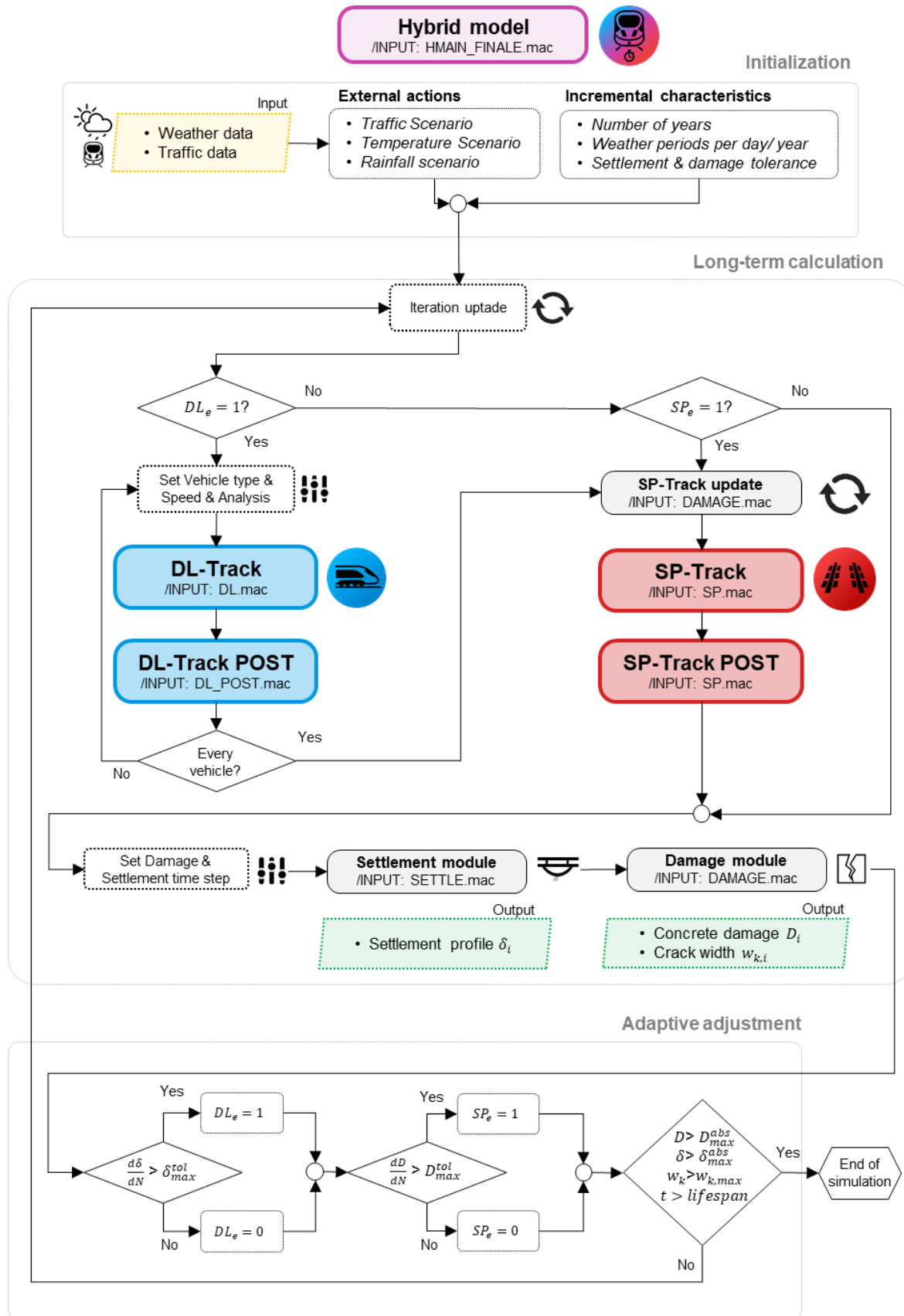


Figure 4.6: Long-term calculation process of the HI-Track model

Overall, there are hundreds of input variables that can be set according to the needs and specifications of a certain scenario, giving the HI-Track a high potential to deliver design and maintenance guidelines thus pursuing the main goals of the thesis.

The most important and longest stage of the HI-Track is the **long-term calculation**. Firstly, in this stage, the HI-Track is required to assemble both sub-models, DL-Track and SP-Track to create the model libraries as an initial iteration so to generate short-term responses. This first iteration is also responsible for the modelling of the initial condition of the track, namely a soil compaction phase and a shrinkage and temperature cracking stage. In what concerns the compaction phase, it is simulated a month worth of traffic (approximately 100k cycles and explained after in the next chapter) to stabilize the initial soil settlement, emulating the initial test runs after construction.

Regarding the initial cracking, the model simulates a month of traffic and temperature loads at a reduced time step and track update (daily) so “weak” cracking zones as the mortar links between panels or transversal cuts can crack and create a “breathing zone” for future imposed displacements. In the absence of this initial calculation at a small time step, the concrete damage would be considerably larger with larger areas deteriorated due to a large updating cycle. A large damage time step is convenient during most of the track’s operation life but not in the early years, in which the importance to foster initial track deterioration at a small-time step is noticed in Figure 4.7.

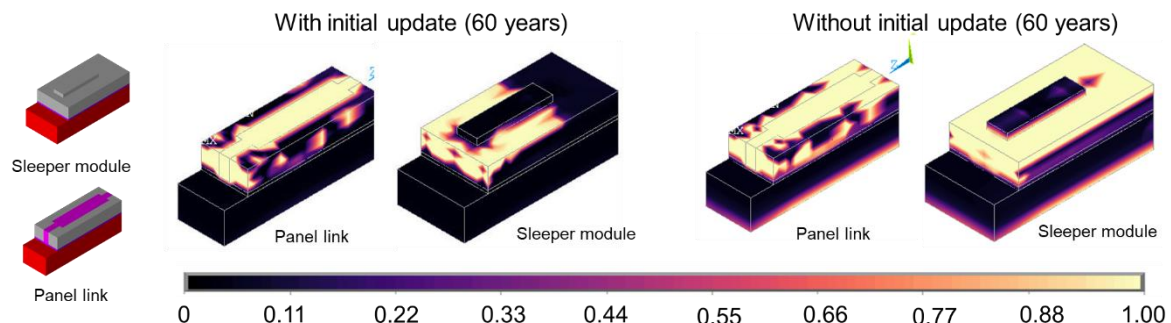


Figure 4.7: Concrete damage comparison between adaptive initial update and without of the panel link and sleeper module of a pre-fabricated slab track system after 60 years for an extreme climate scenario

With the adaptive time step in the first iterations, temperature and traffic loads are redistributed in a more realistically manner by representing the localized damage near the weakest point (panel link) as intended. In this case, the mortar link between the panels is cracked and loses its stiffness and the main damage inflicted on the track is related to temperature gradients and train loads. If no detailed update is performed, and uniform temperature cycles are aggregated in the first iteration, uncontrolled cracking is formed in the entire slab, which would lose stiffness rapidly.

Figure 4.8 shows the effect of the different seasons on track damage. Only damage due to tensile strains is noticeable. The main cause for this damage is negative temperature gradients in severe

winters (tensile damage in the top of the slab) and positive temperature gradients in the summer (tensile damage near the sleeper) due to Poisson effect in a compression state. Additionally, in this first iteration, several days of each season are simulated to accelerate the track's damage for a different range of temperature values.

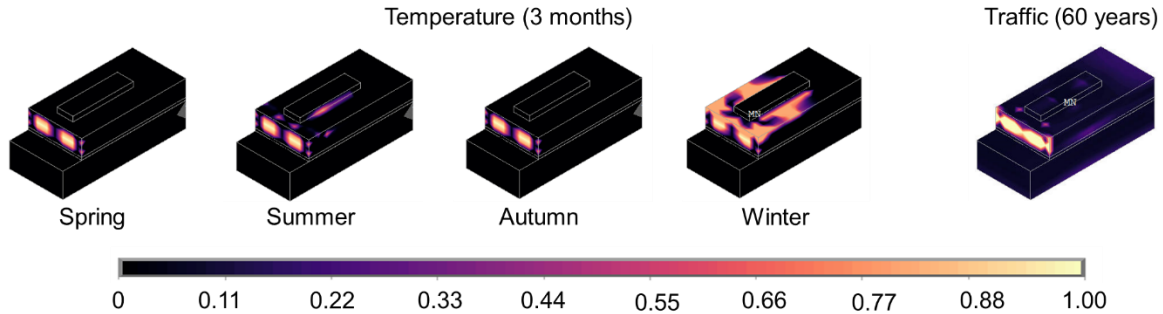


Figure 4.8: Effect of temperature and traffic on concrete slab track damage

After the first iteration calculation, the required parameters are generated and ready to be implemented in later iterations (long-term phase) as an initial track condition. In this next phase, the HI-Track model uses a smart approach by applying different time steps to each short-term model (DL-Track and SP-Track). Since $\partial D / \partial N$ i.e. the change in deterioration per cycle does not change significantly between iterations, and in this sense, there is no need to update the track properties in every load cycle and thus save computing time.

It is assumed that the cumulative damage between ΔN cycles is constant and $\partial D / \partial N$ is only updated every ΔN . This ΔN can vary between the two sub-models since both deals with different deterioration phenomena, e.g. DL-Track calculations are vital for the different settlement rates of the soil, that shows higher growth rates in the early days of the track operations and on the other hand, slab deterioration and cracking is mainly controlled by the SP-Track model. In this case, concrete cracking can have different growth rates, mainly at the end of the lifespan, that don't match the update requirements of the DL-Track. To simplify this process, two boolean variables are created to control the sub-models calculation, DL_e and SP_e . These control variables are defined posteriorly in the next section as a result of the adaptive adjustment.

This difference between ΔN_{SP} and ΔN_{DL} bring concern regarding the hypotheses that small increments can assure the additive property of track damage accumulation. Although not linear, if the time step is small enough to compare with the overall expected final deterioration.

In Figure 4.9 and 4.10, it can be observed the effect of the time step in two distinct deterioration phenomena. These charts concern about the implementation of mixed traffic scenarios (90 high speed trains and 10 freight trains) and how often the track profile is updated. Since the load sequence is important for track settlement, for periods longer than a week, there is a shred of clear evidence that larger time steps result in lower settlement rates, since heavy loads raised by the freight train are postponed to a later moment, in which the soil presents a higher level of consolidation for the current permanent strain. Also, longer time steps lose the detail of atmospheric actions due to seasonal variations. Herein on, the minimum time step is one week

as a result of the balance between the computational accuracy and conservative results.

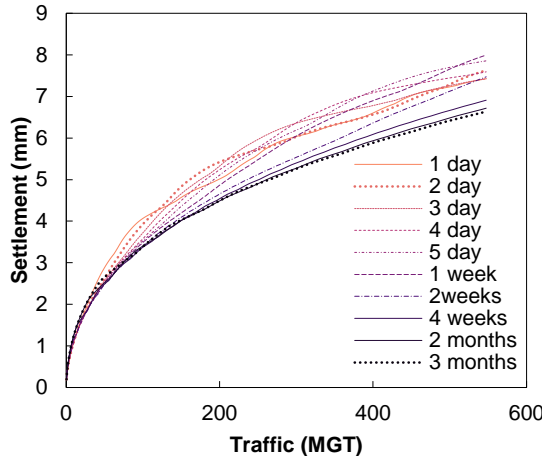


Figure 4.9: Influence of the calculation time step for settlement progression for a mixed traffic scenario

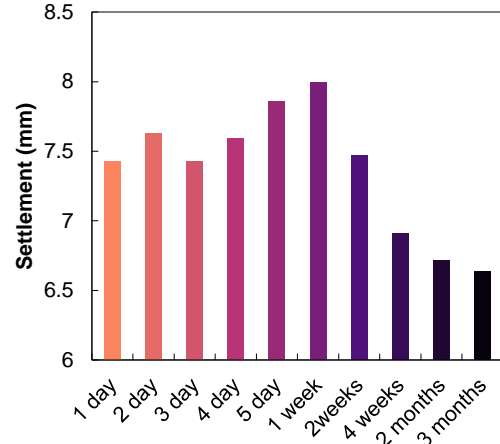


Figure 4.10: Absolute values of settlement for different calculation time steps for a mixed traffic scenario

In what regards the damage time step after the initial iteration, the progress update for a typical traffic and weather scenario (e.g. Frankfurt – Cologne high speed line weather scenario later explained in Chapter 6) does not imply a noticeable difference from a 1 to a 2-year time step (Figure 4.11). This leads to a usual time step of 2 years since it is the minimum time step for reasonable time computation. This time stepping method is carefully chosen so that HI-Track can calculate accurate results while being efficient as possible. Moreover, the long-term simulation can be divided into four main modules: iteration update, DL-Track calculation, SP-Track calculation and deterioration update.

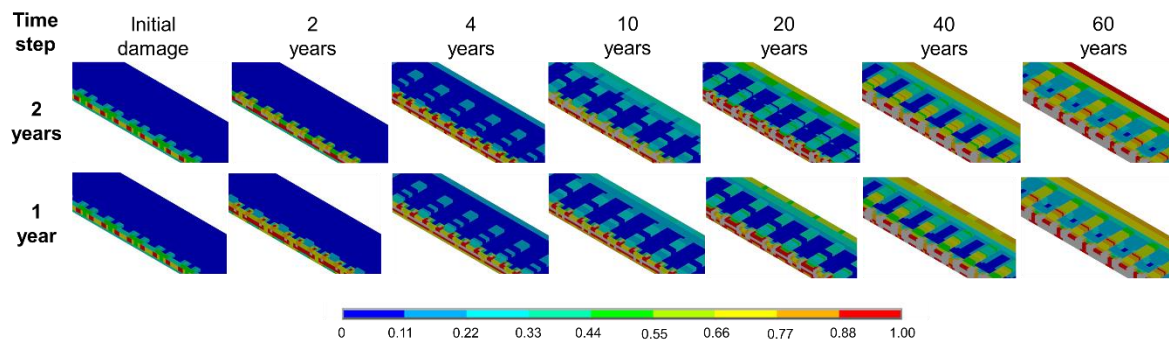


Figure 4.11: Comparison between a 1 and a 2 year time step in the loss of stiffness of the CSL for 60 years

In the iteration update stage, the HI-Track performs the following checking process:

- The iteration number is updated and checks if any of the sub-models DL-Track and SP-Track require to be updated and calculated.
- If necessary, the DL-Track is assembled and calculated with a stiffness update before the static calculation to predict the rail profile levelling.
 - o The analysis is changed to dynamic and a new train/track interaction set of forces

is calculated until the next update. If it is a mixed traffic scenario, there is another step calculation for the second set of train/track interaction forces for other vehicles.

- Obtained the track loading data, the HI-Track calls the SP-Track model routine with the respective prior stiffness update and the stress calculation with the new slab damage condition.
- Finally, the previous calculated concrete and soil stress states can be implemented in the deterioration update stage, which will be explained in more detail subsequently in the next subchapters.

So far, the discussion presented concerns the calculation methods, leaving aside on how often each model is updated. The **adaptive adjustment** is an essential feature of the HI-Track model, i.e. the ability to adjust the time step to the track response rate. If a predefined variable reaches a threshold during the iterative process, the hybrid model updates the respective model. With this methodology, substantial saves in computational time are achieved, with lower time steps when the track response changes at a faster pace and vice versa.

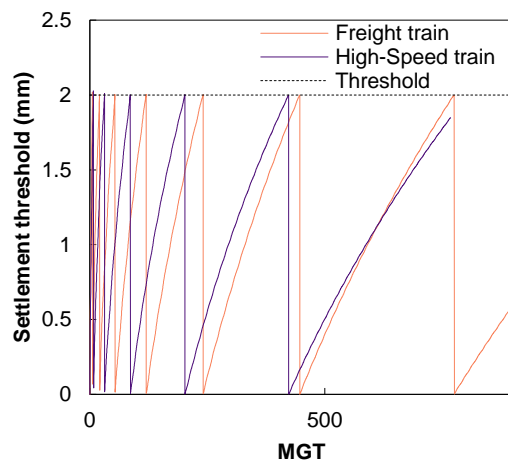


Figure 4.12: Settlement threshold of the HI-Track for the DL-Track calculation

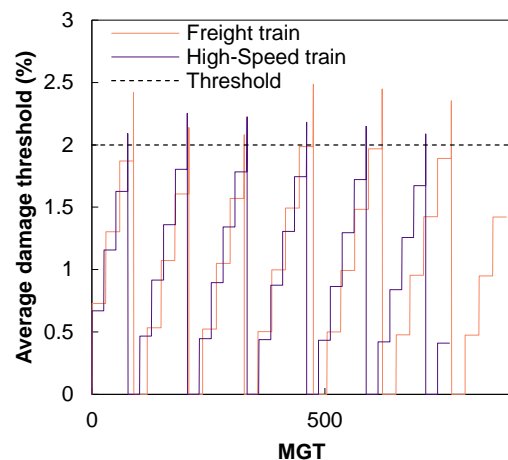


Figure 4.13: Damage threshold of the HI-Track for the SP-Track calculation

In Figure 4.12, the settlement threshold is displayed and the slower rate of settlement progression as the soil consolidates over time are observed. The chosen threshold is a 2mm overall settlement difference between two track updates, and in this particular case, the DL-Track performed dynamic calculation 5 and 7 times for the high speed and freight trains respectively, during the entire simulation. For the track concrete cumulative damage, the established threshold is set to a maximum of a 2% average damage change or 2 years of operation. The 2% average damage increment criterion is employed to avoid losing detail in local damage and the 2-year time step is to keep track of possible changes due to weather seasons. The cumulative damage of the track (Figure 4.13), may seem almost linear, yet, its yearly average value decreases in each year. This shows that the loss of stiffness of the track redistributes the stress the slab as stabilized cracking regime, as illustrated in Figure 4.14. This decreasingly rate

of additional damage in each cycle is in agreement with theoretical results of concrete fatigue, resembling the secondary stage of stabilized concrete cracking. In the freight train scenario, this reduction in the damage rate is more notorious, with a plateau after the 50-year mark. Possibly, if the simulation was continued after the 60-year threshold, the damage rate would start to increase (third stage of concrete fatigue that anticipates fatigue failure and loss of stiffness) due to the decreasingly volume of concrete zones to withstand the loads and unable to redirect the stress by losing stiffness.

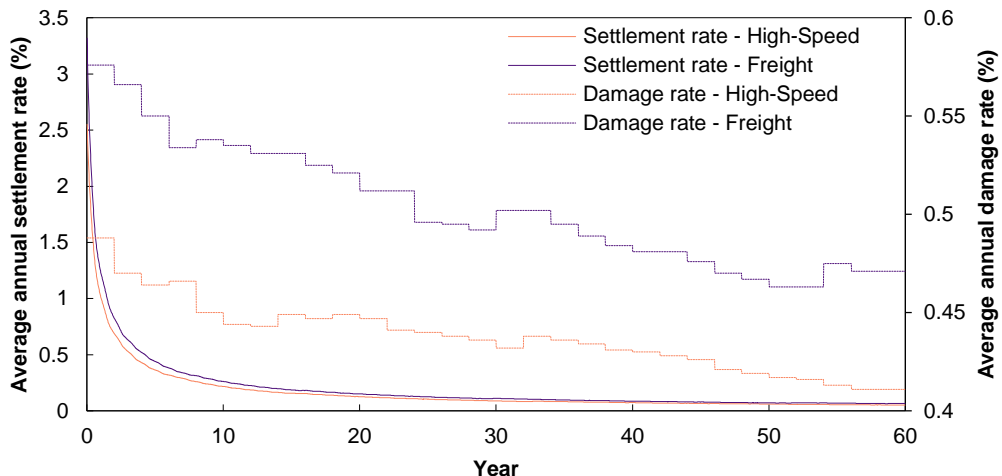


Figure 4.14: Average annual deterioration rate

This definition of the presented threshold, as well as the model architecture itself, are a reflex of the validation and calibration that will be addressed in the next chapter, in an extensive stepwise approach.

4.4.2 SOIL SETTLEMENT PROGRESSION

Permanent deformation of subgrade soil is a common occurring deterioration event when subjected to train loads and weather actions for slab tracks. The main drivers for the development of ballastless systems were the higher structural integrity for speed over 300 km/h and the consequent lower maintenance costs associated with the ballast geometry correction. Although soil settlement in slab tracks is one order of magnitude lower than the ballasted solutions, if the settlement rate is not controlled, significant costs can arise from soil stabilization, thus a relevant reduction in track serviceability. The magnitude of the track has many influencing factors, as the initial geometry quality, traffic characteristics, geotechnical properties and atmospheric conditions.

As previously presented, the common practice for the calculation of railway permanent deformation is based on mechanistic-empirical laws that are a function of vertical strain and stress of the soil. To estimate the total permanent deformation, the subsoil is divided into N layers, and in each layer, the SP-Track calculates the permanent strain in the midpoint from

several vertical alignments as illustrated in Figure 4.15. The permanent soil strains are calculated between with the elastic response of the soil in the SP-Track to be combined with the saturation degree computed in the thermo-hydro-mechanical model, similarly to the work of Ferreira and Teixeira (2012). The saturation degree values in each node of the SP-Track are interpolated from the nodes present in the THM model that do not exactly match location wise. Later, the computed soil settlement is introduced in the DL-Track, that through static analysis, it computes the rail levelling for the current iteration.

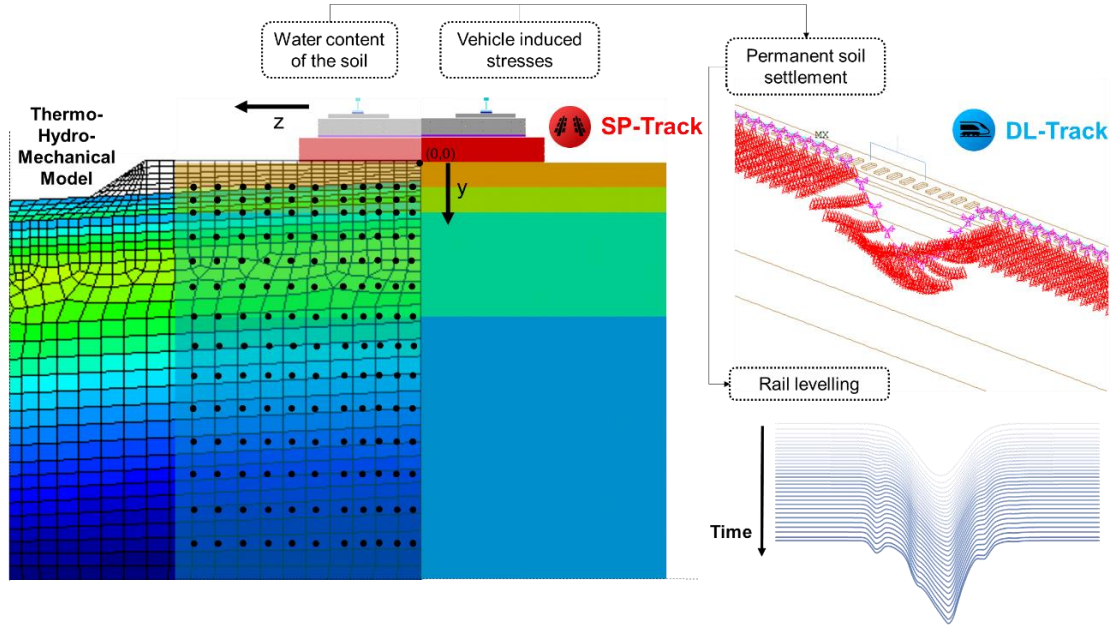


Figure 4.15: Rail levelling calculation process in the HI-Track

Given the detailed hydro-mechanical properties of the embankment soil during the track's lifetime, the empirical analysis performed by Tseng and Lytton (1989), can be implemented to predict permanent deformation, which is integrated into the mechanistic-empirical design guidelines by the AASHTO (ARA, 2004), as follows:

$$\varepsilon_p(N) = \beta_{SG} \cdot \left(\frac{\varepsilon_0}{\varepsilon_r}\right) \cdot e^{-\left(\frac{\rho}{N}\right)^\beta} \cdot \varepsilon_v \quad (4.26)$$

Where ε_p is the permanent deformation associated with an average vertical resilient strain ε_v , N is the number of traffic repetitions, β_{SG} is a calibration factor for the subgrade (usually 1.0), $\varepsilon_0/\varepsilon_r$, ρ and β are material parameters, that are defined by the following equations (Tseng & Lytton, 1989):

$$\log\left(\frac{\varepsilon_0}{\varepsilon_r}\right) = -1.69867 + 0.09121 \cdot W_c - 0.11921 \cdot \sigma_d + 0.91219 \cdot \log(E_{SG}) \quad (4.27)$$

$$\log(\beta) = -0.9730 + 0.0000278 \cdot W_c^2 \cdot \sigma_d + 0.017165 \cdot \sigma_d - 0.0000338 \cdot W_c^2 \cdot \sigma_\theta \quad (4.28)$$

$$\log(\rho) = 11.009 + 0.000681 \cdot W_c^2 \cdot \sigma_d - 0.40260 \cdot \sigma_d - 0.0000545 \cdot W_c^2 \cdot \sigma_\theta \quad (4.29)$$

Where W_c is the water content calculated by the THM model (%), $\sigma_d = \sigma_I - \sigma_{II}$ is the deviatoric stress (psi), $\sigma_\theta = 3p = \sigma_I + \sigma_{II} + \sigma_{III}$ is the bulk stress (psi) and E_{SG} is the subgrade layer Young modulus (psi).

The total permanent deformation is calculated as the sum of the contribution of each layer as follows:

$$\delta_s = \int_0^h \varepsilon_p ds = \sum_{i=1}^{N \text{ layers}} \varepsilon_{p,i} \cdot h_i \quad (4.30)$$

In which δ_s is the total permanent settlement for the considered vertical alignment, N Is the number of sublayers, $\varepsilon_{p,i}$ and h_i are the plastic strain and thickness for the layer i respectively.

As previously described, the stress state of the soil is obtained with the aid of the SP-Track model, in each soil node, while the water content in each node is obtained by the relationship with the saturation level, that is calculated by the THM model developed by T. Ferreira (2015), that is expressed as:

$$W_c = \frac{S_r \cdot e}{G_s \cdot 100} \quad (4.31)$$

With this expression, S_r (%) is the saturation degree of the soil, e is the void ratio (assumed to be 0.33 for a 0.25 porosity level) and G_s is the specific gravity of the soil solid (2.70).

This formulation provides permanent strain of the soil for a determined set of conditions for a total number of load cycles. Since these conditions may vary, as the train load itself (plastic strain) and atmospheric actions that affect soil moisture levels, the cumulative settlement calculation is based on a strain hardening approach. This method used the concept of equivalent traffic, i.e. the equivalent number of load cycles for a determined installed plastic strain level (Figure 4.16).

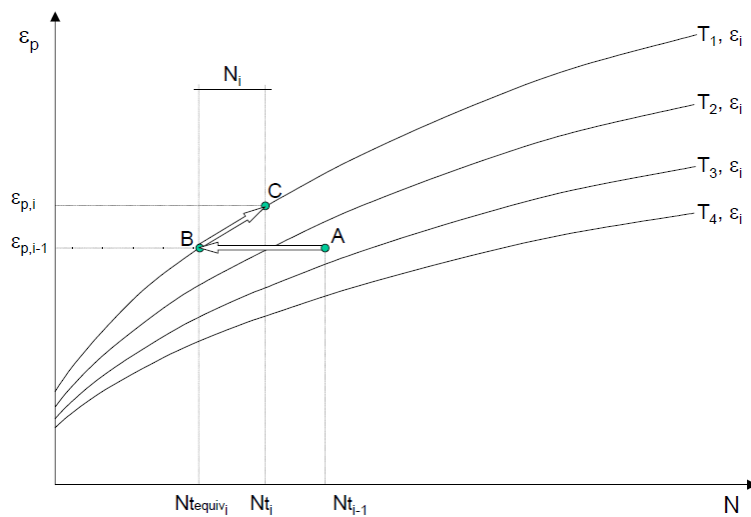


Figure 4.16 Equivalent traffic approach as a strain hardening method for permanent soil deformation

By solving N_{eq} for $\varepsilon_{p,i-1}$, i.e. the previous plastic deformation and having the conditions (stresses, strains and weather data) for the current iteration, an equivalent consolidation level can be obtained for the new time step by adding to N_{eq} the number of traffic load cycles for the

current iteration. This artifice is required since the deformation models deliver a prediction for the total settlement instead of the incremental plastic strain for a traffic time step.

4.4.3 CONCRETE DAMAGE PROGRESSION

Slab tracks are usually designed for high demand corridors subjected to high cycle load fatigue since high speed trains travel faster, freight trains are heavier and the services are more frequent. With these demanding scenarios, concrete fatigue is a growing concern for railway slab track technology, just like concrete pavements for airports and highways.

Regarding the factors that influence concrete fatigue, it is consensual that traffic generated stresses are the main contributors to the cumulated damage paired with environmental loads as thermal-induced stresses. The concrete fatigue is due to internal cracking dispersion, which is important for evaluating the prediction of the fatigue life - currently, this phenomenon has been treated by the scientific community using fracture mechanics modelling.

Models still require a large amount of computational power to small experiment specimens. In this thesis, the methodology used is the mechanistic-empirical approach. The most relevant feature of these models for concrete (a highly heterogeneous material) is their diverse and variability of properties, even for the same specimens and same concrete. This inference is in line with the large number of factors (amplitude, frequency, sequence, etc.) that have an impact on the fatigue life of the concrete.

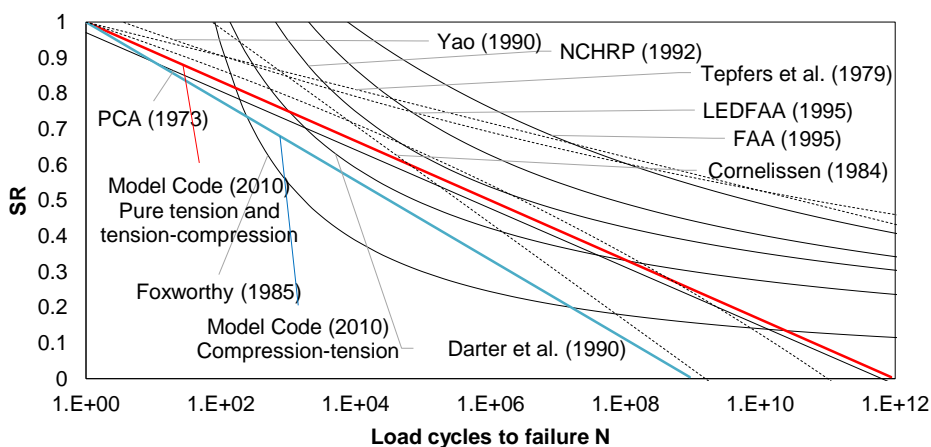


Figure 4.17 Concrete semi-empirical (full line) and empirical (dashed line) fatigue models for flexural stress

Taking this into consideration, a fair amount of scepticism should be considered when evaluating absolute values of cumulative damage in concrete. Nonetheless, performance comparisons between scenarios are possible to address and more interesting to assess. One of the most comprehensive mechanistic-empirical design models in the literature is the proposed concrete fatigue model in the Model Code (2010). For compression, the fatigue life is calculated as that is calculated as follows:

$$N = \begin{cases} N_1, & \log N_1 \leq 8 \\ N_2, & \log N_2 > 8 \end{cases} \quad (4.32)$$

Where:

$$\log(N_1) = \frac{8}{Y-1} \cdot (SR_{cd,max} - 1) \quad (4.33)$$

$$\log(N_2) = 8 + \frac{8 \cdot \ln(10)}{Y-1} \cdot (Y - SR_{cd,min}) \cdot \log\left(\frac{SR_{cd,max} - SR_{cd,min}}{Y - SR_{cd,min}}\right) \quad (4.34)$$

$$Y = \frac{0.45 + 1.8 \cdot SR_{cd,min}}{1 + 1.8 \cdot SR_{cd,min} - 0.3 \cdot SR_{cd,min}} \quad (4.35)$$

Where $SR_{cd,min}$ is the minimum compressive stress ratio, $SR_{cd,max}$ is the maximum compressive stress ratio. The stress ratio SR_{cd} can be calculated as:

$$\gamma_{ED} \cdot \frac{\sigma_c \cdot \eta_c}{f_{cd,fat}} \quad (4.36)$$

σ_c is the installed compressive stress, η_c is an averaging factor for concrete stresses in the compression zone considering the stress gradient (1.0) and $f_{cd,fat}$ is the design fatigue strength that can be calculated as:

$$f_{cd,fat} = 0.85 \cdot \beta_{cc}(t) \cdot \left[f_{ck} \cdot \left(1 - \frac{f_{ck}}{25 \cdot f_{ck0}} \right) \right] \cdot \frac{1}{\gamma_{c,fat}} \quad (4.37)$$

In which, f_{ck} is the characteristic compressive strength of concrete, f_{ck0} is the reference characteristic strength of 10 MPa, $\gamma_{c,fat}$ is a partial safety coefficient (1.25) and $\beta_{cc}(t)$ is a variable dependent on the age of concrete, which is equal to 1 for a 28 day aged concrete.

One of the main goals of the thesis is to predict concrete cracks on the concrete slab track during its lifetime, and since the loss of stiffness to assess the crack width evolution is caused by the induced tensile stress. The HI-Track includes tension-compression, compression-tension or pure tension sequences, being the first the most severe case. For compression-tension load sequences, stress loads with $\sigma_{cm} \leq 0.026 \cdot |SR_{td,max}|$, the fatigue can be calculated as:

$$\log(N) = 9 \cdot (1 - SR_{td,max}) \quad (4.38)$$

For pure tension and tension-compression with $\sigma_{cm} \geq 0.026 \cdot |SR_{td,max}|$, the expression is:

$$\log(N) = 12 \cdot (1 - SR_{td,max}) \quad (4.39)$$

Where $SR_{td,max}$ is the maximum tensile stress ratio, represented by the quotient between the installed tensile stress $\sigma_{t,max}$ and $f_{td,fat} = f_{ctk,005}/\gamma_{c,fat}$

The fatigue analysis of reinforcement bars is not taken into account in the HI-Track model, since this is a rare occurrence for slab tracks due to their supported nature by the subgrade. With the defined fatigue life for certain stress levels, the cumulative concrete damage is calculated using the Palmgren-Miner method:

$$D = \sum_{i=1}^{N \text{ amplitudes}} \frac{n_{si}}{N_{Ri}} \quad (4.40)$$

Where D is the fatigue damage, n_{si} is the number of acting stress cycles at a particular stress range i and N_{Ri} is the number of resisting cycles (fatigue life) for the same stress range i . The cumulated damage in the concrete zone should be less than D_{lim} , usually established at 1, yet could be lower.

From Figure 4.18, one can notice the nonlinearity of the accumulated damage in the slab track with different shifts of track stiffness. Nodes 1 and 2 reach the damage threshold rapidly since their location matches the anchorage of the prestressed tendons, being the tensile generated stresses due to the Poisson effect the main cause of premature damage. Damage in nodes 3 and 4 is mostly derived from flexural stresses, with a more severe case for node 3 that is immediately under the load alignment. Nodes 5 and 6 are localized near the support/ slab joint and more susceptible to weather events, particularly temperature gradients that cause a loss of stiffness in the top of the slab, represented by the decreasing rate of additional damage. On the other hand, node 7 is not significantly affected by damaging actions (temperature and vehicle loads) when compared with other nodes. Overall, during slab track's lifetime, it can be observed that damage accumulation accelerates in each year. This corroborates the loss of stiffness in more heavily loaded zones, that is shifted to less requested zones, as is the case of node 7.

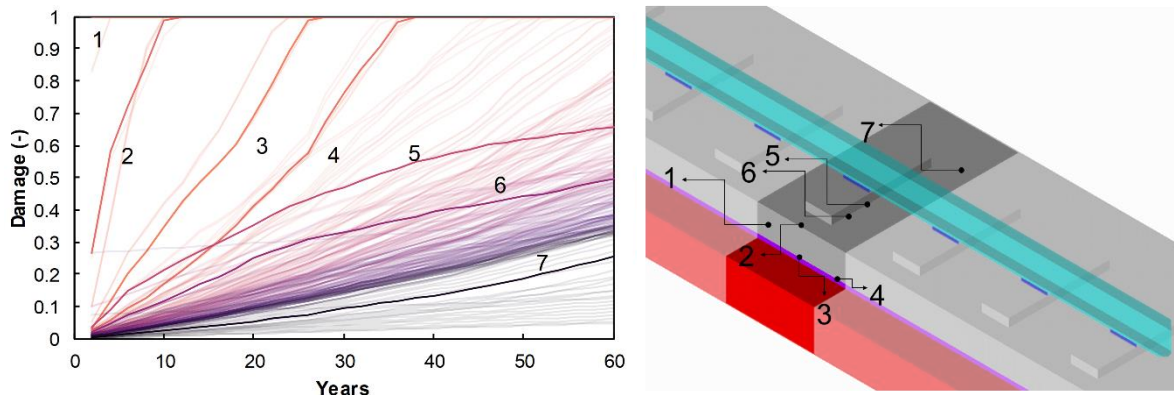


Figure 4.18: Cumulative concrete damage (left) in each node of the sleeper module (right)

Regarding the stress criterion, and since uniaxial stress could lead to over-simplistic results, the HI-Track uses a multi-axial criterion using all three principal stress directions to pitch the most unfavourable scenario for fatigue analysis in each node.

The fatigue life associated with each stress cycle is calculated as the $N_j = \min(N_I, N_{II}, N_{III})$ being N_I , N_{II} and N_{III} the fatigue life associated with the principal stresses in each major direction. Namely, the accumulated damage will be caused by the highest amplitude direction that is the main driver for fatigue progression in concrete-like materials.

Besides, due to temperature loads, there is a daily fluctuation of the vehicle induced stresses, causing load cycles to have distinct amplitudes. To calculate a fatigue damage equivalence of each load cycle, the rainflow algorithm is applied and transform the daily stress cycles into equivalent stress ranges with constant amplitude. With these approaches, the effect of temperature-induced stresses can be included in the fatigue analysis.

4.5 CONCLUDING REMARKS: HIGHLIGHTS AND LIMITATIONS

A set of technical requirements have been defined as the main goals for this thesis; the most relevant of which is the conception and development of a long-term train/ slab track deterioration model. This hybrid model can calculate the track deterioration status of the track (track settlement, concrete fatigue, and crack width evolution) and update the track properties along with the serviceability life.

Unlike the previously presented DL-Track and SP-Track, the HI-Track does not feature finite element modelling in its core, but an interactive routine for both sub-models, which presented itself as challenging compatibility and architectural task to keep the global model as efficient as possible. This step-wise approach in developing the different phases of the hybrid model lead to improvements and functionalities in the sub-models during development as the static rail levelling computation in the DL-Track and the element stiffness update in the SP-Track. One of the main highlights of the HI-Track model is the modular environment in which it was developed that enables a fast adaptation to other empirical laws, that turned out to be more suitable than current ones used.

Also, the adaptive adjustment of the DL-Track and SP-Track calculations results in a significant reduction in computation time, and therefore the model can aspire to go further spatially and temporally. This adaptive adjustment phase was extensively studied to measure the effects of simulation time steps and properties variation threshold on the final results.

For the proposed goals of the thesis, a week time step for settlement and a bi-daily cycle (maximum and minimum) for temperature variations delivers reasonable results.

Possibly, the major simplification for this methodology is the use of mechanistic-empirical laws to model the deterioration of the track since the inherent uncertainty related to the damage process can lead to low accurate results. Besides that, the stochastic nature of the damage should be present in the modelling process to account for the randomness of the concrete-like fatigue and soil settlement. Nevertheless, in the next chapter, a vastly validation and calibration campaign with experimental trials will be conducted to assess the accuracy of the DL-Track and SP-Track (short-term response) and the HI-track (long-term response).

In summary, the HI-Track makes it possible to emulate the long-term behaviour of slab track concrete deterioration and track settlement as well as the study of mixed traffic scenarios, extreme weather events and track heterogeneities. These scenarios and more are going to be addressed in Chapter 6.

5 NUMERICAL VALIDATION AND CALIBRATION USING EXPERIMENTAL MEASUREMENTS

5.1 INTRODUCTION

As mentioned before, the development of the long-term hybrid model and the short-term sub-models required an in-depth validation and calibration process. This comparison with experimental measurements is crucial to building proper confidence and reliability of the numerical model results, from several experimental campaigns in a laboratory and real field environments (in France, Germany, UK and Spain). A large amount of short- and long-term data on slab track was filtered and statistically post-processed to make the comparison possible.

After the development of this hybrid numerical model and its subsequent preliminary verification and proof of concept, the validation and calibration process can be introductoryly performed by analytical or semi-empirical models. This simple approach is quite useful for preliminary validation of the physical coherence of the model. As an example, the DL-Track model was preliminarily validated by comparing results with a beam on Winkler foundation theory and for SP-Track model with Westgard's slab on elastic foundation theory and Boussinesq theory for soil-halfspace stress bulb calculation.

For more advanced modelling and specific scenarios, proper validation of the model requires experimental measurements. However, this type of experimental data is not commonly found, mainly due to the complexity associated with pre-instrumented tracks, which are very expensive and usually kept in a high level of confidentiality by railway administrations. On top of that, data interpretation can be a hard task due to several factors as statistical uncertainty or

malfuncting sensors. Each case-study is as physically characterized (track properties) as possible and the same is valid for the applied loads (rolling stock and weather properties). To enhance the confidence in the model, a parametric study is carried out in each experimental case study if uncertainty in the track properties is expected within a threshold or limiting values. In each case study, the major performance indicators are evaluated within a confidence interval for an envelope with varying values of several parameters (accelerations, stresses, displacements, etc.), usually by graphical verification (signal amplitude, shape, etc.)

This process after the modelling phase is time-consuming and consists of an interactive feedback loop by parametric and sensitivity computations that further improve the debugging and numerical optimization of the model.

5.2 LABORATORIAL SHORT-TERM VALIDATION: CEDEX TRACK Box

5.2.1 CHARACTERIZATION OF THE EXPERIMENTAL SITE

In 2017, multiple railway infrastructure stakeholders performed several tests with a new slab track prototype entitled 3MB developed by Acciona in the CEDEX track box laboratory in Madrid. The CEDEX track box is 21 m long, 5 m wide, 4 m deep and specifically built to test complete railway configurations under high speed and freight trains for speeds up to 450 km/h. Also, it can perform fatigue tests (1 million cycles, i.e. approximately 1 year of operation in one week). The simulation of the train passage is made by imposing unphased loads by 6 hydraulic actuators (3 per rail) placed 1.5 m apart as a function of train velocity (max. 250 kN at 50 Hz).

The experimental section is illustrated in Figure 5.1 and represented by a typical upper and lower embankment, formlayer and subballast layer that was assembled for previous tests in ballasted tracks.

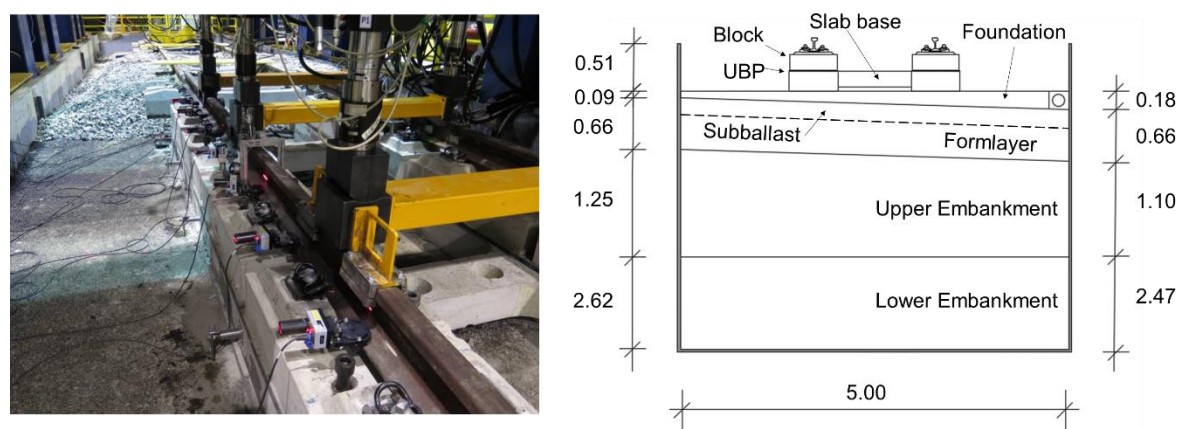


Figure 5.1: Cross section of the 3MB prototype (left) and the track instrumentation (right) present in the CEDEX track box

The upper and lower embankment is a 1.15 m deep clayey sand ($c_s=200$ m/s) and a 1.35 m clayed gravel ($c_s=300$ m/s) respectively. The formlayer is made of well-graded gravel mixed with sand ($c_s=400$ m/s).

The slab foundation is a bituminous layer with a thickness between 9 and 18cm and acts as a levelling layer for the slab track superstructure. The new prototype is a ladder-type slab track (Figure 5.2) with 4 blocks each side to adjust the rail levelling. Each block comprises two rail supports spaced 0.6 m. Detailed dimensions are presented set in Figure 5.2. In the slab interface, an elastomeric layer mitigates the vibration transmitted to the slab. This modular arrangement allows for an easy correction of the track geometry as well as a quick repair and renewal in case of an accident.

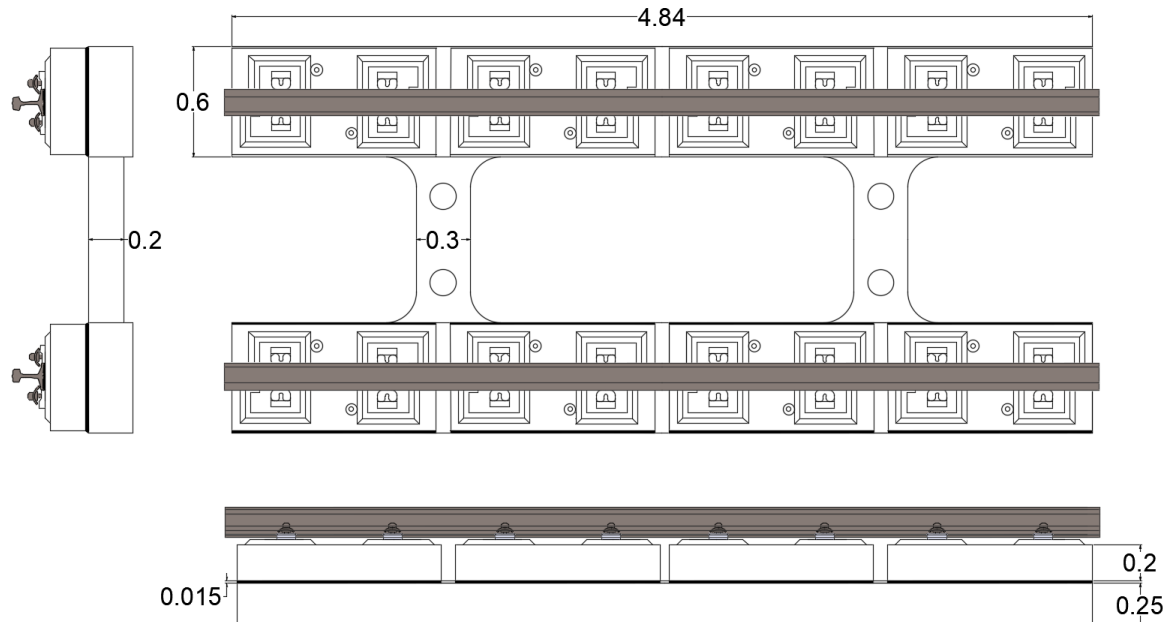


Figure 5.2: 3MB slab track prototype representation

The fastening system is placed into specific holes in the blocks that are filled with cement (Figure 5.3) and a 10 mm railpad with a 35 kN/mm nominal stiffness and a 60EI rail type with a flexural stiffness EI of 6.4155 MNm².

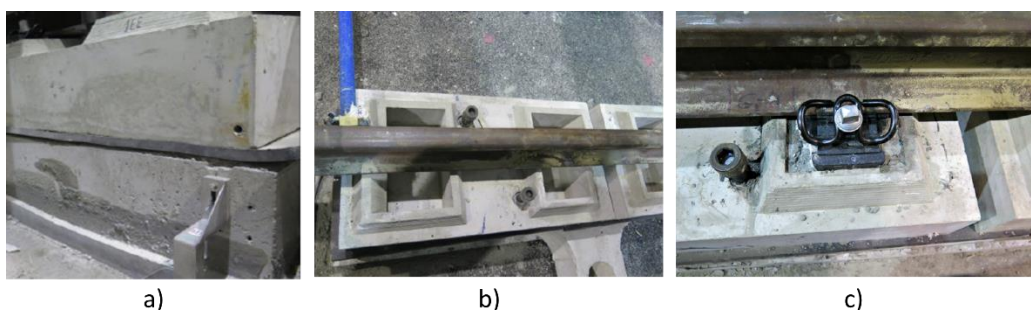


Figure 5.3: 3 MB slab track assembly. a) UBP between the blocks and the CSL. b) Block holes to be filled with cement. c) Installation of the fastening system

The superstructure was manufactured in a controlled environment, therefore its properties were carefully specified and confirmed by testing. On the other hand, the mechanical properties on the substructure are somewhat uncertain. To perform tests on this prototype, the previously tested track configuration (ballasted track) was disassembled and this may have caused

disturbances on the level of soil compaction. Moreover, this also led to the presence of reminiscent subballast layer below the new slab track. The stiffness evaluation of the platform was done through dynamic load tests using a 300 mm diameter plate. This evaluation of stiffness was performed during the construction of the substructure (before the fatigue test). The properties used for modelling are presented in Table 5.1.

Table 5.1: Mechanical properties of the CEDEX track box ballasted track

Element	Mechanical Properties				Geometry
	E / K_p	ν	ρ	ξ	
Rail	200 GPa	0.3	78.5 kN/m ³	0.01	UIC60
Railpad	20/35* kN/mm	-	-	60 kN·s /m	-
Block	15-30 GPa	0.2	25 kN/m ³	0.05	1.15×0.6×0.20
UBP	0.1-0.25 N/mm ²	0.4	20 kN/m ³	0.1	1.15×0.6×0.015
CSL	15-30 GPa	0.2	25 kN/m ³	0.05	$h_{CSL}=0.20$ m
Foundation	50-150 MPa**	0.3	21.5 kN/m ³	0.01	$h_f=0.18$ m
Subballast	50-250 MPa**	0.3	22.3 kN/m ³	0.01	$h_{sub}=0.12$ m
Formlayer	100 - 400 MPa**	0.3	21.5 kN/m ³	0.01	$h_{fr}=0.54$ m
Upper embankment	100 - 400 MPa**	0.4	20.2 kN/m ³	0.01	$h_{emb1}=1.25$ m
Lower embankment	100 - 400 MPa**	0.4	20.2 kN/m ³	0.01	$h_{emb2}=2.57$ m

*Dynamic stiffness

**Aside from the parametric analysis due to the uncertainty of the subgrade layers, the typical stiffness values for the foundation, subballast, formlayer, upper and lower embankment are averagely 80, 170, 165, 160 and 160 MPa respectively.

The prototype was extensively instrumented with potentiometers (relative displacement), LVDT's (absolute displacements), geophones and accelerometers in several positions of the track (rail, block, slab, subballast) with a multitude of static and dynamic tests. Before the starting of any test, 80 000 cycles at 5.5Hz and 20 000 cycles at 3Hz in all actuators were performed to stabilize the track at a simulated speed of 90 km/h.

The static tests were performed with a very slow pace loading aiming at the calculation of the track stiffness. Only the central actuator tests were used for validation, since edge actuators highlight the boundary effect of the slab, leading to significantly lower track stiffness. The dynamic tests were organized at different speeds by the simulated train passages from 40 to 400 km/h.

In what regards the simulated vehicle, the type of train is an EC vehicle type 4 (CEN, 2004a), which is quite similar to the TGV vehicle used in the French high speed lines, whose properties are shown in Table 3.1. Additionally, freight train circulations were tested from 40 to 200 km/h with an axle load of 250 kN, with the EC vehicle type 11.

5.2.2 DL-TRACK AND SP-TRACK NUMERICAL RESULTS

The first step to validate the sub-models DL-Track and SP-Track was to build the geometry and properties defined in Table 5.1, Figure 5.2 and 5.3, to create a finite element version of the 3 MB slab track prototype (Figure 5.4).

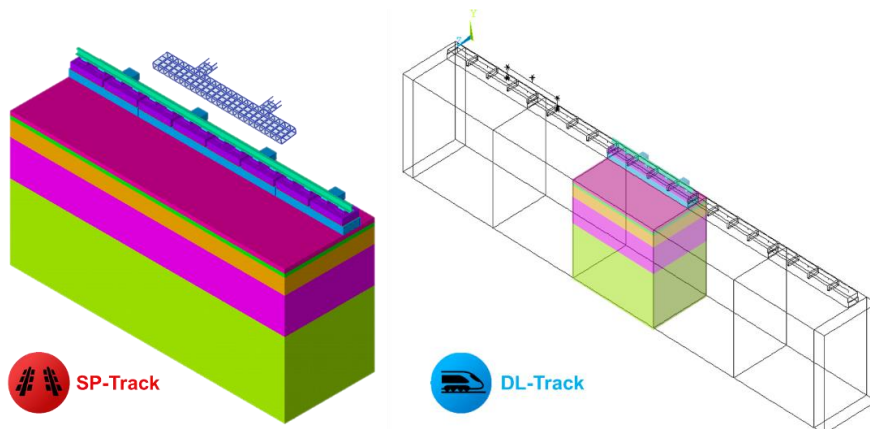


Figure 5.4: SP-Track (left) and DL-Track (right) models of the CEDEX 3MB case study

Although not necessary at this stage (short-term validation), the nonlinear behaviour of the long-term effect on slab tracks is still present as well as the brittle behaviour of the concrete and the bilinear reinforcement model. The length of SP Track is of two panels (1 panel + 2 halves) and the out-of-plane displacement and rotation of end, bottom and outer edge boundaries are restricted, except for the inner edge, which is modelled with a symmetry condition. The static test I was realized in the outer rail with a 150 kN load in each actuator (the maximum load by a 300 kN axle freight train) at a rate of 0.5 kN/s. Figure 5.5 represents the comparison between the experimental static tests and the SP-Track calculations. The calculated vertical displacement for a vertical stiffness of approximately 70 kN/mm is very similar ($|K_{exp} - K_{num}|/K_{num} < 2\%$) to those observed experimentally. To simulate track stabilization, 100 k cycles were applied and this increased the track stiffness to 90 kN/mm - this is probably caused by the elimination of loose clamps in the fastening system at the installation (which could change the original static stiffness of 35 kN/mm). The further away from the loading point (central actuators), the larger the displacement deviation from the SP-Track model and the theoretical approach by Zimmermann (70 kN/mm), since the boundary effects on the rail are not entirely free nor fixed. In the CEDEX track box case, the rails have an additional ordinary concrete sleeper attached that limit the rail rotation but not entirely restrains it (Figure 5.6)

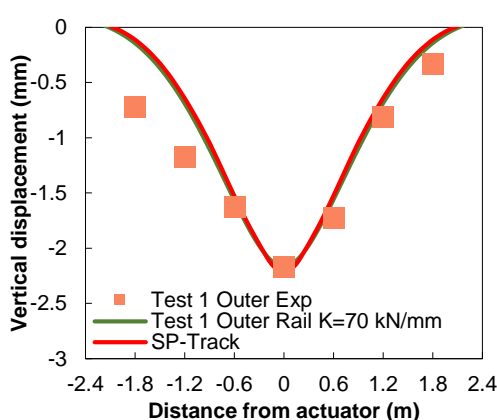


Figure 5.5: Numerical, theoretical and experimental results of 3MB static test for a 150 kN wheel load



Figure 5.6: 3MB static test setup with additional sleepers attached to both ends of the rail

The dynamic validation of DL-Track was far more detailed for the 3MB case study to assess the vibratory behaviour of the track. The major indicators that are going to be used for comparison of the DL-Track dynamic output and the dynamic tests performed in the CEDEX Track box are rail, block, and slab accelerations/ displacements. The DL-Track model will adopt a superelement size of 8 sleepers given the convenience of the 3MB module size and the total length of the track is 24 m (5 modules). This length was the result of an iterative process to achieve a steady-state regime of the vehicle/ track interaction.

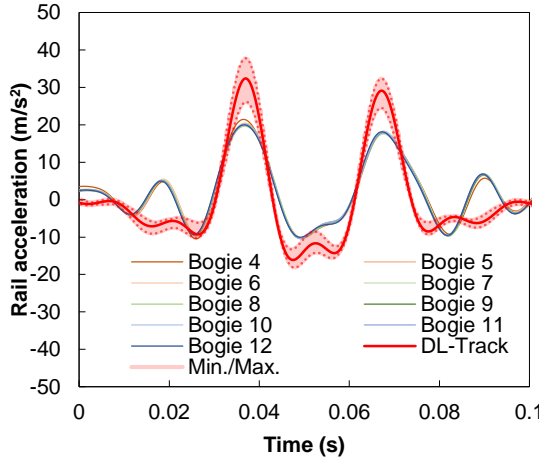


Figure 5.7: Rail acceleration comparison between DL-Track and experimental results for the 3MB case study (360 km/h)

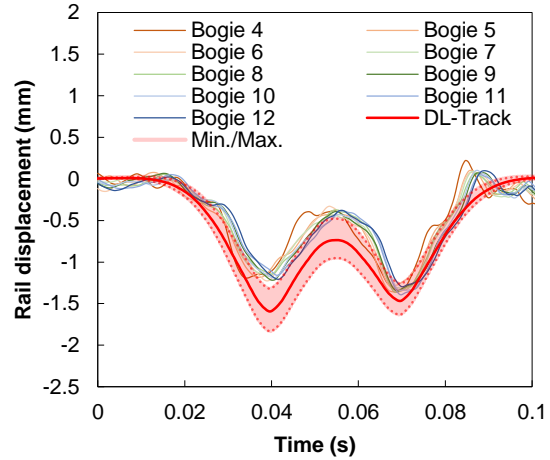


Figure 5.8: Rail displacement comparison between DL-Track and experimental results for the 3MB case study (360 km/h)

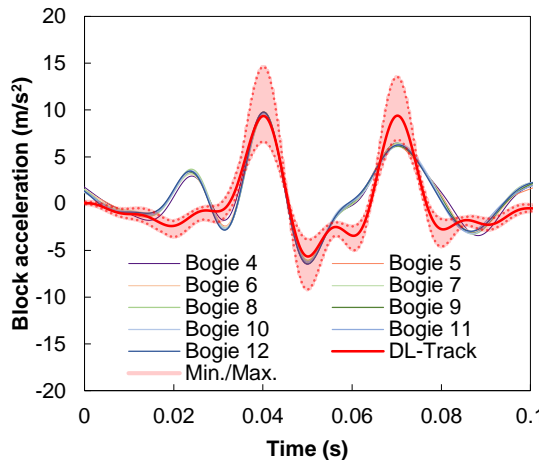


Figure 5.9: Block acceleration comparison between DL-Track and experimental results for the 3MB case study (360 km/h)

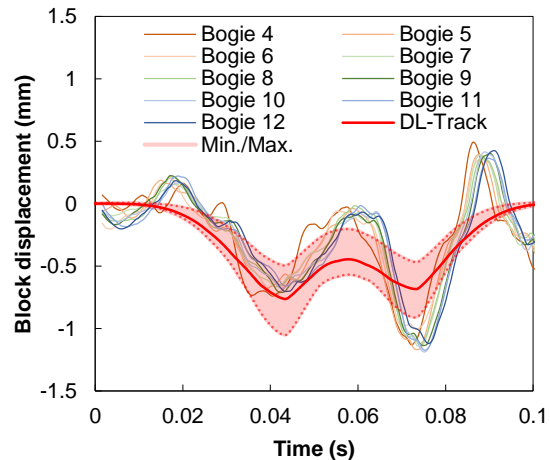


Figure 5.10: Block displacement comparison between DL-Track and experimental results for the 3MB case study (360 km/h)

According to the results displayed in Figure 5.7 to 5.12, the accuracy of the model is low for rail accelerations, with a tendency to overestimate the maximum values ($\approx 20 - 80\%$) for a 100 Hz low-pass filter. The simplified modelling methodology of the rail and railpad (as well as the likely higher stiffness of the railpad) may contribute to this lack of precision. Nevertheless, the model estimates the magnitude order of the acceleration accurately. Regarding rail displacements, the model predictions are also overestimated, again probably due to the likely increase of track

stiffness between the first cycle (70 kN/mm) and the dynamic stabilization (90 kN/mm) since the proportion between the numerical and experimental simulations is similar to the track stiffness ratio respectively.

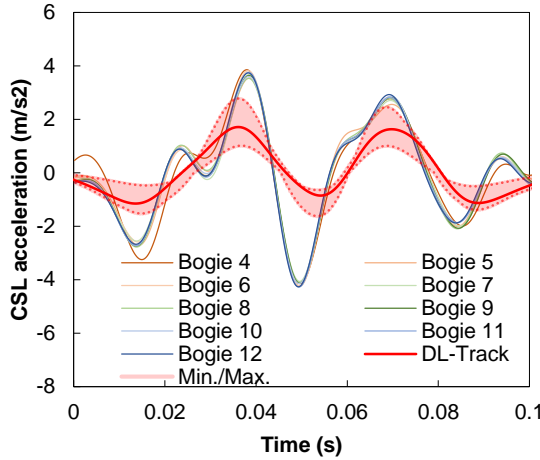


Figure 5.11: CSL acceleration comparison between DL-Track and experimental results for the 3MB case study

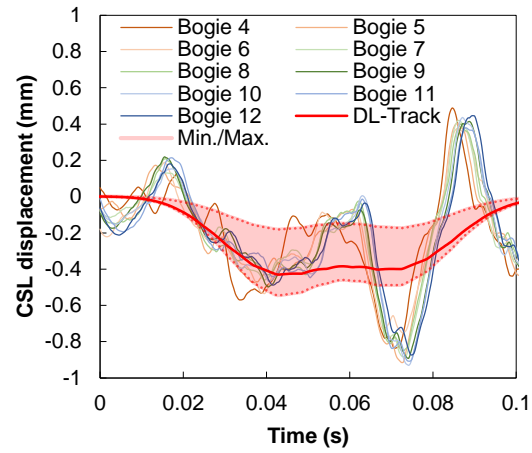


Figure 5.12: CSL displacement comparison between DL-Track and experimental results for the 3MB case study

The dynamic validation and calibration will be centred around the block and concrete slab. A more specific study on the influence of the inherent material uncertainty t is also made. This study concerns the CSL ($10 - 30 \text{ GPa}$) that could be cracked due to shrinkage and thermal effects, the UBP ($\approx 0.05 - 0.25 \text{ N/mm}^3$) that presents a highly nonlinear behaviour dependent on the elastomer deflection, and a range of soil stiffness variations originated from the load plate tests presented in Table 5.1. The platform layers are organized in an ascending stiffness set from S_1 , S_2 , S_3 and S_4 (all layers have a $E_{v2}=100, 200, 300$ and 400 MPa respectively). Due to the fast computation of the DL-Track, a parametric simulation of over 150 runs can be performed effortless, therefore making an extensive parametric analysis possible.

Figure 5.13 to 5.18, present the peak accelerations (filtered for a 100 Hz low bandpass filter) for block and CSL for different high speed train travelling speeds and freight trains. The influence of the UBP properties mainly affects block accelerations as expected and is the element that has the largest variation (=70%) on the overall dynamic behaviour of the track. Nonetheless, the DL-Track can reasonably predict accurate track accelerations for the block and the CSL. Moreover, CSL properties have a marginal impact on the track dynamic behaviour with less than 5% variation while the soil stiffness has a striking effect on CSL acceleration ($\approx 100\%$). The DL-Track tends to a higher match degree for low stiffness soil that can be explained by a decompaction of the soil during the slab track installation. In general, the DL-Track results show a good correlation with experimental results within a time-domain approach. To further study the vibratory content of the results produced by the DL-Track model, the power spectral density in frequency domain spectra and respective variants are computed and presented in Figure 5.19 to 5.22. Although the artificial representation of the train passage through unphased actuator loads,

the rail frequency spectrum obtained by the numerical model resembles the experimental case with a notorious contribution of the axle spacing ($\approx 30\text{Hz}/3\text{m}$).

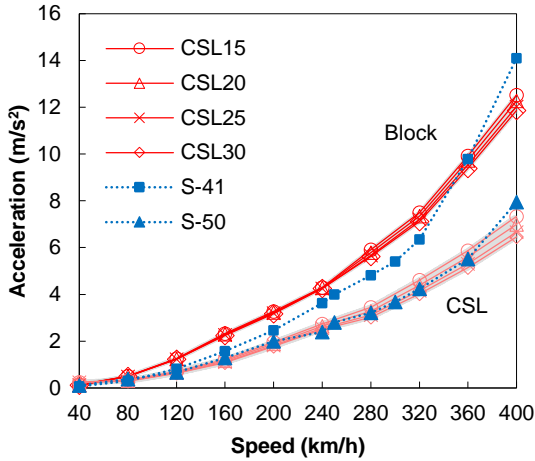


Figure 5.13: Influence of CSL properties and speed on the 3MB slab track accelerations for high speed trains

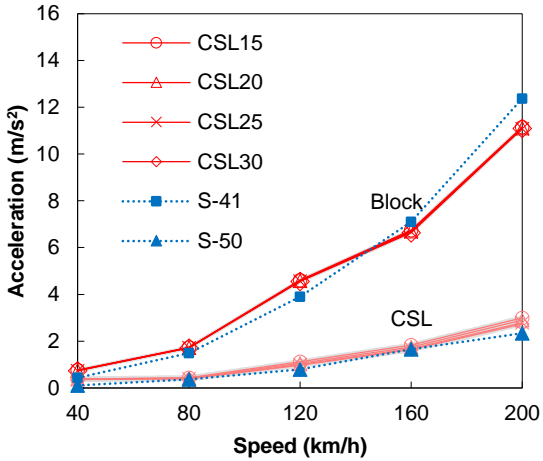


Figure 5.14: Influence of CSL properties and speed on the 3MB slab track accelerations for freight trains

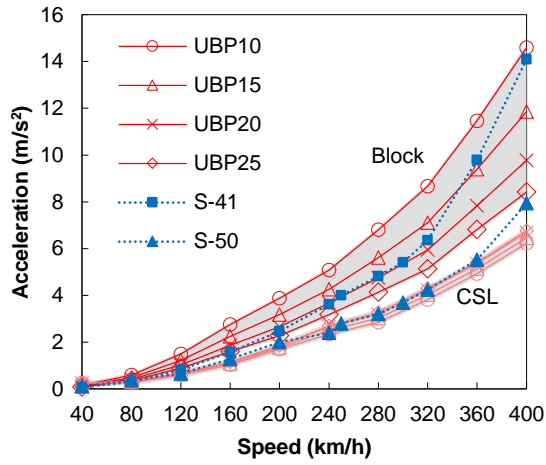


Figure 5.15: Influence of UBP properties and speed on the 3MB slab track accelerations for high speed trains

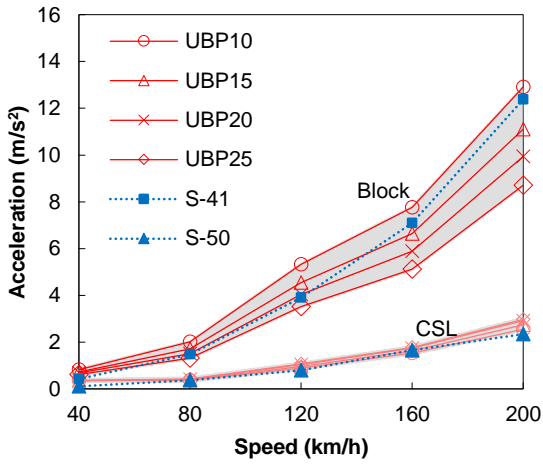


Figure 5.16: Influence of UBP properties and speed on the 3MB slab track accelerations for freight trains

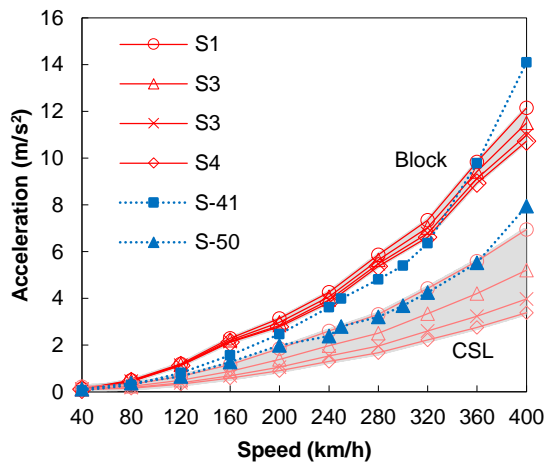


Figure 5.17: Influence of platform properties and speed on the 3MB slab track accelerations for high speed trains

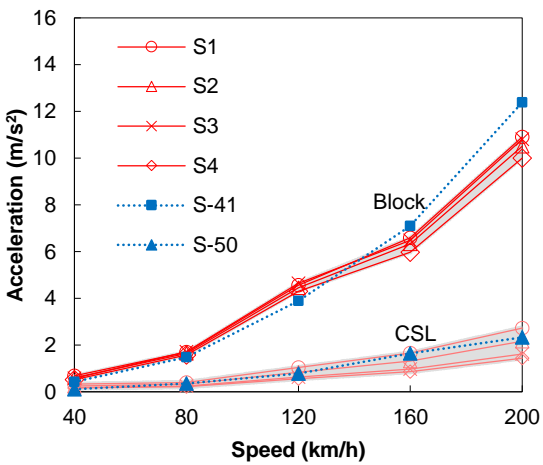


Figure 5.18: Influence of platform properties and speed on the 3MB slab track accelerations for freight trains

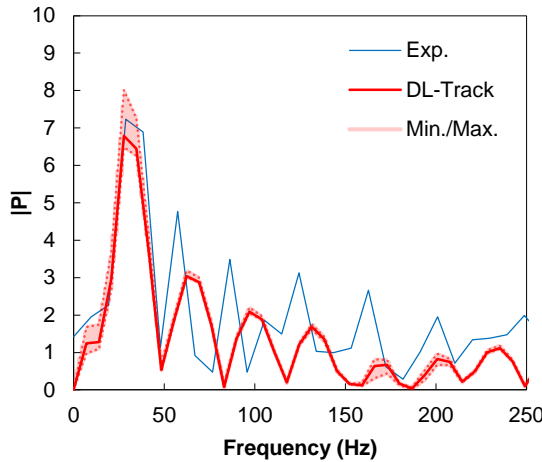


Figure 5.19: Frequency domain of experimental and numerical 3MB rail accelerations for a high speed train circulating at 360 km/h

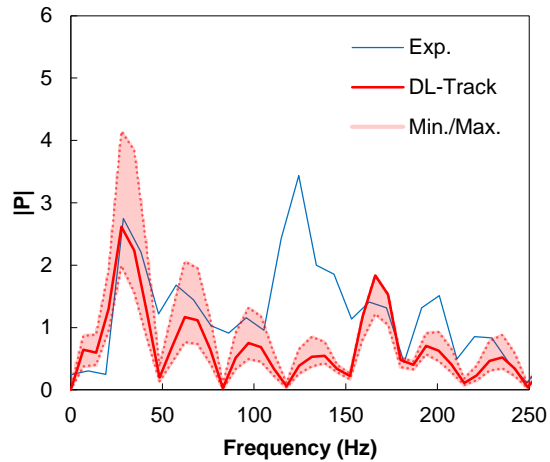


Figure 5.20: Frequency domain of experimental and numerical 3MB block accelerations for a high speed train circulating at 360 km/h

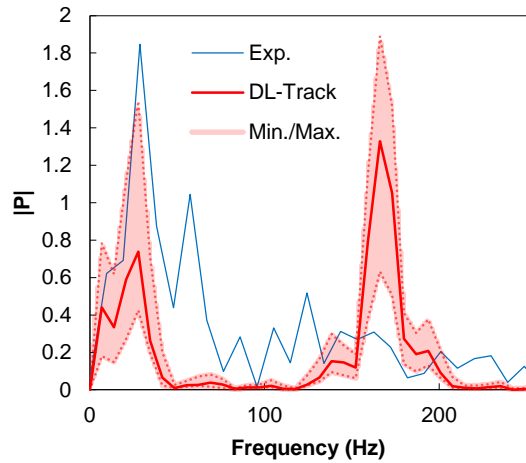


Figure 5.21: Frequency domain of experimental and numerical 3MB CSL accelerations for a high speed train circulating at 360 km/h

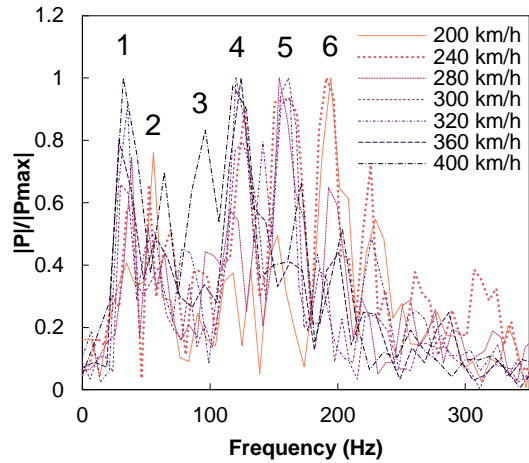


Figure 5.22: Normalised frequency domain of experimental 3MB block accelerations for a high speed train

Aside from the time history signals validation, the frequency content of both numerical and experimental shall be address to assess the limitations of these methods. From Figure 5.19 to 5.21, the frequency power spectral density of rail, block and CSL accelerations are shown with experimental and numerical results. The numerical results are presented with the confidence range previously addressed.

The spectrum of rail frequency is in a relatively good agreement between numerical and experimental measurements, with numerical peaks matching the experimental ones with reduced deviations. The block system shows a meaningful contribution of the 120 Hz modal frequency behaviour ($\approx 0.8\text{om}$), particularly associated with the block end to 2nd sleeper frequency (4) that is not captured by the numerical model. Nonetheless, this observation may have been caused by a laboratorial phenomenon related to the actuators, which may have been captured depending on the position of the accelerometers installed the block and on their

sensitivity to this second (observed) sleeper frequency. The frequency spectrum of the concrete slab shows two major contributions in the DL-Track results by the axle (≈ 33 Hz) and the sleeper (≈ 167 Hz). The latter was not captured in the experimental results. This is mainly due to the effect of the absence of wheel rolling in the experimental setup. The use of hydraulic actuators 1.5 m apart cannot fully simulate the wheel passage and load effect in each sleeper. This is one of the limitations of experimental test rigs regarding track infrastructure. In Figure 5.22, the normalization of the frequency power spectral density is computed for different train speeds, in which is possible to notice the influence of the track geometry as wavelength sources (Table 5.2 and Figure 5.23) for the modal behaviour of the track. This characterization helps to clarify the effect of the actuator frequency and configuration on the experimental setup. In Figure 5.21 this phenomenon is well described with an absence of the actuator frequency in the numerical results and the sleeper frequency in the experimental measurements. For the CSL, the actuator loading highlights frequencies around 67 Hz, while the rolling wheel loading excites the track primary at the sleeper wavelength range (167 Hz) for a train speed of 360 km/h. In this respect, the frequency range under study should be carefully assessed for an accurate representation, yet for the proposed goals of this thesis, the DL-Track results look promising.

Table 5.2: Modal frequencies of the 3MB by the passage of a train

Mode	Wavelength (m)	Frequency (Hz)
Axle (1)	3	33
Actuator (2)	1.5	67
Block (3)	1.2	83
Block end to 2 nd sleeper (4)	0.8	125
Sleeper (5)	0.6	167
Block end to 1 st sleeper (6)	0.5	200

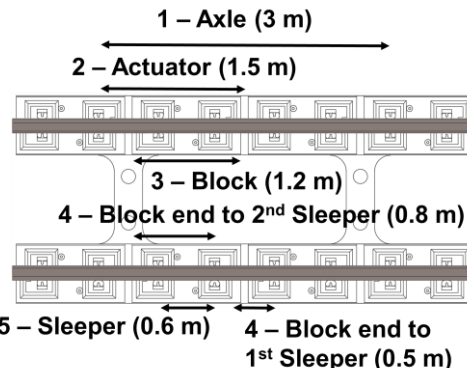


Figure 5.23: Wavelength sources in the 3MB case

5.2.3 LONG-TERM PRELIMINARY RESULTS

For a preliminary validation of the long-term model, the 3MB prototype was included in the HI-Track model for the long-term study of concrete slab tracks. For these simulations, the length of the dynamic model was increased to 9 superelements (72 sleepers) and the nonlinear model SP-Track kept the 16 sleepers (one module plus two halves at each end to simulate real traffic operation. In this simulation, 90 daily TGV type trains were used during the 60 years used in modelling, which corresponds to the lifespan of the slab track. The dynamic amplification is triggered by an initial soil settlement of 1 mm for a 20 m chord. Since atmospheric phenomena are not yet included in this version of HI-track, the empirical law adopted for permanent soil deformation used is the one proposed by Li and Selig (1996):

$$\varepsilon_p(\%) = a \cdot \left(\frac{\sigma_d}{\sigma_s} \right)^m \cdot N^b \quad (5.1)$$

In which sigma σ_d is the soil deviatoric stress, σ_s is the compressive strength of the soil, N is the number of load cycles and a , b and m are soil parameters, according to soil types presented in Table 5.3:

Table 5.3: Model parameters for the empirical soil settlement law proposed by Li and Selig (1996)

Model parameters	Lean Silt (QS3)	Heavy Silt (QS2)	Lean Clay (QS1)
a	0.64	0.84	1.1
b	0.1	0.13	0.16
m	1.7	2.0	2.0

Figure 5.24 and 5.25 present the cumulative evolution of soil settlement in a 3MB slab track system for 60 years. The modular effect on the longitudinal settlement of the soil gets worse over time (sleeper 23, 31, 39, 47). The main reason for this finding is the lack of mechanical connection between panels, which causes this systemic deterioration - this is a design flaw that should be addressed in detail in future improvements. It should be noted that this numerical test is a proof of concept to show that the HI-Track can model the physical coherence of train track interaction and soil settlement. Figure 5.26 shows the final longitudinal settlement for 60 years for different soil types and different speeds.

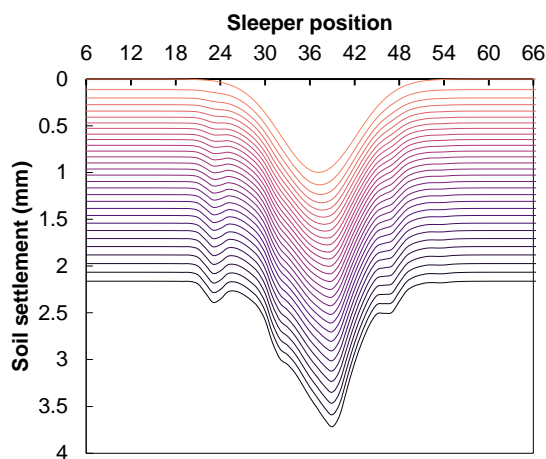


Figure 5.24: Longitudinal rail levelling evolution during 60 years of operation

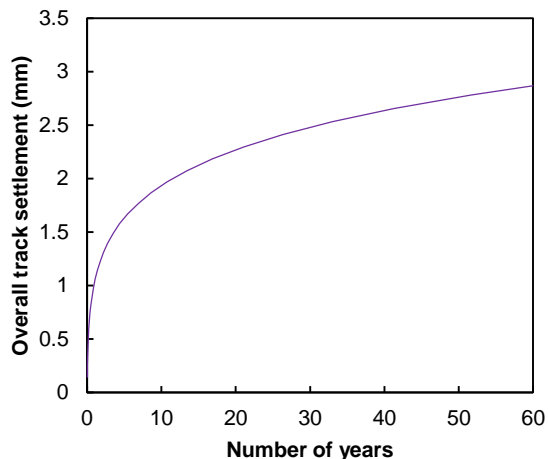


Figure 5.25: Maximum settlement of the soil during 60 years of operation

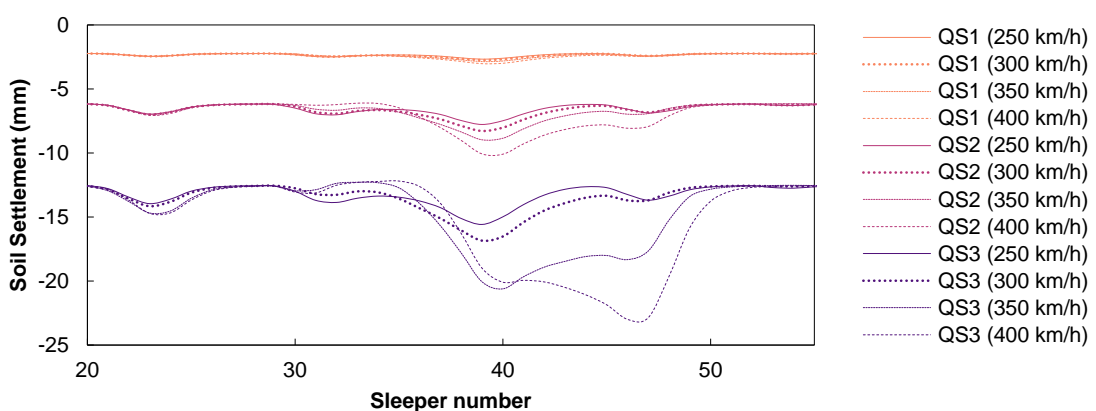


Figure 5.26: Cumulative plastic soil settlement for different train speeds and soil types

The effect of train velocity is well-captured by the HI-Track model using polynomial growth. Also, the heterogeneity of the track is observed by its effect on the evolution of the downstream settlement - i.e. the settlement pattern after the initial defect that increases dramatically even more by the influence of speed and soil quality.

Likewise, the proof of concept for long-term concrete damage was also made using the Model code (2010) approach being the results presented in Figure 5.27. The platform soil used was a QS3 soil as the worst-case scenario.

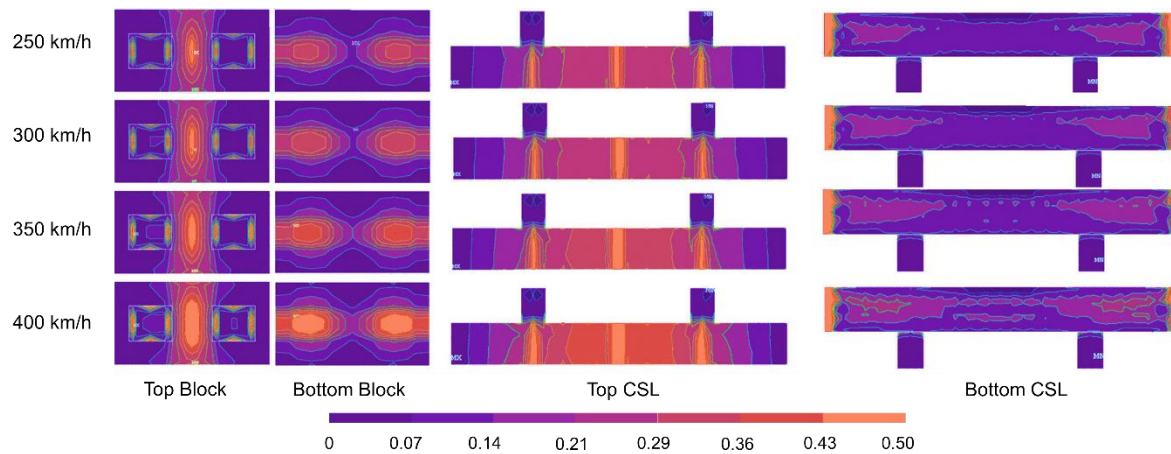


Figure 5.27: Concrete damage on the 3MB slab track (blocks and CSL base) after 60 years of traffic operations for different speeds

The top block shows the shear stress fatigue in the centre of the block and the bending stresses at the bottom under each support – bending and shear stresses increases with higher speed and lower bearing capacity of the soil. In the concrete slabs, the damage caused by shear stresses from the individual blocks can be noticed, as well as the asymmetry of the damage pattern. This is due to the train/track interaction after the initial defect and therefore different sleeper reactions longitudinally. The lower bottom surface of the track is not affected by the bending effect of the slab due to its structural layout. The assembly of blocks and the absence of a mechanical link between panels reduce bending stresses in the concrete slab.

5.3 FIELD SHORT-TERM VALIDATION

5.3.1 CHAUCONIN CASE STUDY

The experimental section carried out in the Chauconin transition zone is a ballasted – slab track transition located in the LGV-Est Européene between Paris and Strasbourg (Figure 5.28). This experimental campaign was conducted by the French operator SNCF, who collected performance measurements in: i) different types of railway track (ballasted and ballastless); ii) the transition zone (displacements and accelerations) with the passage of real train compositions (TGV Réseau UM and MS).



Figure 5.28: LGV-Est high speed line (left) and Chauconin transition site (right)

This LGV high speed line does not require the construction of numerous viaducts or tunnels and almost of its entire length is in ballasted track, except for a 2 km experimental section of slab tracks close to the city of Meaux. The construction of this experimental section was proposed by SNCF to RFF (Réseau Ferre de France) aiming to study and acquiring experience in railway slab tracks. The French patented Stedef slab track system was used. This system is characterized by a two-level elastic adjustment with an easy replacement of the biblock sleepers and two-staged concrete slab pouring. The track grid is similar to that of the ballasted track of the same line (UIC60) and it was used a Pandrol Fastclip fastening system with a 90 kN/mm vertical stiffness railpad. The main difference in the track grid lies on the bi-block sleeper (SATEBA D453IP). To reach the same track elasticity that is guaranteed by the ballast layer and subballast, the biblock sleeper is encased by an elastomer capsule that contains the second elastic level with an under sleeper pad (USP) with 25 kN/mm at the bottom. This elastomer capsule is embedded in a layer of fibrous filler concrete that fills the previously casted trench-shaped concrete slab (Dieleman et al., 2008).

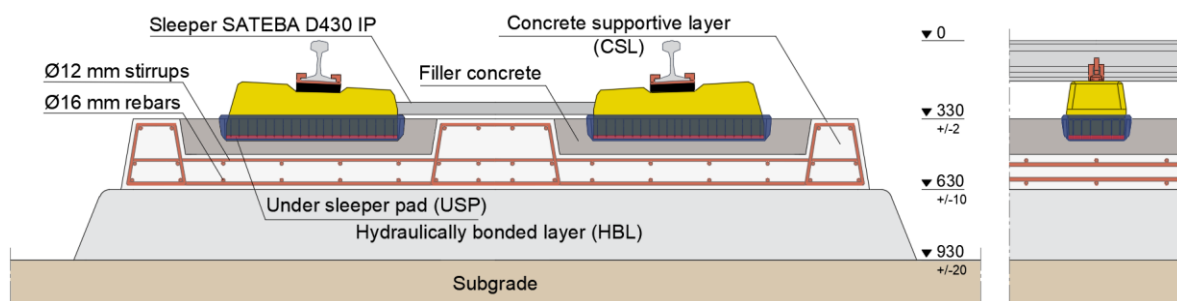


Figure 5.29: Scheme of the Stedef system used in Chauconin case study (units in mm)

The first stage of concrete pouring (C25/45 strength class) uses a paving machine in the form of a trench which will serve as support for the second stage of pouring. The longitudinal and transversal reinforcement contains a polyurethane waterproofing screen to prevent water infiltration and consequent reinforcement corrosion. The second stage of concrete pouring uses a C30/37 propylene fibre reinforcement concrete (density of fibres of 900 g/m³ of concrete) -the positioning of rail and sleeper is adjusted in this pouring. Lastly, there is a hydraulically bonded layer, whose function is to ensure the durability of the entire structure.

For rolling stock operation at the LGV-Est in circulation on the slab track section, TGV-Réseau (SNCF) and ICE (DB) operate, yet the measurements recorded are only those corresponding to TGV-Réseau movements. The TGV-Réseau US (Unité Singulière) has 10 coaches (double in case of the MS-Unité multiple) with a spacing of 14 and 18.7 m between bogies for the motor coaches and passenger coaches. The rolling stock data is presented in Table 3.1. Figure 5.29 and Table 5.4 show the track properties provided by the research department of SNCF used for the modelling.

Table 5.4: Geometrical and mechanical properties of the Stedef slab track system present in the Chauconin case study

Element	Mechanical Properties				Geometry
	E / k_p	v	ρ	ξ	
Rail	200 GPa	0.3	78.5 kN/m ³	0.01	UIC60
Railpad	90/120* kN/mm	0.25	9 kN/m ³	60 kN·s /m	290×150×9 mm ³
Sleeper	43 GPa	0.2	25 kN/m ³	0.05	731×296×210
USP	21/35* kN/mm	0.4	20 kN/m ³	0.1	731×296×12 mm ³
CSL 1 st phase	38 GPa	0.2	25 kN/m ³	0.05	$h_{CSL1}=0.15$ m
CSL 2 nd phase	34 GPa	0.2	25 kN/m ³	0.05	$h_{CSL2}=0.092$ m $A=903$ mm ²
Steel bracket	200 GPa	0.3	78.5 kN/m ³	0.01	$I_z = I_y = 461\ 000$ mm ⁴ $J=922\ 000$ mm ⁴
HBL	23 GPa	0.2	20 kN/m ³	0.01	$h_{HBL}=0.281$ m
Embankment	100 MPa	0.3	18 kN/m ³	0.01	$h_{emb}=4$ m

After the FE model assembly (DL-Track and SP-Track) and the iterative sensibility analysis for the size and mesh of each model, which result in a 40-sleeper dynamic model and a 21-sleeper model for the static SP-Track modelling. Since only the validation of short-term responses is envisaged for this case, the SP-Track will use a dual symmetry simplification at the axle of the track and the load axis, since no heterogeneities are taken into account. The final versions of the sub-models are presented in Figure 5.30. Every element is modelled as described in Chapter 3, except for the steel bracket module – which is modelled as an Euler-Bernoulli beam in both models.

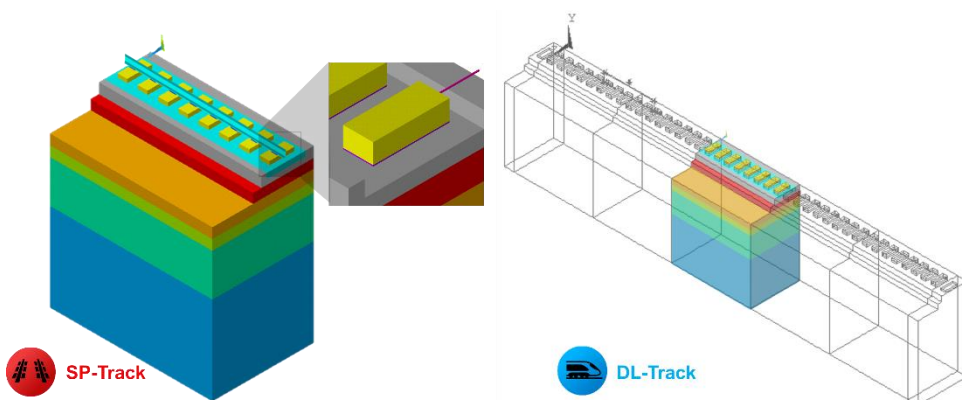


Figure 5.30: SP-Track and DL-Track sub-models of the Chauconin case study

The available data in the experimental slab track section (Figure 5.31) was statistically post-processed to produce a confidence interval from the 5 to the 95 percentile (assuming a Gaussian normal distribution, as well as the average signal amplitude, both for displacements and accelerations). Apart from the DL-Track sleeper acceleration and displacement caused by the

passage of a TGV Réseau train at 230 km/h, a quasi-static EMW vehicle (10 tonnes per axle at 15 km/h) was tested.

The comparisons between the experimental and the numerical results from the DL-Track (TGV) and SP-Track (EMW) are presented in Figure 5.32 and 5.33. The evaluated top sleeper accelerations are unfiltered measurements for a 230 km/h TGV-Réseau passage and show a very good correlation with the experimental measurements with close approximation with the average peak acceleration values. Since time history signals are not available, a time-domain comparison is not possible. Also, the quasi-static displacement (EMW vehicle) and dynamic displacements (TGV) are overestimated in both cases. In the case of the TGV dynamic passage, the results are contained in the confidence interval, however, the EMW results are slightly over the 95% confidence interval. This appraisal leads to a likely lower vertical stiffness of the track than the one simulated by the DL-Track and SP-Track.

Nevertheless, and taking into consideration the inherent uncertainty of the track properties, it can be assumed that both DL-Track and SP-Track can deliver reasonably accurate track accelerations and displacements for real high-speed case studies.



Figure 5.31: Circulation of TGV Réseau trains in the LGV-Est (left), sleeper accelerometers (centre) and potentiometers (right)

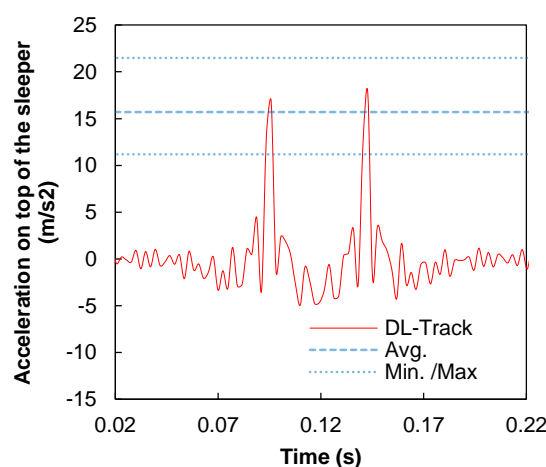


Figure 5.32: Comparison between measured and calculated sleeper accelerations in the Chauconin test site for a TGV train at 230 km/h

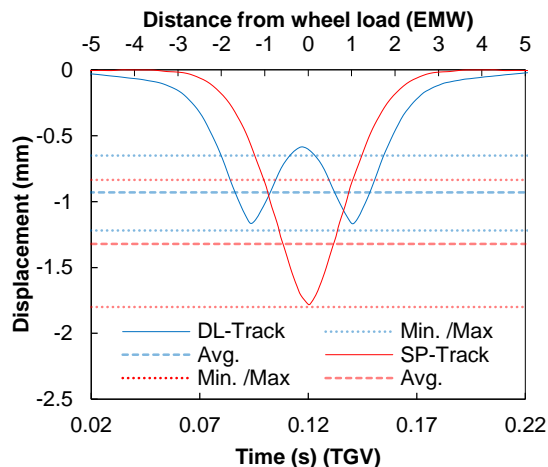


Figure 5.33: Comparison between calculated and measured track displacements for a TGV train at 230 km/h (sleeper) and an EMW vehicle (rail)

5.3.2 BENICASSIM CASE STUDY

In order to create technical assistance for the construction and homologation of concrete slab tracks, the Spanish Ministerio de Fomento, ADIF and TIFSA created a slab track workgroup and built an experimental section between Las Palmas de Castellón and Oropesa de Mar on the Valencia-Tarragona line in 2002 (Figure 5.34). Six types of the most commonly used non-ballasted tracks in Europe were built (Edilon, Rheda Dywidag, Rheda 2000, Stedef, Getrac, ATD) with at least one section in an embankment and another in cutting.



Figure 5.34: Valencia – Tarragona line (left) with Rheda 2000 system (centre) and Stedef system (right)

This experimental campaign was composed of 3 phases, the first of which was a preliminary study in which the necessary information on the different typologies was gathered. The second phase focused on the control and data collection regarding the construction and operation. The last phase consists of processing the data and assess the conclusions employing periodic track inspection. The second phase was divided into 4 experimental campaigns from January 2004 to February 2007 collecting track parameters such as vertical stresses (yy) in the multilayer system, track displacements, reinforcement stresses and strains, vibration and noise.

The numerical validation of the Benicassim case study is only focused on the two elastic level Stedef system and the embedded sleeper system Rheda 2000. The Stedef concrete slab track system used in the experimental trial shows slight differences from the Chauconin case study typology (mainly the reinforcement and CSL thickness) and is presented in Figure 5.35. The first phase concrete uses a C30/37 class strength concrete with a slab thickness of 30 cm (for a total height of 470 mm with the 2nd phase C35/45 concrete pouring) and there is no central block (only one trench for the concrete pouring). The track grid is composed by UIC60 rails, a 90 kN/mm Nabla fastening system, a biblock sleeper U41-GV and a 21 kN/mm under sleeper pad. The concrete reinforcement is made of 24 Ø20 longitudinal rebars equally spaced and Ø16 stirrups with a 400 mm spacing.

The monolithic Rheda 2000 follows the typical construction standards recommended in Chapter 2 and illustrated in Figure 2.5. The concrete slab uses a C35/45 class strength concrete with a 246 mm slab height with embedded B355W60M sleepers. The fastening system is an IOARV 300.1 with a vertical stiffness of 22.5 kN/mm where the vast majority of the systems' elasticity is comprised. Apart from the steel truss of the biblock sleeper, the reinforcement grid is formed by a 20 Ø12 and a Ø12 mm stirrup with a 600 mm spacing.

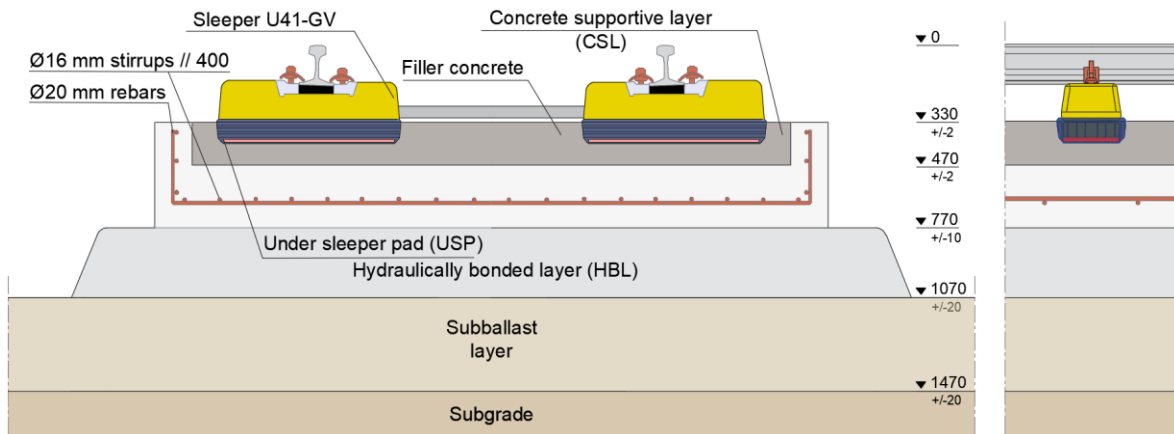


Figure 5.35: Scheme of the Stedef system used in Benicassim case study (units in mm)

Both systems share a 30 cm thick HBL, a 40 cm subballast with a Young modulus of 120 MPa and $\nu=0.25$ (current values for Spanish high speed lines) and a soil platform that has been modelled 4 meters deep and $E_{v2}=80$ MPa and $\nu=0.3$ (minimum recommended value for slab tracks according to the Spanish homologation guidelines). The remaining mechanical properties (rail, sleepers, CSL, HBL, etc) and boundary conditions for this model were assumed as equivalent to previously presented models since no additional data were available. The numerical models developed for this case study are presented in Figure 5.36.

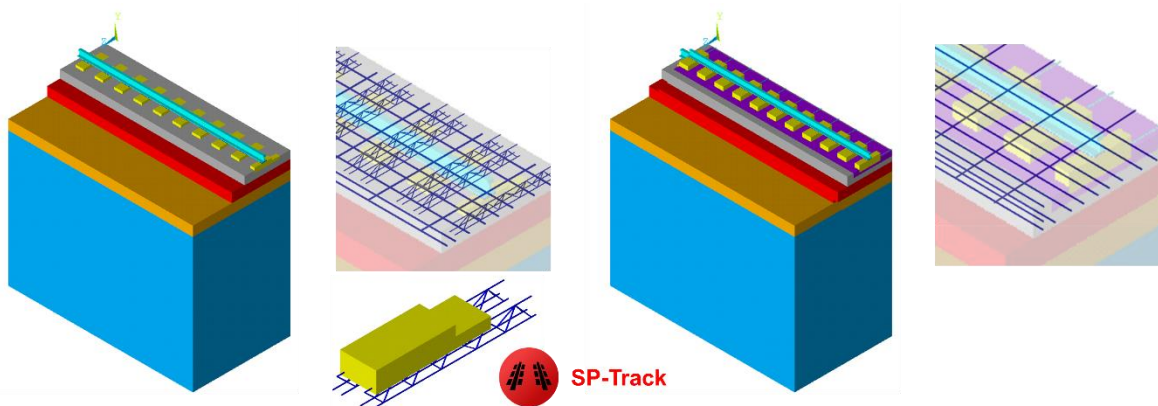


Figure 5.36: SP-Track sub-models representation of the Benicassim case study with the Rheda 2000 system (left) and Stedef system (right)

During these 4 experimental campaigns, the operational traffic was composed by regional (17.2 ton/axle) and freight trains (22 ton/axle) and higher speed trains as the Euromed (17.2 ton/axle) and Arco/ Talgo (17 ton/axle at 230 km/h). In the modelling process, only the circulation of the most conditioning vehicles is considered – this corresponds to the freight and the Arco/Talgo train. Both systems evaluated have sections in cutting and embankment zones, which can affect significantly the substructure stiffness. The assumed embankment section features a 120 MPa subballast and an 80 MPa soil platform, while the cutting system features a 400 MPa subballast and a platform. Moreover, the maximum and minimum measured temperatures are 37.5 and 9.5 °C respectively. Given that there are no time-dependent data regarding the temperature, combinations with the maximum and minimum temperature are added to the simulations. Due

to the fast computational time of HI-Track, multiple combinations are easily implemented and calculated.

Figure 5.37 and 5.38 present the comparison between the results of the numerical hybrid model and the experimental measurements. The experimental measurements are presented as the range of results from the 4 distinct data collection campaigns and the numerical data from the uncertainty linked to material properties. In what concerns track deflection, the HI-Track can guarantee accurate displacement predictions with an adequate degree of detail. The accuracy of the model decreases as the depth of the experimental measurement increases - this agrees with the notion that the modelling of substructure layers is more uncertain in depth. In both systems, stiffer subgrade layers lead to more precise results when compared to the experimental measurements range. This shows that the specific stiffness of the subgrade is higher than the recommended Spanish guidelines. Although not as accurate as of the track displacement, the vertical stiffness can be reasonably predicted at a multilayer level, with every numerical result being predicted between the spectrum of the experimental measurement, except for the HBL-Subballast interface for the Stedef system and the CSL-HBL for the Rheda 2000. Although the stress predictions for the Stedef case in the HBL-Subballast interface are outside the range of experimental results, the calculation is still very close (<10%). Moreover, the spectrum of experimental stresses under the HBL is higher for the Stedef system than for the Rheda 2000. This is not physically consistent, since the height of the HBL must be equivalent in both systems, and the CSL is about 40 cm in the Stedef case and only around 25 cm for the Rheda 2000 case. Possible causes of this deviation may be a sensor error/ miscalibration or a reduced thickness in the Stedef slab track in comparison to the specific value of the project.

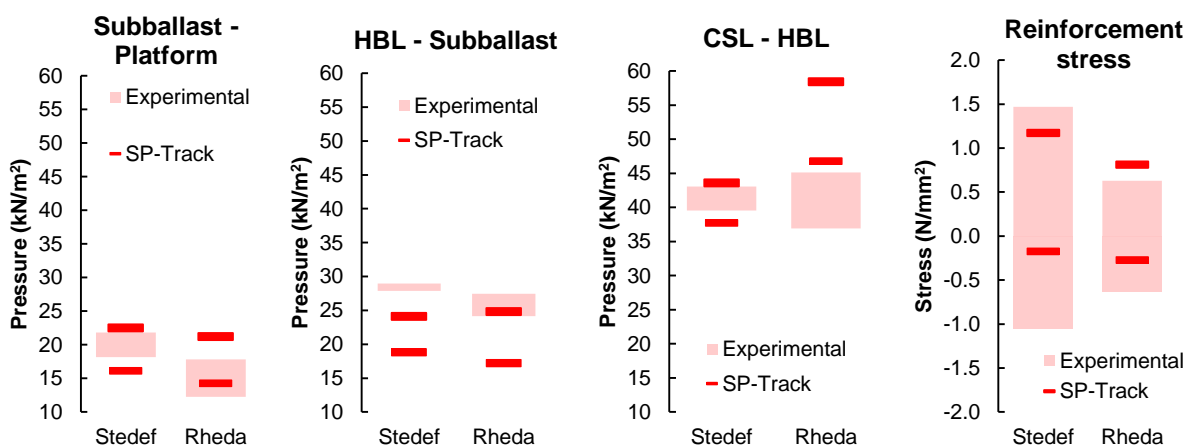


Figure 5.37: Comparison of calculated and experimental ranges of layer and reinforcement stresses for the Benicassim case study

Similarly, in the CSL-HBL interface the numerical predictions are off the experimental range for the Rheda 2000, by a small margin (<7%). Again, the CSL-HBL vertical stresses should be notoriously higher for the Rheda 2000 due to the different total CSL thicknesses. This indicates the occurrence of sensor malfunctioning or different-than-expected (and assumed in modelling) properties of the subgrade.

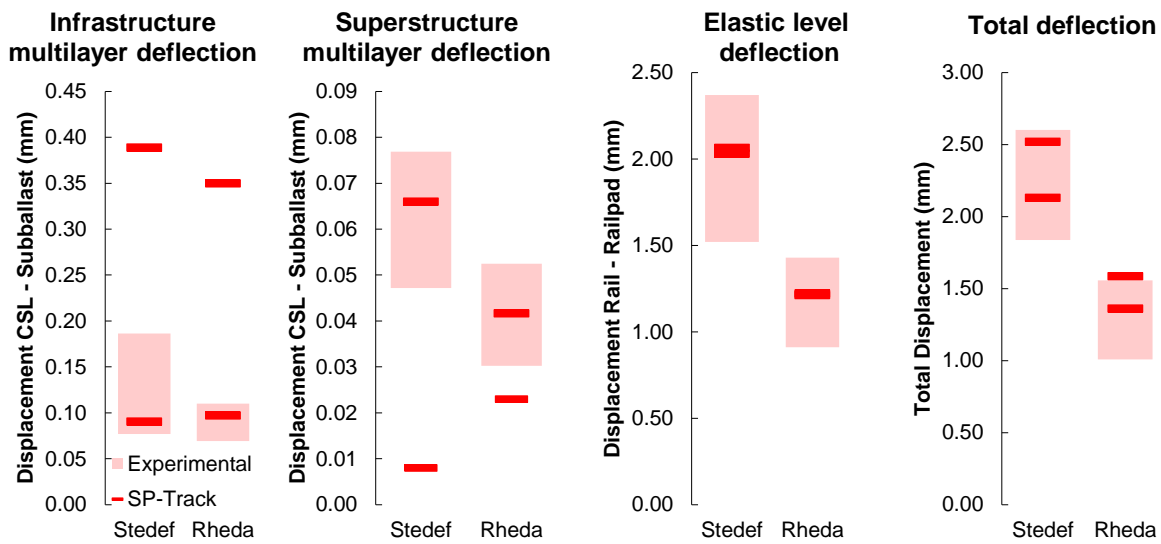


Figure 5.38: Comparison between calculated and experimental displacements for the Benicassim case study

Furthermore, the reinforcement stresses show a good correlation with the experimental records, presenting a very low-stress level – this shows that the main role of the reinforcement in slab track systems is related to crack control under shrinkage and temperature loads rather than as a structural solution for vehicle loads if no extraordinary conditions arise.

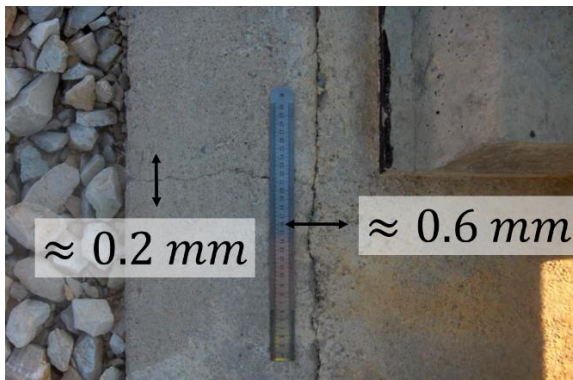


Figure 5.39: Crack width in the Rheda 2000 of the Benicassim site after 1 year of operation

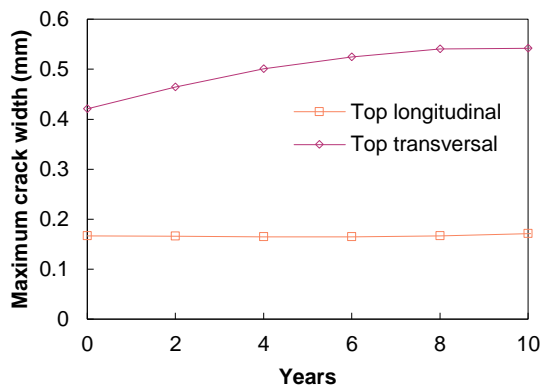


Figure 5.40: Calculation of crack width by the HI-Track model for the Rheda 2000 case study

Although limited, crack width data was available for the Rheda 2000 case (Figure 5.39) after the end of the second experimental campaign (after 1 year of operation). By visual observation, crack width reaches 0.2 mm and 0.6 mm in the longitudinal and transversal direction respectively. Data regarding external actions for modelling purposes is unavailable, which leads to major assumptions related to temperature variations and traffic operations. To validate the order of magnitude of crack widths, a temperate climate (presented in Figure 5.46 and 5.47) and a 30 000 ton/day traffic (50 Arco/Talgo trains with 28 axles of 17 t and 7 freight trains with 46 axles with 22t) are assumed. The numerical calculations are presented in Figure 5.40, with a strong physical coherence, in particular, the larger crack widths in the transversal direction caused by the temperature gradient warping. The effect of the initial damage and the stabilization for

longitudinally top cracks are also captured by the model. The results of the model are similar to those of the experimental observations, which indicates a good correlation with the order of magnitude for crack widths. Nevertheless, the level of unknown parameters and associated uncertainty is high, and the reliability of the results should be carefully examined.

5.4 LABORATORIAL LONG-TERM VALIDATION: GRAFT-II

The Geo-pavement and railways accelerated fatigue testing facility (GRAFT-II) is one of the most comprehensive full-scale experimental test rig specialized to test the fatigue of railway track configuration located at Heriot-Watt University in Edinburgh, UK. The train passages are simulated with a phased cyclic load equipped with hydraulic actuators (Figure 5.41) with a maximum load of 120 kN. The different load phases allow the emulation of different speeds and simulate the short- and long-term behaviour of the track, with multiple years of train service condensed under a week of testing. The slab track model tested was the precast Bögl system (Figure 2.8) that was custom built for this experimental campaign. The typical Bögl slab track features a 200 mm thick slab with a C45/55 concrete class strength prestressed laterally (6 Ø0.6" tendons) with a 90% pulling force Si860 steel and ordinary 28 Ø10 mm longitudinal rebar, 2 Ø8 mm stirrups spaced 0.6m and 3 pass through steel rods Ø20 mm that is bolted between panels (mechanical link). Nevertheless, the reinforcement is not presented in this tested panel, since the study of concrete damage and crack width is not intended for this long-term study.

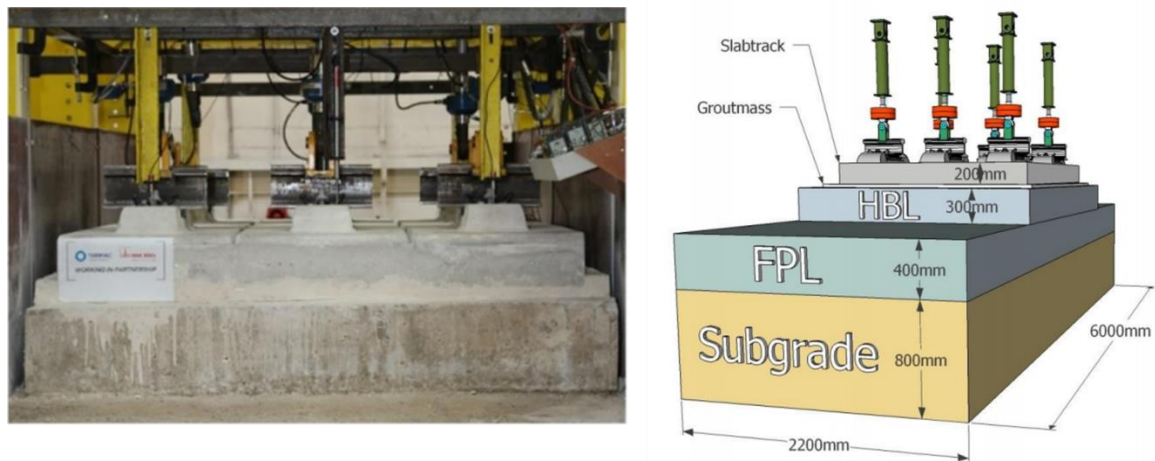


Figure 5.41: Bögl slab track system present in the GRAFT-II laboratory

The rail fastening system is a Vossloh 300-1 with a static stiffness of 22.5 kN/mm and dynamic stiffness of 40 kN/mm and the rail is UIC60. The CSL is a 200 mm slab with a C35/45 concrete (20-36 GPa) and a 300 mm HBL with a C10/12 concrete (7.5-18.0 GPa). Between the CSL and the HBL, a 40 mm gap was filled with cement grout as in the original system (22.5 GPa).

The subgrade is divided in a 400 mm frost protective layer (FPL) with a deflection modulus of $E_{v2} \geq 120$ MPa and an 800 mm-platform soil with $E_{v2} \geq 60$ MPa according to the German guidelines (yet, soil tests for both layers indicate a Young modulus of 400/500 MPa). Both soils consisted of granular limestone with optimal moisture of 4.5%, specific gravity of 2.69 and

maximum dry density of 22.5 kN/m^3 . For the model validation, it is assumed that the moisture content is invariable during testing.

The axle load for the static and cyclic loading is simulated by each actuator with a 50% load to the middle sleeper and 25% to the adjacent ones, to emulate the behaviour of a beam on an elastic foundation. The dynamic tests were performed under full loading in each sleeper. This approach can lead to satisfactory results when static or pseudo-static loads are applied, nonetheless, dynamic tests lead to very low accelerations on the track compared to the complete rail-railpad system. Still, only track settlements are evaluated because the soil stress cycles could be considered as pseudo-static, and therefore the HI-Track train/track interaction calculations of soil settlement are comparable with the experimental results.

The experimental campaign was divided in four tests, two statics and two dynamic cyclic tests, being the latter divided into 2 phases characterized in Table 5.5. The static tests are not assessed for the numerical validation of the HI-Track:

Table 5.5: Cyclic test phases performed in the Bögl slab track system in GRAFT-II

	Actuator load	Frequency	Cycles
Phase I	58.86 kN	5.6 Hz	1.17 M
Phase II	83.34 kN	2.5 Hz	2.2 M

The load frequencies are calculated according to the bogie spacing of the trains intended to be emulated ($\approx 17.8 \text{ m}$) for operating speeds of 360 km/h and 160 km/h.

The data acquisition is composed by 27 channels for the slab track (5 pressure cells on the FPL, 6 load cells, 6 LVDT's in each actuator, and 7 LVDT's in each sleeper and the slab mid-point, and 3 accelerometers in 3 sleepers. Nevertheless, only the readings of the LVDTs placed on the sleepers and of load cells were available for the numerical model validation.

By evaluating the evolution of track displacement during the duration of the test, it is possible to withdraw and post-process the track settlements, which are illustrated in Figure 5.42.

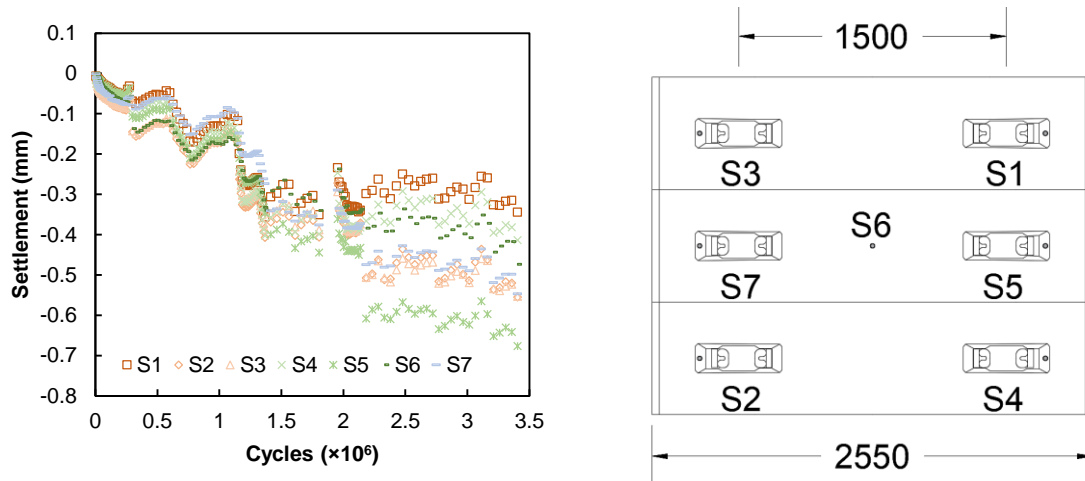


Figure 5.42: Post-processing settlement data (left) from LVDT sensors installed in the slab (right)

The hybrid numerical model HI-Track is intended to represent the real-life track circulation and their interaction with the track; therefore, the load application will differ from the laboratorial test at GRAFT-II. Instead, the SP-Track and DL-Track sub-models are modelled with full longitudinal domains (Figure 5.43) with real vehicle models with axle load equivalent to the dynamic tests and vertical domains are respected to simulate the vertical stiffness.

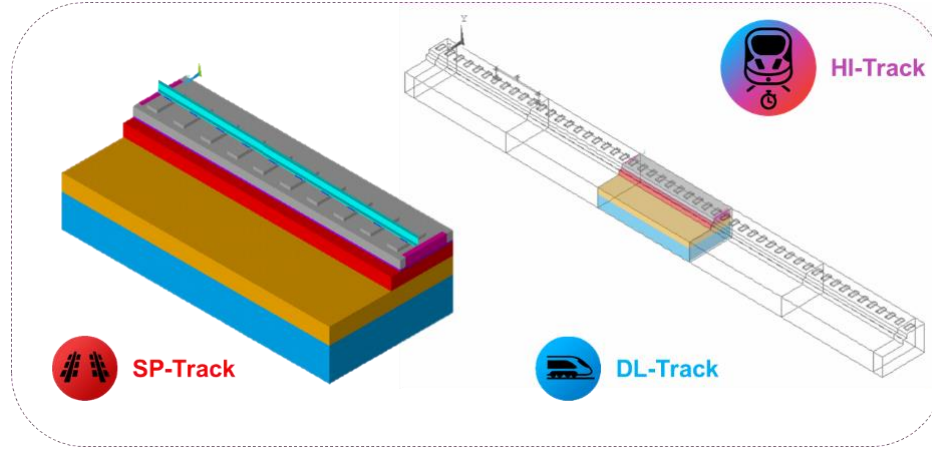


Figure 5.43: HI-Track model representation of the GRAFT-II case study with the Bögl system

The vehicle suspension and wheel and bogie are simulated to the TGV type previously presented, being the only difference the carbox mass that matches the tested actuator loads. The calculation of both DL-Track and SP-Track to predict an almost pseudo-static response of the soil may be perceived as unjustified since differential settlement and concrete fatigue is negligible. Nevertheless, since track geometry and track damage do not vary significantly, both models are updated to the bare minimum and keep the simulation efficient. Both the longitudinal domain and mesh size are the result of an iterative process, and the lateral and vertical domain is defined by the laboratory setup.

All properties used in the numerical model are the result of laboratorial tests, as in the soil layers, on data from the literature, or information from manufacturers. These properties are reported in Table 5.6:

Table 5.6: Geometrical and mechanical properties of the Bögl slab track system present in the GRAFT-II case study

Element	Mechanical Properties				Geometry
	E / k_p	v	ρ	ξ	
Rail	200 GPa	0.3	78.5 kN/m ³	0.01	UIC60
Railpad	30/40* kN/mm	0.25	9 kN/m ³	60 kN·s /m	200×150×9 mm ³
CSL	43 GPa	0.2	25 kN/m ³	0.05	$h_{CSL}=0.20$ m
HBL	18 GPa	0.2	25 kN/m ³	0.05	$h_{HBL}=0.30$ m
CAM	25 GPa	0.3	25 kN/m ³	0.05	$h_{CAM}=0.04$ m
Formlayer	100-500 MPa	0.3	21.4 kN/m ³	0.01	$h_{fr}=0.40$ m
Subgrade	100-500 GPa	0.4	20.9 kN/m ³	0.01	$h_{sub}=0.80$ m

Again, subgrade properties are prone to uncertainty since static tests could affect the consolidation level of the soil layers. Thus, a range from 100 to 500 MPa is going to be simulated as a parametric analysis on the track settlement.

Furthermore, two settlement mechanistic-empirical models are going to be implemented in this analysis as an attempt to encompass the uncertainty related to the subgrade soil. The first is the work developed by Tseng & Lytton (1989) and the second is the work of Selig & Li (1996), both discussed previously in 5.2.3. In the model developed by Tseng & Lytton (1989), a 100 and 400 MPa Young modulus range of the soil as input for the empirical model is used. In the case of the law formulated by Selig & Li (1996), high-quality lean silt with a 70 KPa and 100 KPa compressive strength, in order to mimic the expected soil properties present in the laboratory. The results are shown in Figure 5.44.

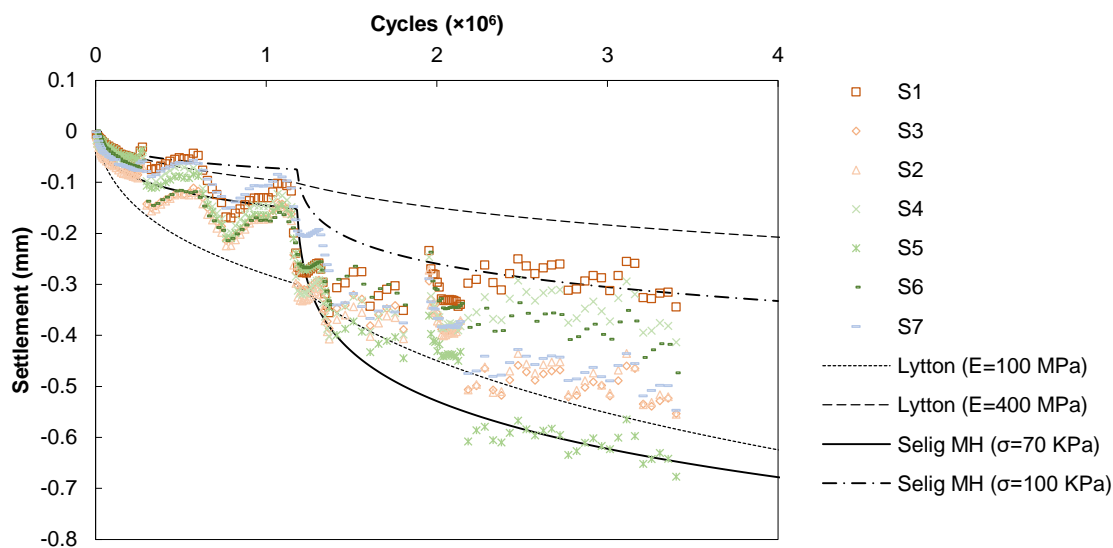


Figure 5.44: Comparison between experimental and calculated soil settlement for the Bögl case study in GRAFT-II

The 100 MPa Lytton model version slightly overestimated the settlement for the phase I of the cyclic dynamic testing, while the 400 MPa version has a good matching for the phase II, and vice-versa. This suggests that the soil stiffness takes a value between these two limits and that the settlement rate after the change of phase is not properly predicted by the HI-Track model, which indicated that possible soil disturbances during the calibration process of the phase II loading and frequency could change the soil compaction level and alter the equivalent traffic strain level of the soil. Also, the Lytton and Tseng model is not calibrated for this level of soil stiffness, so the 400 MPa case forecast should be carefully addressed for its accuracy. Moreover, the Selig and Li model concludes that the actual behaviour of the lean silt soil shows a good correlation for 70 and 100 KPa compressive strength, and it better represents the change between cyclic dynamic phase change than the Lytton model.

Both variants suggest that the actual behaviour of the soil is between the limits defined (deflection modulus between 100-400 MPa and soil compressive strength between 70-100 kPa) which makes the long-term soil approach by the HI-Track reasonably reliable to predict soil permanent deformation by mechanistic-empirical models at a preliminary level with the available data.

5.5 FIELD LONG TERM VALIDATION

5.5.1 HANNOVER-BERLIN HIGH SPEED LINE CASE: CONCRETE SLAB DAMAGE

The Hannover-Berlin high-speed railway is a 258 km high speed line that opened in September 1998 and the first German line mostly constructed with a ballastless track (Figure 5.45).

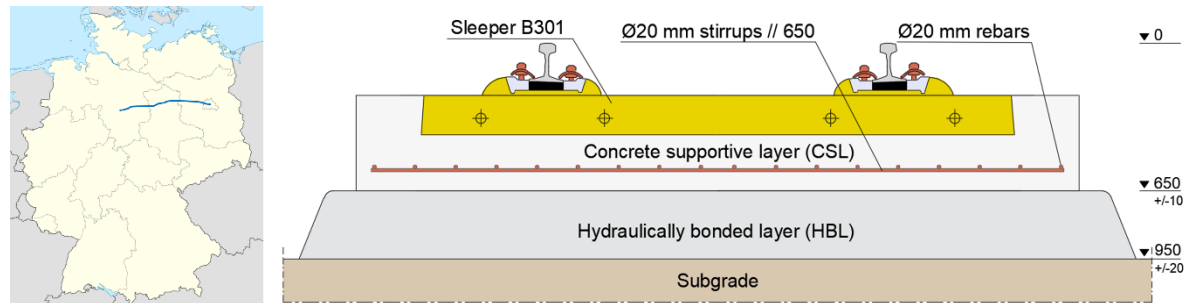


Figure 5.45: Hannover-Berlin high speed line (left) and scheme of the Rheda Classic system used (units in mm)

The system used is the Rheda Classic, a system closely related to the predecessor Rheda 2000. Similarly to Rheda 2000, is an embedded sleeper system with continuous longitudinal reinforcement, being the main differences the implementation of a monoblock B301 sleeper with passing through holes for the reinforcement and the bi-phased concrete slab, i.e. a first phase in a trench-like shape and the infill concrete to embed the sleepers, see Figure 5.45. There is a lack of available information regarding the track properties of this ballastless system, so standard properties found in the literature and the German guidelines are used for modelling. These properties are summarized in Table 5.7 and the HI-Track is illustrated in Figure 5.50.

Table 5.7: Geometrical and mechanical properties of the Rheda Classic slab track system present in the Hannover – Berlin high speed line

Element	Mechanical Properties				Geometry
	E / k_p	v	ρ	ξ	
Rail	200 GPa	0.3	78.5 kN/m ³	0.01	UIC60
Railpad	22.5 kN/mm	0.25	9 kN/m ³	60 kN·s /m	200×150×9 mm ³
Sleeper	45 GPa	0.2	25 kN/m ³	0.05	B301
CSL	10-30 GPa	0.2	25 kN/m ³	0.05	$h_{CSL}=0.20\text{ m}$
HBL	28 GPa	0.2	25 kN/m ³	0.05	$h_{HBL}=0.30\text{ m}$
Foundation	120 MPa	0.3	22.3 kN/m ³	0.01	$h_f=0.30\text{ m}$
Formlayer	120 MPa	0.3	22.3 kN/m ³	0.01	$h_{fr}=0.40\text{ m}$
Upper emb.	80 MPa	0.4	20.2 kN/m ³	0.01	$h_{emb1}=1.25\text{ m}$
Lower emb.	80 MPa	0.4	20.2 kN/m ³	0.01	$h_{emb2}=3.25\text{ m}$

In what regards external actions in the track, the operation at the time of the data collection consists in average daily traffic of 36 000 ton/day, which can be expressed as 75 ICE trains per day and circulations at a commercial speed of 300 km/h. Since track damage is the main topic to assess in this validation case study, temperature and rainfall data are required to be implemented in the HI-Track model. In Figure 5.46 and 5.47, the average annual uniform temperature and temperature gradients for the Hannover/Berlin region are represented. Concerning the average rainfall intensity in the same region, the Köppen-Geiger climate

classification attributes a Cfb (oceanic climate) with around 630 mm per year, which is quite similar to the climate in Barcelona used to validate the thermo-hydro-mechanical model. The phreatic level used was set to 3 m below the embankment.

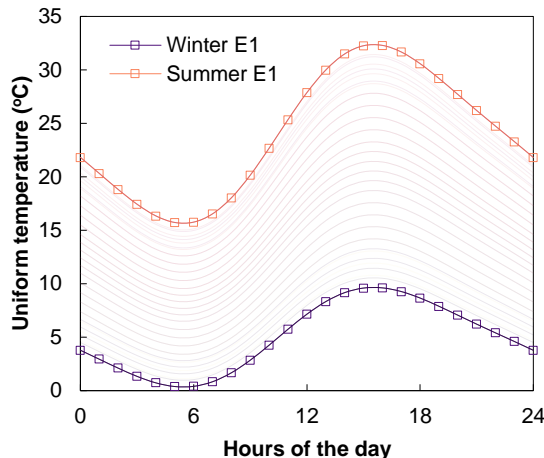


Figure 5.46: Uniform temperature variation during the year used for the Hannover – Berlin case study

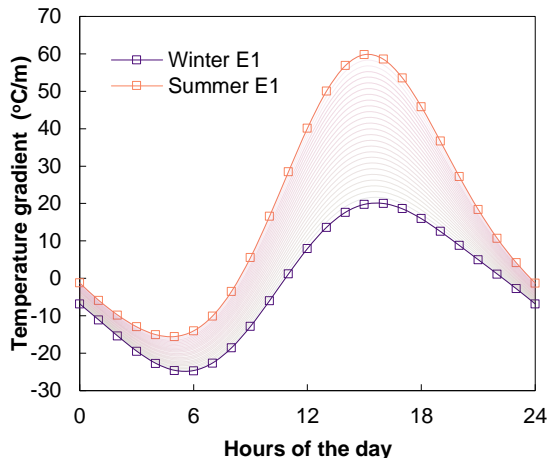


Figure 5.47: Gradient temperature variation during the year used for the Hannover – Berlin case study

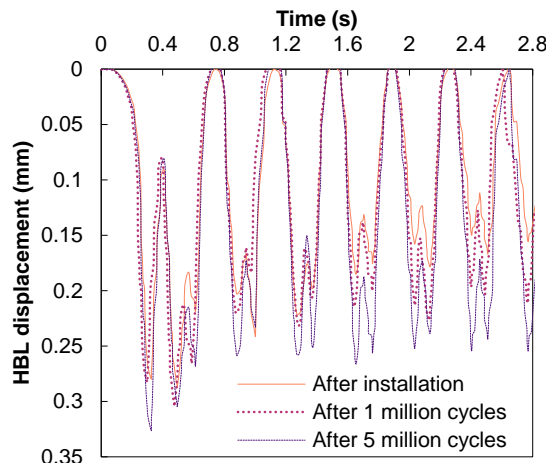


Figure 5.48: HBL displacement of the Rheda Classic system present in the Hannover - Berlin high speed line at different times

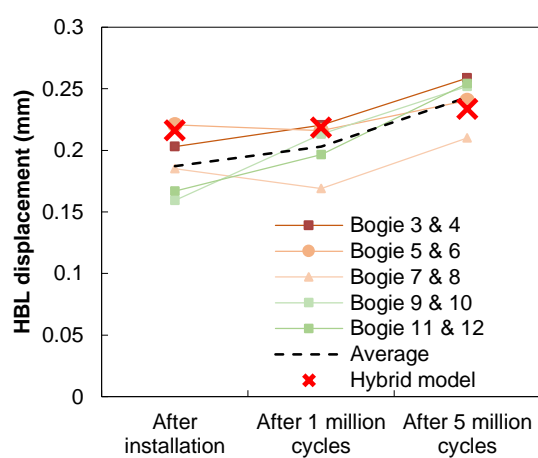


Figure 5.49: Comparison between calculated and experimental HBL displacements at different times

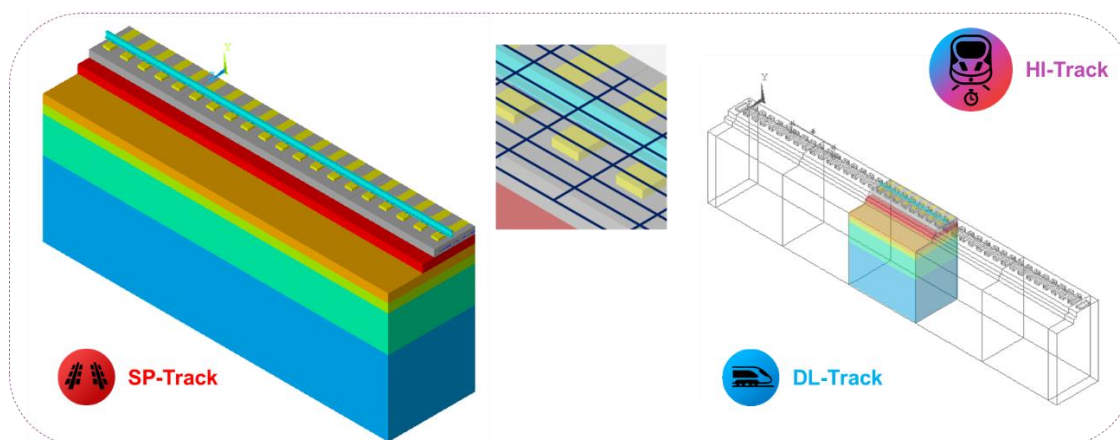


Figure 5.50: HI-Track model representation of the Hannover – Berlin high speed line case study

The experimental measurements recorded were divided into three phases: After installation (September 1998), after 1 million cycles (November 1999) and after 5 million cycles (May 2004). In each phase, the HBL displacement was registered (Figure 5.48). In each experimental campaign, the HBL increases due to the passage of ICE trains from 0.19 mm to 0.20 mm (after 1 million cycles) and to 0.24 mm (after 5 million cycles), which is a fairly linear increase of 0.01 mm/million cycles. This is physically coherent with the steady secondary phase of concrete damage. Figure 5.49 shows the average HBL displacement for multiple bogies and compares it with the HI-Track results. Despite being within the range of track displacements, the HI-Track shows a slower deterioration rate (≈ 0.04 mm/million cycles) that may be justified by various uncertainties unable to be accurately addressed as construction quality of the CSL, HBL and soil platform. In Figure 5.51 and 5.52, the cumulative concrete damage on the track using the Model Code (2010) methodology explained in chapter 4 is shown. Two main fatigue phenomena can be observed: i) the temperature fatigue on the top surface in the vicinity of the sleeper – here, the induced stresses are caused by the temperature gradient; ii) the flexural fatigue at the bottom of the CSL caused by train loads, that rapidly stabilizes after a certain number of cycles.

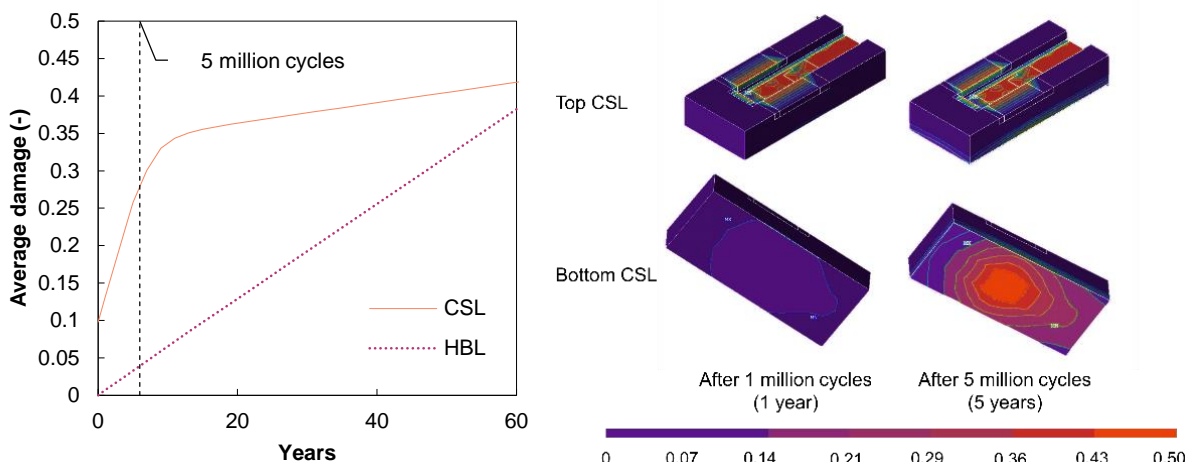


Figure 5.51: CSL and HBL damage for the Rheda classic case study

Figure 5.52: Calculation of concrete damage in one CSL sleeper module for the Rheda Classic case study

Figure 5.51 better elucidates the fast rate of concrete deterioration for a later stabilization after the tenth year. This deterioration is mainly due to temperature effects. On the other hand, the HBL follows a linear trend in the cumulative concrete damage, since only the train load is applied to this layer (the layer is protected from significant temperature variations). It is important to note that this stabilization of cumulative damage in the concrete slab is highly dependent on the model time step update in the early years of the track's lifetime. Since the track stiffness update in the HI-Track is performed once a year, the first stage of concrete cracking occurs later during operation, as if the update were performed on daily basis, to account for full temperature cycles. Notwithstanding, for validation purposes, this time step discretization is sufficient to characterize the first phase of concrete damage at the end of the 5 millionth cycle.

These several stages of concrete damage are illustrated in Figure 5.53, in which it can be comprehended the first initial damage of concrete until year 5-10, followed up by a secondary

phase of intermediate steady cracking that transitions to the final stage of uncontrolled cracking at the year 280 that precedes the failure by concrete fatigue.

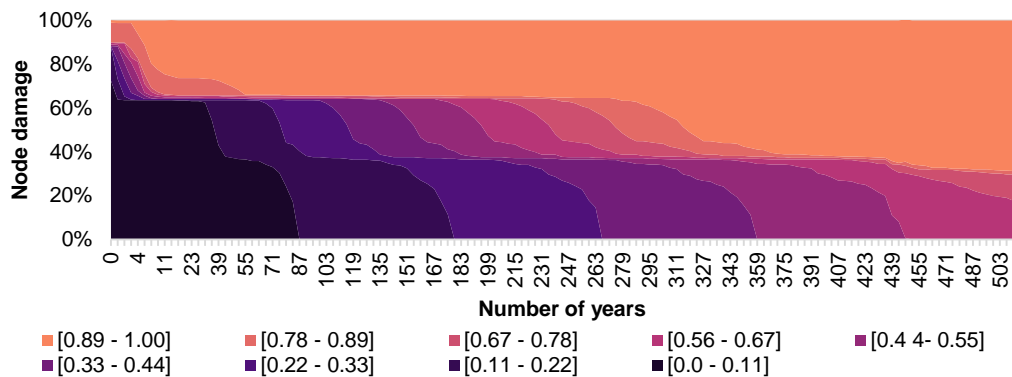


Figure 5.53: Evolution of nodal damage distribution in the CSL

In addition to the uncertainty related to brittle materials like concrete, multiple factors can affect the evolution of track displacement rate after millions of cycles, such as subgrade properties variation in terms of stiffness or specific hydrological properties or heterogeneities, unforeseen traffic. So, the model's ability to predict the order of magnitude of the concrete loss of stiffness is satisfactory as a numerical tool to compare different scenarios, later to be presented.

5.5.2 COLOGNE-FRANKFURT HIGH SPEED CASE: THM BEHAVIOUR OF THE SOIL

The Cologne-Frankfurt high-speed line is one of the most important slab track high speed lines in Europe, stretching 177 km, and has commercial speeds of 300 km/h (Figure 5.54). The trains are third-generation ICE trains with more power to circulate in the line's high grades (up to 4%), which is only possible with slab track technology. As in the case study of the previous subchapter, the information related to the track structure is scarce and usually confidential, so the track element properties used for modelling are taken from literature and manufacturers' reports. The slab track system used in the Cologne-Frankfurt high speed line is the Rheda 2000 and the properties used are those already presented in Table 5.7. The experimental setup was set at km 72.6 between Limburg and Wiesbaden/ Mainz and several odometers were installed to measure the soil settlement after the construction of the track.

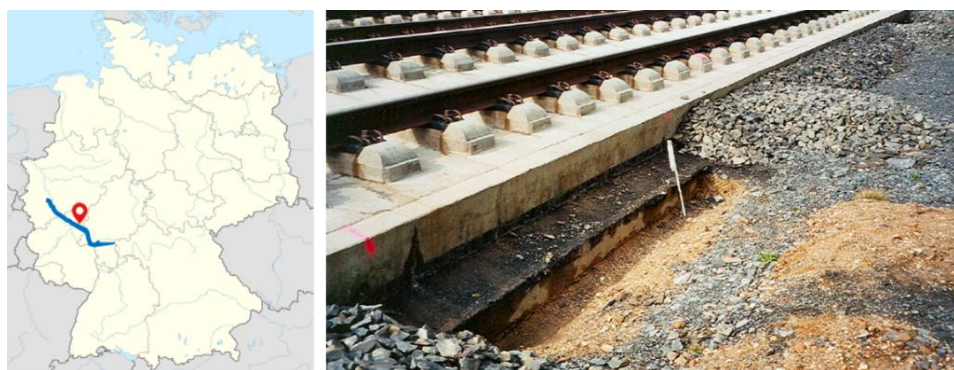


Figure 5.54: Cologne-Frankfurt high speed line (left) and soil settlement in the Rheda 2000 system (right)

Figure 5.55 presents the timeline of settlement progression after the embankment construction of the track in May 2001 and subsequent compaction interventions until August 2002 and the end of the settlement records in October 2004. After the line opening, the average daily train circulation was 75 ICE trains (32 axles) circulating at 300 km/h.

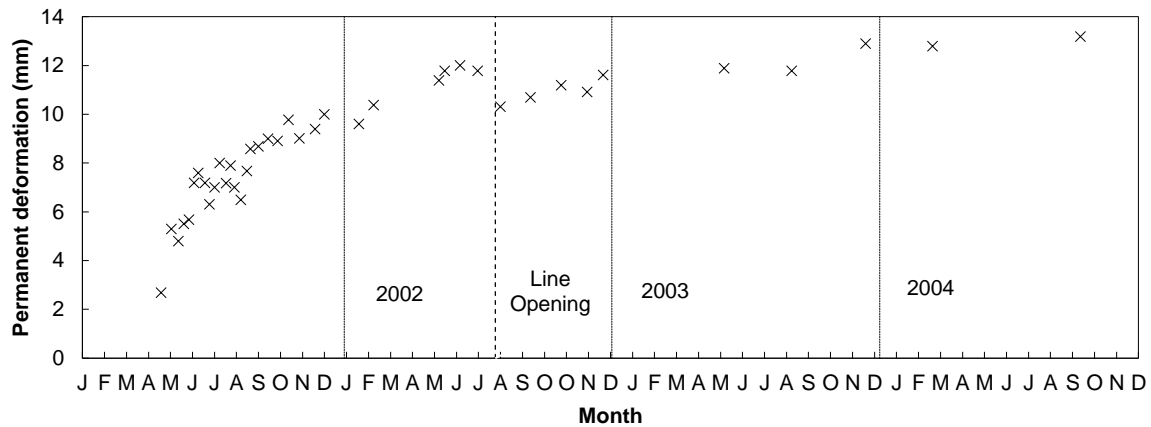


Figure 5.55: Soil settlement after construction in PK. 72.6 in the Cologne – Frankfurt high speed line

The purpose of this subchapter is the validation and calibration of the thermo-hydro-mechanical behavior of the soil in the long-term, thus atmospheric actions should be carefully addressed for implementation in the model. As in the previous experimental case in the Hannover-Berlin high speed line, the weather and climate conditions are very similar to the Cologne-Frankfurt, so the temperature loads and rainfall intensity are those previously used.

In order to simulate the compaction level of the soil before the line opening, initial traffic was iteratively calculated to match the soil consolidation level until August 2002, and it was established at 100 000 load cycles. Also, a parametric assessment was included in the validation process regarding the initial condition of the hydraulic properties of the soil, namely the groundwater table from 1 to 5 meters below the embankment. This parametric analysis is useful to address the high uncertainty related to the soil conditions and more important than the soil stiffness, which range should be controlled since the test was conducted in an embankment. The results of the simulations are illustrated in Figure 5.56.

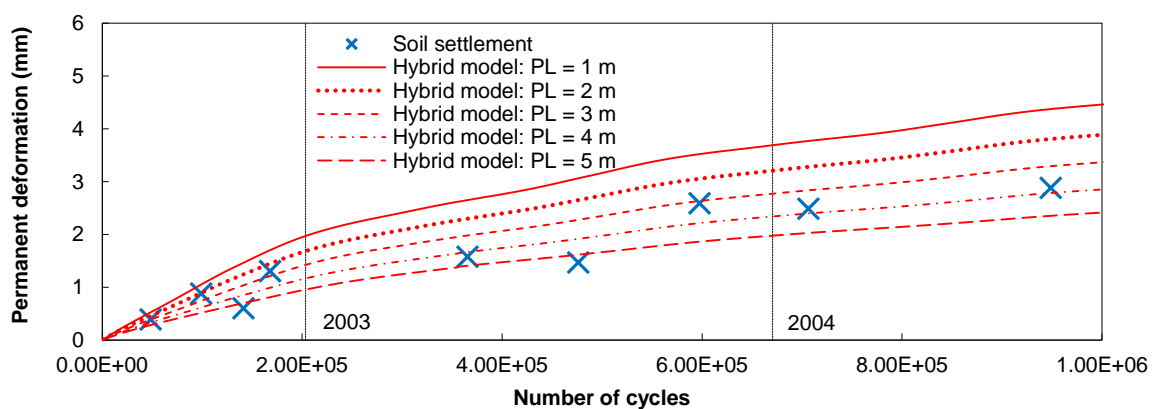


Figure 5.56: Comparison between experimental and numerical soil settlement results for the Cologne-Frankfurt high speed line

The numerical results indicate a good correlation with the experimental data for various phreatic levels with a tendency for better matches with deeper saturation levels as expected, according to the efficient drainage design. In the model predictions, it is possible to observe the seasonal settlement fluctuations around winter months due to a higher saturation level of the soil due to more frequent rainfall.

This calibration and validation of the coupled HI-Track/ THM model foster the confidence in the hybrid numerical model to predict long-term soil settlement for slab track systems and incorporate this calibration in future scenarios to develop future design guidelines.

5.6 CONCLUDING REMARKS

This chapter was dedicated to the validation and calibration of the numerical model HI-Track. Calculation of the short-term accelerations, displacements and stresses and long-term soil settlement and concrete loss of the stiffness of concrete elements during the lifetime.

During the validation with experimental measurements, multiple slab track systems were evaluated and compared in the short- and long run for laboratorial and field campaigns. The different case studies modelled show the flexibility and versatility of the HI-Track and its ability to suitably predict track responses. The summary of available data is outlined in Table 5.8.

Table 5.8: Available experimental data for the validation and calibration of the HI-Track model

Case study	Country	System	Vehicle	Short-term variables					Long-term variables ε_p, D, w_k
				Rail a, δ, σ	Sleeper a, δ, σ	CSL a, δ, σ	HBL a, δ, σ	Subgrade a, δ, σ	
CEDEX Track box	Spain	β MB	– TGV – Freight train	●●○	●●○	●●○	○○○	●●○	○○○
Chauconin	France	Stedef	TGV	○○○	●●○	○○○	○○○	○○○	○○○
Benicassim	Spain	– Stedef – Rheda 2000	– Arco/ Talgo – Freight train – TGV	○●●	○●●	○●●	○●●	○●●	○○●
GRAFT-II	UK	Bögl	– Regional train	○○○	○○○	○○○	○○○	○○○	●○○
Hannover-Berlin HS line	Germany	Rheda Classic	ICE	○○○	○○○	○○○	○●○	○○○	○○○
Cologne – Frankfurt HS line	Germany	Rheda 2000	ICE	○○○	○○○	○○○	○○○	○○○	●○○

By far, the most comprehensive experimental case study was the β MB slab track prototype tested in the CEDEX Track Box that took the most amount of model simulations and contributed vastly to the confidence on short-term accuracy of the DL-Track and SP-Track sub-models. Besides,

two real high speed European railway lines (the Chauconin and Benicassim case studies) were used to screen out possible limitations of the test rig loaded by the hydraulic actuators. The Benicassim case study was quite important for the validation of the predictions of stress levels at different interfaces of the track configuration. Both experimental case studies were fundamental to validate the short-term response calculation of DL-Track and SP-Track.

Moving to the long-term behaviour of slab tracks, the number of experimental campaigns are scarce due to the complexity, instrumentation required and duration of the tests. Also, since all dedicated slab tracks lines are recent solutions for high-demand railway lines, there are no longstanding records from experiments related to long-term deterioration.

Nonetheless, some experimental trials were addressed in this validation process, having each one a specific goal to examine the model's reliability for a particular deterioration phenomenon. The most controlled and instrumented experimental study is the GRAFT-II case study, which was used to validate the soil settlement methodology employed by the hybrid numerical model. This case study was complemented by the Cologne-Frankfurt high speed line case study to enhance the results' accuracy concerning the effect of atmospheric actions on the permanent deformation of the soil.

Concerning the concrete damage of slab tracks, the validation process was far more challenging. Firstly, due to the lack of dedicated experimental cases with real vehicle traffic and secondly due to the demanding task of accurately and reliably predict concrete deterioration subjected to high-frequency train and temperature loads, shrinkage, creep, among others. The Benicassim, Hannover-Berlin and Cologne-Frankfurt high-speed case studies held little information available on the experimental track section, which reduces the reliability of the model. Still, the model results show similar orders of magnitude and theoretical significance that provides reasonable confidence on concrete deterioration for at the very least, a comparative result assessment between scenarios.

The results obtained during the validation process enable claiming that the HI-Track is capable to predict track responses accurately during the lifetime, mainly for the concrete superstructure layers and track settlement. Table 5.9 summarizes the reliability degree of the numerical model in the calculation of the track responses from accuracy levels, • – reasonable, •• – satisfactory, ••• – strong.

Table 5.9: Reliability level of the numerical model

	Short-term variables			Long-term variables		
	a	δ	σ	ε_p	D	w_k
Rail	•	•••	••			
Sleeper	•••	•••	••			
CSL	•••	•••	••		•	
Reinforcement		•••	•••			••
HBL		•••	••		•	
Subgrade	••	•••		•••		

Concluding, HI-Track is a valid numerical model to calculate the short- and long-term behaviour

of high-demand slab tracks subjected to high speed and freight trains and atmospheric actions in a dual approach between DL-Track and SP-Track. This calibration process plays a vital role on the model development, in particular, the numerical parameters as the initial condition of the track damage, and initial soil permanent strain level, as well as boundary conditions and mesh size, time step, etc.

The next following chapter will be focused on different scenarios that will aid on design guidelines, which in turn deliver maintenance requirements to be implemented in future in life cycle decision support tools.

6 SLAB TRACK STRUCTURAL BEHAVIOUR AND GUIDELINES FOR OPTIMIZED DESIGN

6.1 INTRODUCTION

In this chapter, the main results of the hybrid model developed in the thesis are assessed to evaluate the long-term response of the slab track configuration. The system evaluated is the Bögl slab track system (presented in detail in Figure 6.1), since it is one of the most widespread systems worldwide (a combined total of more than 4000 km of track length). Its structural functioning is quite similar to CRTS-II and CRTS-III that account for more than 20 000 km in the Chinese high speed network.

This chapter is divided into 3 parts: definition of scenarios, calculation, and design recommendations. Firstly, a list of scenarios specifically defined to comply with the design goals of the study is presented. Next, several simulations aiming to optimize the design of the track are conducted as well as the post-processing of the results, and finally, a critical analysis is delivered with a set of guidelines for future slab track designs.

According to the literature review presented in Chapter 2 and the research questions addressed in chapter 1, the HI-track is used to evaluate the performance and resilience of the slab track system Bögl (Figure 6.2) for a wide variety of scenarios. The model goes further and implements several ultimate limit state scenarios to evaluate the long-term performance of the slab track system when subjected to extreme atmospheric and train actions. The model is also used to predict the need for early maintenance according to different thresholds.

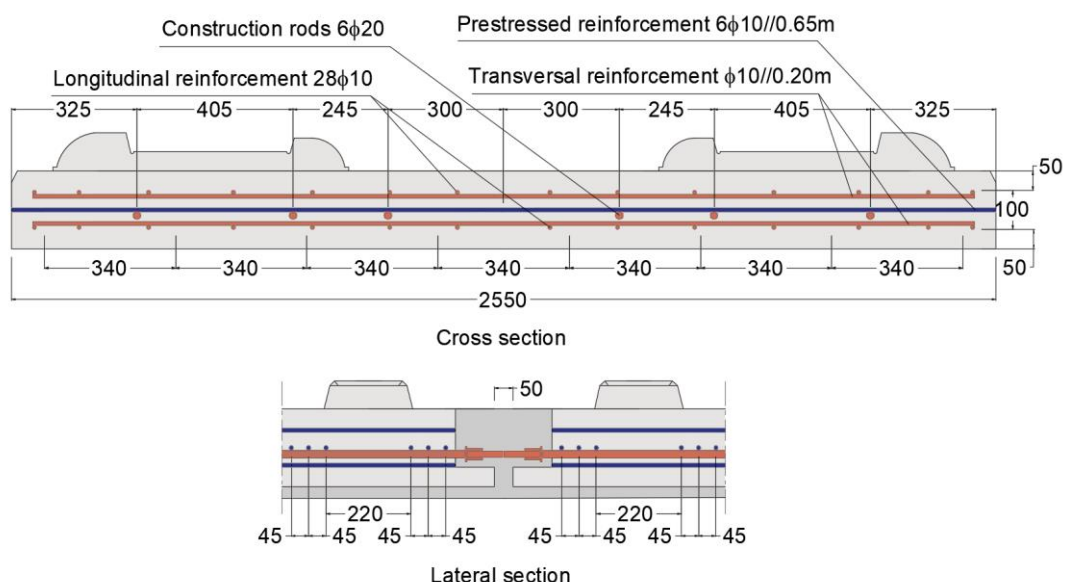
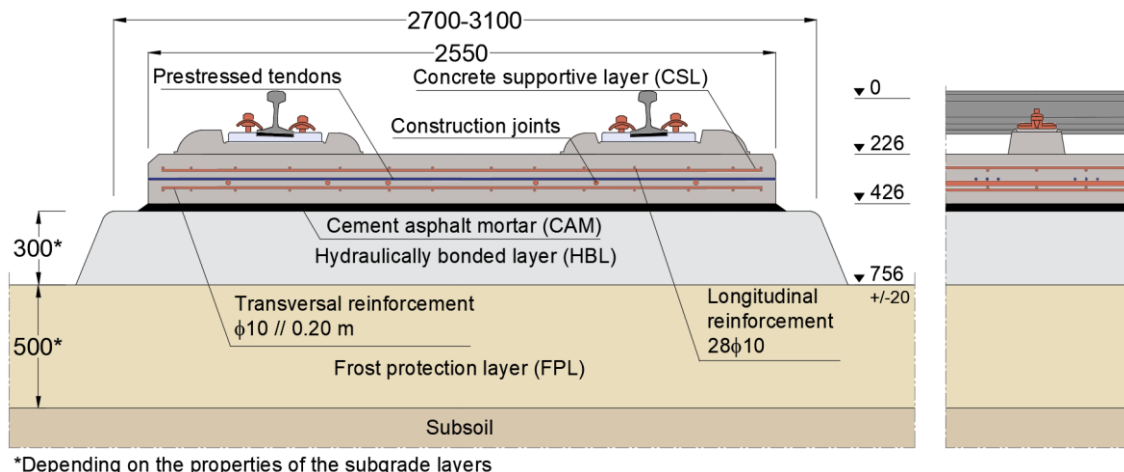


Figure 6.1: Detailed representation of the Bögl slab track system to be used in the HI-Track

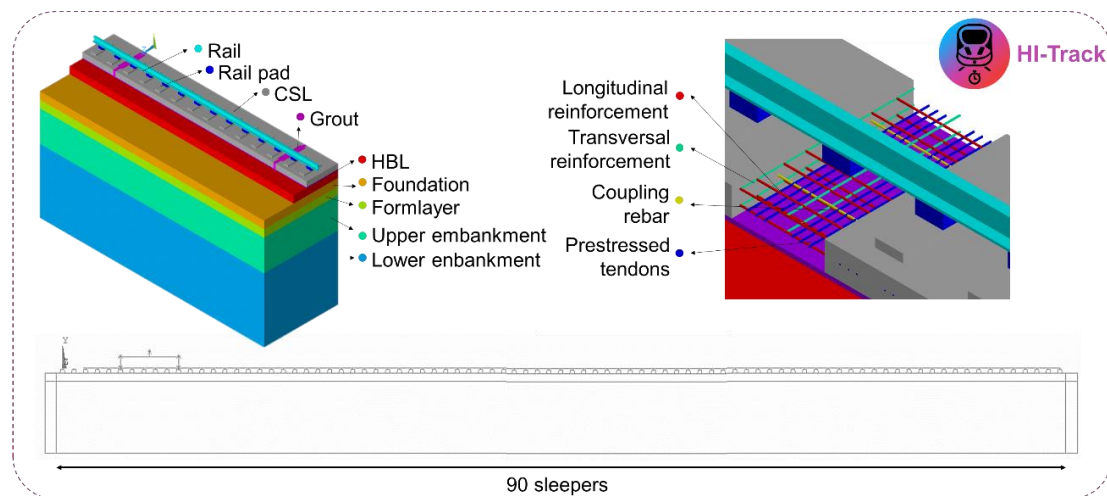


Figure 6.2: HI-Track representation of the Bögl slab track

The scenarios evaluated in this chapter cover important issues that are pertinent to railway infrastructure managers and are divided into 4 groups (Figure 6.3): vehicle operation, weather events, track design and track condition.

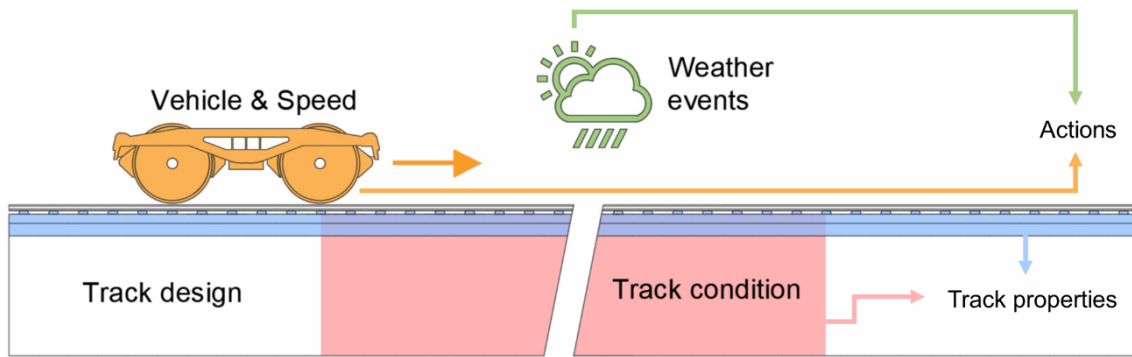


Figure 6.3: Scenarization scheme divided into actions (vehicle and weather actions) and track properties (design and condition)

In what concerns vehicle operation, two different vehicles are modelled: a CHR₃ high speed used in the Chinese high-speed network and a standard 250 kN/ axle freight train – the properties of both are defined in Figure 3.5 and Table 3.1 in Chapter 3.

The traffic conditions are simulated as close as possible to real operation scenarios, and they comprise 3 main intervals for simplicity:

- The maintenance period, in which there is no traffic (to allow maintenance works). The interruption of traffic is modelled as an 8-hour period in the case of high-speed traffic and as a 2-hour window for freight and mixed traffic.
- The operation period, which is divided into freight and high-speed traffic:
 - o Usually, high-speed traffic is set to respond to passenger demand with a 16-hour interval (7 am to 11 pm) with a 5 trains per hour frequency (80 trains per day);
 - o The freight traffic scenarios are defined with a 2-train/h frequency and can run on the track for a maximum of 22 hours (1 am – 11 pm).

The schedule of the traffic conditions is illustrated in Table 6.1.

Table 6.1: Traffic conditions of the scenarios to be studied

Vehicle Scenario	#	hour										◀	23	24
		1	2	▶	◀	6	7	▶	◀	23	24			
High speed traffic	T ₁	Maintenance (M)				5 High speed trains/ h						M		
Freight traffic	T ₂	M	2 Freight train /h									M		
Mixed traffic	T ₃	M	2 Freight trains /h		5 High speed trains/ h							M		

Regarding weather scenarios, they are divided into temperature (E) and rainfall (R). Each is modelled with 3 scenarios. In the case of temperature, the standard scenario (E₁) is as an approximate temperature response of humid subtropical (Cfa) climates as several cities in Japan and China (e.g. Tokyo and Shanghai) and an oceanic climate as many cities in Germany (e.g. Frankfurt) according to the Köppen climate types. The data to be used in the model is collected from the Climate Data Library of the International Research Institute for Climate and Society (IRI) and Lamont-Doherty Earth Observatory (LDEO) (IRI & LDEO, 2019). The E₁ temperature

scenario is characterized by a cold January (yet not freezing) and hot temperate summers (July and August). E₂ and E₃ are based on extreme temperature variations from cold desert climates (BWk), in which already slab track lines were constructed, namely in the Urumqi region in China, known to have high-temperature differentials. The cyclic temperature differentials are calibrated with data from a local Meteorological Bureau in Guangzhou, China (Zhu et al., 2018).

The standard temperature gradient from scenario E₁ varies from -25 °C to 20 °C during the winter peak and from -15 °C to 60 °C during the summer peak. The weather data shows the minimum and maximum gradients occur at 6 am and 3 pm. For simplicity, the daily uniform temperature variation follows the same trendline. E₂ and E₃ scenarios take a similar variation curve with higher absolute values recorded in extreme temperature regions of China (X. Liu et al., 2011). The adopted values for uniform and differential temperature variations are presented in Table 6.2 and the daily variation is illustrated in Figure 6.4 and 6.5, respectively. Also, the yearly uniform temperature variation (the differential temperature variation follows the same trend) is depicted in Figure 6.6. It is very important to mention that these temperature scenarios intend to represent real weather actions, nonetheless, they are fictitious scenarios that seek to take the slab track system to extreme limits, namely E₂ and E₃ scenarios.

Although the maximum values can be registered occasionally in several sites worldwide, the persistence of those temperature loads for several days in a row is unlikely. Nonetheless, climate change can bring more extreme weather and more frequent occurrences, hence it can narrow this difference.

Table 6.2: Maximum and minimum variations of uniform and gradient temperature during the year for the temperature scenarios

Scenario	Winter				Summer			
	TU (°C)		TG (°C/m)		TU (°C)		TG (°C/m)	
	min.	max.	min.	max.	min.	max.	min.	max.
E ₁	-25	20	0	10	-15	60	16	33
E ₂	-35	20	-33	8	-15	70	7	40
E ₃	-45	20	-42	10	-15	80	7	50

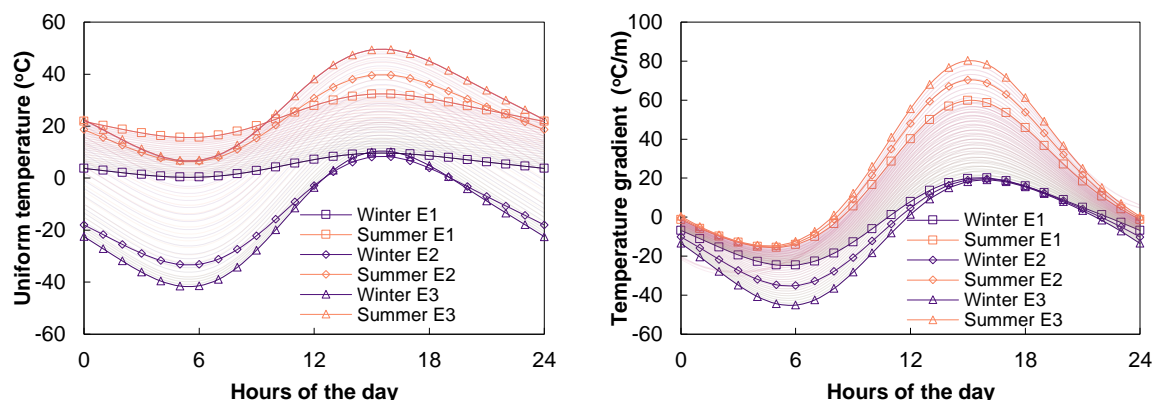


Figure 6.4: Uniform temperature variation along the day to the proposed scenarios E₁, E₂ and E₃

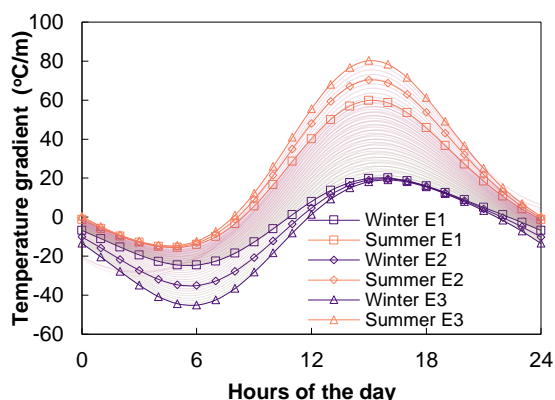


Figure 6.5: Temperature gradient variation along the day to the proposed scenarios E₁, E₂ and E₃

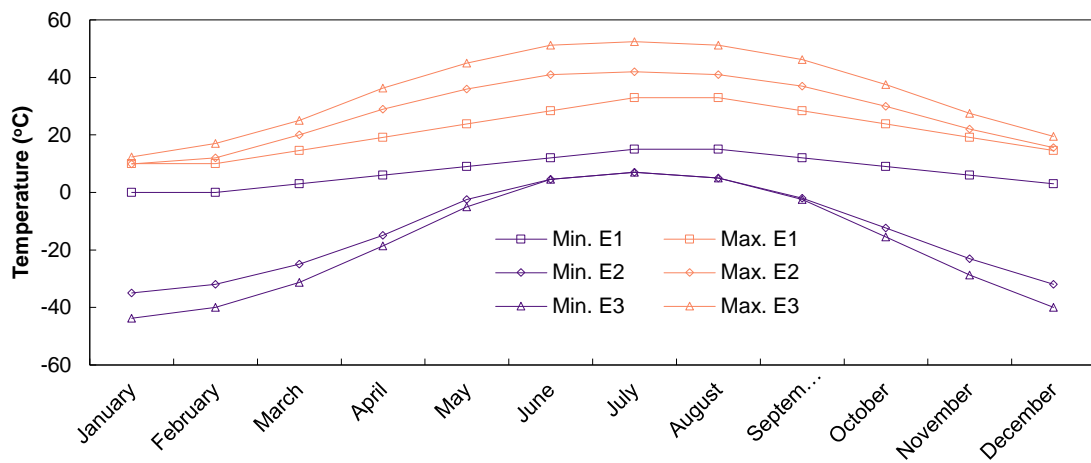


Figure 6.6: Uniform temperature variation along the year to the scenarios E1, E2 and E3

In relation to rainfall events, the standard scenario (R1) reflects an Mediterranean climate around 800 mm of rainfall per year with atmospheric data collected from the city of Barcelona. Taking this in mind, the data is considered in the finite element thermo-hydro-mechanical model and demonstrated in Figure 4.3. The saturation level of the soil is then calculated with the defined soil characteristics (typical embankment $E_v \approx 80$ MPa for high speed lines) with the aggregation of multiyear atmospheric annual data. Moreover, the groundwater table can be variable which has a considerable impact on the water present in the soil. The atmospheric data is transverse to R2 and R3 scenarios, having only as a difference the phreatic level in each one. For easiness, the phreatic level can artificially represent extreme rainfall, and in this case, R1, R2 and R3 scenarios have a phreatic level at 5, 4 and 1 meter.

Taking into consideration the track optimization, the improvements to be studied are related to feasible manufacturing processes in the ballastless system. Highly standardized features, such as geometry, fastening systems and rail type are excluded from the analysis deliberately since this is the common practice of the industry. With this in mind, feasible design improvements are focused on the concrete elements of the track, as the CSL and HBL. Also, railpads have a large impact on slab track performance (namely, the vertical elasticity) and a broad range of railpad stiffness is tested: from the lowest available in the market to the commonly used in ballasted tracks.

In the case of concrete, different strength classes considered: C30/37 and C40/C50. The C35/45 strength class is the standard class of the models developed in this thesis. Note that the standard Bögl slab track uses a C45/55 high strength concrete, but to perform a more representative analysis applicable to similar slab tracks, C30/37 to C40/50 strength classes are implemented in the simulations. Aside from strength class, a fibre reinforced concrete (FRC), of the C35/45 strength class, is used to evaluate the higher performance of fibre reinforced concrete to tensile concrete fatigue and crack control. Also, recycled aggregate concrete is used to evaluate its implementation as a sustainable alternative for slab track construction without compromising standard performance.

Concerning the reinforcement of concrete, 2 scenarios are implemented: a B1 scenario, in which the longitudinal rebar is increased from 10 mm to 12 mm, and B2 scenario, in which a high-performance system with longitudinal prestressed tendons similar to the CRTS-III system, mainly used in extreme temperature environments to control cracking (since this system is expensive).

To finish track optimization, different thicknesses for the subbase (HBL) are studied to draw conclusions related to their influence on the overall damage effect of the system.

The last scenario category is related to track defects and is subdivided in rail profile, track deficiencies and soil heterogeneities. This last scenario category serves to closely emulate real cases of track defects that are likely to occur and affect operation. Rail defects are simulated by a sinusoidal Dirac delta type defect, which is similar to those found in real tracks:

$$s(x) = \delta_{disp} \times e^{-\left(\frac{(x-x_{disp})}{w_{disp} \times \left(\frac{3}{14}\right)}\right)^2} \quad (6.1)$$

Where $s(x)$ is the rail displacement, x the distance to the origin referential, x_{disp} is the distance of the centre of the settlement and w_{disp} is the settlement wavelength. Rail defects are grouped in 3 scenarios (P1, P2 and P3), that are represented by a standard defect of 1 mm for a 20 m chord (standard defect for every simulation), a more advanced defect of 5 mm for a 20 m chord and a defect with a smaller chord (1 mm for a 10 m chord), respectively. Regarding superstructure defects, they can take some various configurations: drainage deficiency, bad construction quality of the subbase, loss of prestressed force, defective expansion joints, defective sleepers and a poor soil compaction quality (D1 – D6). Finally, the last subset of track conditions is related to soil heterogeneities and was used to study the behaviour of the slab as a “bridge” over defects. This subset is divided into two groups: the soft soil group, which assesses the slab capacity to absorb positive bending moments and the transition group, which evaluates the track resilience to unforeseen shear stresses not accounted for in the design calculation.

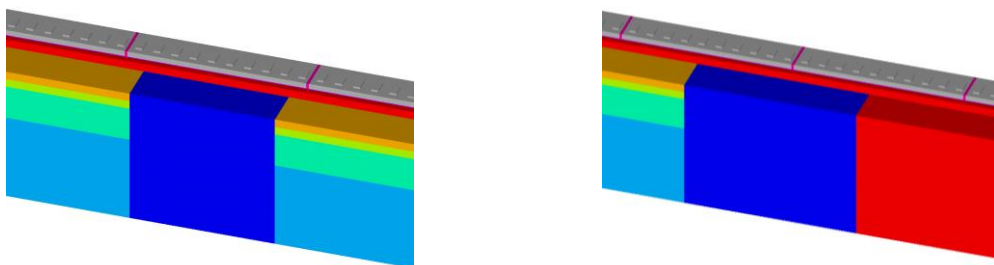


Figure 6.7: Bending moment/ soft soil scenario (left) and shear force/ transition scenario (right)

These scenarios are represented in Figure 6.7, with soft soil sections (blue) and rigid soil sections (red). The soft soil section is used to study the capacity of the slab to span over this defect (Figure 6.7, left). The other group (Figure 6.7, right) is the emulation of a transition between soft soil to a very stiff platform, e.g. a bridge transition with precedent poor embankment compaction. This is mainly to study the slab capacity to resist negative bending moments and shear force due to the very sudden stiffness transition, a phenomenon that is not likely to occur.

These scenarios dataset intends to explore most weaknesses of slab track systems and how they behave in a short- and long-term perspective when submitted to cyclic vehicle and weather actions. In Table 6.1, the 4 categories of scenarios are described and every variable to simulate is listed. All standard features are present in every scenario unless the studied feature is assessed directly. The combination of scenarios is illustrated in Table 6.4, for a total of 42 simulations.

Table 6.3: Scenarization variables

Train operation		Weather actions	
Actions	V120 – Speed of 120 km/h for freight trains V160 – Speed of 160 km/h for freight trains V250 – Speed of 250 km/h for high speed trains V300 – Speed of 300 km/h for high speed trains V350 – Speed of 350 km/h for high speed trains V400 – Speed of 400 km/h for high speed trains	E1 – Standard temperature climate E2 – Severe temperature climate E3 – Extreme temperature climate R1 – Standard precipitation climate R2 – Severe precipitation climate R3 – S precipitation climate R4 – Standard precipitation climate for drainage deficiency	
	Track design		Track condition
	P20 – 20 KN/mm railpad P35 – 35 KN/mm railpad P50 – 50 KN/mm railpad P90 – 90 KN/mm railpad CS1 – C30/37 concrete class strength CS2 – C35/45 concrete class strength CS3 – C40/50 concrete class strength CF – C35/45 fibre reinforced concrete CR – C35/45 recycled aggregate concrete H1 – 25 cm HBL thickness H2 – 30 cm HBL thickness H3 – 35 cm HBL thickness B10 – Standard Bögl reinforcement scheme B8 – 8 mm reinforcement scheme B2 – 12 mm longitudinal rebar Bps – Longitudinal prestress	S1//20 – Rail defect of 1 mm amplitude within a 20 m chord S5//20 – Rail defect of 5 mm amplitude within a 20 m chord S10//20 – Rail defect of 10 mm amplitude within a 20 m chord S1//10 – Rail defect of 1 mm amplitude within a 10 m chord D1 – Drainage deficiency D2 – Subbase construction deficiency (30% HBL stiffness) D3 – Loss of transversal prestress D4 – Expansion joint malfunctioning D5 – Missing fastening system D6 – Low soil compaction S10 – Soft soil (10 MPa) S20 – Soft soil (20 MPa) S40 – Soft soil (40 MPa) S60 – Soft soil (60 MPa) T10 – Transition: soft soil (10 MPa) T20 – Transition: soft soil (20 MPa) T40 – Transition: soft soil (40 MPa) T60 – Transition: soft soil (60 MPa)	

Table 6.4: Parametric analysis simulations

#	High Speed	Freight	Temp.	Rainfall	Pad	CSL	Reinf.	HBL	Rail profile	Track	Soil
1	V250	-	E1	R1	P35	C35/45	B10	H30	S1//20	-	-
2	V300	-	E1	R1	P35	C35/45	B10	H30	S1//20	-	-
3	V350	-	E1	R1	P35	C35/45	B10	H30	S1//20	-	-
4	V400	-	E1	R1	P35	C35/45	B10	H30	S1//20	-	-
5	-	V120	E1	R1	P35	C35/45	B10	H30	S1//20	-	-
6	-	V160	E1	R1	P35	C35/45	B10	H30	S1//20	-	-
7	V300	V120	E1	R1	P35	C35/45	B10	H30	S1//20	-	-
8	V400	V160	E1	R1	P35	C35/45	B10	H30	S1//20	-	-
9	V300	-	E2	R1	P35	C35/45	B10	H30	S1//20	-	-
10	V300	-	E3	R1	P35	C35/45	B10	H30	S1//20	-	-
11	V300	-	E1	R2	P35	C35/45	B10	H30	S1//20	-	-
12	V300	-	E1	R3	P35	C35/45	B10	H30	S1//20	-	-
13	V400	V160	E3	R3	P35	C35/45	B10	H30	S1//20	-	-
14	V300	-	E1	R1	P20	C35/45	B10	H30	S1//20	-	-
15	V300	-	E1	R1	P50	C35/45	B10	H30	S1//20	-	-

Table 6.4: Parametric analysis simulations (Continued)

#	High Speed	Freight	Temp.	Rainfall	Pad	CSL	Reinf.	HBL	Rail profile	Track	Soil
16	V300	-	E1	R1	P90	C35/45	B10	H30	S1//20	-	-
17	V300	-	E1	R1	P35	C30/37	B10	H30	S1//20	-	-
18	V300	-	E1	R1	P35	C40/C50	B10	H30	S1//20	-	-
19	V300	-	E1	R1	P35	FRC	B10	H30	S1//20	-	-
20	V300	-	E1	R1	P35	RAC	B10	H30	S1//20	-	-
21	V300	-	E1	R1	P35	C35/45	B8	H30	S1//20	-	-
22	V300	-	E1	R1	P35	C35/45	B12	H30	S1//20	-	-
23	V300	-	E1	R1	P35	C35/45	Bps	H30	S1//20	-	-
24	V300	-	E1	R1	P35	C35/45	B10	H25	S1//20	-	-
25	V300	-	E1	R1	P35	C35/45	B10	H35	S1//20	-	-
26	V300	-	E1	R1	P35	C35/45	B10	H30	S5//20	-	-
27	V300	-	E1	R1	P35	C35/45	B10	H30	S10//20	-	-
28	V300	-	E1	R1	P35	C35/45	B10	H30	S1//10	-	-
29	V300	-	E1	R4	P35	C35/45	B10	H30	S1//20	D1	-
30	V300	-	E1	R1	P35	C35/45	B10	H30	S1//20	D2	-
31	V300	-	E1	R1	P35	C35/45	B10	H30	S1//20	D3	-
32	V300	-	E1	R1	P35	C35/45	B10	H30	S1//20	D4	-
33	V300	-	E1	R1	P35	C35/45	B10	H30	S1//20	D5	-
34	V300	-	E1	R1	P35	C35/45	B10	H30	S1//20	D6	-
35	V300	-	E1	R1	P35	C35/45	B10	H30	S1//20	-	S10
36	V300	-	E1	R1	P35	C35/45	B10	H30	S1//20	-	S20
37	V300	-	E1	R1	P35	C35/45	B10	H30	S1//20	-	S40
38	V300	-	E1	R1	P35	C35/45	B10	H30	S1//20	-	S60
39	V300	-	E1	R1	P35	C35/45	B10	H30	S1//20	-	T10
40	V300	-	E1	R1	P35	C35/45	B10	H30	S1//20	-	T20
41	V300	-	E1	R1	P35	C35/45	B10	H30	S1//20	-	T40
42	V300	-	E1	R1	P35	C35/45	B10	H30	S1//20	-	T60

6.2 PERFORMANCE INDICATORS

An important methodology to assess the track performance is the definition of a set of short- and long-term parameters that enable the comparison between scenarios. These performance indicators are going to be used in the previously described simulations as standardized control points, and they can be divided into short- and long-term parameters (see Table 6.5).

Table 6.5: Performance indicators

Short-term variables	Geometric	Long-term variables		
		CSL	CAM & HBL	
acc_{CSL} - Concrete supportive acceleration (m/s^2)	y_{rail} - Vertical rail profile (m)	$D_{CSL\ TOP/BOT}$ - Slab top/bottom average damage (-)	D_{CAM} - CAM average damage (-)	
acc_{form} - Formlayer overall acceleration (m/s^2)	y_{soil} - Vertical soil settlement (m)	$D_{CSL\ TOP/BOT}$ - Slab link top/bottom average damage (-)	$D_{CAM\ L}$ - CAM link average damage (-)	
F_c - Contact force of the first wheel (1 bogie) (N)		$D_{CSL\ SLEEPER}$ - Sleeper average damage (-)	$D_{HBL\ TOP/BOT}$ - HBL top/bottom average damage (-)	
q_{soil} - Maximum deviatoric stress on the platform soil (N)		$w_{k\ trs}$ - Transversal crack width on slab top (mm)	$w_{k\ trs}$ - Transversal crack width on slab top (mm)	
		$w_{k\ top/bot}$ - Longitudinal crack width on slab top/ bottom (mm)	$w_{k\ top/bot}$ - Longitudinal crack width on slab top/ bottom (mm)	

The short-term variables are CSL and formlayer accelerations, wheel/ rail contact forces and the level of deviatoric stress of the soil. Long-term variables are divided into geometry deterioration and concrete damage. The latter is subdivided in damage in the CSL and base layers (CAM and HBL). The geometric variables encompass the longitudinal levelling profile of the rail and soil, that is evaluated as the vertical coordinate of each rail/ soil node in the model. The concrete fatigue, however, is grouped in different zones to compute average concrete damage that will be of most importance to compute crack width. The different damage zones are illustrated in Figure 6.8 and 6.9. CSL PS zones (module and link) are excluded from the performance indicators since they have a high concentration of stresses, and, therefore, premature damage according to the damage law used. The mortar link zone is also removed from the model since it holds no significant structural role and has premature damage due to thermal expansion.

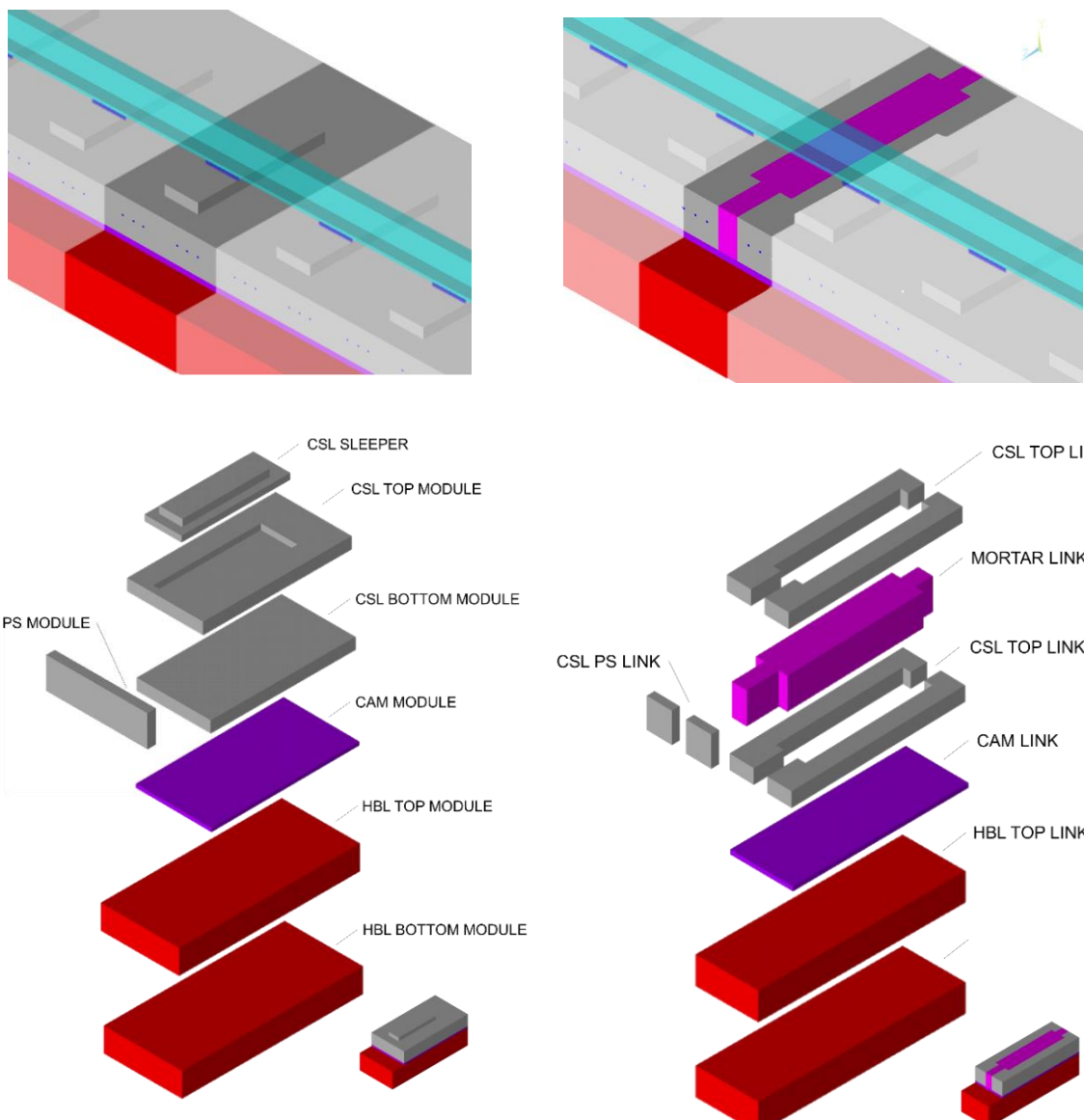


Figure 6.8: Concrete zones of a Bögl slab track slice (one sleeper)

Figure 6.9: Concrete zones of a Bögl slab track link

In what concerns the limiting values, 3 main design thresholds are assumed in which if at least one of them is surpassed, maintenance interventions to correct or replace the element in question are required. These 3 design thresholds are the geometric tolerances of the rail profile (that indirectly preserve short-term safety of the train ride), concrete damage (avoid failure by loss of stiffness) and crack width (ensure track's durability to atmospheric actions).

Considering the admissible rail profile levelling, the Chinese code TB106621 (Professional Standard of the People's Republic of China, 2009) suggests a 15 mm threshold settlement. If the settlement is regular, the threshold settlement is increased to 30 mm, the track vertical radius R_v (m) to a certain train speed V (km/h) can be calculated according to the following equation:

$$R_v \geq 0.4V^2 \quad (6.2)$$

According to crack width evolution, this process is indirectly controlled by a 0.8-0.9% reinforcement ratio to limit cracks to 0-0,5 mm. The Japanese guidelines are adopted to open track sections. These guidelines are used to divide the maintenance needs into three categories A ($w_k \geq 0.2$ mm), which requires immediate and rapid repair; B ($0.1 \text{ mm} < w_k < 0.2 \text{ mm}$), which calls for preparation of a rapid process; and class C ($w_k \leq 0.1$ mm), in which cracks are merely registered to assess their evolution. This threshold is applied for top cracks that are subjected to weather actions, and probably the threshold for bottom cracks is not as stringent, since water infiltration is not as severe as in top cracks. Therefore, no adjustment is going to be considered in the case of bottom cracks.

The threshold for concrete damage is more complex to define since failure by concrete fatigue is a complex phenomenon, thus a simplification is used according to the concrete pavement standards of concrete fatigue of 50% of slabs cracked without any bearing capacity (Smith & Roesler, 2004). As a simplification, a 50% damage level for a zone is adopted as the threshold for an intervention (panel removal or demolishing and reconstruction). It is important to mention that certain nodes in the slab can reach 100% damage; nevertheless, this occurs at the microscale and has no practical consequences at the scale of structural response. Likewise, the HBL follows the same threshold to study the concrete damage. Although this damage approach carries a fair amount of uncertainty, the goal of this threshold is to provide a comparison spectrum for each scenario, including how soon the thresholds are reached in each scenario.

6.3 TRAIN OPERATION DURING LIFETIME

6.3.1 TRAIN SPEED

The effect of the train speed is simulated in 4 existent scenarios for the most typical situations and for hypothetical scenarios to be applied in the near future in numerous slab track corridors worldwide (350 km/h and 400 km/h).

Overall track settlements can be identified in Figure 6.10 and 6.11. The graphs show a trend and a stationary value of around 10.7 mm for a defect-free track and an amplification of the defect

due to the dynamic interaction between the train and the track. This interaction is highlighted to the growing deviation of the maximum settlement down the track, being higher with the speed, as expected. Figure 6.11 shows the maximum settlement evolution over the life period of the track - the most notorious feature is the faster settlement rate of scenario 4 (400 km/h), which puts a larger deterioration on the geometric quality of the track. A big effect on the track geometry is noticed with a 23%, 63% and 125% increase in the rail profile settlement for the increase of speed to 300 km/h, 350 km/h and 400 km/h, respectively (Figure 6.13).

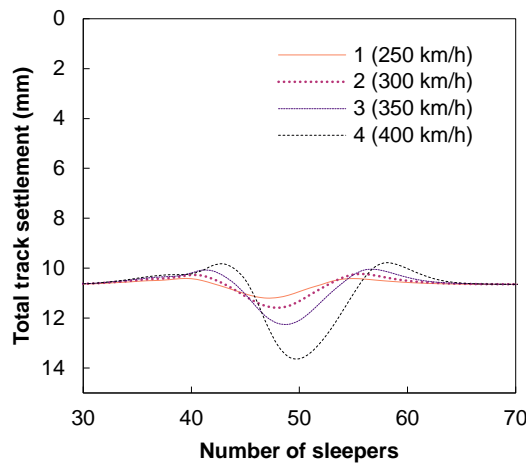


Figure 6.10: Effect of train speed on the longitudinal soil settlement

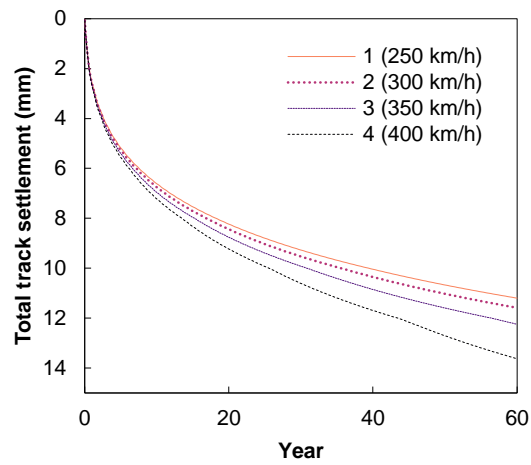


Figure 6.11: Effect of train speed on the progress of the maximum soil settlement

This can be observed in the contact force evolution, as shown in Figure 6.12 (5%, 19%, and 46% increase. The rate of soil settlement differs along with the rail profile since the track can bear some settlement; it is important to note that some of these defects might never happen since maintenance works could occur in the meantime.

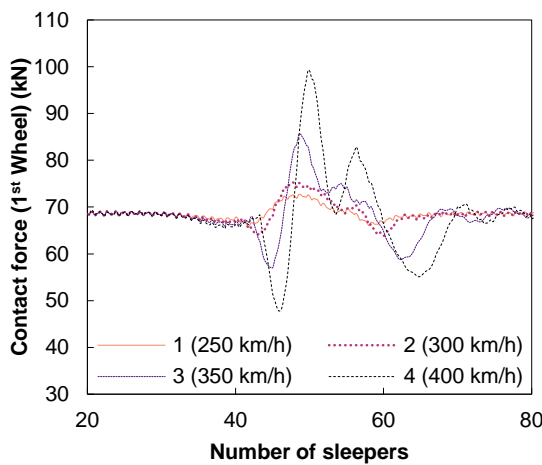


Figure 6.12: Effect of train speed on wheel/rail contact force after 60 years of operation

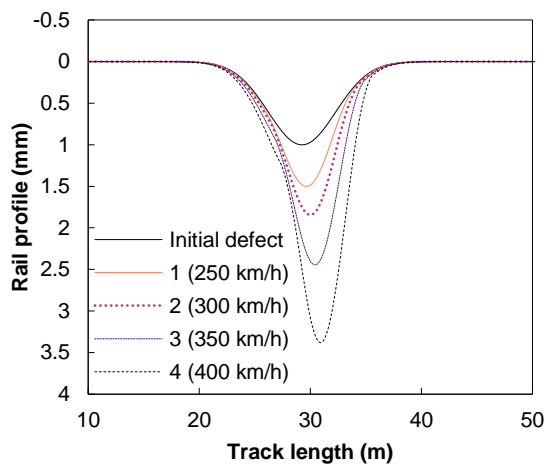


Figure 6.13: Effect of train speed on the rail profile deterioration after 60 years of operation

In terms of concrete damage, the findings are as expected. The damage evolution is mainly driven by the flexural behaviour of the slab due to the train load. This justifies the higher damage in the CSL bottom, see Figure 6.14.

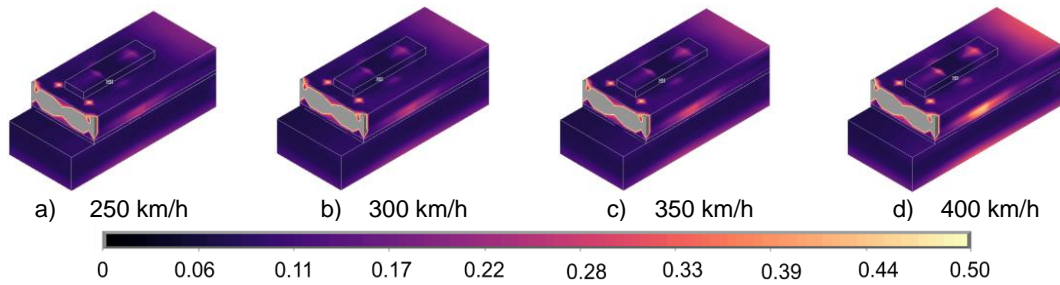


Figure 6.14: Concrete damage level due to flexural stresses caused by vehicles for different speeds

Figure 6.15 presents the cumulative concrete damage of a single node, particularly the most stringent node under flexural stresses (C node). A slow-down in the concrete damage in this node is evidenced during the final years of operation due to loss of stiffness in that concrete zone (since stress is redistributed to nodes of concrete zones that are less damaged, therefore, stiffer).

The relevant role of the CSL layer in the supporting capacity of the structure is observed. As shown in Figure 6.16, the 400 km/h scenario puts a lot of additional stress on the track – this may lead to a significant increase in maintenance costs. In relative terms, the HBL bottom experiences higher changes in concrete damage, mainly due to the singular effect of the train load, excluding the effect of temperature loads.

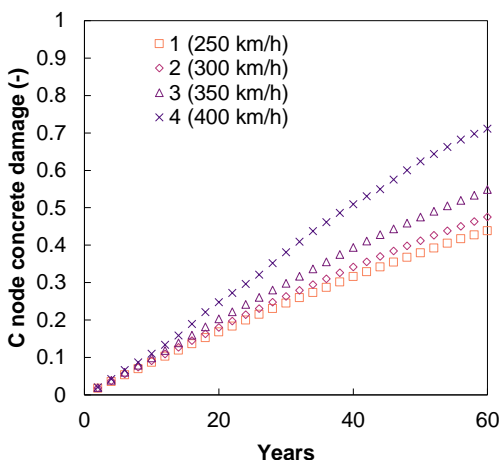


Figure 6.15: Effect of train speed on C2 node concrete damage after 60 years of operation

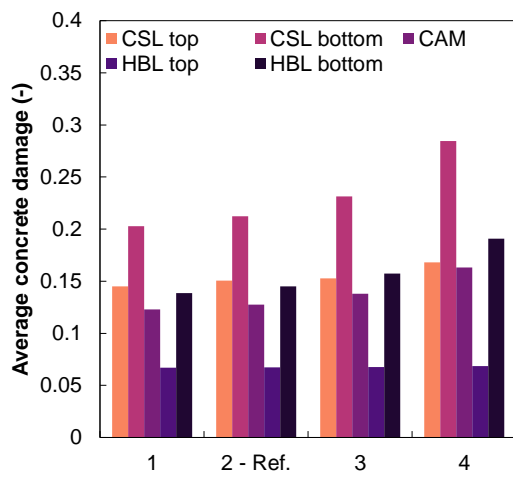


Figure 6.16: Effect of train speed on the final damage per concrete zone

The slab link exhibit larger damage due to a weaker flexural capacity, that could result in higher infiltration possibility in this zone due to mortar voids (Figure 6.17 and 6.18).

Crack width evolution is another topic that brings concern to the durability of the entire structure. Figure 6.19 shows that speed has little influence on the top crack width, since the measured reinforcement stress is collected at the same time of the most unfavourable scenario, which in this case corresponds to measuring stress in the bottom reinforcement stress. Yet this is not the most unfavourable situation for the top crack width. This is the reason why scenario 4 (400 km/h) for some periods has a smaller crack width compared to other speeds. Nevertheless, due to the loss of stiffness in the CSL, top cracks will eventually become more sensitive to the train speed.

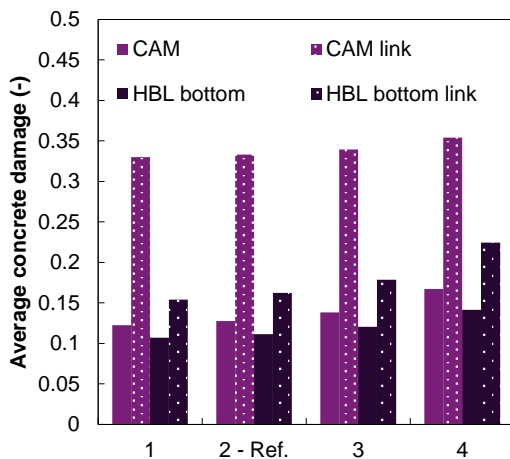


Figure 6.17: Comparison between the open module and link damage for different concrete zones after 60 years of operation

On the other hand, bottom cracks (Figure 6.20) follow an expected trend, where a significant increase of crack width for the 400 km/h scenario in which possible maintenance is due at the 40 years is observed (assuming the hypotheses taken by the HI-Track model). For a 350 km/h speed, maintenance is only required at the very end of the track's lifespan, and for scenarios 1 (250 km/h) and 2 (300 km/h), no maintenance is required. Similarly, to other parameters, bottom cracks increase 4%, 12% and 34% for 300 km/h, 350 km/h and 400 km/h, when compared to a 250 km/h standard.

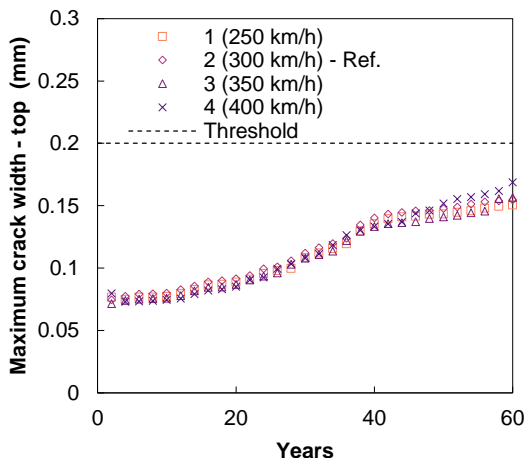


Figure 6.19: Effect of train speed on maximum crack width on the slab top after 60 years of operation

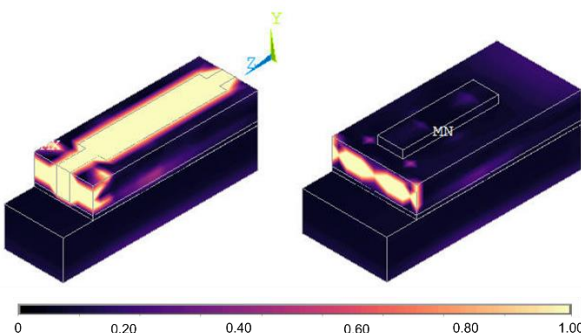


Figure 6.18: Comparison between concrete damage plots between the open module and link zones after 60 years of operation

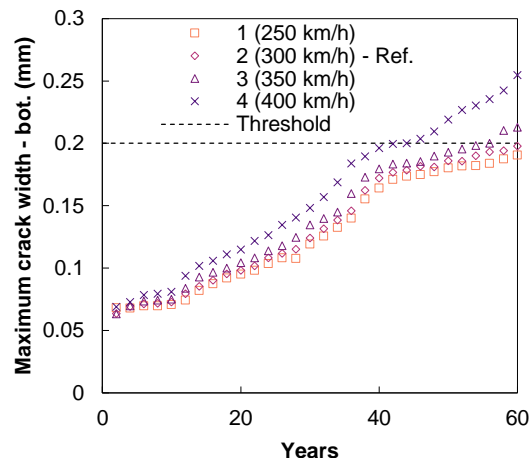


Figure 6.20: Effect of train speed on maximum crack width on the slab bottom after 60 years of operation

6.3.2 VEHICLE TYPE

In this section, several scenarios with different vehicles (a CHR₃ high-speed train and a standard freight train) and combinations of operation between them are tested to study the influence of the vehicle type on the slab track behaviour during the lifetime.

By observing Figure 6.21 and 6.22, the severity of freight trains on the overall track settlement is found, with an increase of almost 60% in track settlement when compared to the same million gross tonnes passages of the standard 300 km/h high speed train. Although the mixed traffic scenarios exhibit a 25% increase in the open track settlement, the presence of freight trains slightly levels the track profile, causing a lower differential settlement when compared to the scenarios 2 and 4, which present the same high speed circulations as scenario 7 and 8, respectively (see Figure 6.23). Scenarios with only one type of train and train speed are prone to systematic failures, and in this case, amplified differential settlements. Also, little impact is observed between scenario 5 (120 km/h) and 6 (160 km/h). Hence, for lower speeds (<200 km/h), freight train speed has little influence on track settlement.

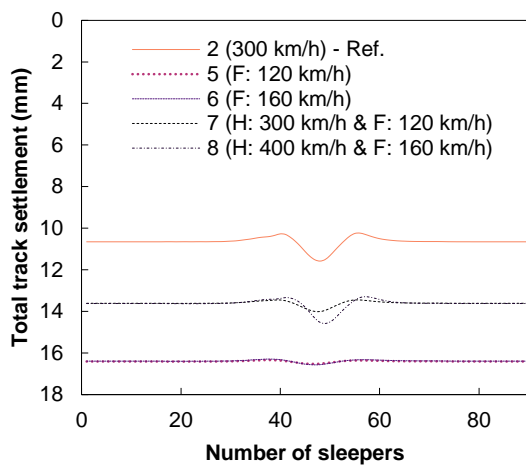


Figure 6.21: Effect of vehicle type on overall track settlement profile after 60 years of operation

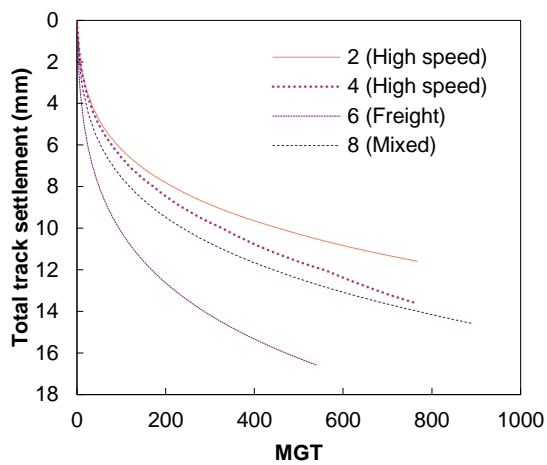


Figure 6.22: Effect of vehicle type on overall track settlement evolution after 60 years of operation

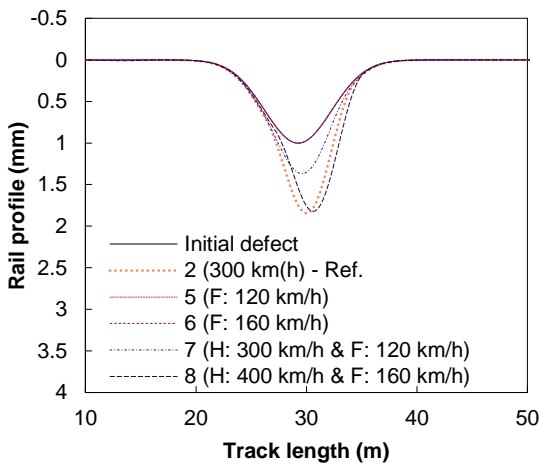


Figure 6.23: Effect of vehicle type on the rail profile after 60 years of operation

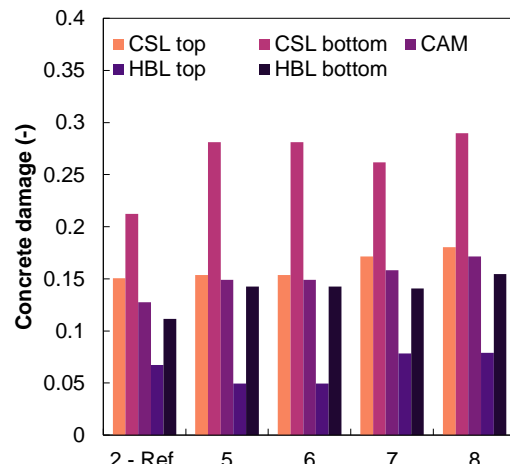


Figure 6.24: Effect of vehicle type on the final damage per concrete zone

A significant influence of freight trains on track damage is that related to fast pace deterioration at an early stage when compared to the same million gross tonnes passages of a high-speed train (Figure 6.25). In this figure, point B is a control node near the fastener.

On the contrary, high-speed trains cause higher damage at more advanced stages of the slab

track life cycle, mainly due to the high frequency and amplified loading. At the 20-years mark, the freight scenario 5 has 51% more cumulated damage than the mixed traffic scenario 8, and, at the end of tracks' service life, the difference is only 2%. Overall damage by concrete zone is not that notorious (Figure 6.24). At 20 years in, the exclusive freight traffic scenarios present a 35% higher damage than the standard high-speed case, and at the end of the 60 years, the difference only drops to 32%. Taking in mind the comparison with million gross tonnes passages, this phenomenon is also evidenced in Figure 6.26, in which the freight scenario has a negative concavity for the average damage at the CSL bottom, while the high-speed scenario presents a positive concavity. Also, by direct comparison, the mixed traffic scenario starts with higher damage and is overtaken by the high speed scenario at mid-lifespan of the slab track.

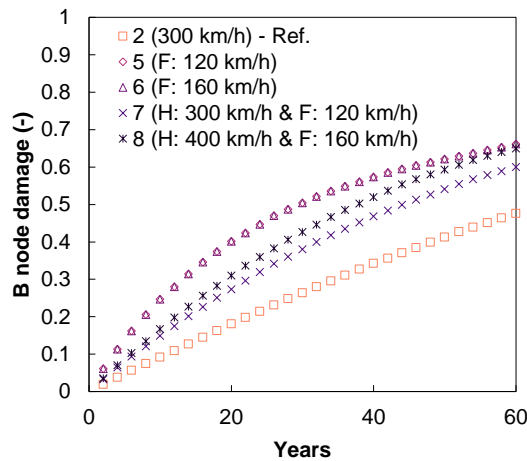


Figure 6.25: Effect of vehicle type on concrete block damage after 60 years of operation

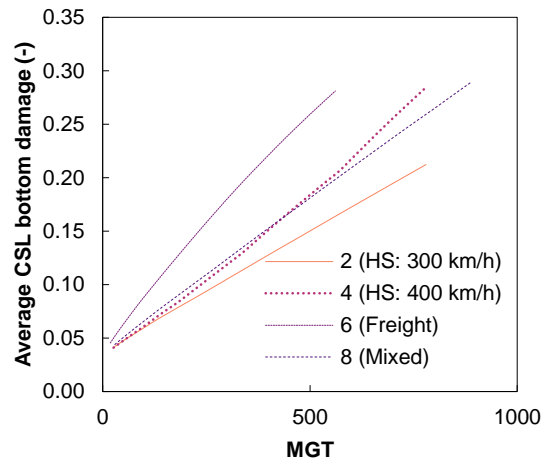


Figure 6.26: Effect of vehicle type on the average CSL bottom damage

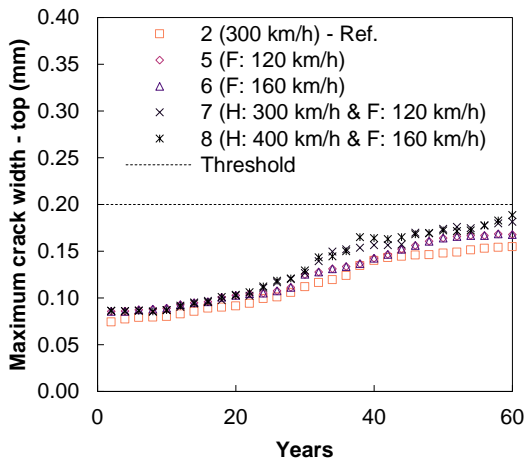


Figure 6.27: Effect of vehicle operation on maximum crack width on the slab top after 60 years of operation

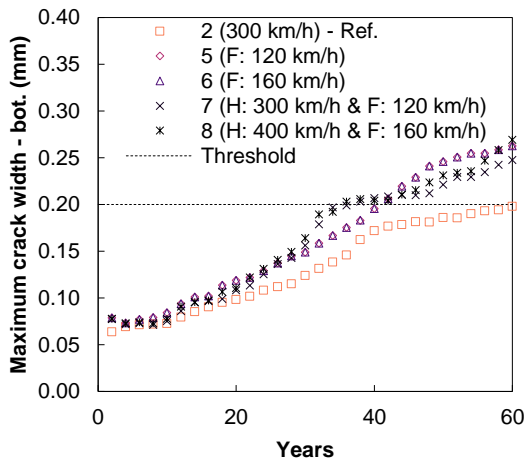


Figure 6.28: Effect of vehicle operation on maximum crack width on the slab bottom after 60 years of operation

Regarding crack width (Figure 6.27 and 6.28), similar to the speed scenarios, the top cracks do not reach the maintenance threshold, while the bottom cracks reach the same level around 30 to 40 years. This bottom cracking requires early injection for the mixed traffic (30 years) and then stabilizes until it is overtaken by the freight scenario. This is explained by the fact that at the

30-year level, the freight scenarios lost more concrete stiffness than the mixed traffic scenarios, and vice versa after the 40-year period (Figure 6.29).

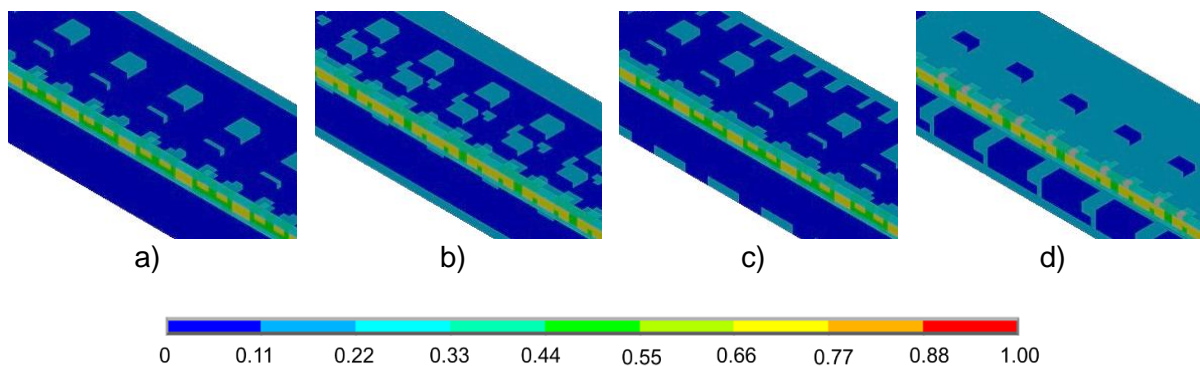


Figure 6.29: Loss of concrete stiffness in the CSL and HBL for a) freight scenario at 35 years, b) mixed traffic scenario at 35 years, c) freight scenario at 50 years and d) mixed traffic scenario at 50 years

6.4 EXTREME WEATHER EVENTS

6.4.1 TEMPERATURE

Slab tracks are subjected to atmospheric actions - mainly temperature loads, which cause relevant structural damage as reported by multiple scholars (X. Liu et al., 2011; Song et al., 2014; Wan & Yang, 2018; J. Wang et al., 2019). Slab tracks are built worldwide, sometimes in construction sites with harsh climates including large annual temperature difference, daily temperature difference and high gradients, continuous high temperatures.

Damage process in joints is of major importance for the overall damage of the structure (Cai et al., 2019). In the case of the evaluated Bögl slab track system (a prefabricated system), the expansion joints have high quality. In the case of in situ construction (like Rheda 2000 or Stedef), extra scrutiny should be applied to assure a well-functioning temperature performance. Results from Wang et al. (2019) show that negative temperature gradients are one of the main responsible factors for tensile concrete fatigue.

In terms of temperature-related scenarios, track settlement and rail profile are almost the same among themselves, with differences lower than 2%, justified by higher stress on the platform soil caused by a lower bending capacity of the track (less stiffness).

When it comes to track damage, the temperature scenarios cause great impact. Additional damage is mainly concentrated on the top surface of the CSL and is observed right after the first years (Figure 6.30). This results in an early loss of stiffness as it was almost an ultimate state action, instead of a long-term damaging phenomenon. Thus, the majority of damage is caused in the first year and a steady damage accumulation is caused by the traffic over time. According to the simulations, the early loss of stiffness of the CSL causes the damage accumulation to shift to the HBL (which is mostly protected from temperature actions) as seen in Figure 6.31, which presents a lower damage rate for scenarios 9 and 10.

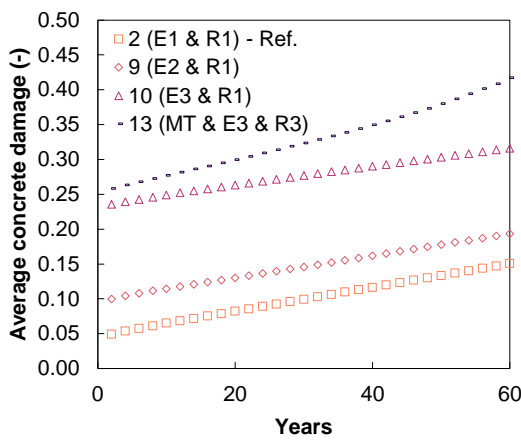


Figure 6.30: Effect temperature scenarios on average concrete damage after 60 years of operation

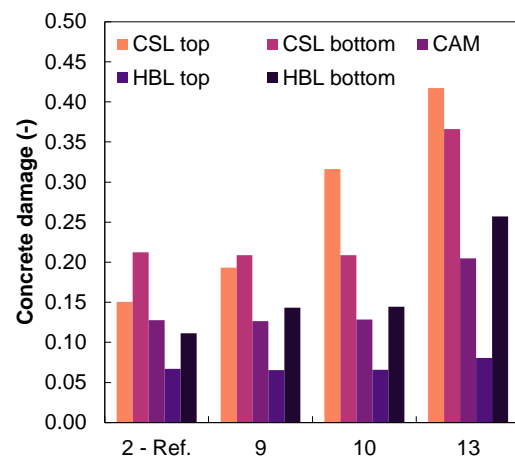


Figure 6.31: Effect of temperature scenarios on the final damage per concrete zone

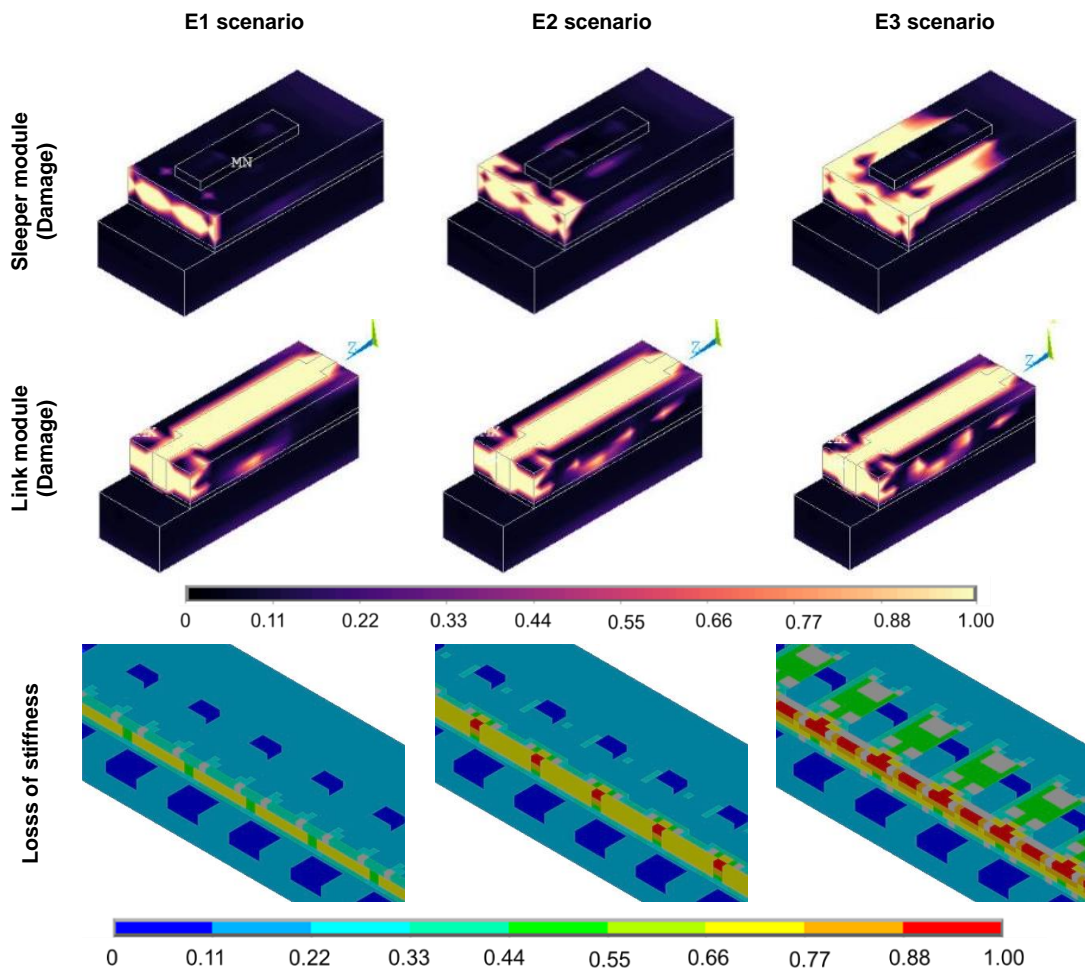


Figure 6.32: Effect of extreme temperature scenarios on concrete damage and loss of stiffness

In Figure 6.32, the final damage after 60 years for the temperature scenarios is illustrated, showing the influence of temperature actions on the CSL. For scenario 2 (E1 standard) the damage is concentrated in the link that accommodates all the expansions of the track, behaving

like an expansion joint. The other points of damage are in the transversal prestressed zone and bending related damage in the link zone between panels. In this standard scenario, the effect of temperature is not significant since it is all absorbed by the mortar link between panels, acting as a cracking point. For scenarios 9 and 10, the uniform temperature presents a moderate effect, mainly visible in the vicinity of the linking studs, and the temperature differential is the most damaging, causing a great amount of concrete deterioration at the top of the slab. This effect is mainly caused by negative gradients during the winter periods, causing tension on the upper part of the slab and consequently reach the tensile damage strength. This deterioration is concentrated in the outer edge of the panels – this is also shown in Figure 6.32.

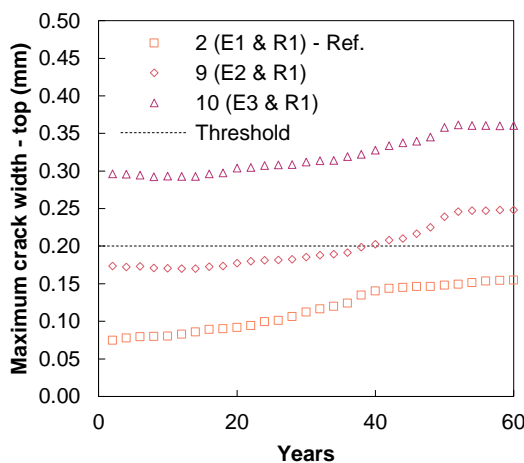


Figure 6.33: Effect of temperature scenarios on maximum crack width on the slab top after 60 years of operation

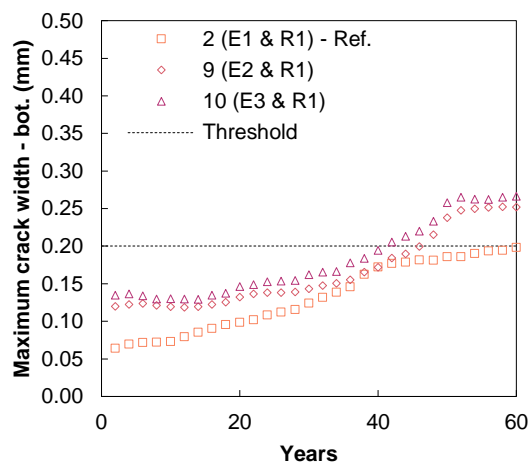


Figure 6.34: Effect of temperature scenarios on maximum crack width on the slab bottom after 60 years of operation

This concrete damage results in significantly higher crack widths at the top of the slab (Figure 6.33). In the case of scenario 9 (E2 climate), maintenance intervention is required before the end of the 40-year period. For scenario 10, the extreme temperature scenario acts as an ultimate state combination load and maintenance to seal the top cracks is required from the first load cycle. Due to the stiffness loss in the upper slab, the concrete damage and crack width advance at a steady state after the load temperature; nevertheless, significant maintenance is required on the slab to inject cracks. The bottom of the slab is more protected from temperature actions, nevertheless, the overall loss of stiffness causes larger cracks at the same magnitude level for E2 and E3 scenarios (Figure 6.34).

These results aid in concluding that temperature has a key role in slab damage, even when appropriate expansion mechanisms are used. This occurs mainly when extreme temperature gradients, which cause the slab to warp, are present. Nevertheless, if a proper functioning of the expansion joint is guaranteed, concrete damage and crack width can be controlled without major interventions, such as panel replacements. It is important to point out that this performance to extreme temperatures is achieved by transversal prestressed tendons that control the effect of the temperature gradient and the excessive warping of the slab, otherwise the slab will suffer irreversible damage, as observed in Figure 6.35.

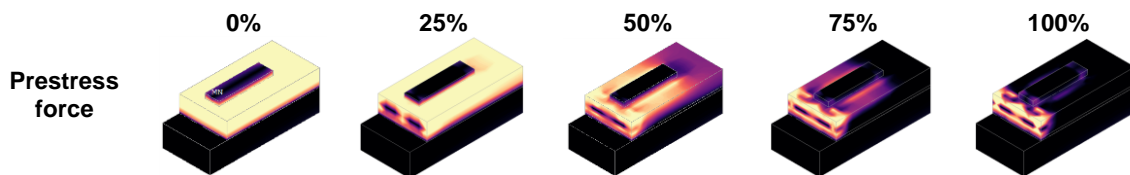


Figure 6.35: Effect of transversal prestressed tendons on the track damage for an E2 scenario

6.4.2 RAINFALL

Climate change brings new challenges. The previous subchapter discussed temperature scenarios and, due to climate change, extreme weather events will become more frequent and severe (e.g. extreme precipitation that could cause flooding). Thus, extreme precipitation is modelled indirectly as a variation of the phreatic level, since the phreatic level increases the saturation degree of the soil and therefore larger permanent deformations. In this section, an extreme action scenario (13) is added with extreme temperature and rainfall and mixed traffic.

According to Figure 6.37, maximum overall settlement for scenario 11 (R₂) increases almost 40% more when compared to the reference scenario, and twice as much for the extreme rainfall scenario. Regarding the differential settlement, more severe precipitation events result in a deeper concavity for the same initial defect as expected. The lower settlement before the defect is due to the lower dynamic stresses on the soil (Figure 6.36) since the vehicle is “projected” right before the defect, resulting in less vehicle weight being directly applied to the track. The same phenomenon occurs while exiting the defect. This occurs in this scenario because systematic operation is being simulated. In scenario 13, these bumps are attenuated due to the presence of mixed traffic.

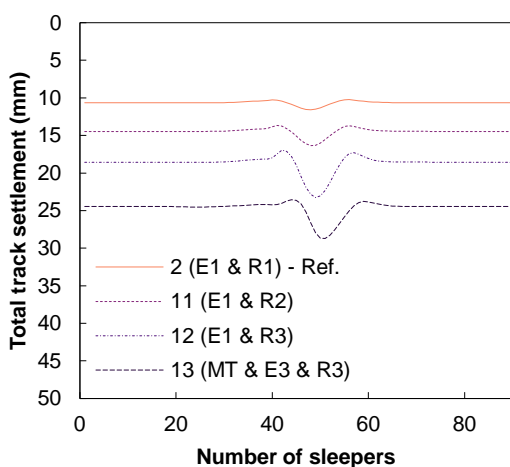


Figure 6.36: Effect of rainfall scenarios on the longitudinal soil settlement

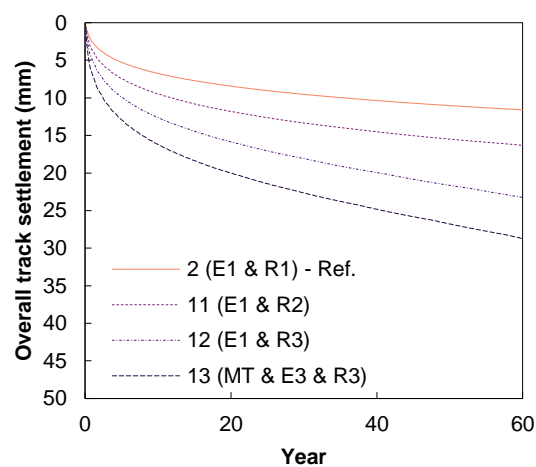


Figure 6.37: Effect of rainfall scenarios on the progress of the maximum soil settlement

This extra dynamic amplification due to geometry deterioration causes larger bending stresses in the CSL (4% and 19% for R₂ and R₃ respectively). The scenario 13 presents significant higher damages, mainly by the added severity of the additional traffic and extreme temperature, acting almost as a worst-case scenario. When compared to the scenario 10 (E₃ climate), the CSL top

damage increased 32% with the added rainfall and mixed traffic effect, with a greater contribution of the inclusion of the rainfall scenario (2/3 of the damage approximately).

CSL and HBL bottom damage can show the deterioration without the effect of the temperature. The damage increases by 30% and 42% approximately when compared with the extreme mixed traffic scenario 8, being this increase explained by the major part of it by the rainfall. This larger damage increase is illustrated in the average damage of the CSL bottom in Figure 6.38 and 6.39. Notwithstanding, the damage is below the maintenance threshold for the simulated properties.

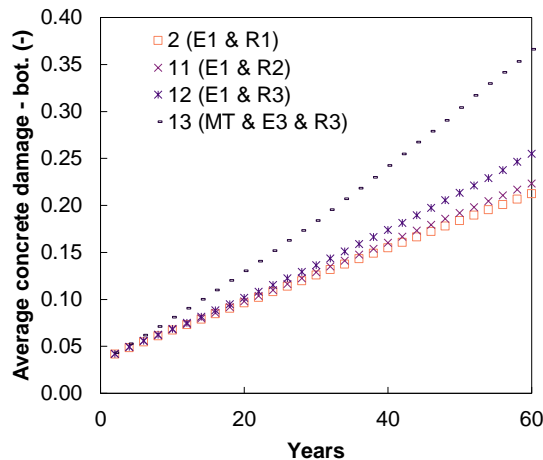


Figure 6.38: Effect of temperature scenarios on average CSL bottom damage

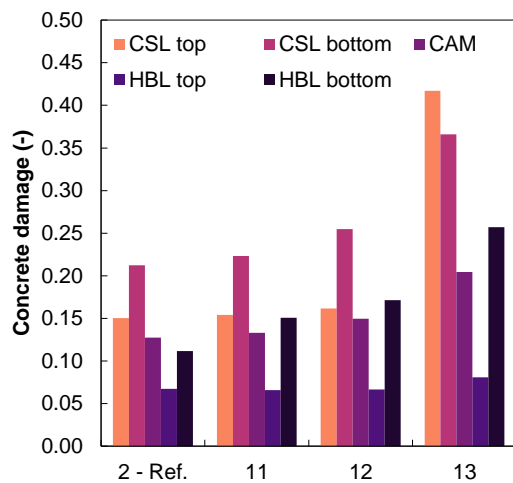


Figure 6.39: Effect of temperature on the final damage per concrete zone

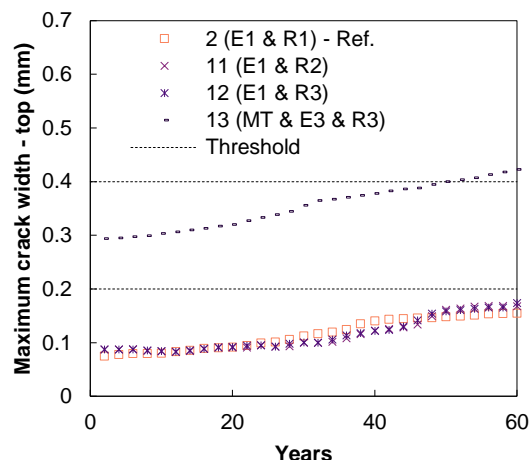


Figure 6.40: Effect of rainfall scenarios on maximum crack width on the slab top after 60 years of operation

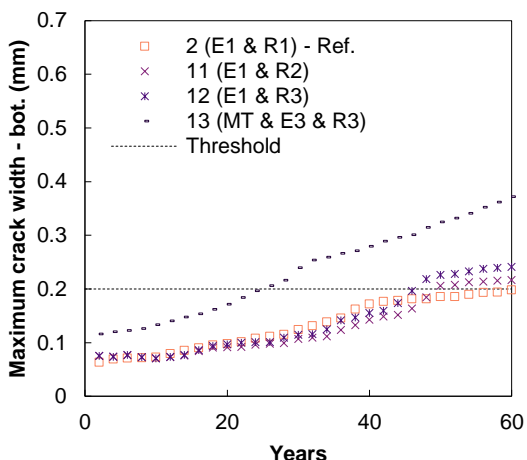


Figure 6.41: Effect of rainfall scenarios on maximum crack width on the slab bottom after 60 years of operation

Regarding crack width, rainfall does not affect maintenance needs related to crack injection significantly (in what concerns both top and bottom cracks). Nonetheless, scenario 13 is the worst-case scenario again from an external action point of view, with significant maintenance works required both for an early age (due to the temperature) and at around 48 years of service life (due to top crack sealing maintenance needs shown in Figure 6.40). Also, for bottom cracks (Figure 6.41), the maintenance threshold is reached after the 20-year mark. Interestingly,

extreme rainfall affects more the short-term behaviour of the track than extreme temperature, mainly by the geometric deterioration of the track.

6.5 STRUCTURAL TRACK DESIGN FOR ENHANCED SHORT- AND LONG-TERM PERFORMANCE

6.5.1 RAILPAD

Railpad is an influential and important stiffness's values are between 40 to 70 kN/mm, and therefore 3 scenarios are designed with a 20 kN/mm (similar to the Rheda 2000 system), a 50 kN/mm (significantly stiffer than usual) and a 90 kN/mm railpad (similar to what is applied on ballasted tracks).

As expected, stiffer railpads provoke higher stresses on the subjacent layers, therefore causing larger permanent deformations on the soil (Figure 6.42), yet in very small variations (+/- 3%) and not that relevant for long-term settlement. Stiffer railpads seem to neutralize the speed effect on the settlement shift downwards the track.

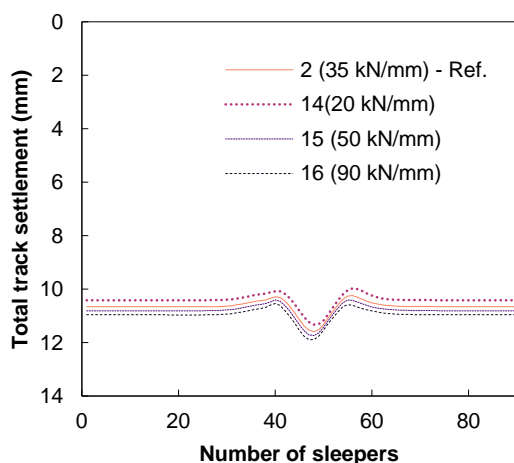


Figure 6.42: Effect of railpad stiffness on the longitudinal soil settlement

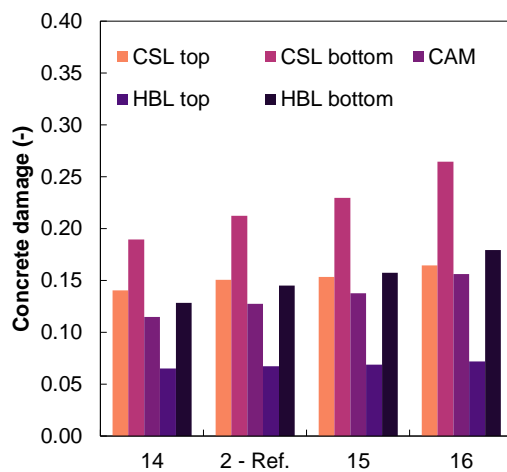


Figure 6.43: Effect of railpad stiffness on the final damage per concrete zone

Concerning track damage (Figure 6.43), the railpad presents a slightly higher influence with a - 11% and 8% variations for a 20 kN/mm and 50 kN/mm railpads for flexural fatigue in the CSL bottom, respectively. Similar deviations are found in CAM and HBL. As expected, the 90 kN/mm presents a 25% increase in the slab's bottom damage.

Also, as expected, stiffer railpads increase cracks width, being less relevant for top cracks (Figure 6.44), nevertheless, bottom cracks can be visibly affected (Figure 6.45). For a 20 kN/mm, the maintenance requirement is not reached, with a 5% reduction when compared with the 35 kN/mm reference case. The 90 kN/mm presents a 21% increase in the bottom crack with, anticipating possible maintenance interventions in more than 15 years compared to the reference case.

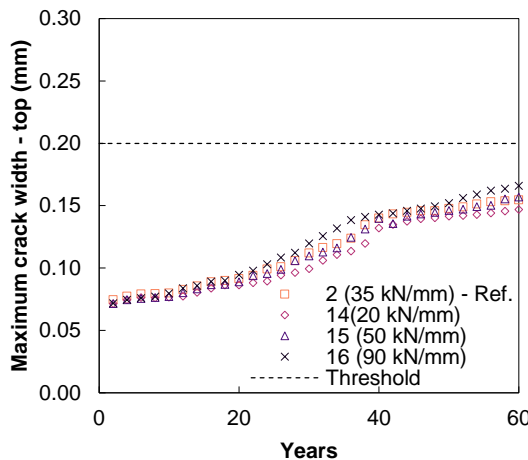


Figure 6.44: Effect of railpad stiffness on maximum crack width on the slab top after 60 years of operation

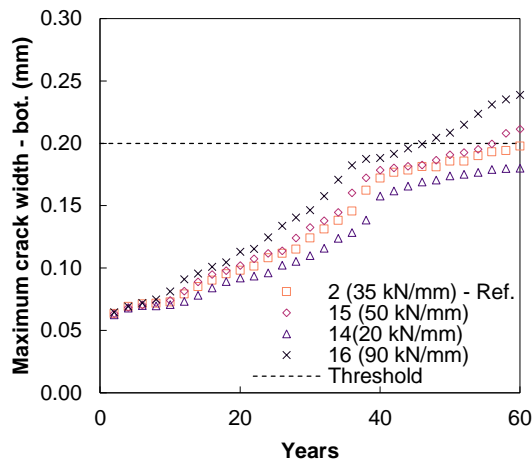


Figure 6.45: Effect of railpad stiffness on maximum crack width on the slab bottom after 60 years of operation

By observing the long-term deformation of the soil and the concrete damage/ crack width evolution a relationship between the railpad stiffness and the increased deterioration in these two phenomena is found: higher railpad stiffness leads to higher damage in the track. Nevertheless, there are some aspects that HI-Track is not taking into account. First, from an operational standpoint, in which lower railpad stiffness requires more energy consumption by the train to move and also higher maintenance in rail-related deterioration.

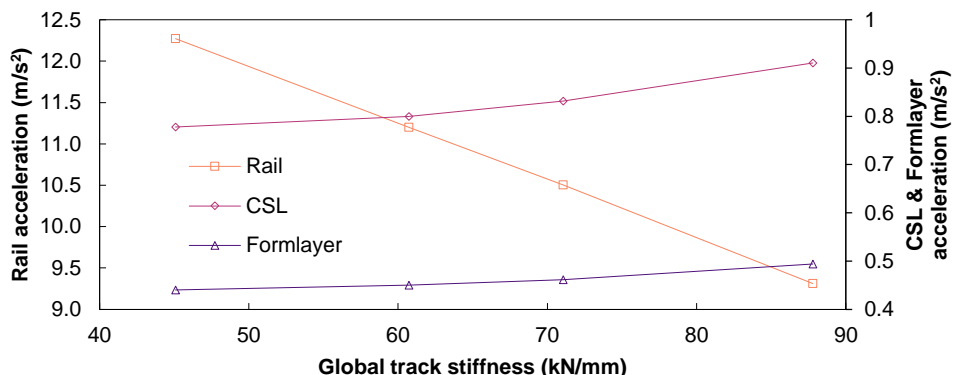


Figure 6.46: Slab track accelerations under a 300 km/h high speed train for a 100 Hz band pass filter

According to Figure 6.46, it is possible to notice the inverse relationship between accelerations in the rail and supporting layers when it comes to railpad stiffness. By that fact, it can be observed that rail deterioration is more likely to arise for lower railpad stiffness since higher acceleration levels can lead to higher chances of rail wave wear and head checks (Z. Li et al., 2008). On the other hand, higher acceleration levels for the CSL and formlayer are coherent with the higher damage observed in these two structural layers.

As a consequence, and according to the work of Teixeira (2004) in ballasted tracks, an optimum value for the global track stiffness can be achieved for slab tracks. As stated by the obtained results, the 35 kN/mm value can be close to an optimum railpad stiffness for the Bögl system taking in mind track deterioration and energy consumption. Flexible tracks lead to higher

chances of rail-related fatigue and higher energy consumption by the train movement, and otherwise, stiffer tracks cause higher rates of track settlement and concrete damage.

6.5.2 CONCRETE SUPPORTIVE LAYER

An important parameter to control the concrete deterioration is its strength class, whose tensile strength is the key player in concrete damage and crack control performance. Hence 4 scenarios are simulated to evaluate 4 types of concrete (aside from the standard C35/45) and their properties are shown in Table 6.6:

Table 6.6: Concrete design properties (CEN, 2004b)

Symbol	Description	C30/37 #14	C35/45 #2	C 40/50 #15	FRC #16	RAC #17
f_{ck} (MPa)	Characteristic cylinder compressive strength	30	35	40	35	35
f_{ctm} (MPa)	Mean tensile strength		2.90	3.21	3.51	5.39
E_{cm} (MPa)	Elastic modulus		32 837	34 077	35 220	34 077
						23 854

Simulations 14 and 15 resort to concrete strength class C30/37 and C35/45, respectively. The mechanical properties of all concrete mixes were those assumed in Eurocode 2 for each strength class. The remaining concrete is unusual variants that could offer their potential to slab track construction.

The FRC (fibre reinforced concrete) can attain a larger tensile strength at a low cost (Madhkhan et al., 2013; Y. Yang et al., 2015) and thus is important to tensile damage due to flexural and temperature-induced stresses. It is assumed that is the same specified compressive resistance as the standard C35/45 scenario and that the elastic modulus remains the same. For the discussed scenarios, the used fibre reinforced concrete uses steel fibres, and the mean tensile strength is assumed to be equal to the splitting tensile strength calculated through:

$$f_{ctm} = \alpha + \beta \times \left(v_f \times \frac{l}{d} \right)^{\chi} \times \sqrt{f'_c} \quad (6.3)$$

This expression is the result of a regression analysis presented by Musmar (2013), whose parameters were found to be $\alpha = 0.614$, $\beta = 0.4$ and $\chi = 1.029$. The remaining parameters are the volumetric fibre content (v_f), the length/diameter ratio of the steel fibre (l/d) and the compressive strength of the concrete (f'_c). Reports from the HS2 project in the UK suggest a volumetric fibre content between 0.25% and 2% and a length/diameter ratio between 60 and 90, hence the adopted values are 1% and 75 respectively, which results in a mean tensile strength of 5.39 MPa.

In what concerns recycled aggregate concrete, the advantages in its use are mainly focused as a sustainable choice for slab tracks, since slab tracks stretch hundreds or even thousands of kilometres in some corridors, so the concrete demand for such works is high. The properties of

the RAC are quite similar to natural concrete for the same specified compressive strength stress (C35/45). However, the tensile strength drops approximately 10/15% and the Young modulus is reduced by 30% for concrete of the C35/45 strength class (Pacheco et al., 2019). These assumptions were based on a metanalysis and are valid for the material properties' assumptions of Eurocode 2. For this strength class, the tensile strength is limited by the (weak) strength of coarse recycled aggregates and the f_{ctm}/f_c ratio decreases; conversely, the tensile strength of lower strength classes is not as affected by the strength of (weak) recycled aggregates (the mortar phase is weaker than the coarse aggregates) and the f_{ctm}/f_c ratio is larger.

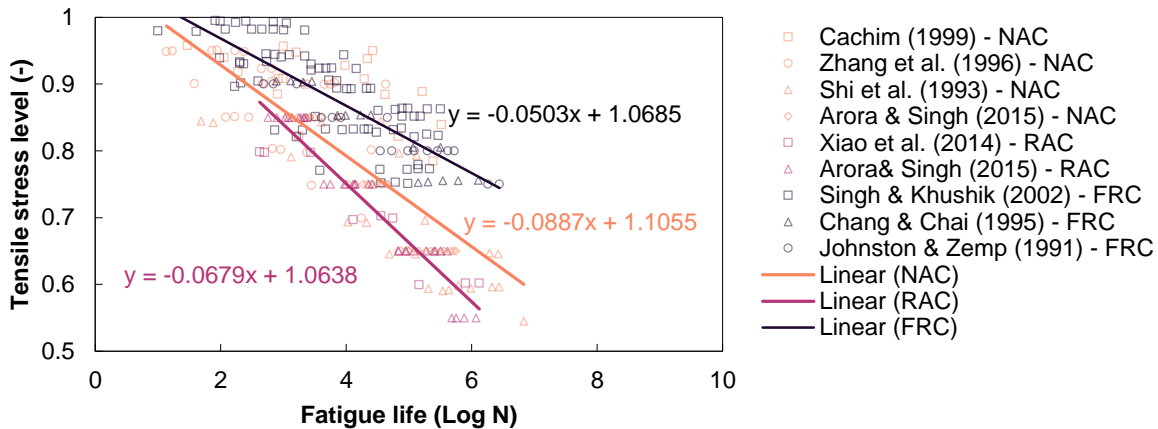


Figure 6.47: S-N curve of NAC, RAC and FRC under bending cyclic loading

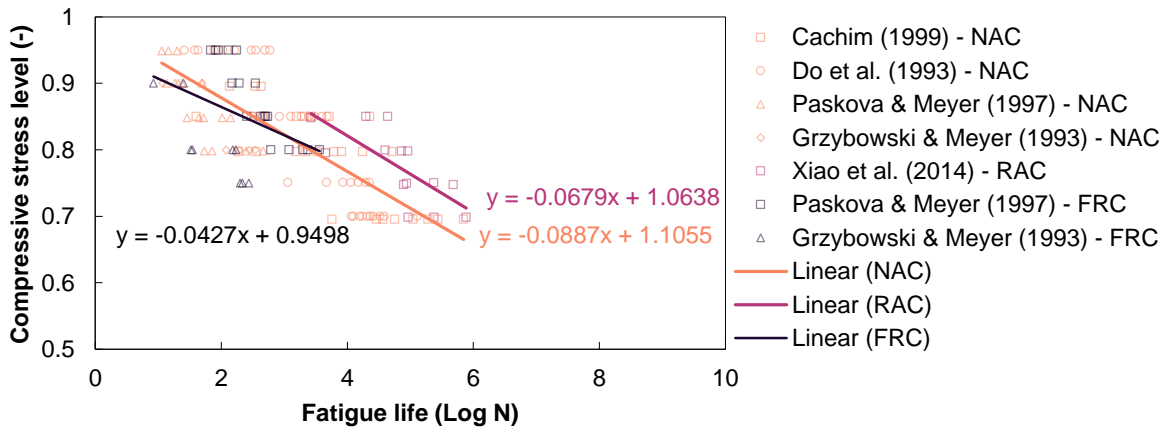


Figure 6.48: S-N curve of NAC, RAC and FRC under uniaxial compressive cyclic loading

Due to the different mechanical properties, RAC and FRC present different Wöhler curves, namely due to the nature of the recycled aggregates and the percentage level in the concrete mixture, as the fibre volumetric content and length/ ratio for FRC. With this in mind, several studies in concrete fatigue were evaluated, in natural aggregate concrete (Arora & Singh, 2016; Cachim, 1999; Do et al., 1993; Grzybowski & Meyer, 1993; Paskova & Meyer, 1997; X. P. Shi et al., 1993; B. Zhang et al., 1996), recycled aggregate concrete (Arora & Singh, 2016; Xiao et al., 2013, 2014) and fibre reinforced concrete (Chang & Chai, 1995; Johnston & Zemp, 1991; M. K. Lee & Barr, 2004; Singh & Khushik, 2002). The concrete fatigue studies were selected according to 100% recycled aggregates content for RAC and the volumetric fibre content of 1% to FRC. Although

these studies are not directly designed for pavement engineering, the selected tests use the flexural bending test to assess the tensile fatigue concrete, that is closely related to the tests performed directly for pavement analysis. Nonetheless, for comparison, plain concrete fatigue studies are also included to evaluate in a broader sense the effect of RAC and FRC in the fatigue life of the system. Figure 6.47 and 6.48 present the compressive and tensile fatigue results for the different concretes, respectively. By observing the figures above, it is possible to find that for compressive loading, the NAC, FRC and RAC are quite similar, being the RAC the one that shows a better performance, nevertheless, using a conservative philosophy, the concrete damage law for compression stresses is the same adopted in Chapter 4. For flexural fatigue and most important for damage assessment, the recycled aggregate concrete has a reduction in the flexural capacity of around 20%. On the other hand, FRC presents a 25% increase under flexural loading, however, there is not going to be applied a corrective factor and adopt an over-conservative approach for the upcoming simulations.

Regarding the simulations, concrete quality presents a low influence on the track geometry deterioration and indirectly, it also has a smaller impact on the short-term response of the overall system, nevertheless track vibrations could be a risen concern if important thresholds are not met during the track's lifespan. On the other hand, concrete damage is strongly affected by the concrete quality. Figure 6.49 and 6.50 illustrates the average concrete damage on the top and bottom of the concrete slab, respectively. On top of the slab, the deterioration rate is quite similar only with small differences due to the dominance of compressive stresses under mainly flexural loads which are low. The big difference among the various concrete qualities is the initial damage caused by the daily temperature cycles, and in this case, the FRC shows a better performance than the C40/50, although the deterioration rate is higher on the first. This is because the initial damage is controlled by the tensile strength under cyclic thermal loads and the progressive damage is controlled by the compressive strength, in the case of the top of the CSL. Conversely, the CSL bottom presents a larger difference, being the C30/37 the concrete with the poorest performance after the RAC. The difference between using a lower strength class concrete (C30/37) is 15%, whereas increasing to C40/50 only drops the overall damage to 4%. Also using RAC could be a sustainable choice for projects that favours recycled aggregates availability and ease of transport since the bottom damage only reduces 5% when compared with the NAC simulation. Said that this concrete could be applied in tunnels (controlled environment) without compromising performance and even if the project requirements entail high-performance concrete, RAC can also be vastly used in the subbase layer without relevant additional deterioration.

In both zones, FRC stands out with the best performance, mainly in the flexural fatigue performance with more than 30% less damage when compared with the standard C35/45 concrete. The 10% damage level is reached for the bottom CSL at 39 years of operation, almost 18 years after when compared with the standard C35/45. It is important to strengthen the fact

that the Wöhler curve used for the FRC simulation is conservative since the fatigue life is larger for this kind of concrete, thus an even better performance can be achieved.

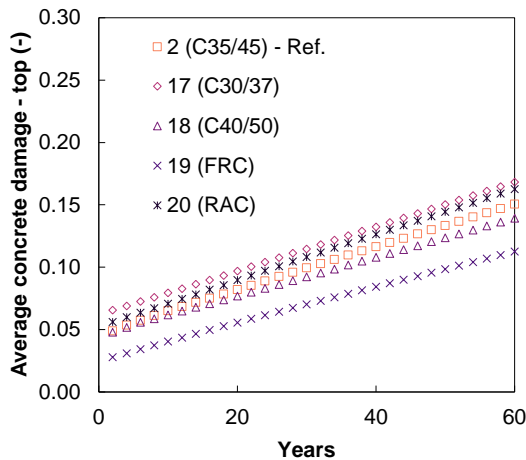


Figure 6.49: Effect of concrete quality scenarios on average CSL top damage

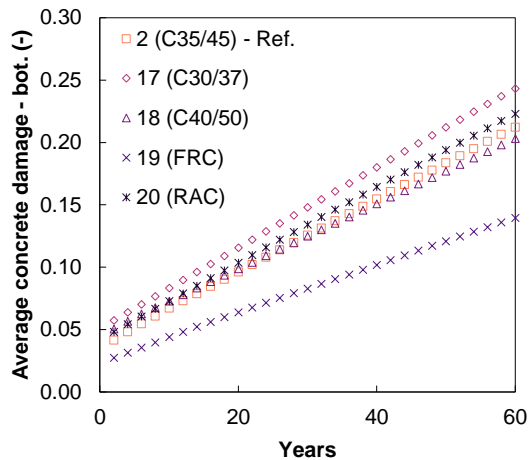


Figure 6.50: Effect of concrete quality scenarios on average CSL bottom damage

Also, according to Figure 6.51, it is possible to notice the concrete quality on the HBL bottom, in which the RAC have the worst performance. Despite having slightly lower damage (and consequently lower loss of stiffness) in the CSL than the C_{30/37}, the RAC presents a lower Young's modulus which is reflected in lower participation in the bending capacity of the system, thus a lower portion of the load is applied to the HBL. In Figure 6.52 can be observed the final concrete damage of the different evaluated concrete types.

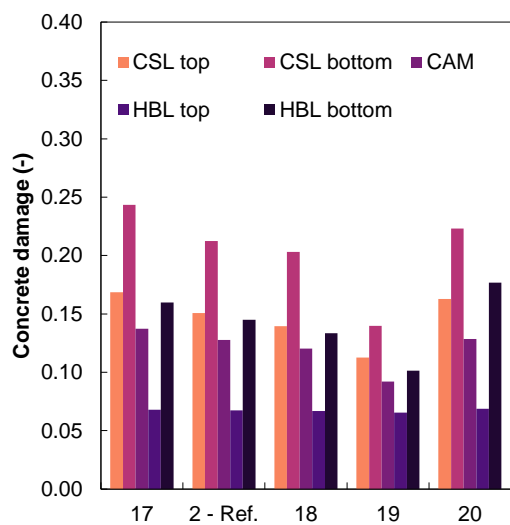


Figure 6.51: Effect of concrete quality on the final damage per concrete zone

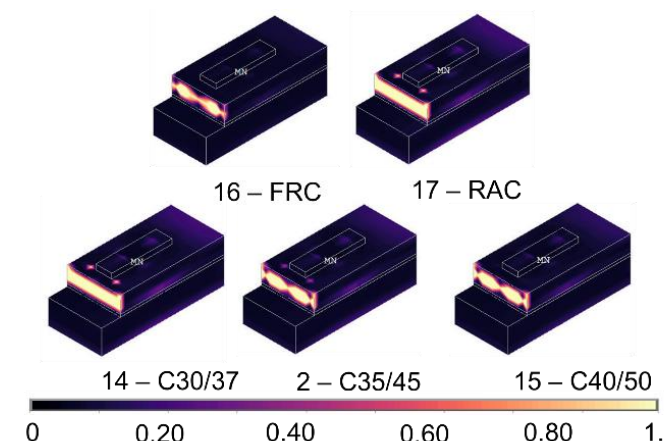


Figure 6.52: Effect of concrete quality on the final damage plot of the sleeper module

In matters of concrete cracking, the concrete quality does not influence significantly after 60 years. For example, for the 0.1 mm alert point, the top cracks for the several concrete simulations, are observed between 15 and 21 years, while the FRC postpones this alert level by almost 20 years. In both top and bottom cracks, the FRC does not need any major maintenance procedures regarding crack injection, presenting itself as a potential high-performance design.

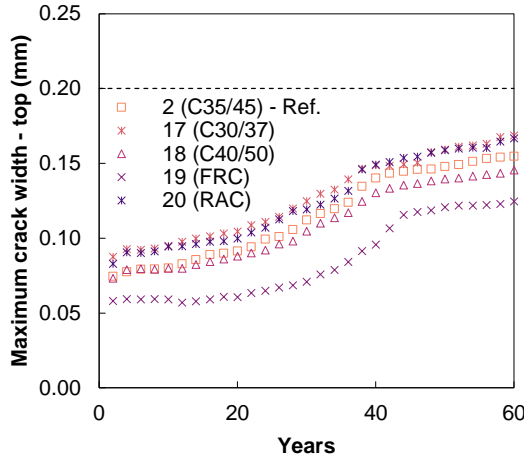


Figure 6.53: Effect of concrete type on maximum crack width on the slab top after 60 years of operation

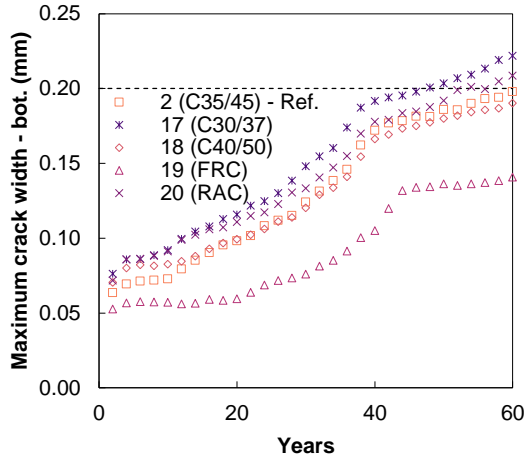


Figure 6.54: Effect of concrete type on maximum crack width on the slab bottom after 60 years of operation

6.5.3 REINFORCEMENT

Reinforcement detailing in ballastless tracks are mainly used for crack control (Lichtberger, 2005) with a mechanical ratio of around 0.8-0.9%. In the case of the Bögl system, mechanical percentage of reinforcement ($\frac{A_{s,fy,d}}{b \times d \times f_{cd}}$) is 0.43% (excluding the linking studs). This abnormal low reinforcement percentage is reasoned by the transversal prestress tendons featured in this system. Variants with Ø 12 mm (0.62%) and Ø 8 mm longitudinal rebar versions (0.28%) are going to be simulated, as well as a longitudinal prestress version (LPS).

In what regards settlement and damage, the differences are almost null, with a small negative variation ($\approx 1\%$) for the Ø 12 mm scenario and vice versa for the Ø 8 mm scenario. This is justified by the fact that a larger steel ratio causes less stress to be directed to the concrete and less overall damage, although being in a residual effect.

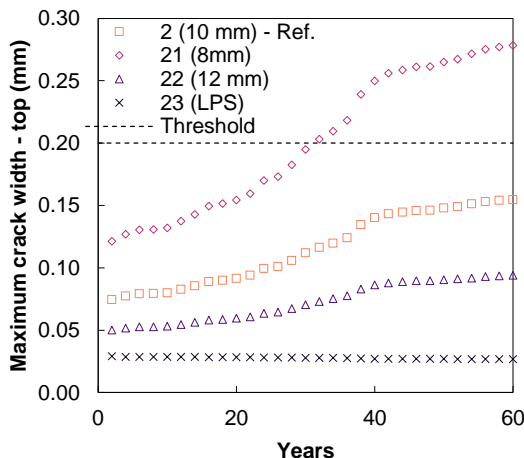


Figure 6.55: Effect of longitudinal rebar size on maximum crack width on the slab top after 60 years of operation

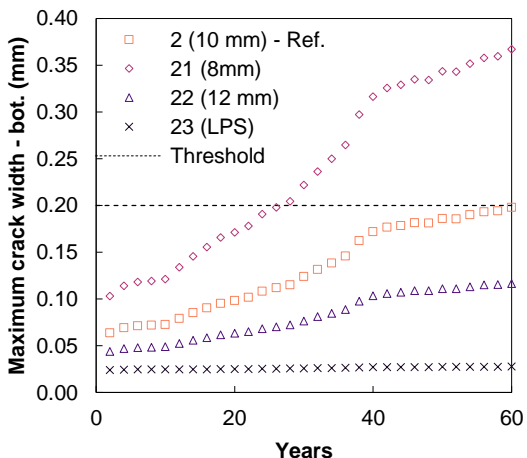


Figure 6.56: Effect of longitudinal rebar size on maximum crack width on the slab bottom after 60 years of operation

In what concerns crack control, the reinforcement presents a massive influence. In Figure 6.55 and 6.56 it is possible to observe that by reducing the longitudinal rebar diameter from 10 to 8 mm, the crack width increased 80% requiring injection at the 30-year mark, something not required to the standard scenario. For the bottom crack width, the threshold is reached at 26 years of operation. On the other hand, the 12 mm scenario reduces the crack width by almost 40% compared with the standard case and the longitudinal prestress reaches an 80% reduction. Despite these reductions, for standard applications, the 10 mm reinforcement scheme does not present significant maintenance in terms of crack injection, thus an increase in the rebar diameter would entail significant construction costs without a great difference in the maintenance costs. Likewise, the longitudinal reinforcement shows high performance in crack width control (crack widths under 0.05 mm for the entire lifespan of the slab track), nevertheless, this is a costly solution, only used in extremely cold climates. Better reinforcement schemes are mostly justified by temperature-induced actions.

6.5.4 HYDRAULICALLY BONDED LAYER

Although being labelled as a sub-layer/ subbase, the HBL plays an important role (Lichtberger, 2005) in track's durability, mainly by controlling the level of soil stresses. To evaluate its performance on the track's fatigue life, 2 scenarios are assessed by varying the HBL thickness in 5 cm. Said that two simulations are performed with a 25 cm HBL (#24) and 35 cm (#25).

In overall track damage, for the evaluated HBL thicknesses, there is not a relevant impact in track damage with an increase of 4% for flexural fatigue in the CSL for the 25 cm HBL version and a 4% decrease if a 35 cm is used. Concrete cracks are also with variations around +/- 3%.

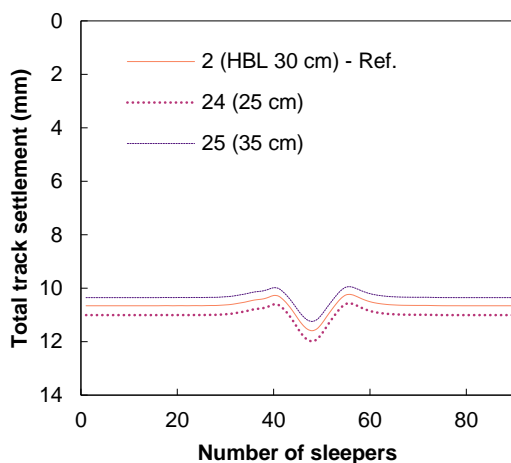


Figure 6.57: Effect of HBL thickness on maximum crack width on the slab top after 60 years of operation

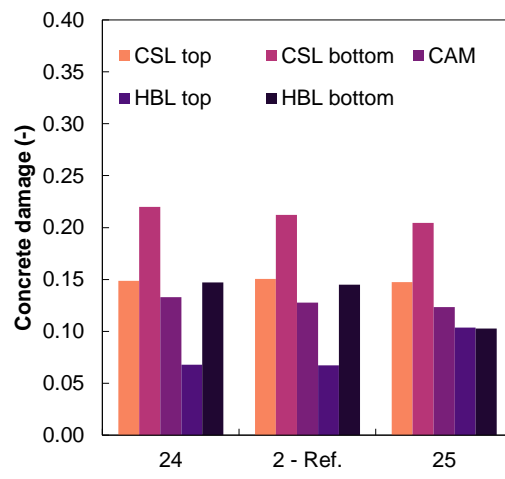


Figure 6.58: Effect of HBL thickness on the final damage per concrete zone

Track settlement is also not relevantly affected with deviations under 4% for the 25 cm HBL version and 2.8% for the 35 cm HBL version. This is an indication that the HBL is already on a near optimum design as expected (for being an important element in construction economy), in which an increase in the thickness will have marginal variations on track response on short- and

long-term spectra and a reduction under 25 cm could lead to increased deterioration of the CSL and track geometry and leading to substantial maintenance costs.

As depicted in Figure 6.57 and 6.58, the HBL damage itself suffers little impact in reducing the thickness to 25 cm (+1.5%), mainly by the fact that the flexural capacity of the system is guaranteed by the CSL. In the case of the 35 cm HBL, the flexural fatigue is reduced by almost 30%. These design improvements can present better results for longitudinally heterogeneous soils that will be addressed later in this chapter.

6.6 EFFECT OF TRACK QUALITY CONDITION DURING LIFETIME

6.6.1 GEOMETRIC QUALITY

An initial rail profile defect is a common deterioration type that can influence track degradation significantly, thus the geometry quality can influence the maintenance regime.

To assess the effect of the rail levelling, 3 scenarios are simulated using Dirac-type sinusoidal defects: a 5 and 10 mm amplitude settlement within a 20 m wavelength, and a 1 mm amplitude defect within a 10 m wavelength. It is worthy to mention, that different wavelengths present different maintenance thresholds according to equation 6.1.

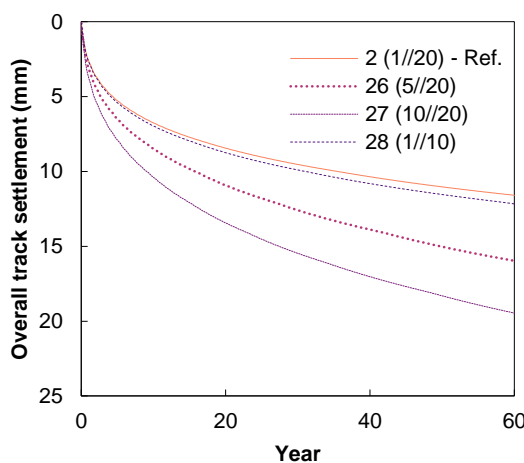


Figure 6.59: Effect of initial rail profile on the progress of the maximum soil settlement

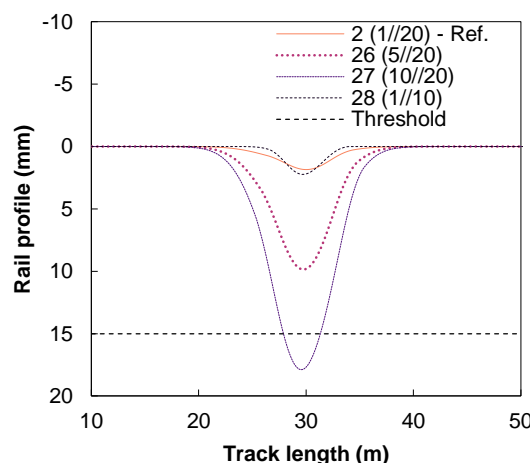


Figure 6.60: Effect of initial rail profile on the rail profile deterioration after 60 years of operation

Figure 6.59 and 6.60 present the global track settlement and the rail profile respectively, and it can be noticed that the disparity on how the settlement evolves according to the initial amplitude. The standard case (1//20) increases from 1 mm to 1.85 mm (85%) in 60 years, and for the initial settlement of 5 mm, the increase was 4.85 (final 9.85) and for the 10 mm scenario, it was 7.9 mm, surpassing the settlement maintenance threshold, thus requiring geometry corrections before the end of the lifespan (at the 20-year level). Maintenance interventions could be applied with different thresholds and this could result in different life cycle costs since near failure thresholds tend to be more onerous than early-detected deterioration.

The 10 m wavelength scenario results in a 2.23 mm settlement after 60 years, which is a 20% increase compared with the 20 m wavelength, nevertheless the comfort of the passengers is significantly lower (Figure 6.63). If the initial settlement was 2 mm instead of 1 mm, the maintenance threshold (3.75 mm) of the rail profile is reached after 45 years, which indicates the importance of the initial geometry quality for low wavelength defects.

Also, an initial settlement has some influence on the CSL's damage according to Figure 6.61 and 6.62 in which the scenario #27 (10//20) presents the most damage when compared with the remaining initial settlement scenarios. Due to flexural stresses at the bottom of the CSL, the scenario #28 (1//10) reaches the $\frac{1}{4}$ damage threshold (0.125) at the year 26.4 which is 3.4 years before the standard scenario, while the scenario #26 (5//20) and #27 (10//20) reach this threshold 9.6 and 16.5 years before the standard case. Figure 6.63 and Figure 6.64 show the dynamic amplification due to the higher settlement on the track. This dynamic amplification results in a growing rate of deterioration for the scenario #27 (bottom) until the $\frac{1}{4}$ damage level. After this damage level, the damage rate is reduced, mainly explained by the loss of CSL stiffness (see Figure 6.62).

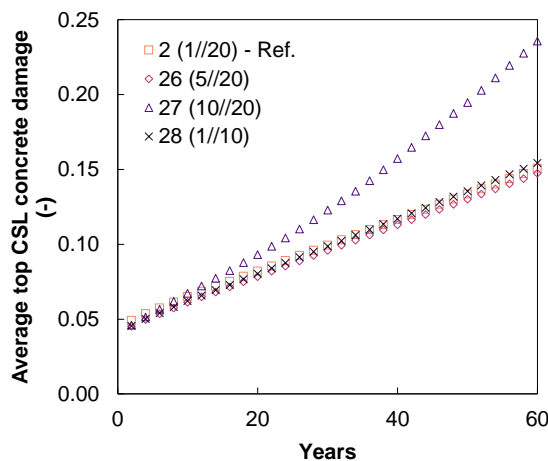


Figure 6.61: Effect of initial rail profile on concrete damage on the CSL top

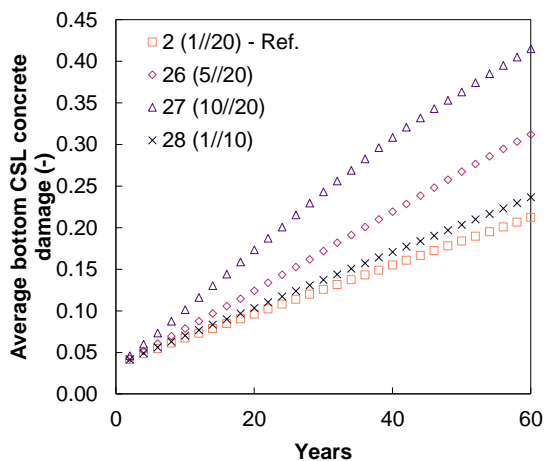


Figure 6.62: Effect of initial rail profile on concrete damage on the CSL bottom

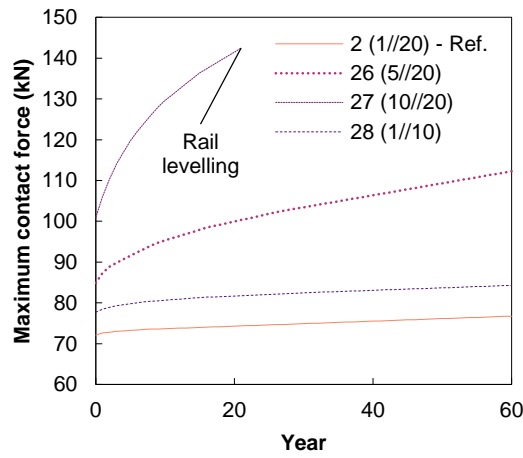


Figure 6.63: Effect of initial rail profile on contact force evolution during the lifetime

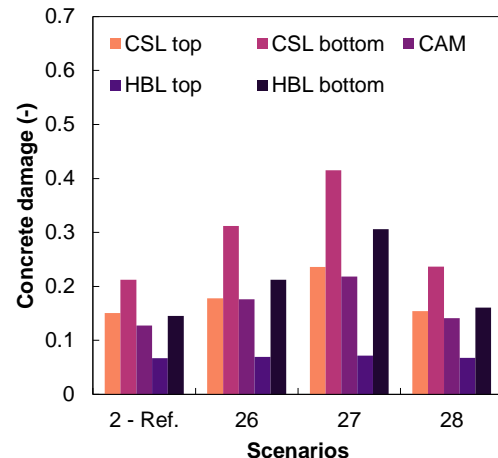


Figure 6.64: Effect of initial rail profile on the final damage per concrete zone

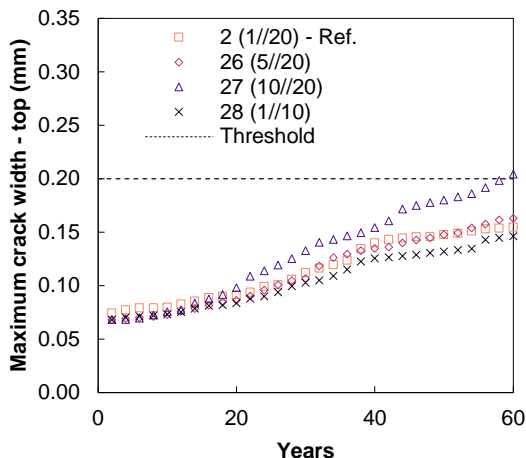


Figure 6.65: Effect of initial rail profile on maximum crack width on the slab top after 60 years of operation

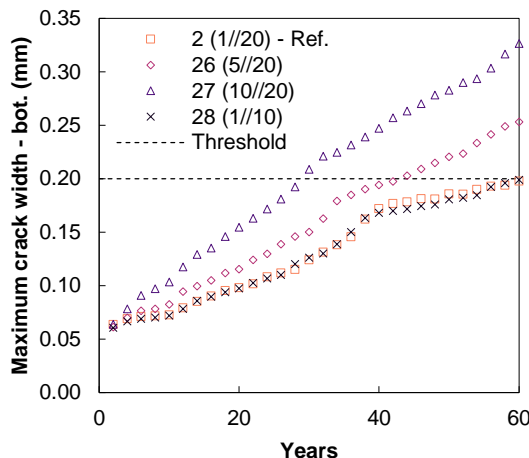


Figure 6.66: Effect of initial rail profile on maximum crack width on the slab bottom after 60 years of operation

As observed in Figure 6.65 and 6.66, the severity of the initial settlement is also felt in the crack width evolution with maintenance required according to the maintenance threshold for the scenario #27 (10//20) more than 30 years before the standard case for the bottom cracks. Also, in the slab top, the crack width intervention limit is reached within the lifespan of the track for scenario 27, mainly driven by the loss of stiffness. In this line, the initial settlement is important, not only for the geometric quality deterioration but as well as the structural damage in the track that can reach noticeable levels, leading to unforeseen maintenance interventions.

6.6.2 CONSTRUCTION QUALITY

This subsection presents a wide variety of defects that could arise during construction of the Bögl slab track system that could be grouped **in infrastructure design** (drainage deficiency and low soil compaction), **in site construction errors** (subbase stiffness reduction and expansion joint malfunctioning) and **module manufacturing**: prestress loss and defective railpad support.

First, in what regards infrastructure design, drainage deficiency is assumed as the lack of capacity by the drainage system to redirect rainwater to the water collectors and significantly increase the water content of the soil. To model this scenario, it is assumed that the concrete slab track has 100% permeability and water content of the soil levels are calculated by the thermo-hydro-mechanical model. The low soil compaction is simulated through a reduction of the initial equivalent traffic of 100 000 cycles to 10 000 cycles, which will increase the early stage of the settlement.

Scenario #30 (low soil compaction) presents a modest increase in the overall track settlement (12.5%) as depicted in Figure 6.67. Also, almost no change in the rail profile of the track is observed (6.2%) and therefore a marginal increase in track damage as shown in Figure 6.68. This states that the proposed lower level of soil compaction has a small impact on the geometry quality of the track. Nevertheless, it is a high standard soil, and if a lower soil compaction is performed on a lower quality platform soil, track settlement will certainly bring geometry

problems and all consequences associated with. On the other hand, scenario #29 (drainage) has a major impact on the soil settlement, presenting the largest settlement among the simulated scenarios so far and requiring heavy maintenance on the track at the 48-year mark.

Also, the differential settlement is almost 7 times larger than the standard case, which can indicate significantly more frequent longitudinal levelling maintenance. This geometric degradation is easily reflected in the growing damage under the slab observed in scenario #29 (drainage), where damage starts to accelerate at the 20 years (4 mm//20 m).

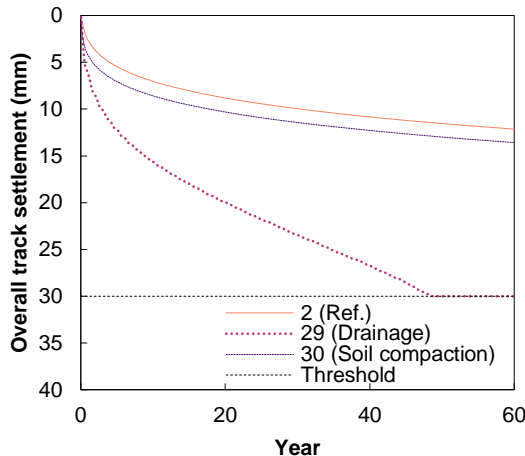


Figure 6.67: Effect of infrastructure design on the progress of the maximum soil settlement

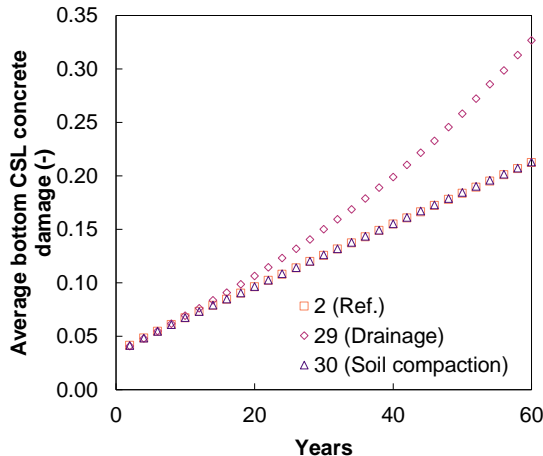


Figure 6.68: Effect of infrastructure design on concrete damage on the CSL top

Additionally, crack width progress does not require significant maintenance interventions for the top cracks during lifetime of the track (Figure 6.69); yet lateral bottom cracks require maintenance 15 years before the standard case scenario #2 (Figure 6.70). Scenario #30 (low soil compaction) presents little influence on the crack width progress.

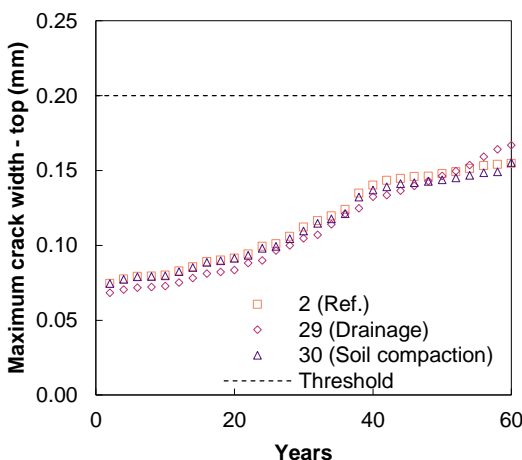


Figure 6.69: Effect of infrastructure design on maximum crack width on the slab top after 60 years of operation

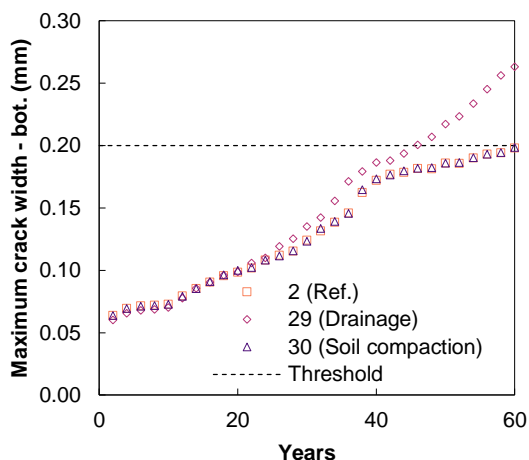


Figure 6.70: Effect of infrastructure design on maximum crack width on the slab bottom after 60 years of operation

For construction design, the subbase stiffness reduction scenario (#31) presents a 70% reduction of the common Young's modulus for the HBL and the expansion joint malfunctioning (#32) is

modelled by the movement restriction between panels, e.g. accumulation of debris in the expansion joint.

In what concerns the long-term settlement of the track, these 2 scenarios are not significant. The subbase stiffness reduction only increases the overall settlement by 5%, and the expansion joint has a marginal increment, only by 1% justified by a stiffness loss more evident in the slab.

Additionally, track's damage is slightly affected by the subbase loss of stiffness with a 7% increase in the CSL bottom. Thus, the importance of the quality of the subbase is less relevant than other elements, presenting little influence over the 10 to 30 GPa spectrum. Conversely, the expansion joint malfunctioning makes the temperature loads act as an almost ultimate state load that requires the total replacement of the panel. This is an extreme scenario that only occurs when a design flaw is unsupervised. In this respect, expansion joints play a crucial role for the temperature design of the track, however, it is necessary to emphasize that such a damaging phenomenon would hardly occur in the studied slab track system unless unlikely specific conditions are met. The mortar filled voids in between panels act as expansion joints as a "weak" link in the continuous structure, hence when panel expands or contracts, the "weakest" link will crack. In regular scenarios, the mortar links act as a non-structural element, and by undergoing some temperature load cycles, they crack and lose stiffness. However, for normal track operation, uniform temperature loads will not cause significant damage. Significant damage (due to slab warping) is caused by differential temperature.

Finally, the last defects are related to the **manufacturing** of the slab track panels, that although being prefabricated in a highly controlled environment, could present possible flaws. These flaws are assessed as prestress loss during the cast of the panels (#33) and loose clamp supporters (#34), that will not assure proper rail support. This last defect could occur during construction or operation by a missing fastening system. The prestress loss scenario is modelled with no pulling force whatsoever and the missing fastening system scenario is simulated by the removal of the railpad element from the models.

The number of defective sleepers is an important feature to assess the damage that these defects can cause to the railway system. A single defective sleeper may not cause a substantial effect on the contact force and many defective sleepers in a row may cause safety issues and a high risk of derailment. In this sense, the number of defective sleepers is chosen to maximize the concrete damage caused in order to keep an operational ride safety. It is assumed that a contact force higher than 30% of the static axle load must occur at all train passages. A parametric study on the effect of speed and the number of defective sleepers on the wheel/ rail contact force was assessed and summarized in Figure 6.71 and 6.72. Certain combinations of train speed and number of defective sleepers would not occur in real-life scenarios since safety precautions would not allow it. Hence, by following the aforementioned derailment safety criterion, for a speed of 300 km/h for the high speed vehicle in this analysis, the number of defective sleepers that could occur in railway operations should be less than 2.

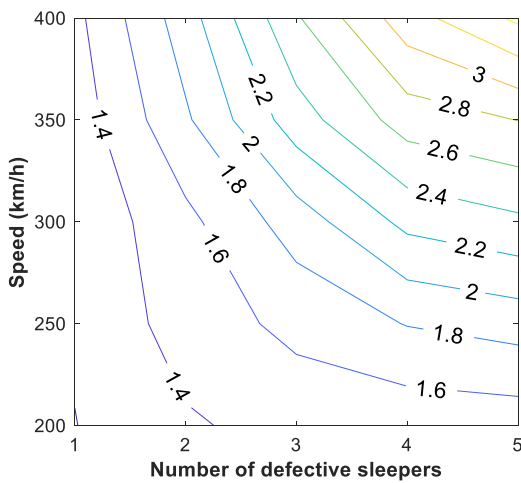


Figure 6.71: Maximum wheel/ rail contact force for different combinations of train speed and number of defective sleepers

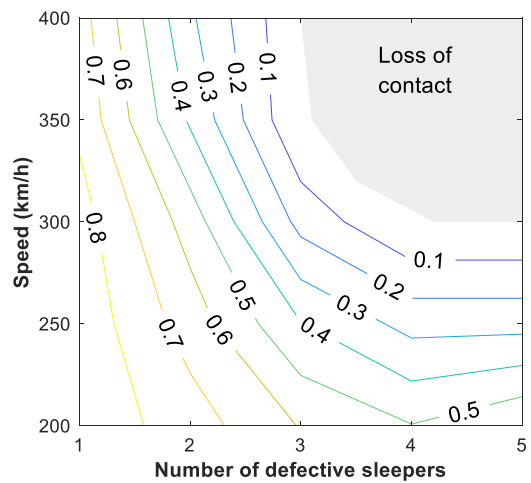


Figure 6.72: Minimum wheel/ rail contact force for different combinations of train speed and number of defective sleepers

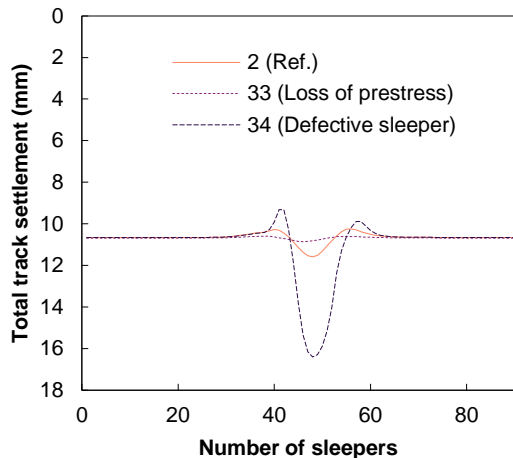


Figure 6.73: Effect of module manufacturing on the soil settlement profile deterioration after 60 years of operation

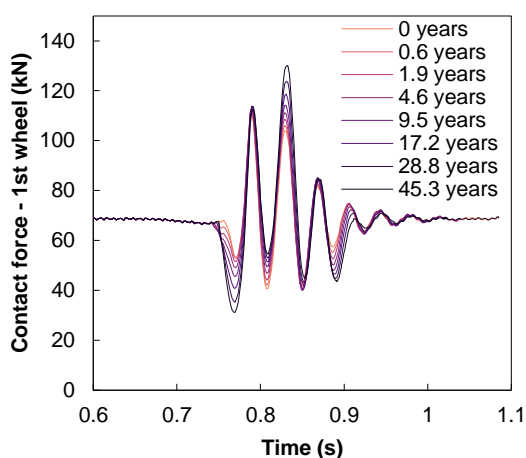


Figure 6.74: Effect of defective sleepers on wheel/ rail contact force during track's lifetime for scenario 31

From Figure 6.73 and as predicted, the loss of prestress presents almost no difference in track settlement compared to the reference case (+0.2%), however, the defective sleeper creates a noticeable disturbance in the longitudinal levelling of the track due to the amplified dynamic interaction between the train and the track. Yet the cumulated damage on the track for the defective sleeper is almost 80% higher when compared with the standard case due to the contact force that causes a higher rate of damage progression (Figure 6.74). For the same scenario #34, the 0.125 damage level (1/4 fatigue life) is reached 20 years earlier than in the standard case as shown in Figure 6.75. Also, in this scenario, the maintenance intervention related to top crack width could be required almost 30 years earlier than the standard case (Figure 6.77). Every concrete zone (Figure 6.76) increases around 30-80% for the defective sleeper scenario that is concentrated around the punctual defect. This shows the importance of preventive maintenance in case of fastener/clamp replacement.

In both Figure 6.75 and 6.76, the lower deterioration of the prestress loss (scenario #33) when

compared with the standard scenario stands out as it is not expected to occur when this feature is active. The main reason is the methodology architecture of the damage accumulation by the rainflow algorithm that includes the stress amplitude variation, i.e. only the stress ratio variation is considered, neglecting the initial stress condition. Hence, the cumulated damage is even lower than the reference case since the load range is identical but there is no damage caused by the prestress application. Also, the transversal prestress does not play a major influence in the flexural induced stresses that are mainly oriented longitudinally.

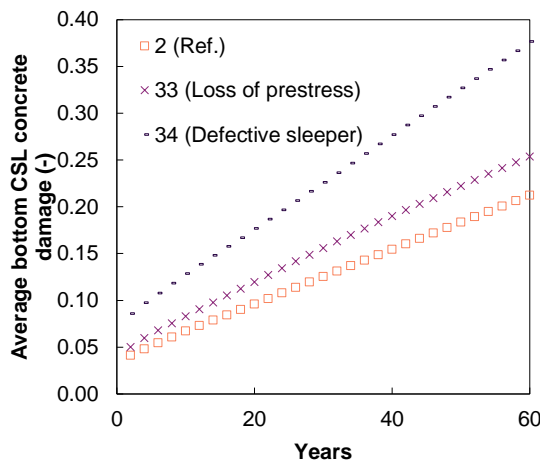


Figure 6.75: Effect of module manufacturing on concrete damage on the CSL top

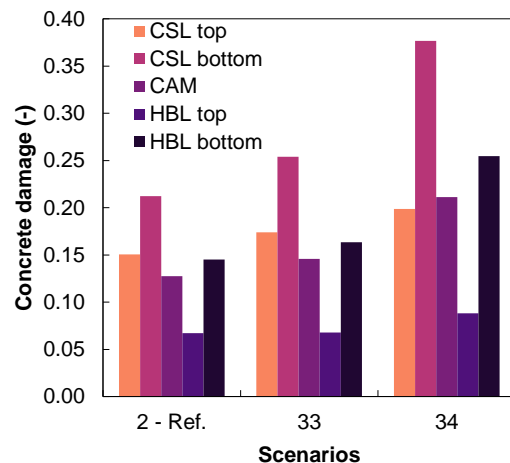


Figure 6.76: Effect of module manufacturing on the final damage per concrete zone

In Figure 6.77, as expected, the bottom crack width progression is slightly worse than the reference case with the active prestress, yet the difference is very small. Nonetheless, besides the additional concrete deterioration and marginal improvement on bottom crack control, transversal prestress serves a different purpose, i.e. to control the crack width in the transversal direction due to thermal expansions of the track, mainly the temperature gradients that cause slab warping.

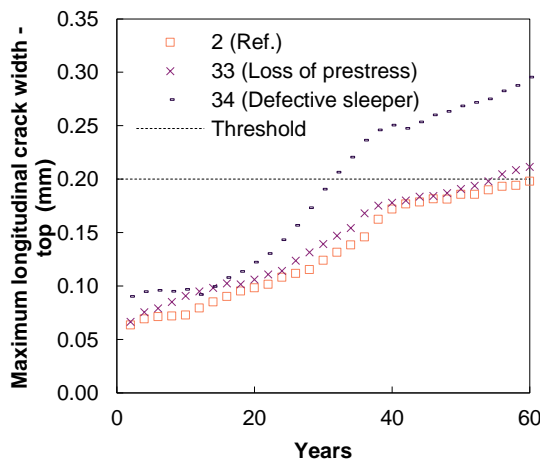


Figure 6.77: Effect of module manufacturing on maximum longitudinal crack width on the slab top after 60 years of operation

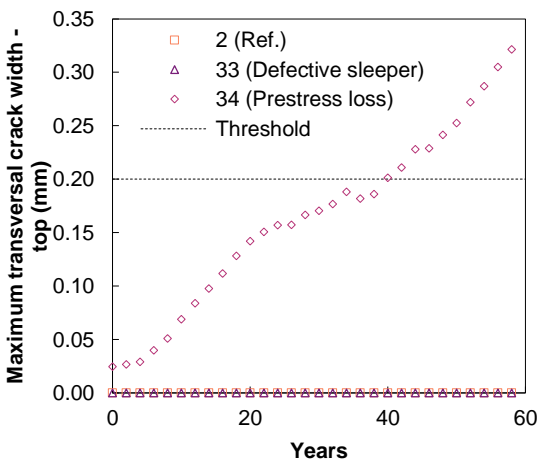


Figure 6.78: Effect of module manufacturing on maximum transversal crack width on the slab top after 60 years of operation

Without the transversal prestress, transversal cracks are no longer null due to the compression state that prevents them to progress, and maintenance is required at the 40-year mark (Figure 6.78). These conclusions are in concordance with other slab track systems that relinquish the transversal prestress and require additional maintenance in what regards crack injection, nonetheless, the crack width range are within usual values in the literature ($\approx 0.2 - 0.4$ mm) as reported by Ripke (2010). If the weather scenario is more severe, the prestress loss is emphasized by reducing the resiliency of the track. The tensile stress level during the negative temperature gradients during severe winters is strongly affected by the transversal prestress that prevents significant temperature damage to occur on the track. Overall, the transversal prestress brings coveted resiliency features that can tackle extreme temperature gradients.

6.6.3 TRACK HETEROGENEITIES

Sudden track heterogeneities can occur even in cases of proper design. These heterogeneities can have a large impact on the structural integrity of the entire system. Heterogeneities may be related to soft soil sections, culverts, tunnels, or bridges transitions that can cause accelerated deterioration of both soil and track structure. To study the effect of track heterogeneities on slab track structure, two scenarios are considered: a soft soil transition to study the positive bending moment of the slab and a poorly designed embankment- platform transition to studying the effect of the negative bending moment and shear force on the slab track (Figure 6.7).

The soft soil has an assumed stiffness of 10 MPa and for the transition case, the soft soil acts as a design flaw on the transition embankment to a very stiff platform (5 GPa) (e.g. tunnel, bridge, rocky outcrop, etc). Since a long section of soft soil will cause the entire track to lay down on the platform and a short section will cause the track to behave like a “bridge” over the soft soil, there is a length of the soft soil section that maximizes the bending moment and shear force for the soft soil and transition scenarios respectively. Due to the fast computation times of the HI-Track, hundreds of short-term simulations can be performed to estimate the length of the soft soil section for both scenarios.

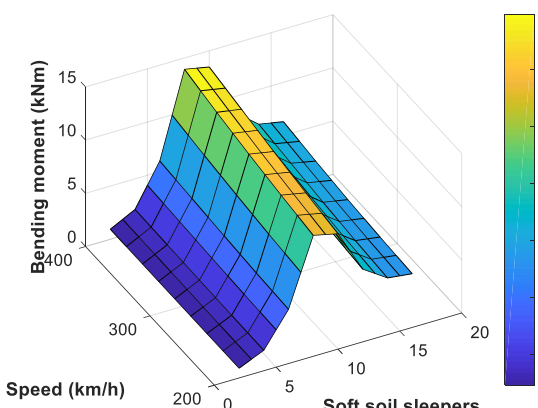


Figure 6.79: Bending moment for different train speeds and number of soft soil sleepers

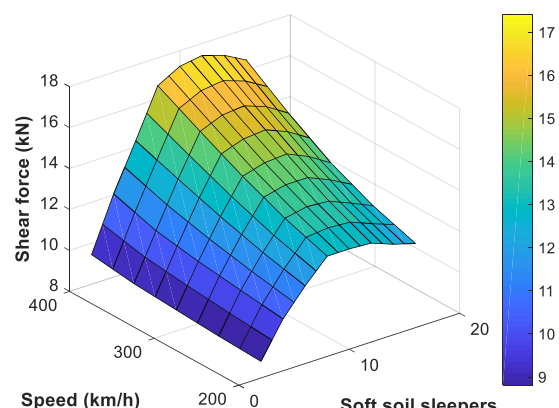


Figure 6.80: Shear force for different train speeds and number of soft soil sleepers

Through Figure 6.79 and 6.80, it is possible to conclude that a length of 8 and 10 sleepers are the spans that maximize the bending moment and shear force for the soft soil and transition scenarios respectively. These results are only valid for the 10 MPa soft soil reference since different soil stiffness implies different spans to maximize the bending moment and shear force. Higher soil stiffness will cause the “optimum” span to decrease and therefore the bending moment and shear force will decrease. Since these spans and the maximum values do not vary significantly, by simplicity, these spans are kept constant for soft soil and transition scenarios.

Eight scenarios (soft soil and transition scenarios for 10, 20, 40 and 60 MPa soils) are studied to assess the severity of soil stiffness transitions in slab track performance.

One of the biggest issues with soft soils is the excessive track settlement that occurs at a fast pace. Figure 6.81 and 6.82 represent the overall track settlement for the soft soil and transition scenarios. In both situations, the 10 MPa soil causes the occurrence of excessive settlement, with soil stabilization techniques after 10 years for the transition case and 12 years for the soft soil. In case for the 20 MPa case, the maintenance intervention is delayed for the 15-year and 20-year mark for the soft soil and transition, respectively.

For a 40 MPa soil, the soft soil does not require heavy soil maintenance before the 60-year life span, yet the transition case requires at the 48-year mark. Interestingly, the 60 MPa soil case does not follow the same trend, and the transition case is less severe (16 mm against 18 mm of the soft soil case), being the main reason the balance between the span (8 sleepers vs 10 sleepers) and the evolution of the wheel/rail contact force. Figure 6.83 shows the evolution of the maximum wheel/rail contact force in the early years for both the soft soil and the transition cases. For the 10 and 20 MPa soils, the transition case presents a higher maximum contact force than the soft soil case that is inverted for the 40 and 60 MPa due to the different span. If the span was the same in both cases, the transition would have higher contact forces.

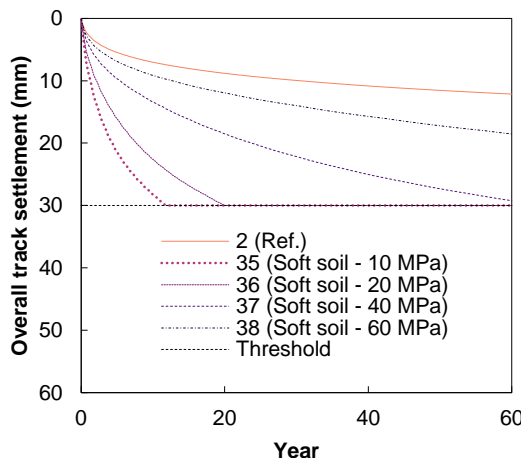


Figure 6.81: Effect of soft soil scenarios on the progress of the maximum soil settlement

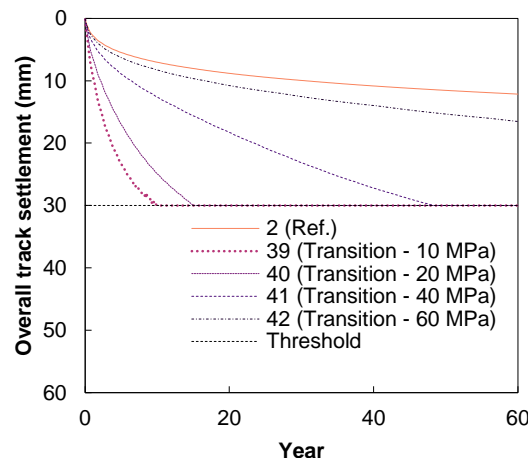


Figure 6.82: Effect of transition soil scenarios on the progress of the maximum soil settlement

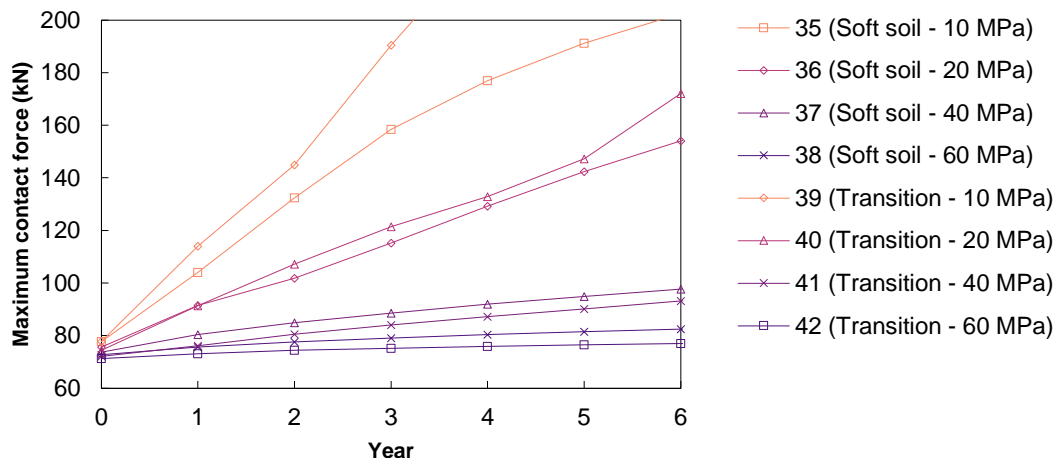


Figure 6.83: Effect of track heterogeneities on maximum contact force evolution

Regarding the rail profile, the maintenance needs occur significantly sooner in both cases when compared with the reference scenario (soft soil and transition case) with longitudinal levelling at around 4.5 – 6.5 years (10 MPa of contact force), 8–9 years (20 MPa) and 35 – 37 years (40 MPa). Although expensive, this maintenance procedure is accounted for by the fastening system vertical adjustment capabilities. These case scenarios are extreme situations that would require a speed restriction to the circulating traffic in a real-life situation, nonetheless, this assessment of the scenarios intend to deliver the slab resiliency to extreme induced stresses.

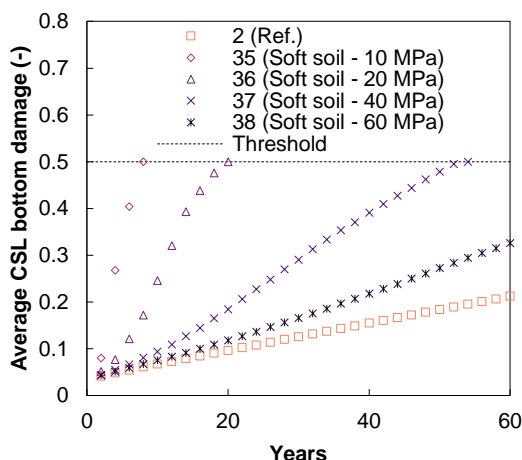


Figure 6.84: Effect of soft soil scenarios on the average CSL bottom concrete damage

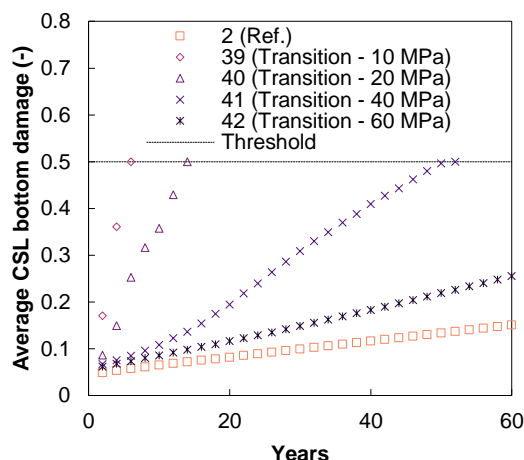


Figure 6.85: Effect of transitions scenarios on the average CSL bottom concrete damage

However, the first major intervention requirement is due to failure by concrete fatigue (Figure 6.84 and 6.85) and requires the reconstruction of the slab track – therefore, this type of failure should be avoided at all costs. In case of the soft soil, the most prominent failure induced stress is by the positive bending moment (CSL bottom) and for the transition scenario is the analogous negative bending moment combined with high shear stress.

Although lower absolute bending moments, the shear-induced stresses cause higher damage on the top of the slab. At the 10 MPa level, the slab is behaving almost as a bridge reaching the failure threshold at the 6-year mark (8 for the soft soil). The level of damage during this period

would be highly noticeable since the wheel/rail contact force can easily reach 4 times as much as the initial track configuration, meaning that significant improvements in the soil or speed restrictions would be undertaken. By increasing the soil stiffness, notable improvements are observed in the tracks damage due to the extra bearing capacity of the soil. If the soil stiffness is larger than 50 MPa, there is no failure by concrete fatigue during the lifetime for the properties simulated. These findings are in close coherence with the soil guidelines used worldwide for slab track as discussed in section 2.3.1.

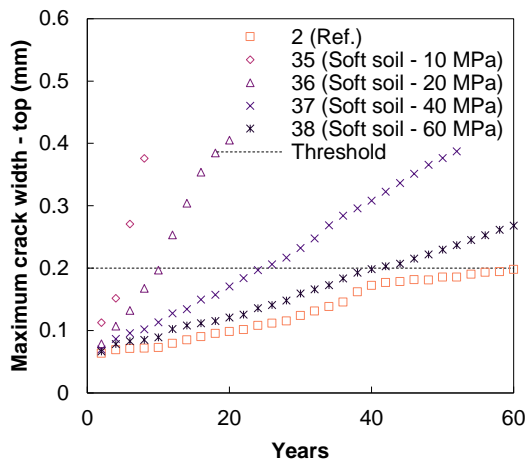


Figure 6.86: Effect of soft soil scenarios on maximum crack width on the slab top after 60 years of operation

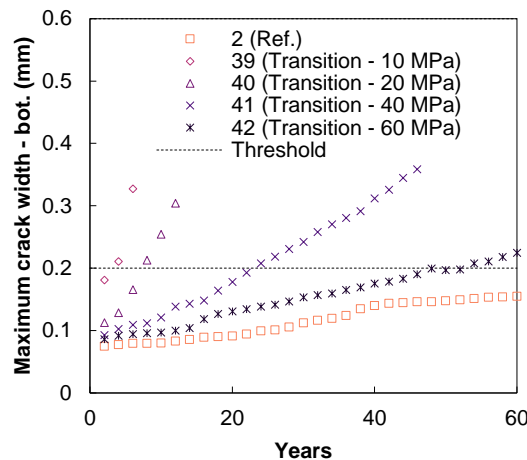


Figure 6.87: Effect of transition scenarios on maximum crack width on the slab top after 60 years of operation

Similarly, the crack width for the 10 MPa reaches the maintenance threshold before the 5 year-mark for both cases (Figure 6.86 and 6.87). Higher quality soil postpones drastically the crack injection intervention, thus bringing the importance magnitude of sudden platform stiffness in slab tracks. Small variations as the 60 MPa soil section lead to increased (but manageable) maintenance requirements, as the slab spans over the section as a “bridge” without a significant increase of concrete damage. Lower values of the platform stiffness cause a premature failure by concrete fatigue, i.e. heavy works on the platform soil must be performed before structural damage start to develop, and more importantly, ride safety starts to compromise the train operation, mainly for the 10 and 20 MPa cases. For the 40 and 50 MPa cases, the short-term responses, although higher, are more controlled and the damage starts to be more concerning that the ride safety.

Also, as expected, if unforeseen scenarios as cases of high shear-induced stress occur, the performance of the slab is weaker when compared with the scenarios related to bending performance. This is due to the limited shear reinforcement present in the slab. Although the effect of the shear stresses is present, the hybrid model is mainly designed to calculate crack widths due to bending moments, i.e. cracks in the transversal direction. In this regard, the HI-Track model may underestimate the width of shear-induced cracks.

6.7 OPTIMIZED DESIGN FOCUSING ON LONG-TERM PERFORMANCE

6.7.1 GENERAL ASSUMPTIONS

In this subchapter, the design optimization of slab track is mainly focused on limit track settlement, concrete long-term damage, and concrete width. Other deterioration phenomena could also have been addressed as rail fatigue, fastening deterioration or cement asphalt mortar damage, however, they are outside the scope of this dissertation and this version of HI-Track.

In previous subchapters, it was found that similarly to ballasted track, to control track settlement aside from soil stabilization (most effective, yet very expensive) is to limit the soil pressure and improving the load distribution. The most effective methods to control track settlement indirectly are through changes in railpad stiffness or HBL thickness. To limit concrete damage, the main key driver is the reduction of the stress ratio in the slab, or by reducing the induced stresses or by increasing the tensile strength of the concrete. Finally, to limit the crack width the most effective method is the reinforcement scheme. Thus, in this chapter, some of these slab track design improvements are implemented to reduce track deterioration and enhance the short term performance subjected to extreme scenarios, particularly the most challenging scenarios previously addressed: Platform heterogeneities and real-life scenarios with extreme temperature, rainfall and mixed traffic operation.

The implemented track design solutions are softer railpads, several ratios of steel fibre in concrete mixtures, higher rebar diameters, longitudinal prestress and thicker subbases.

6.7.2 IMPACT OF TRACK DESIGN ON SOFT SOIL PLATFORMS

The same soft soil scenarios from the previous subchapter are implemented in this subsection, but the design of the slab tracks was changed as shown in new scenarios of Table 6.7.

Table 6.7: Parametric analysis simulations focusing on slab track optimization for platform heterogeneities

#	High Speed	Freight	Temp.	Rainfall	Pad	CSL	Reinf.	HBL	Rail profile	Track	Soil
43	V300	-	E1	R1	P35	FRC0.5%	B10	H30	S1//20	-	S10
44	V300	-	E1	R1	P35	FRC1%	B10	H30	S1//20	-	S10
45	V300	-	E1	R1	P35	FRC1.5%	B10	H30	S1//20	-	S10
46	V300	-	E1	R1	P35	C35/45	Bps	H30	S1//20	-	S10
47	V300	-	E1	R1	P35	C35/45	B10	H35	S1//20	-	S10
48	V300	-	E1	R1	P35	FRC0.5%	B10	H30	S1//20	-	T10
49	V300	-	E1	R1	P35	FRC1%	B10	H30	S1//20	-	T10
50	V300	-	E1	R1	P35	FRC1.5%	B10	H30	S1//20	-	T10
51	V300	-	E1	R1	P35	C35/45	Bps	H30	S1//20	-	T10
52	V300	-	E1	R1	P35	C35/45	B10	H35	S1//20	-	T10

In this parametric study, 10 new scenarios are presented, 5 for the soft soil case and 5 for the transition case. When in presence of a lack of soft soil bearing capacity, design configurations capable to withstand high induced stresses are the most effective. Taking this into consideration, three different steel fibre content ratios (calculated by equation 6.3) are incorporated in the

concrete mixture. By using 0.5, 1 and 1.5% content ratios, the estimated tensile strength of the concrete increases to 4.49, 5.39 and 6.3 MPa respectively. The alternative is to reduce the generated stresses by increasing the flexural capacity of the track (thicker subbase) or by actively reduce the stress state of the slab (longitudinal prestress). For this study, the same initial conditions and track properties are maintained. The railpad and the rebar size are not included since the design improvements are not expected to be relevant since the most demanding deterioration phenomena, in this case, is the concrete damage.

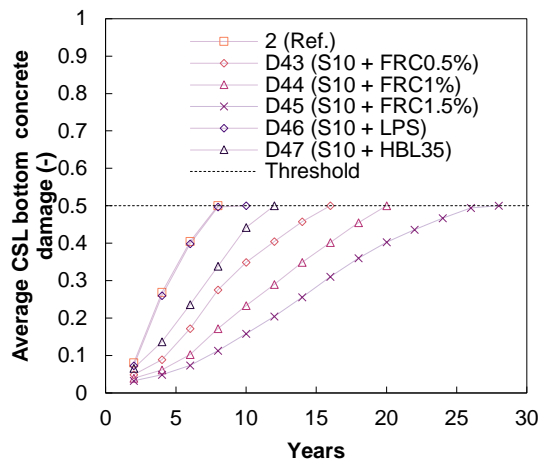


Figure 6.88: Effect of design improvements on the average CSL bottom concrete damage for soft soil scenarios

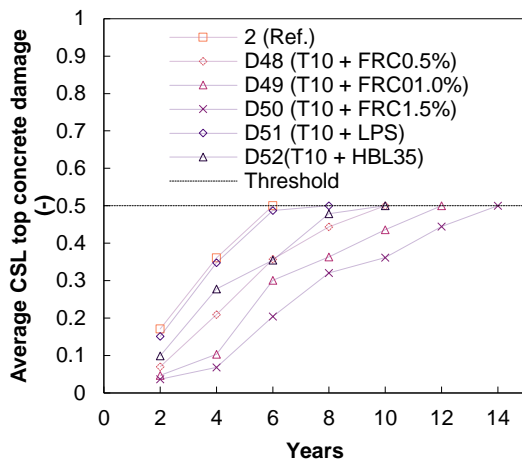


Figure 6.89: Effect of design improvements on the average CSL top concrete damage for transition scenarios

Figure 6.88 and 6.89 present the damage evolution until the threshold failure is reached in the CSL bottom and top for the soft soil and transition, respectively. In the soft soil case, the reference case reaches the failure threshold at the 8-year mark, and every design configuration postpones the damage failure, being the FRC the most effective element to postpone by 8, 12 and 20 years for the 0.5, 1 and 1.5% fibre content included in the concrete. The thicker 35 cm HBL layer provide an 18% less damage in the CSL bottom that is reflected in a 4-year delay until damage failure is reached. In this case, the HBL solution presents a vastly better performance when compared with simulation #25 (3.6% for the bottom CSL) that present no heterogeneities, which enhance this layer as an important element to increase long term performance when subjected to track heterogeneities. The longitudinal prestress present almost no difference regarding concrete damage, due to methodology of the damage accumulation algorithm explained aforementioned.

For the transition case, the design improvements are slightly less effective, being the best solution again the 1.5% steel fibre content concrete that advances the slab replacement by 8 years, more than duplicating the operation life for this scenario. The remaining design configurations follow the same rank in what concerns the most damaged zone of the slab. These weaker results are once again justified by lower shear strength of the slab that was not meant to withstand these level of shear stresses on a regular basis.

In terms of crack width, Figure 6.90 and 6.91 present a similar trend to the effectiveness of the design improvements, and in this case, the longitudinal prestress is the most effective design configuration to control the crack width with a notorious improvement for the transition and soft soil cases. The second most effective solution is unsurprisingly the 1.5% steel fibre content concrete that postpones the crack injection by 8 years in the soft soil case and 4 years in the transition case. In both cases, the 1.5% steel fibre content practically duplicates the time of the first crack injection intervention.

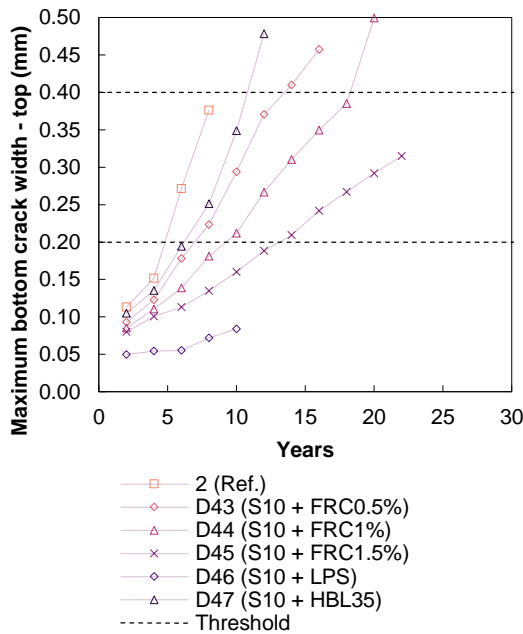


Figure 6.90: Effect of design improvements on maximum crack width on the slab top for soft soil scenarios after 60 years of operation

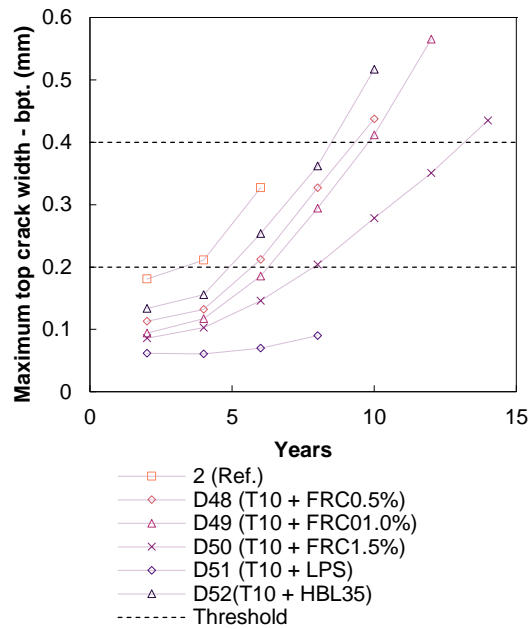


Figure 6.91: Effect of design improvements on maximum crack width on the slab bottom for transitions scenarios after 60 years of operation

Concerning the HBL, the maintenance interval is increased by 29% and 50% for the soft soil and transition case respectively. These results are theoretically sound since a thicker HBL provide a larger improvement of the shear capacity of the slab by proportion when compared with the bending capacity of the entire system. Note that these are not design solutions that will solve the situation, since these scenarios require immediate intervention and are not intended to withstand these actions. Nevertheless, this assessment is intended to demonstrate that for less severe soft soil situations (40/ 60 MPa), these new design configurations can significantly postpone the maintenance thresholds and possible fatigue phenomena.

6.7.3 TRACK DESIGN RESILIENCE UNDER EXTREME WEATHER EVENTS AND OPERATION SCENARIOS

Unlike the previous subchapter, this section is focused on extreme operation conditions, and not construction nor design flaws that require to be corrected, i.e. these scenarios are not fixable and require the slab track resiliency to operate on. The reference scenario for this case is scenario #13, which combines the most severe mixed traffic operation (90 high-speed trains at 400 km/h

and 12 freight trains with 250 kN/ axle at 160 km/h), rainfall (R₃) and temperature (E₃). Once again, the fibre reinforced concrete, longitudinal prestress and the thicker HBL are included, and also, a softer railpad and larger rebar diameter are implemented since their effect could be important in the damage (railpad) due to mixed traffic and the crack width control (rebar size) due to the temperature. To enhance the slab track performance, 7 improved design scenarios are proposed in Table 6.8.

Table 6.8: Parametric analysis simulations focusing on slab track optimization for extreme weather and operation scenarios

#	High Speed	Freight	Temp.	Rainfall	Pad	CSL	HBL	Reinf.	Rail profile
53	V400	V160	E ₃	R ₃	P ₃₅	FRC0.5%	B ₁₀	H ₃₀	1//20
54	V400	V160	E ₃	R ₃	P ₃₅	FRC1%	B ₁₀	H ₃₀	1//20
55	V400	V160	E ₃	R ₃	P ₃₅	FRC1.5%	B ₁₀	H ₃₀	1//20
56	V400	V160	E ₃	R ₃	P ₃₅	C _{35/45}	B ₁₂	H ₃₀	1//20
57	V400	V160	E ₃	R ₃	P ₃₅	C _{35/45}	B _{ps}	H ₃₀	1//20
58	V400	V160	E ₃	R ₃	P ₂₀	C _{35/45}	B ₁₀	H ₃₀	1//20
59	V400	V160	E ₃	R ₃	P ₂₀	C _{35/45}	B ₁₀	H ₃₅	1//20

In what regards to settlement, all solutions only achieve a mild reduction that is negligible with the fibre reinforced concrete under -0.5% deviations, only justified by a minor loss of stiffness. As expected, the reinforcement solutions also present almost null deviations. Most direct effect solutions achieve larger variations, as the 35 cm HBL with a 6% reduction in the overall settlement, and the softer railpad (20 kN/mm) achieve a 9% reduction, that in this case reveals that actively reducing the dynamic forces is more effective than to improve the load distribution by using a thicker HBL since the load is already well distributed. This difference is more notorious in the geometric deterioration of the rail profile, in which the reference case presents a 4.46 mm for a 20 m chord after 60 years or 900 MGT, and the 20 kN/mm and 35 cm HBL presents 2.74 mm (-38.5%) and 3.54 mm (-20.6%), respectively.

In what regards to concrete damage (Figure 6.92 and 6.93), the simulations present quite different results. At the top of the slab, which is mainly affected by the prejudicial impact of the temperature gradients, the most effective solutions are the ones with higher tensile strength – therefore, FRC designs are associated to the scenarios that present the best performance. Furthermore, the reinforcement scenarios do not present major variations, however, the longitudinal prestress solution applies an initial stress level that is detrimental to the concrete damage performance when compared to reference scenarios.

Moreover, the softer railpad presents a better performance in reducing the concrete damage in the CSL (-9.4% for top and -23.3% for bottom) than the thicker HBL (-2.7% and -9.2% for top and bottom respectively), enhancing the idea that mitigates the transmitted forces from the rail to the CSL plays a major role in the damage progress of the slab.

Despite being a demanding scenario, failure by concrete fatigue is not expected to occur for most of the proposed design configurations nor any major maintenance due to concrete damage. Yet,

the durability of the concrete slab should not be neglected, and the crack width evolution is assessed during the track's lifetime, depicted in Figure 6.94 and 6.95.

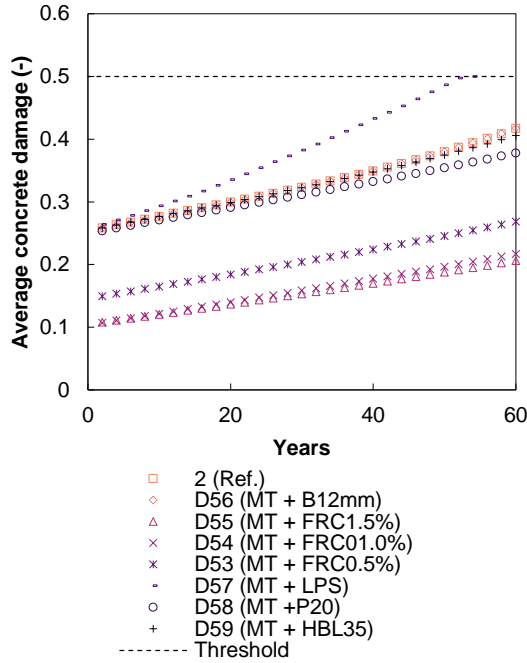


Figure 6.92: Effect of design improvements on the average CSL top concrete damage for extreme weather and operation scenarios

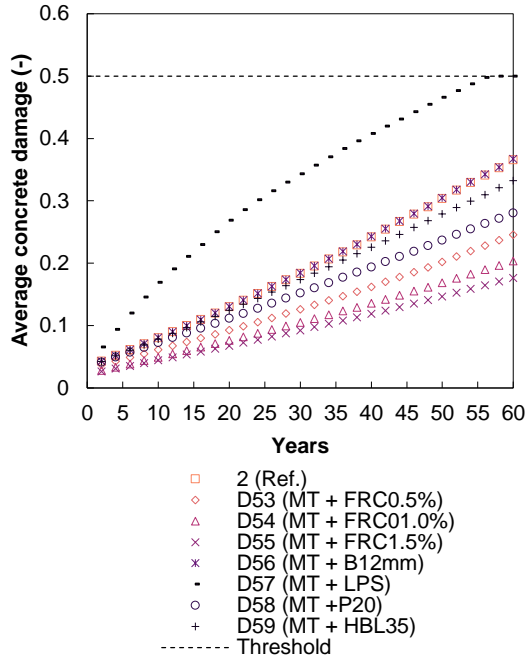


Figure 6.93: Effect of design improvements on the average CSL bottom concrete damage for extreme weather and operation scenarios

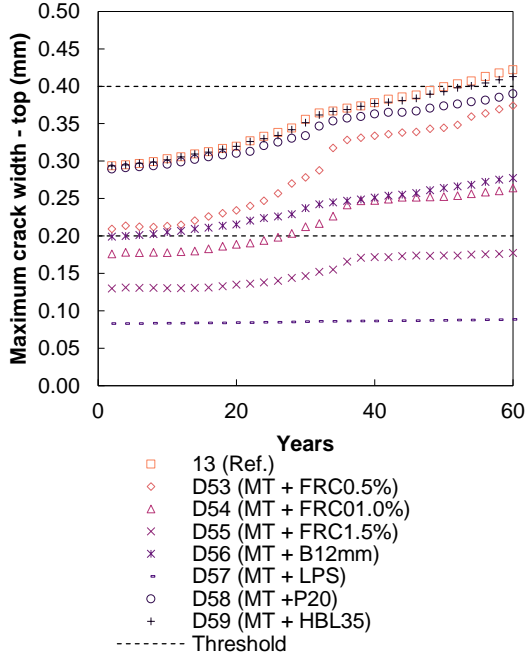


Figure 6.94: Effect of design improvements on maximum crack width on the slab top for extreme weather and operation scenarios after 60 years of operation

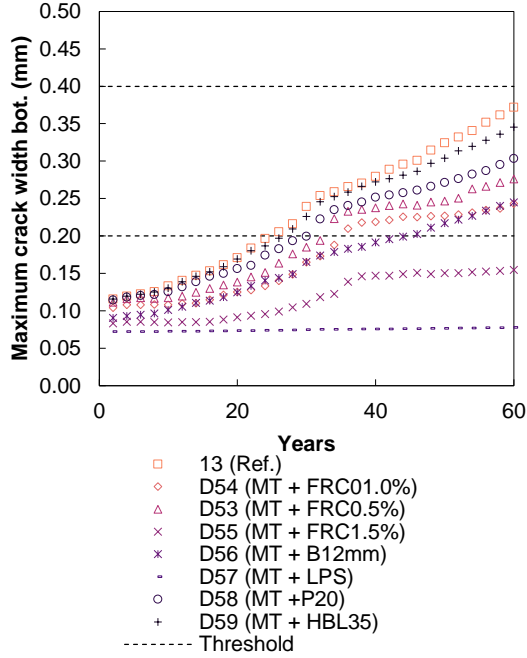


Figure 6.95: Effect of design improvements on maximum crack width on the slab bottom for extreme weather and operation scenarios after 60 years of operation

Due to the extreme temperature simulated climate, the width of top cracks reaches large values and, in most cases, the temperature cycles cause such large cracks that crack injection is required early in the operation life of the track. A remarkable performance is the use of longitudinal prestress that keeps the crack width below 0.1 mm during the entire lifespan of the track,

evidencing its usefulness to extreme climate with high-temperature gradients. Moreover, the 1.5% fibre content concrete also presents a high performance without ever reaching the maintenance threshold.

6.8 PERFORMANCE AND COMPARATIVE ASSESSMENT OF THE SLAB TRACK BEHAVIOUR IN SHORT- AND LONG-TERM

6.8.1 MAINTENANCE REQUIREMENTS

The HI-Track model is capable to deliver multiple track responses in short-term (accelerations, displacements, stresses) during several years of the track's operation, resulting in cumulative concrete damage and settlement. Moreover, the model can also predict when maintenance thresholds are going to be reached and establish maintenance interventions according to correspondent tolerances.

It is important to notice that there is currently an inherent uncertainty related to the track intervention needs due to the empirical laws used in the HI-Track model, in which the conditions they were developed could distort the results. However, the extensive calibration and validation of the model allow for solid confidence in the relative results among scenarios and it is of great interest to use the HI-Track to predict the level of maintenance required compared to a standard scenario. With this numerical tool, track interventions can be estimated when they will occur during the track's lifetime and wherein the track they are needed and which intervention is set to be implemented (according to the thresholds defined in section 6.2), hence a possible life cycle cost assessment can be roughly calculated.

Table 6.9 presents the first maintenance intervention that concerns track settlement and rail levelling. On the right side, the maintenance required is soil stabilization, that is considered heavy works on the track and should be avoided at all costs due to economic drawbacks from construction works and track unavailability. Almost every scenario keeps the overall track settlement under control, except scenarios in which the track condition was affected, as the case of the drainage deficiency scenario and the platform defects scenarios. In the worst-case simulated (10 MPa soft soil section), both soft soil and transition scenarios require soil stabilization for the 10-12-year range and the rail profile levelling to the 4-7 years range. Early intervention would be applied since the short-term response would compromise track safety. If a 30% minimum static axle load is adopted as ride safety threshold, heavy maintenance should be implemented at the 2-year and 1.6-year mark for the soft soil and transition scenarios. For the 20 MPa case, the maintenance interventions are reduced roughly to half for the soft soil scenario and 50% for the transition scenario. In this case, a short-term threshold is still the defying serviceability design criterion for operational restrictions at the 4.5-year mark (soft soil scenario) and 3.2 years (transition scenario). For 40 and 60 MPa, the most stringent variable is still the

short-term performance of with 30% of the contact force threshold at the 15th and 17th year of operation respectively, yet no geometric threshold is surpassed.

Table 6.9: Number of years required to reach rail levelling and settlement maintenance thresholds

		Settlement threshold				Rail profile threshold			
		25%	50%	75%	100%	25%	50%	75%	100%
Speed	1 (250 km/h)	14.74	-	-	-	-	-	-	-
	2 (300 km/h)	13.73	-	-	-	-	-	-	-
	3 (350 km/h)	12.50	-	-	-	-	-	-	-
	4 (400 km/h)	11.16	-	-	-	-	-	-	-
Freight Traffic	5 (F: 120 km/h)	4.71	41.58	-	-	-	-	-	-
	6 (F: 160 km/h)	4.67	40.99	-	-	-	-	-	-
Mixed Traffic	7 (H: 300 km/h & F: 120 km/h)	7.11	-	-	-	-	-	-	-
	8 (H: 400 km/h & F: 160 km/h)	6.62	-	-	-	-	-	-	-
Weather	9 (E ₂ & R ₁)	13.33	-	-	-	-	-	-	-
	10 (E ₃ & R ₁)	13.22	-	-	-	-	-	-	-
	11 (E ₁ & R ₂)	5.16	44.64	-	-	-	-	-	-
	12 (E ₁ & R ₃)	2.45	16.75	55.43	-	41.01	-	-	-
	13 (MT & E ₃ & R ₃)	1.24	7.81	29.39	-	50.29	-	-	-
Railpad	14 (20 kN/mm)	14.76	-	-	-	-	-	-	-
	15 (50 kN/mm)	13.31	-	-	-	-	-	-	-
	16 (90 kN/mm)	12.71	-	-	-	-	-	-	-
Concrete	17 (C ₃₀ /37)	13.71	-	-	-	-	-	-	-
	18 (C ₄₀ /50)	13.73	-	-	-	-	-	-	-
	19 (FRC)	13.73	-	-	-	-	-	-	-
	20 (RAC)	13.59	-	-	-	-	-	-	-
Reinf.	21 (8mm)	13.71	-	-	-	-	-	-	-
	22 (12 mm)	13.71	-	-	-	-	-	-	-
	23 (LPS)	13.72	-	-	-	-	-	-	-
HBL	24 (25 cm)	12.57	-	-	-	-	-	-	-
	25 (35 cm)	15.11	-	-	-	-	-	-	-
Settlement	26 (5//20)	7.25	49.73	-	-	0.00	17.72	-	-
	27 (10//20)	4.44	27.43	-	-	0.00	0.00	1.70	20.50
	28 (1//10)	12.52	-	-	-	0.00	41.52	-	-
Construction defects	29 (Drainage)	1.41	8.82	27.25	48.45	20.72	42.72	57.00	-
	31 (Subbase construction)	12.12	-	-	-	-	-	-	-
	33 (Loss of prestress)	13.73	-	-	-	-	-	-	-
	32 (Expansion joint)	13.26	-	-	-	-	-	-	-
	34 (Defective sleeper)	7.72	54.32	-	-	15.52	-	-	-
	30 (Soil compaction)	7.70	-	-	-	-	-	-	-
Soft soil	35 (Soft soil - 10 MPa)	0.80	2.50	5.60	11.78	0.57	1.36	2.47	6.56
	36 (Soft soil - 20 MPa)	1.34	4.41	9.89	19.98	1.54	2.84	5.73	8.77
	37 (Soft soil - 40 MPa)	2.94	12.67	31.03	-	2.77	10.62	21.10	37.27
	38 (Soft soil - 60 MPa)	6.13	35.46	-	-	11.87	-	-	-
Transition	39 (Transition - 10 MPa)	0.79	2.26	4.64	10.01	1.13	1.78	2.77	4.47
	40 (Transition - 20 MPa)	1.41	4.09	8.26	15.06	1.16	3.50	5.64	7.87
	41 (Transition - 40 MPa)	3.57	13.86	28.64	48.38	5.74	14.20	23.99	34.67
	42 (Transition - 60 MPa)	7.71	47.32	-	-	22.99	-	-	-

In what regards the rail profile, unlike soft soil and transition scenarios, the initial defect of 10 mm (#27 scenario) is more severe as expected and requires maintenance after 20 years of operation. The rail profiling does not involve heavy works and it can perform through the vertical adjustment of the fastening system (+/- 50 mm), that although being an expensive maintenance procedure, is much less onerous than soil stabilization. Since the rail profile threshold is reached before the overall settlement, a lower rail profile threshold could be defined to avoid the occurrence of large dynamic forces, hence postponing the soil stabilization. In this

case of no early intervention, a larger number of rail longitudinal profiling would be required, and that is reflected in additional maintenance costs. Therefore, it suggests the concept of a balance between the rail profile levelling threshold and consequent costs of levelling and the cost of soil stabilization in the case of soft soils.

Another deterioration phenomenon that requires heavy maintenance when a threshold is reached is the concrete damage that causes failure by fatigue (the concrete slab loses its stiffness and structural integrity) and consequent removal and replacement of the panels, and in precast systems, the reconstruction of the section which causes severe traffic disruptions.

Table 6.10: Number of years required to reach concrete damage maintenance thresholds for each scenario

		CSL damage				HBL damage threshold			
		0.125	50%	75%	100%	25%	50%	75%	100%
Speed	1 (250 km/h)	31.30	-	-	-	-	-	-	-
	2 (300 km/h)	29.79	-	-	-	-	-	-	-
	3 (350 km/h)	27.87	-	-	-	-	-	-	-
	4 (400 km/h)	24.68	52.70	-	-	-	-	-	-
Freight Traffic	5 (F: 120 km/h)	18.94	50.75	-	-	-	-	-	-
	6 (F: 160 km/h)	18.94	50.75	-	-	-	-	-	-
Mixed Traffic	7 (H: 300 km/h & F: 120 km/h)	22.39	56.64	-	-	-	-	-	-
	8 (H: 400 km/h & F: 160 km/h)	20.51	50.29	-	-	-	-	-	-
Weather	9 (E ₂ & R ₁)	16.73	-	-	-	-	-	-	-
	10 (E ₃ & R ₁)	1.06	10.71	-	-	-	-	-	-
	11 (E ₁ & R ₂)	28.82	-	-	-	-	-	-	-
	12 (E ₁ & R ₃)	26.79	58.87	-	-	-	-	-	-
Railpad	13 (MT & E ₃ & R ₃)	0.97	1.94	48.54	-	-	-	-	-
	14 (20 kN/mm)	34.46	-	-	-	-	-	-	-
	15 (50 kN/mm)	27.09	-	-	-	-	-	-	-
	16 (90 kN/mm)	22.66	55.95	-	-	-	-	-	-
Concrete	17 (C _{30/37})	22.86	-	-	-	-	-	-	-
	18 (C _{40/50})	30.05	-	-	-	-	-	-	-
	19 (FRC)	52.16	-	-	-	-	-	-	-
	20 (RAC)	26.94	-	-	-	-	-	-	-
Reinf.	21 (8mm)	29.79	-	-	-	-	-	-	-
	22 (12 mm)	30.10	-	-	-	-	-	-	-
	23 (LPS)	31.99	-	-	-	-	-	-	-
HBL	24 (25 cm)	28.58	-	-	-	-	-	-	-
	25 (35 cm)	31.29	-	-	-	-	-	-	-
Settlement	26 (5//20)	20.15	46.38	-	-	-	-	-	-
	27 (10//20)	13.26	31.06	52.10	-	-	-	-	-
	28 (1//10)	26.37	-	-	-	-	-	-	-
Construction defects	29 (Drainage)	24.44	48.71	-	-	-	-	-	-
	31 (Subbase construction)	27.51	-	-	-	-	-	-	-
	33 (Loss of prestress)	43.15	-	-	-	-	-	-	-
	32 (Expansion joint)	0.29	0.57	0.86	1.14	-	-	-	-
	34 (Defective sleeper)	9.29	34.64	59.67	60.00	-	-	-	-
Soft soil	30 (Soil compaction)	29.64	-	-	-	-	-	-	-
	35 (Soft soil - 10 MPa)	2.48	3.81	5.57	8.00	43.50	-	-	-
	36 (Soft soil - 20 MPa)	6.14	10.10	13.50	20.00	-	-	-	-
	37 (Soft soil - 40 MPa)	13.79	26.19	38.42	54.00	-	-	-	-
Transition	38 (Soft soil - 60 MPa)	21.63	46.02	-	-	-	-	-	-
	39 (Transition - 10 MPa)	1.47	2.83	4.20	6.00	0.58	1.16	1.73	5.00
	40 (Transition - 20 MPa)	3.22	5.95	10.49	14.00	0.84	1.68	6.61	9.91
	41 (Transition - 40 MPa)	12.33	24.85	36.56	-	11.88	17.36	23.27	32.56
	42 (Transition - 60 MPa)	22.71	58.51	-	-	26.29	46.67	-	-

In Table 6.10, it may be observed that, for most scenarios, failure of concrete is not a common damage limit state, with the vast majority under the 25% damage level by concrete zones (it is assumed that failure occurs when a concrete zone reaches a average concrete damage of 0.5).

Scenarios such as mixed traffic, 400 km/h high speed trains and the influence of geometric quality of the track (initial settlement, heavy rainfall, drainage deficiency, defective sleeper, etc.) require slightly more attention, achieving damage levels over 0.25.

Scenarios with malfunctioning expansion joints are by far the most severe scenarios in what concerns track damage, making the temperature effect a single ultimate state action reaching the top CSL damage over 0.5 on one daily cycle. As observed previously, the soft soil and transition scenarios are case studies that are vulnerable to high stresses causing an early failure by concrete fatigue. In the case of the soft soil, the main induced stresses are caused by bending moments, thus the slab acts as the major element in the bending capacity and takes most of the damage, and almost no damage is directed to the HBL. On the other hand, shear loading is the main induced stress driver in the transition scenarios, and in this case, both slab and HBL share a similar shear force resistance, hence both elements present failure relatively at the same time.

Both track settlement and failure by concrete damage are deterioration phenomena that are not expected during the track's lifetime since it implies substantial economic losses. On other hand, crack width control is a degradation phenomenon that requires close surveillance and maintenance, to avoid further damage due to water infiltration in the slab, causing reinforcement corrosion and larger settlements (higher soil saturation due to rainwater infiltration). In Table 6.11, it is possible to notice a relationship between track damage and crack width progress. Immediate maintenance on top cracks is not required for most scenarios, nonetheless, scenarios with extreme temperature, track initial conditions (soft soil, transitions, etc.) and implementation of lower rebar diameters must be carefully addressed. Yet, by far the most influential mechanism of top cracking in slab tracks is the concrete contraction and expansion caused by temperature. In extreme cases such as the E₃ scenario, the slab structure is subjected to early interventions, notwithstanding the crack progress stabilizes after the first load cycles due to a controlled concrete stiffness loss. This resiliency to extreme weather events can be an essential feature for the upcoming future in which climate change can endanger current transport infrastructure. Despite the bottom cracks being less susceptible to thermal effects, they require frequent maintenance due to the flexural stresses. More than ¾ of the scenarios envisage bottom crack injection (mainly side cracks) except for improved design solutions.

Table 6.11: Number of years required to reach crack width maintenance thresholds for each scenario

		Top cracking threshold				Bot. cracking threshold			
		25%	50%	75%	100%	25%	50%	75%	100%
Speed	1 (250 km/h)	1.40	28.06	59.04	-	1.59	22.67	37.29	-
	2 (300 km/h)	1.34	24.74	52.81	-	1.57	21.01	36.50	-
	3 (350 km/h)	1.40	27.09	56.86	-	1.58	18.01	34.68	55.90
	4 (400 km/h)	1.40	26.25	49.35	-	1.58	13.57	30.40	43.48
Freight Traffic	5 (F: 120 km/h)	1.17	17.64	43.27	-	1.27	13.72	30.23	40.84
	6 (F: 160 km/h)	1.17	17.65	43.26	-	1.27	13.71	30.22	40.84

Table 6.11: Number of years required to reach crack width maintenance thresholds for each scenario (Continued)

		Top cracking threshold				Bot. cracking threshold			
		25%	50%	75%	100%	25%	50%	75%	100%
Speed	1 (250 km/h)	1.40	28.06	59.04	-	1.59	22.67	37.29	-
	2 (300 km/h)	1.34	24.74	52.81	-	1.57	21.01	36.50	-
	3 (350 km/h)	1.40	27.09	56.86	-	1.58	18.01	34.68	55.90
	4 (400 km/h)	1.40	26.25	49.35	-	1.58	13.57	30.40	43.48
Freight Traffic	5 (F: 120 km/h)	1.17	17.64	43.27	-	1.27	13.72	30.23	40.84
	6 (F: 160 km/h)	1.17	17.65	43.26	-	1.27	13.71	30.22	40.84
Mixed Traffic	7 (H: 300 km/h & F: 120 km/h)	1.16	18.83	34.18	-	1.29	18.23	29.07	36.45
	8 (H: 400 km/h & F: 160 km/h)	1.16	17.56	36.00	-	1.29	16.56	28.07	35.44
Weather	9 (E ₂ & R ₁)	0.58	1.15	1.73	38.78	0.83	1.67	33.86	46.09
	10 (E ₃ & R ₁)	0.34	0.68	1.01	1.35	0.74	1.49	22.76	41.05
	11 (E ₁ & R ₂)	1.15	32.38	48.13	-	1.32	28.25	42.70	49.44
	12 (E ₁ & R ₃)	1.15	29.85	47.31	-	1.32	22.01	38.79	46.33
	13 (MT & E ₃ & R ₃)	0.34	0.68	1.02	1.36	0.86	1.72	14.89	24.74
Railpad	14 (20 kN/mm)	1.40	30.11	-	-	1.60	25.24	39.19	-
	15 (50 kN/mm)	1.40	26.30	55.07	-	1.57	18.95	34.68	56.10
	16 (90 kN/mm)	1.39	22.77	48.34	-	1.55	15.59	30.60	46.27
Concrete	17 (C ₃₀ /37)	1.14	14.43	45.16	-	1.31	12.15	30.58	47.50
	18 (C ₄₀ /50)	1.36	28.60	-	-	1.42	20.43	37.33	-
	19 (FRC)	1.72	40.79	-	-	1.90	37.91	-	-
	20 (RAC)	1.21	20.14	40.98	-	1.39	12.66	34.73	52.91
Reinf.	21 (8mm)	0.83	1.65	16.52	31.24	0.97	1.94	14.86	26.59
	22 (12 mm)	1.99	-	-	-	10.57	38.81	-	-
	23 (LPS)	-	-	-	-	-	-	-	-
HBL	24 (25 cm)	1.40	24.08	54.19	-	1.58	19.04	35.81	58.58
	25 (35 cm)	1.40	27.94	57.88	-	1.59	21.94	37.10	-
Settlement	26 (5//20)	1.46	25.62	52.26	-	1.63	14.16	29.93	42.89
	27 (10//20)	1.46	20.32	38.13	58.51	1.56	8.87	18.88	28.91
	28 (1//10)	1.46	28.16	-	-	1.65	20.99	35.96	-
Construction defects	29 (Drainage)	1.47	28.06	52.25	-	1.66	20.37	33.15	45.85
	31 (Subbase construction)	1.47	29.11	-	-	1.65	22.69	36.82	-
	33 (Loss of prestress)	29.73	-	-	-	24.12	36.18	-	-
	32 (Expansion joint)	0.12	0.25	0.37	0.50	0.23	0.45	0.68	0.90
	34 (Defective sleeper)	1.34	22.02	41.87	-	1.11	14.09	25.02	31.20
	30 (Soil compaction)	1.47	29.93	-	-	1.66	23.75	37.73	-
Soft soil	35 (Soft soil - 10 MPa)	4.29	5.52	6.89	8.53	0.89	1.77	3.91	4.81
	36 (Soft soil - 20 MPa)	6.34	11.83	15.06	19.34	1.27	3.49	6.99	10.10
	37 (Soft soil - 40 MPa)	1.38	20.71	35.26	50.45	1.44	7.41	16.10	24.67
	38 (Soft soil - 60 MPa)	1.34	25.26	52.06	-	1.51	11.65	28.29	40.67
Transition	39 (Transition - 10 MPa)	0.55	1.11	1.66	3.27	1.62	6.11	7.56	8.75
	40 (Transition - 20 MPa)	0.88	1.77	5.16	7.46	7.17	14.39	15.85	17.40
	41 (Transition - 40 MPa)	1.08	3.48	16.24	22.93	18.45	26.57	35.14	42.93
	42 (Transition - 60 MPa)	1.16	11.95	28.98	52.45	14.33	27.30	45.67	-

From Table 6.12 to 6.14, the maintenance improvements of the enhanced design solutions are presented with the respective postponed interventions reflecting and highlights on how efficient a certain design solution is. These improved design solutions feature feasible changes in the industry that can have a significant impact on the overall performance of slab tracks. Improvements as lower railpad stiffness, better performance concrete, different reinforcement schemes and thicker HBL are studied as countermeasures to mitigate the need of track maintenance when subjected to extreme scenarios, such as soft soil, transitions, extreme weather and mixed traffic.

In almost every scenario, the most effective design to control track settlement is the thickness of the HBL, but by a small margin that probably would not be economically viable when compared with other design solutions. More effective solutions are direct soil stabilization or a more efficient drainage system. Softer railpads (20 kN/mm) reduce the dynamic stresses on the platform, that in the case of the extreme scenarios presents better performance than a 35 cm HBL.

Table 6.12: Number of years required to reach rail levelling and settlement maintenance thresholds for improved design solutions

			Settlement threshold				Rail profile threshold			
			25%	50%	75%	100%	25%	50%	75%	100%
Design (soft soil)	35 (Soft soil - 10 MPa)		0.80	2.50	5.60	11.78	0.57	1.36	2.47	6.56
	D43 (S10 + FRC0.5%)		0.80	2.52	5.59	11.69	0.98	1.50	2.83	4.19
	D44 (S10 + FRC1%)		0.80	2.50	5.58	11.66	0.98	1.50	2.83	4.18
	D45 (S10 + FRC1.5%)		0.80	2.50	5.58	11.62	0.98	1.50	2.83	4.18
	D46 (S10 + LPS)		0.80	2.50	5.60	11.79	0.97	1.49	2.84	4.25
	D47 (S10 + HBL35)		0.92	2.91	6.63	13.86	1.11	1.99	3.86	5.20
Design (transition)	39 (Transition - 10 MPa)		0.79	2.26	4.64	10.01	1.13	1.78	2.77	4.47
	D48 (T10 + FRC0.5%)		0.83	2.35	4.73	9.59	1.13	1.80	2.81	4.41
	D49 (T10 + FRC1.0%)		0.86	2.37	4.76	9.48	1.14	1.83	2.85	4.46
	D50 (T10 + FRC1.5%)		0.86	2.38	4.75	9.40	1.14	1.83	2.85	4.47
	D51 (T10 + LPS)		0.81	2.29	4.66	9.94	1.10	1.72	2.69	4.33
	D52 (T10 + HBL35)		1.00	2.79	5.70	11.02	1.40	2.51	3.08	5.41
Design (Extreme weather & mixed traffic)	13 (MT & E3 & R3)		1.24	7.81	29.39	-	50.29	-	-	-
	D53 (MT + FRC0.5%)		1.24	7.82	29.46	-	50.87	-	-	-
	D54 (MT + FRC1.0%)		1.24	7.83	29.49	-	51.01	-	-	-
	D55 (MT + FRC1.5%)		1.24	7.81	29.50	-	51.15	-	-	-
	D56 (MT + B12mm)		1.24	7.81	29.39	-	50.29	-	-	-
	D57 (MT + LPS)		1.24	7.82	29.46	-	50.29	-	-	-
	D58 (MT + P20)		1.30	8.49	34.05	-	-	-	-	-
	D59 (MT + HBL35)		1.29	8.47	33.08	-	-	-	-	-

Table 6.13: Number of years required to reach concrete damage maintenance thresholds for each scenario for improved design solutions

			CSL damage				HBL damage threshold			
			25%	50%	75%	100%	25%	50%	75%	100%
Design (soft soil)	35 (Soft soil - 10 MPa)		2.48	3.81	5.57	8.00	43.50	-	-	-
	D43 (S10 + FRC0.5%)		4.87	7.51	10.93	16.00	-	-	-	-
	D44 (S10 + FRC1%)		6.65	10.58	14.98	20.00	-	-	-	-
	D45 (S10 + FRC1.5%)		8.53	13.77	18.70	28.00	-	-	-	-
	D46 (S10 + LPS)		2.56	3.89	5.66	9.99	34.56	-	-	-
	D47 (S10 + HBL35)		3.66	6.28	8.71	12.00	1.49	9.07	13.36	23.83
Design (transition)	39 (Transition - 10 MPa)		1.47	2.83	4.20	6.00	0.58	1.16	1.73	5.00
	D48 (T10 + FRC0.5%)		2.79	4.55	6.40	10.00	1.46	4.62	5.60	6.88
	D49 (T10 + FRC1.0%)		4.22	5.48	8.32	12.00	4.54	5.34	6.33	8.13
	D50 (T10 + FRC1.5%)		4.83	6.79	10.33	14.00	4.90	5.97	7.41	9.32
	D51 (T10 + LPS)		1.65	3.00	4.39	8.00	0.58	1.16	1.74	5.04
	D52 (T10 + HBL35)		2.29	3.69	6.32	10.00	4.12	7.73	12.06	18.16
Design (Extreme weather & mixed traffic)	13 (MT & E3 & R3)		0.97	1.94	48.54	-	-	-	-	-
	D53 (MT + FRC0.5%)		1.67	33.26	-	-	-	-	-	-
	D54 (MT + FRC1.0%)		11.82	-	-	-	-	-	-	-
	D55 (MT + FRC1.5%)		12.76	-	-	-	-	-	-	-
	D56 (MT + B12mm)		0.97	1.94	48.47	-	-	-	-	-
	D57 (MT + LPS)		0.95	1.90	28.35	53.99	-	-	-	-
	D58 (MT + P20)		0.99	1.97	58.80	-	-	-	-	-
	D59 (MT + HBL35)		0.97	1.94	49.97	-	52.90	-	-	-

Concrete damage can be drastically reduced by using a higher quality concrete that postpones

the panel removal and triples the lifespan in case of flexural induced stresses or doubles it in the case of shear-induced stresses scenarios. For bending and shear fatigue stresses in extreme scenarios, a thicker HBL (35 cm) plays a relevant role with a reduction by 50% of the damage rate in the CSL. For the last design scenario series subjected to extreme actions, the concrete quality is the element that has a direct influence on concrete damage, especially to delay the damage threshold easily reached by the extreme temperature. For example, the 0.25 damage level (1/2 of the lifespan) is reached in the early years (less than 2 years), and by implementing a 0.5% steel fibre content, this threshold is only reached by the 33-year mark, and if a 1.0% content is used, the 0.25 damage level is not reached during the track's lifetime. As expected, the effectiveness of the steel fibre concrete is enhanced in stress scenarios with bending majority stresses. The difference between increasing from 1.0 to 1.5% steel fibre content in bending scenarios leads to a 34% increase in concrete damage performance. In a shear-dominated scenario, the increase in performance is only 13% and for extreme weather scenarios with heavy traffic, only 8%. For the extreme weather and mixed traffic, the HBL improvement is only noticed by the increased bending capacity with a 3% performance increase in the CSL damage and a decrease in the HBL itself due to a greater influence on the track's vertical stiffness. Instead of increasing the bending capacity of the track and consequently reduce track concrete damage, the application of softer railpads by actively reduce dynamic loads is more effective than a thicker HBL.

Table 6.14: Number of years required to reach crack width maintenance thresholds for each scenario for improved design solutions

			Top cracking threshold				Bot. cracking threshold			
			25%	50%	75%	100%	25%	50%	75%	100%
Design (soft soil)	35 (Soft soil - 10 MPa)		4.29	5.52	6.89	8.53	0.89	1.77	3.91	4.81
	D43 (S10 + FRC0.5%)		8.15	10.56	14.26	19.55	1.08	2.47	4.98	6.97
	D44 (S10 + FRC1%)		11.66	17.35	20.99	-	1.18	3.18	6.54	9.24
	D45 (S10 + FRC1.5%)		15.94	-	-	-	1.25	3.94	9.21	13.11
	D46 (S10 + LPS)		23.62	-	-	-	2.17	-	-	-
	D47 (S10 + HBL35)		1.84	7.80	10.13	12.55	0.95	1.90	4.50	6.21
Design (transition)	39 (Transition - 10 MPa)		0.55	1.11	1.66	3.27	1.62	6.11	7.56	8.75
	D48 (T10 + FRC0.5%)		0.89	1.77	4.45	5.70	10.59	11.10	11.61	12.48
	D49 (T10 + FRC1.0%)		1.06	2.52	4.96	6.27	6.52	11.67	-	-
	D50 (T10 + FRC1.5%)		1.17	3.67	6.14	7.87	7.81	15.01	17.38	-
	D51 (T10 + LPS)		1.62	-	-	-	-	-	-	-
	D52 (T10 + HBL35)		0.75	1.50	3.51	4.91	10.44	11.02	11.60	12.59
Design (Extreme weather & mixed traffic)	13 (MT & E3 & R3)		0.34	0.68	1.02	1.36	0.86	1.72	14.89	24.74
	D53 (MT + FRC0.5%)		0.48	0.96	1.43	1.91	0.90	1.79	23.56	32.40
	D54 (MT + FRC1.0%)		0.57	1.14	1.70	26.62	0.96	1.92	28.16	35.09
	D55 (MT + FRC1.5%)		0.77	1.54	31.21	-	1.20	26.29	45.01	-
	D56 (MT + Bi2mm)		0.50	1.00	1.50	3.46	1.10	9.38	28.09	44.43
	D57 (MT + LPS)		1.21	-	-	-	1.39	-	-	-
	D58 (MT + P20)		0.35	0.69	1.04	1.38	0.87	1.75	18.02	30.04
	D59 (MT + HBL35)		0.34	0.68	1.02	1.36	0.86	1.73	15.28	26.45

In what concerns crack width, the proposed design solutions have a significant influence on track's maintenance. By far the best performance is the longitudinal prestress solution that limits the crack width under 0.05 mm for every scenario, being a solution to be implemented in

extreme temperature amplitude zones, mainly in China (CRTS-III variant). This variant is quite expensive being only used when the durability of the structure is threatened by extreme weather and an effective crack control is desired. Additionally, steel fibre concrete is an efficient solution to control crack width, by postponing maintenance threshold by twice as much when compared to the C35/45 concrete for extreme track conditions. This reduces the need for prompt maintenance giving time and redundancy to the infrastructure manager, hence reducing the risk of the vulnerability of the entire system. The performance is over enhanced for extreme weather scenarios with no immediate intervention predicted during lifetime if a 1.5% fibre content solution is used.

6.8.2 SCORING AND COMPARATIVE ASSESSMENT

A comparative assessment among modelling scenarios is now presented. A short and long-term perspective is provided. The short-term perspective is divided into acc_{CSL} , acc_{form} , F_c and q_{soil} , while the long-term performance is divided into 3 groups: Geometry deterioration (y_{soil} and y_{rail}), slab deterioration ($D_{CSL\ TOP}$, $D_{CSL\ BOT}$, $w_{k\ trs}$, $w_{k\ top}$, $w_{k\ bot}$) and HBL deterioration (D_{CAM} , $D_{HBL\ TOP}$, $D_{HBL\ BOT}$). By using these variables, a performance scoring system is proposed to compare the slab track performance of each scenario.

Figure 6.96 to 6.97 present some examples of web charts used to aid the visualization of the different impacts of each scenario on the calculated response. These charts represent the percentage deviation of each variable to a certain scenario compared to a reference scenario and they are essential to establish the basis of the scoring system.

As an illustration on what can be comprehended more easily, Figure 6.96 shows the more significant influence of speed towards track acceleration (almost 100% increase from 300 to 400 km/h) rather than the contact force and the deviatoric soil stresses. Concerning the analysis of damage, the geometry quality of the rail is one of the most sensitive damage criteria, followed by the bottom CSL damage and bottom crack width.

— 1 (H: 250 km/h) — 2 (H: 300 km/h) - Ref. — 3 (H: 350 km/h) — 4 (H: 400 km/h)

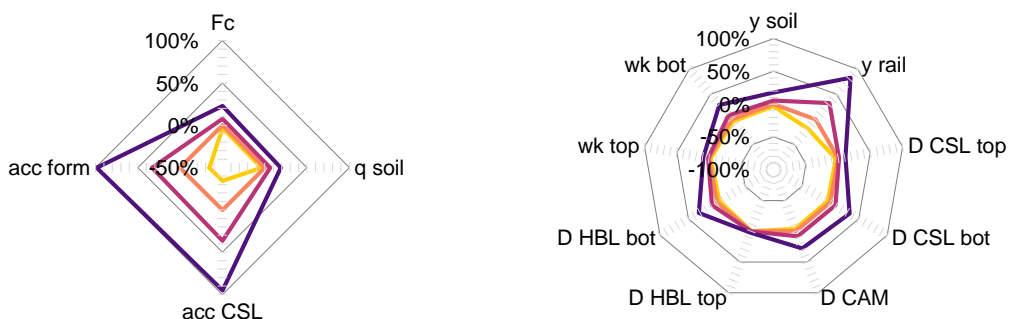


Figure 6.96: Web plot of the speed effect on slab track short-term behaviour

Figure 6.97: Web plot of the speed effect on slab track long-term behaviour

These web plots are presented in Annex A.1 for the standard scenarios 1-42 discussed in this chapter to clarify how the performance indicators interact with external actions, track design and track condition. Additionally, Annex A.2 presents a sensitivity analysis on track actions, design and condition and the effect on short- and long-term performance to better sustain some conclusions regarding track design and resiliency.

Furthermore, the previously proposed scenarios are going to be evaluated through a scoring system that enables a certain level of comparison between scenarios and evaluate the performance level of each one in 4 categories: 1 short-term (*ST*) and 3 long-term, subdivided in geometry (*LT_{GEO}*), CSL (*LT_{CSL}*), HBL deterioration (*LT_{HBL}*). For each category, the performance score is calculated as in the formulae presented below:

$$SC_j = \log(\alpha_j \times (A_j - P_j) + 1), \quad j = \{ST, LT_{GEO}, LT_{CSL}, LT_{HBL}\} \quad (6.4)$$

For $j = ST$

- $A_j = acc_{CSL}^1 + acc_{form}^1 + F_c^1 + q_{soil}$
- $P_j = 0$
- $\alpha_j = \frac{\sin(\frac{\pi}{2})}{2}$

For $j = LT_{GEO}$

- $A_j = y_{soil}^1 + y_{rail}^1$
- $P_j = (L_{span} - M_{soil}^{1st}) + (L_{span} - M_{rail}^{1st})$
- $\alpha_j = \frac{1}{2}$

For $j = LT_{GEO}$

- $A_j = D_{CSL\ TOP}^1 + D_{CSL\ BOT}^1 + w_{k\ TOP}^1 + w_{k\ BOT}^1 + w_{k\ TRV}^1$
- $P_j = (L_{span} - M_{CSL\ D}^{1st}) + (L_{span} - M_{wk}^{1st})$
- $\alpha_j = \frac{\sin(\frac{2\pi}{5})}{2}$

For $j = LT_{HBL}$

- $A_j = D_{HBL\ TOP}^1 + D_{HBL\ BOT}^1 + D_{CAM\ TOP}^1 + w_{k\ BOT}^1 + w_{k\ TRV}^1$
- $P_j = (L_{span} - M_{HBL\ D}^{1st})$
- $\alpha_j = \frac{\sin(\frac{2\pi}{3})}{2}$

In these formulae, $\alpha_j \times (A_j - P_j)$ is the normalized area of the polygon that makes the web chart as illustrated in Figure 6.96 to 6.97. Each vertex of the polygon represents a normalized performance variable. The proportion P_j is a tie breaker in scores that reach the maintenance threshold, and in that case, the sooner the maintenance intervention (M^{1st}) in the lifespan of the structure (L_{span}), the higher the penalization in the performance score. Finally, the logarithm is an artifice to reduce the spectrum boundary and ease the perception of the overall score to compare with other scenarios. Finally, the score is normalized from 0 (best) to 100 (worst) are represented in Table 6.15.

As it may be observed, the scenarios may be compared using the performance score of each indicator and certain deterioration mechanisms are highlighted. For a short-term perspective, it is possible to assess and compare certain scenarios that show similar short-term responses as the effect of speed and most importantly, the track geometry and condition. For example, scenario #38, with a 60 MPa soft soil section (300 km/h), presents a similar score as scenario #8 for high demand mixed traffic. For a lower platform stiffness, the short-term performance decreases sharply which supports the need for soil stabilization, although the slab structural integrity can withstand for a certain period, as already mentioned.

Concerning geometry deterioration, as expected, soft soil platform scenarios have the worst performance. Additionally, drainage and initial traffic defects have a greater impact on the final geometry score followed by heavy traffic and extreme rainfall events. If the designed soil platform and initial geometry quality are maintained within the design limits, no major issues are expected during the lifetime of the railway corridor. It must be stated that the best scenarios for geometry performance are the freight scenarios, due to a low deterioration of the rail profile associated with a reduced variation in the differential settlement. Nevertheless, this analysis may be misleading if the model assumption and architecture are not taken into account, since a homogeneous soil is considered in these scenarios. The rail profile is not significantly affected by a large overall soil settlement, since the track settles at the same rate. If a heterogeneous soil is considered, even by small margins (as it occurs in real case conditions), this geometry deterioration score would be poorer.

Table 6.15: Proposed performance score level of each scenario

		ST	GEO	CSL	CAM & HBL
Speed	1 (250 km/h)	7.35	0.00	1.49	0.46
	2 (300 km/h)	7.80	0.06	1.68	0.58
	3 (350 km/h)	8.99	0.28	2.84	0.87
	4 (400 km/h)	13.84	1.05	6.51	1.84
Freight Traffic	5 (F: 120 km/h)	0.00	0.00	6.98	1.09
	6 (F: 160 km/h)	0.03	0.00	6.98	1.09
Mixed Traffic	7 (H: 300 km/h & F: 120 km/h)	6.90	0.19	7.95	1.72
	8 (H: 400 km/h & F: 160 km/h)	16.96	0.51	8.84	2.39
Weather	9 (E ₂ & R ₁)	7.80	0.08	10.90	0.53
	10 (E ₃ & R ₁)	7.80	0.09	22.19	0.57
	11 (E ₁ & R ₂)	8.00	1.51	4.31	0.70
	12 (E ₁ & R ₃)	8.79	8.73	5.57	1.24
	13 (MT & E ₃ & R ₃)	18.78	11.06	34.44	4.80
Railpad	14 (20 kN/mm)	7.71	0.02	1.26	0.28
	15 (50 kN/mm)	7.97	0.09	2.78	0.88
	16 (90 kN/mm)	8.01	0.11	5.55	1.56
Concrete	17 (C ₃₀ /37)	7.80	0.07	5.03	0.88
	18 (C ₄₀ /50)	7.79	0.06	1.41	0.38
	19 (FRC)	7.71	0.06	0.50	0.00
	20 (RAC)	7.80	0.07	3.54	0.90
Reinf.	21 (8mm)	7.83	0.06	18.28	0.58
	22 (12 mm)	7.75	0.06	0.64	0.58
	23 (LPS)	7.80	0.06	0.00	0.58
HBL	24 (25 cm)	7.82	0.13	2.06	0.68
	25 (35 cm)	7.78	0.01	1.54	0.34
Settlement	26 (5//20)	13.02	7.69	6.89	2.56
	27 (10//20)	28.75	40.29	13.69	6.41
	28 (1//10)	8.64	0.22	1.80	0.95
Construction defects	29 (Drainage)	10.39	44.88	6.62	2.85
	31 (Subbase construction)	7.91	0.15	1.63	0.03
	33 (Loss of prestress)	7.80	0.06	5.85	0.58
	32 (Expansion joint)	7.80	0.08	100.00	1.49
	34 (Defective sleeper)	18.48	4.37	10.95	5.20
Soft soil	30 (Soil compaction)	7.90	0.32	1.45	0.62
	35 (Soft soil - 10 MPa)	100.00	97.44	53.28	37.12
	36 (Soft soil - 20 MPa)	57.77	92.39	46.33	30.68
	37 (Soft soil - 40 MPa)	43.59	57.14	20.63	16.99
	38 (Soft soil - 60 MPa)	16.78	9.74	7.56	5.14

Table 6.15: Proposed performance score level of each scenario (Continued)

		ST	GEO	CSL	CAM & HBL
Transition	39 (Transition - 10 MPa)	16.81	99.34	51.74	82.62
	40 (Transition - 20 MPa)	12.66	95.22	45.81	79.09
	41 (Transition - 40 MPa)	9.48	66.00	28.59	26.72
	42 (Transition - 60 MPa)	8.05	5.17	4.86	1.05

Aside from the external weak platform and lack of bearing capacity, concrete damage and crack width progress is mainly affected by the temperature, with failure issues if a malfunction occurs at the expansion joints. Also, reinforcement plays a major role in crack control, as well as the concrete quality that also shows good behaviour for long-term fatigue.

Finally, the HBL damage is fairly contained in most scenarios with minor differences in high load cases as initial rail profile quality and defective sleepers. Nonetheless, the platform bearing capacity causes the worst performance in the HBL damage with significant deviations from other scenarios. This is due to the main function that the HBL holds: to transfer dynamic loads to the soil uniformly. If a platform heterogeneity emerges, the HBL will naturally accumulate more damage, to uniform soil stresses.

In Table 6.16, the design improvements in terms of performance score are presented and some conclusions are drawn. In what regards short-term responses, each scenario presents improvements, even marginal as illustrated by the concrete quality which can improve the short-term response due to the higher capacity to maintain higher structural stability. A noteworthy performance is attributed to the 35 cm HBL that improved the bending capacity and the dynamic performance of the track. The extreme weather scenario and the mixed traffic presents a homogeneity in the short-term improvements aside from the soft railpad and thicker HBL. Since instantaneous responses of the track are intrinsically linked to geometry deterioration, the best performance scenarios are again the use of soft railpads and a thicker HBL. Short-term responses are not evaluated in the transition scenarios since the short-term sensors are located after the transition zone and are not comparable with the remaining scenarios.

Table 6.16: Proposed performance score level of each improved design scenario

		ST	GEO	CSL	CAM & HBL
Design (soft soil)	35 (Soft soil - 10 MPa) - Ref.	100.00	97.44	53.28	37.12
	D43 (S10 + FRC0.5%)	74.61	98.65	46.69	33.88
	D44 (S10 + FRC1%)	74.42	98.67	31.33	44.17
	D45 (S10 + FRC1.5%)	74.54	98.72	22.76	29.24
	D46 (S10 + LPS)	72.71	98.56	18.42	48.61
	D47 (S10 + HBL35)	55.02	97.09	53.15	94.42
Design (transition)	35 (Soft soil - 10 MPa) - Ref.	-	97.44	53.28	37.12
	D48 (T10 + FRC0.5%)	-	99.62	53.57	92.00
	D49 (T10 + FRC1.0%)	-	99.65	41.81	90.00
	D50 (T10 + FRC1.5%)	-	99.65	38.45	67.00
	D51 (T10 + LPS)	-	100.00	19.11	100.00
	D52 (T10 + HBL35)	-	98.40	58.11	76.30

Table 6.16: Proposed performance score level of each improved design scenario (Continued)

		ST	GEO	CSL	CAM & HBL
Design (extreme weather & mixed traffic)	D ₅₃ (MT + FRC0.5%)	18.78	11.06	34.34	4.80
	D ₅₄ (MT + FRC1.0%)	13.65	10.92	25.50	1.54
	D ₅₅ (MT + FRC1.5%)	13.72	10.89	15.91	0.82
	D ₅₆ (MT + B ₁₂ mm)	18.71	10.89	1.42	0.48
	D ₅₇ (MT + LPS)	18.78	11.06	24.30	4.81
	D ₅₈ (MT + P ₂₀)	18.78	11.01	9.65	14.15
	D ₅₉ (MT + HBL ₃₅)	13.25	4.83	28.08	2.10
		14.59	7.36	32.07	2.76

As discussed previously, concrete damage is highly influenced by concrete quality. As it may be observed, a 1.5% steel fibre content with extreme weather and mixed traffic scenario has the same SC_{CSL}^{LT} score as the 300 km/h standard scenario. Reinforcement schemes also have an impact on this performance score, mainly due to the crack control variables. Still related to the CSL and HBL score, it can be noticed that some design improvements have a worse score compared with the reference case. This is mainly caused by a delay in track maintenance (in this case concrete damage) that enables the formation of large cracks that affect the performance score. As an example, better concrete types can actively reduce the CSL damage and postpone slab maintenance, nonetheless, the HBL continues to accumulate extra damage.

In conclusion, this scoring system must be used with caution since limitations can be pointed as every performance indicator has the same weight, which can lead to misleading findings. A detailed and careful approach should be considered with the effects of intervention cost, maintenance frequency, quality thresholds among others. Notwithstanding, this scoring system provides a quick comparison tool between the very distinct scenarios for a rapid assessment of track performance.

6.9 CRITICAL ANALYSIS OF SLAB TRACK DESIGN AND GUIDELINES

The main goal of this chapter was to use the developed HI-Track model as a numerical tool to predict the short-term and long-term behaviour of slab tracks and to deliver design guidelines through an extensive assessment. The performance indicators are only focused on certain short-term responses and long-term predictions within the scope of this thesis. All the conclusions and recommendations do not take into consideration other deterioration phenomena, such as rail fatigue, fastening system wear and CAM-related deterioration.

In the previous subchapters, multiple simulations were run and complemented with an additional sensitivity analysis (Annex A.2) and the effect of external actions, track design and track condition on several damage progressions during the track's lifetime was analyzed. Table 6.17 summarizes the main findings, by presenting an easy-to-visualize analysis of the influence of each parameter on track deterioration. This table is the result of multiple cross-referenced simulations.

Table 6.17: Influence of actions and track condition on slab track long-term performance

		Geometry deterioration	Concrete Fatigue	Crack width
Actions	Speed	••	••	•
	Freight	••	•••	••
	Rainfall	••••	••	••
	Temperature	•	•••	•••••
Track condition	Initial Profile	•••••	•••	•••••
	Drainage	•••••	•••	••
	Transv. Prestress	•	•	•••*
	Expansion joints	•	•••••	•••••
	Defective sleeper	•••	•••	•••
	Soil compaction	••	•	•
	Soft soil	•••••	•••	•••••

*Longitudinal crack width

The results of the aforementioned table follow the conclusions obtained to the proposed level of service and weather scenarios and should be closely examined before a generalization about the phenomena is made. As in multiple track dynamic studies performed by several authors, speed influence is studied and its effect is observed exponentially with a 100% increase in track accelerations and a 20% in the contact force that during the track's lifespan. This results in an 82% increase for the rail profile levelling and 34% and 29% higher concrete damage and cracks width respectively. Although this substantial rise in track vibrations and deterioration, it is not a significant design issue since the slab track system is designed to withstand such speeds. Currently, the main limitation is related to operation and maintenance costs for the vehicle. An example is the 380 km/h homologated line from Beijing to Shanghai that was reduced to 300 km/h from 2011 until 2017 and restored to 350 km/h by a new version of a CR Series train that enhances the speed limit to the vehicle instead of the track, being capable to withstand speeds over 400 km/h without major maintenance requirements.

In what concerns the vehicles, freight trains cause higher levels of overall settlement and significantly more damage in the CSL and HBL. Although this additional damage, mixed traffic scenario does not present major maintenance interventions aside from crack injection. For relatively high quality and homogeneous soil, track geometry is under the maintenance threshold. Taking into consideration the assumed simplifications of the model, this topic should be further studied with the influence of soil heterogeneity and different track profiles.

A coveted feature that was included in the HI-Track model was the ability to simulate extreme weather events, such as intense rainfall and extreme temperature scenarios. Both can cause significant damage and crack width evolution by extreme heat and cold waves. In what concerns rainfall, heavy rain considerably increases track settlement, yet no maintenance threshold is surpassed (if the proper design is considered during the construction phase). Extreme

temperatures as hot temperatures (slab dilation and compression) and cold temperatures (slab warping) cause severe initial damage on the track. In contrast to what was observed for rainfall events, events of extreme temperature may result in the crack width intervention threshold being surpassed and maintenance is required. Nevertheless, no traffic disruption maintenance is expected (panel removal or soil stabilization) on both extreme atmospheric actions which enhance the track resiliency to climate adversity as well as very high speed and high axle load.

Apart from external actions, track conditions can have a relevant negative effect that may require heavy maintenance that disrupts the traffic as problems related to initial track profile and drainage defects, which may lead to expensive soil or embankment stabilization. Initial track defects higher than 7 mm for a 20 m chord and 2 mm for a 10 m chord (for a 300 km/h CHR₃ train vehicle with 90 circulations per day) will reach the maintenance threshold before the end of a 60-year lifespan.

Moreover, concrete damage is not a relevant concern for most expectable scenarios, however, the proper functioning of expansion joints or miscalculated temperature design tolerances can lead to structural failure. The latter is difficult to occur since the Bögl slab track has a cracking control zone between the panels with the grouting and transversal cuts for that matter, but another cast in situ solutions could present these problems.

For both differential settlement and soft soil sections that force the slab to act as a “bridge” over the defect are by far the most severe cases that should be fixed with immediate action to keep the same level of service. These simulations intend to represent the worst case scenarios that reveal that soft soil sections higher than 50 MPa do not cause any major maintenance works for track settlement or panel removal, which match with the German recommendations of a minimum $E_{v2} \geq 45$ MPa for embankments for existing tracks. These platform problems could also result in higher shear stresses leading to unexpected damage on the slab.

Table 6.18: Influence of track design optimization on slab track deterioration

	Geometry deterioration	Concrete Fatigue	Crack width
Railpad	••	••	••
CSL (FRC)	•	••••	•••
Long. Prestress	•	•••••	•••••
Reinforcement	•	•	••••
HBL	••	••	•

Some of these extreme cases previously mentioned were simulated with various design improvements to mitigate the deterioration level. These counter-measuring solutions are represented in Table 6.18, that shows how effective each design improvement is on reducing track deterioration (within the range of properties previously evaluated in this chapter). The scale is correlated with Table 6.17 to help visualize how much damage can be avoided by a design point of view. As an example, the 2-level geometry deterioration caused by the effects of speed

and freight (represented in Table 6.17) can be compensated by a softer railpad, and a 3-level crack width progress caused by the lack of transversal prestress can be fixed by an improved fibre reinforced concrete.

The design improvement can take two approaches: (i) reduce the vibratory energy that reaches the slab and fastening system vicinity, HBL or soil layers (which will redirect the damage elsewhere); (ii) increase the track strength to track deterioration.

As an example, to reduce the vibratory and dynamic loads is the introduction of softer railpads. Softer railpads have a positive outcome in all evaluated deterioration types leading to less maintenance and extend the track's lifespan, nevertheless, this balance can cause higher rail fatigue, vehicle wear and high energy costs which were not addressed.

Furthermore, a thicker HBL can reduce track damage but by a limited margin with low influence for thicknesses above 30/35 cm (except for severe soft soil conditions) and also thicknesses below 20/25 cm can lead to early damage and reduced track lifespan, which indicates a balanced thickness of 25-30 cm for earthworks sections using current construction standards.

Since the CSL is the principal layer of the superstructure and responsible for the structural integrity, direct improvements on the slab are influential. Concrete tensile strength is one of the main factors for crack control and damage, being the steel fibre reinforced concrete an attractive solution for slab tracks, and already implemented in some variants of Bögl slab track and the Stedef system. Considering that slab track systems are mainly designed for serviceability limit states, higher tensile stress strength on concrete is a design feature more effective than in conventional building construction, in which the main design codes are limited by ultimate limit states. Nevertheless, some steel fibre concrete show some difficulties to be cast as a heterogeneous fibre orientation mixture that increases the uncertainty regarding a true isotropic behaviour of the concrete. This can result in a lower Young modulus and tensile stress strength, yet the performance is acceptable for most scenarios. Also, the sustainable solution of recycled aggregate concrete can be applied in slab track projects with a high concrete usage.

Additionally, the reinforcement detailing is an effective measure to control the crack width evolution in situations that for example, are expected to occur minor changes in track condition. More advanced configurations as the longitudinal prestress, are the most effective way to control crack width, particularly for extremely low temperatures, however, it is very expensive and only used when no alternative exists.

In synthesis, track design plays a varied role on slab track deterioration with certain features prevailing as more practical design solutions as the reinforcement scheme in crack control width and the concrete quality on concrete damage and loss of stiffness. Although some severe scenarios require direct intervention on the crack condition, as very soft soil platform and drainage deficiency, slab track systems present itself as a robust and compelling level of low maintenance and a resilient track form for high demand railway operation.

7 FINAL REMARKS

7.1 CONCLUSIONS

Rail traffic is reaching new limits in terms of train speed, axle load and frequency. To cope with these new demand standards, ballastless tracks emerge around the globe as high performance, long-life and low maintenance solutions.

The main goal of this thesis was the conception, development and validation of a versatile three-dimensional train-track-soil system model using the finite element method so that it can accurately simulate the short- and long-term response of the track under the train and atmospheric actions. Along with this goal, the following research questions were used as reference benchmarks to fulfil the main contributions of this work:

1. How can slab track solutions be modelled for an accurate long-term response?
2. Which degradation mechanisms are relevant for slab track deterioration during lifetime?
3. Which slab track features are significant for long-term fatigue analysis?
4. How to develop an accurate maintenance operation scheduler aiming at life cycle cost assessment?

To answer these questions, the research made for this thesis resulted in the following contributions:

1. Development of a novel numerical tool capable of accurately predict short- and long-term behaviour of slab tracks.
2. Improvements of slab track design for the European requisites for 2030/2050 railways.
3. Decision assistance for the technical feasibility of slab track solutions focusing on longer life cycle and extended lifetime.

The first contribution, the development of a long-term numerical railway track model - HI-Track, was by far the most time-consuming phase of the thesis. The development of the HI-Track model followed a stepwise approach from scratch with thousands of simulations to build confidence in the model as a reliable tool to predict the short- and long-term performance indicators needed to fulfil the goals of the thesis.

In order to model the slab track long-term response with an appropriate level of accuracy, a new model architecture was proposed entitled HI-Track (hybrid & iterative). The main scope of this new architecture is the dual approach between a dynamic train/track simulation – DL-Track (dynamic & linear) and the nonlinear track calculation – SP-Track (static & plastic).

The DL-Track model can compute fast calculations of track accelerations and vibrations by implementing a substructuring technique to reduce the degrees of freedom of the full three-dimensional model. This is achieved by modelling a superelement composed of several track elements (sleepers, CSL, HBL, etc,) (a track “slice”). This modelling technique enables computation times 100 to 500 times faster than a full 3D-FEM model, allowing multiple dynamic calculations per global simulation. This is a singular contribution that makes a long-term simulation feasible with the available computational power, but comes with a cost: accuracy is lost when modelling high-order modal frequencies. Hence, this substructuring technique is not suitable for very modelling high-frequency phenomena (e.g. rail low wavelengths defects). Since the main scope of the thesis is focused on the concrete slab and soil deterioration with model frequencies under 200 Hz, the use of superelements is not an issue, presenting a marginal deviation between the reduced and the full model.

The second sub-model SP-Track is responsible for the detailed calculation of nonlinear soil, concrete and reinforcement stresses and strains and slab bending moment and shear force. This sub-model is far more detailed, and the main advanced feature is the incorporation of an initial concrete damage state that gives a pseudo nonlinear character in the long-term while keeping fast computations during short-term runs. This is crucial to assess the stiffness loss progression and the respective calculation of the crack width during lifetime. In what concerns geometry, SP-Track model features a more detailed fastening system load transfer, expansion joints and contact elements between layers. This system enables the slab to uplift and warp due to the train load and mostly due to temperature loads. This capacity to adequately model temperature effects on the track slab with minimal computational costs was a necessary goal to ascertain the track’s resiliency to extreme weather scenarios and how much damage is caused on the slab.

The long-term calculation of track behaviour is left to the HI-Track that controls the interaction between sub-models and is responsible for the track update according to the response measured in each one of the models. The update of the track condition is computed by mechanistic-empirical formulations with each sub-model output (track accelerations from the DL-track and track stresses and strains from SP-Track to compute concrete damage and soil settlement). Uneven soil settlement leads to amplified track accelerations, which consequently cause faster

concrete deterioration and loss of stiffness, thus accelerating differential settlements and the process is repeated. It is this interaction that empowers the degradation modelling on slab tracks by implementing a full 3D train/track dynamic simulation with nonlinear behaviour.

The developing process was subjected to extensive validation and calibration from multiple literature sources to compass most of the key variables calculated by the model, for short- and long-term responses. This validation was complemented with intermodal comparison (with models already validated with ballasted and slab tracks), laboratorial campaigns (Track Box and GRAFT-II) and the use of pre-instrumented real high-speed lines (Hannover-Berlin, Cologne-Frankfurt and Paris-Strasbourg) for several slab track systems as Rheda 2000, Rheda Classic, Stedef, 3MB and Bögl system. The calibration with these data has leveraged the reliability of the model to predict long-term effects on slab tracks. Long-term data concerning slab track performance is scarce in comparison with short-term measurements (long-term testing is complex and usually made under stringent confidentiality agreements and long-lasting records history of the performance of existing high-speed lines are absent). This can lead to high levels of uncertainty regarding the calculated variables (concrete deterioration and soil permanent deformation). Nevertheless, the data available shows a good correspondence with the calculated results, delivering confidence in the hybrid model. Results as track damage and crack width are not as well validated as other parameters (lack of long history of records), however, an effort was done to compare the magnitude and overall growth with literature review and a physical coherency stepwise comparison with the obtained results. Model validation was one of the most time-consuming milestones of the thesis and presented multiple challenges as part of the available data, requiring extensive statistical post-processing and very disperse modelling for multiple scenarios. Nevertheless, this vast process has enabled to develop and come to a HI-Track model well-equipped and robust and providing reliable predictions on slab track behaviour during its lifespan.

After the validation and calibration, the next phase of the thesis was the improvement and applicability of the model to a wide range of scenarios to test the slab track solution to its design limits. The Bögl slab track system was the elected commercial system to be implemented in the HI-Track and to representatively assess the performance of slab tracks. This choice is justified by its wide application worldwide (the Bögl system is one of the most used ballastless track forms). Also, the slab track category is representative and can easily extrapolate conclusions to other slab track typologies.

The next contribution of the thesis is related to the main degradation mechanisms and causes, and which features can be adjusted to postpone or even avoid such deterioration. The model architecture and development were built to meet the requirements for studying concrete damage and track geometry quality. Other phenomena as rail wear or fastening system fatigue are important for the overall life cycle cost of the entire system but are not addressed in this version of the HI-Track.

The model uses empirical formulations to emulate the cumulative damage on the track, hence in the case of more comprehensive empirical formulation arise with more detailing incorporation of different variables, the hybrid model is prepared to be easily upgraded with such laws. Extreme weather scenarios are simulated through temperature cycles and rainfall events. Temperature is represented as daily temperature variations and gradients directly imposed on the track (rail and CSL) and the rainfall events are modelled through the cumulative soil settlement, indirectly calculated by a THM model that takes into account precipitation, temperature, relative humidity, wind and groundwater table.

The first approach to use the HI-Track for design guidelines is to determine to what level is slab track able to withstand extreme weather and traffic loads. This ability to ensure structural stability and controlled deterioration is a key factor regarding the slab track resiliency and risk vulnerability. The main findings are:

- Train speed and vehicle type have a larger influence on track geometry quality with a 40% increase on track settlement for freight and more than 80% on rail levelling by increasing the speed from 300 to 400 km/h. It is noted that a mixed traffic scenario tends to reduce differential settlements, which matches with real-world applications where mixed traffic reduce the probability of systematic failures.
- In extreme weather scenarios simulated, heavy rainfall and flooding have implications on the plastic permanent strain of the soil and cause poor rail quality geometry during operation (+170% increase of the rail levelling). On the other hand, temperature loads have a significant impact on concrete damage and crack width, being the most conditioning external action on this deterioration type. Uniform temperature variations have a small impact on the Bögl system due to a cracking concentration zone between the module panels that act as a “breathing zone” for temperature expansions and contractions. In that case, gradient temperature cause slab warping and is the main cause of concrete damage mainly negative gradients that cause concrete cracks on top of the slab, since it is the most exposed surface to climate actions.

In synthesis, external severe actions in very extreme scenarios can have a severe impact on slab track deterioration (track settlement and concrete fatigue). On one hand, increasing train speed and axle load cause fairly distributed concrete fatigue and soil plastic deformation, and on the other hand, atmospheric actions achieve more extreme results in both deterioration phenomena. As expected, rainfall has a deeper impact on soil settlement and temperature on concrete fatigue when compared to ordinary operating conditions. However, this additional deterioration is far from maintenance thresholds (except for concrete cracking) which goes along with the main purpose of ballastless tracks to provide operation resiliency to demanding scenarios.

Regarding which features are significant for long-term analysis, multiple track configuration, geometric layout, local soil properties, track defects were assessed in Chapter 7 with critical

analysis in each parameter. Certain features show an important influence on a specific deterioration while having a negligible effect on others. These design factors can be implemented and promote an enhanced track performance and resiliency for particular real-world scenarios, aiming for a particular design goal. Taking into account the included slab track components modelled in the HI-Track, the main design guidelines and recommendations are:

- Soft railpads can reduce track damage and crack width up to 10% when reduced from 35 kN/mm to 20 kN/mm and also decreases CSL and soil accelerations which can reduce the deterioration even further. Notwithstanding, rail accelerations are higher, causing increased rail fatigue, vehicle wheel wear and higher energy consumption by the vehicle, which indicates the existence of an optimum pad stiffness to minimize maintenance and operation costs;
- Concrete class strength has little influence on track damage (less than 5% improvement), yet steel fibre reinforced concrete can achieve a 30% lower concrete fatigue and crack width compared to the standard C35/45. Recycled aggregate concrete, which may make economic and sustainable sense to apply this kind of concrete in slab track construction, has worse performance (reduction of 8% for concrete fatigue damage);
- Reinforcement detailing, namely rebar diameter, has a massive impact on crack control. Reducing the rebar diameter for 10 to 8 mm almost doubles the crack width progress rate. On the other side, a 12 mm diameter can result in a 20-40% lower crack width. If longitudinal prestressed is installed on the panels, a 40-80% reduction is achieved depending on the climate and traffic. Since these enhanced solutions add significant construction costs, they are only used in extreme temperature variations or high chloride environments to avoid steel corrosion and assure the durability of the track.
- The HBL thickness (25 – 35 cm) has diminished effect on concrete damage and track settlement on ordinary operation conditions (<5%) unless in the presence of soft soil sections in which the settlement rate can be shortened by up to 20% and a reduction in 10% for concrete damage. Along with these results, the importance of the HBL is hailed as a fundamental element to provide durability and stability of the track.

Despite the Bögl slab track being representative of the most common ballastless system around the globe, there is a myriad of different systems with very distinct structural behaviour as elaborated in Chapter 2 and these findings should not be generalized to different slab track categories without a careful assessment. Nevertheless, the HI-Track model is a flexible tool capable of modelling different ballastless systems, traffic conditions, temperature variations, rainfall events, and supporting conditions, e.g. bridge/tunnel transitions, slab - ballasted track transitions, culverts, among others. The model is tailored to deliver simulations to study specific parameters for a long-term assessment paired with fast computation.

With this final version of the numerical model, the fourth contribution of this work can be

delivered, which corresponds to the evaluation of track maintenance requirements during the service life supporting programs of life cycle cost assessment. Throughout the simulations, several maintenance thresholds were defined (track settlement, slab damage and transversal and longitudinal crack width) and each scenario was evaluated on how fast or slow that limit was surpassed, giving insights on how frequent and when during the service life does the track require maintenance for the damage phenomena considered. By attributing a cost to maintenance procedures, the operation works, construction and other indirect costs (e.g. ride comfort quality, track availability, environmental impact, etc.), a simple life cycle cost model or a RAMS analysis can be complemented by the results of the HI-Track.

In conclusion, the fast computing dynamic & nonlinear HI-Track model can fulfil a bi-objective optimization goal complying with short-term performance as well as long-term responses. The obtained design recommendations have the potential to incorporate decision support tools for railway stakeholders to increase the feasibility of high-demand slab track corridors.

7.2 LIMITATIONS AND PROSPECTIVE WORK

As future developments, there are some aspects related to modelling techniques and further simulation scenarios that require additional research. Some research opportunities for future works and developments are suggested herein:

1. Further improvement in modelling techniques

Numerical modelling enhancements and complexity will eventually become feasible with growing computational power, as well as more comprehensive modelling tools that enable more accurate and solid predictions of the slab track behaviour.

The **DL-Track** is a model that uses a numerical reduction technique, favouring fast computations, obtaining the best trade-off between calculation time and accurate responses for the track and soil vicinity. These goals could result in an oversimplification of dynamic modelling techniques that could be improved in future works:

- Nonlinear constitutive law for soft railpads that have a frequency-dependent stiffness and a more accurate response at higher frequencies.
- A higher level of detail in the vehicle modelling, as full car multibody dynamics, to study the influence of sprung and non-sprung masses on track short-term response and therefore possible effects on long-term deterioration.
- Application of longer track models to include real-world track vertical levelling sections (>200 m). Using the same substructuring technique, it is believed to keep the simulation under reasonable computational times.
- A detailed evaluation of damping properties of each element coupled with “infinite” model boundaries could provide a proper wave propagation to the soil.

Similarly, the **SP-Track** follow the same computational cost/ result accuracy ratio optimization for the calculation of the stress state of the concrete, reinforcement and soil, yet a fair amount of complexity could be applied:

- A more geometric detailed representation of the fastening system (railpad, clamps, shoulder, bolts, etc.) that would drive for improved stress paths from the rail to the slab, as well as the study of the fatigue on the fastening system.
- Implementation of a more complex “cracked” state as an initial condition for prospective iterations instead of loss of stiffness in each element.
- Concrete curing, hydration and temperature in the early days are proven by the literature to have a significant impact on concrete cracking. The inclusion of these phenomena in early iterations of the HI-Track model may conduct to more accurate crack width progression as well as shrinkage and creep effects during the slab serviceability life.
- A slip-bond law between the reinforcement and the concrete can simulate the adhesion between the two surfaces and increase the reliability of the model regarding crack width progress.
- Although a linear modelling approach to the soil platform is not rough to slab track modelling since the expected soil stresses are low, nonlinear soil models would be desirable for situations on non-consolidated soils or higher stress levels on the subgrade.
- Temperature effects on the CSL and HBL could use a thermal conductivity model. This would avoid temperature gradients being artificially implemented in the model.

The HI-Track model is responsible for couple DL-Track and SP-Track together and updates the track properties of each one. Taken into consideration the architecture of the model, some future works are:

- Adaptive time step threshold in the early years of the service life of the track instead of fixed steps to enhanced crack detection.
- Different empirical formulae should be implemented and compared to track damage and track settlement.
- Since track deterioration is a highly unpredictable set of phenomena, track updating based on stochastic modelling could be adopted. For example, fatigue modelling could be made taking into consideration the stress level and the probability of failure of each element (modelled with a Weibull distribution).
- Direct coupling of the THM model with the HI-Track for a wider range of applications of atmospheric actions and the model update during the lifetime of the track, that includes track permeability and drainage system.

2. Future simulations focusing on design recommendations for a decision support system.

With the final version of the HI-Track, several simulation combinations may be calculated and presented as a standard catalogue for slab track systems with pros and cons for certain parameters. Future calculations could entail:

- Transition designs and the evolution of track deterioration over millions of train passages and climate actions. Slab-track/ ballasted track transitions, as bridge and tunnels would have a high potential to be simulated with limited improvements on the model.
- Study of a different set of vehicles with different speeds to investigate the damage level of each one on the track.
- Assessment of structurally distinct slab track systems as embedded rail systems, floating slab tracks, non-embedded block systems, among others, or study railway elements with different properties, upgrading existing designs.
- Integration of the obtained results and design recommendations in life cycle cost evaluation and contribute as a decision support tool for railway administrations in condition based maintenance programs.

REFERENCES

- ACCIONA. (2017). D 4.3.2: Demonstration of new monitoring techniques. C4R - Capacity for Rail (Report).
- ACI. (1992). ACI 215R-74 - Considerations for design of concrete structures subjected to fatigue loading.
- Aggestam, E., Nielsen, J. C. O., & Bolmsvik, R. (2018). Simulation of vertical dynamic vehicle-track interaction using a two-dimensional slab track model. *Vehicle System Dynamics*, 3114, 1–25.
- Al-Tabbaa, A., & Wood, D. M. (1989). An experimentally based “bubble” model for clay. In Elsevier Applied Science (Ed.), *Proceedings of "Numerical Models in Geomechanics. NUMOG III*, Niagara Falls, Canada.
- Alves Costa, P., Calçada, R., & Silva Cardoso, A. (2012). Track-ground vibrations induced by railway traffic: In-situ measurements and validation of a 2.5D FEM-BEM model. *Soil Dynamics and Earthquake Engineering*, 32(1), 111–128.
- Alves Costa, P., Lopes, P., & Cardoso, A. S. (2018). Soil shakedown analysis of slab railway tracks : Numerical approach and parametric study. *Transportation Geotechnics*, 16(July), 85–96.
- Andersen, L., Nielsen, S. R. K., & Krenk, S. (2007). Numerical methods for analysis of structure and ground vibration from moving loads. *Computers and Structures*, 85(1–2), 43–58.
- Ando, K., Sunaga, M., Aoki, H., & Haga, O. (2001). Development of slab tracks for Hokuriku Shinkansen line. *Quarterly Report of RTRI (Railway Technical Research Institute) (Japan)*, 42(1), 35–41.
- Andrés, A., Gómez, M., & Gutiérrez, L. (2015). Costs and RAMS methodologies (superstructure). Paris, France: C4R - Capacity for Rail (Dissemination Workshop).
- ARA. (2004). Guide for Mechanistic-Empirical Design of New and Rehabilitated Pavement Structures. *NCHRP 1-37A, Report, Final Draft*, Applied Research Associates, Inc. Albuquerque, NM.
- Araujo, N. M. (2010). *High-Speed Trains on Ballasted Railway Track - Dynamic stress field analysis*. PhD Thesis. University of Minho. Portugal.

- Arlaud, E. (2017). *Modèles dynamiques réduits de milieux périodiques par morceaux : application aux voies ferroviaires*. École Nationale Supérieure d'Arts et Métiers.
- Arora, S., & Singh, S. P. (2016). Analysis of flexural fatigue failure of concrete made with 100% Coarse Recycled Concrete Aggregates. *Construction and Building Materials*, 102, 782–791.
- Auersch, L. (2005). Dynamics of the railway track and the underlying soil: the boundary-element solution, theoretical results and their experimental verification. *Vehicle System Dynamics*, 43(9), 671–695.
- Auersch, L. (2012). Dynamic Behavior of Slab Tracks on Homogeneous and Layered Soils and the Reduction of Ground Vibration by Floating Slab Tracks. *Journal of Engineering Mechanics*, 138(8), 923–933.
- Auersch, L., & Said, S. (2017). Track-soil dynamics – Calculation and measurement of damaged and repaired slab tracks. *Transportation Geotechnics*, 12, 1–14.
- Aure, T. W., & Ioannides, A. M. (2010). Simulation of crack propagation in concrete beams using cohesive elements in ABAQUS. In *Transportation Research Record 2154: Journal of the Transportation Research Board* (pp. 12–21). Washington.
- Balendra, T., Chua, K. H., Lo, K. W., & Lee, S. L. (1989). Steady-state vibration of subway-soil-building system. *Journal of Engineering Mechanics*, 115(1), 145–162.
- Barksdale, R. D. (1972). Laboratory evaluation of rutting in base course materials. In *Proc. 3rd International Conference on the structural design of asphalt pavements* (pp. 161–174). University of Michigan.
- Bezin, Y., Farrington, D., Penny, C., Temple, B., & Iwnicki, S. (2010). The dynamic response of slab track constructions and their benefit with respect to conventional ballasted track. *Vehicle System Dynamics*, 48(sup1), 175–193.
- Bian, Xuecheng, Chao, C., Jin, W., & Chen, Y. (2011). A 2.5D finite element approach for predicting ground vibrations generated by vertical track irregularities. *Journal of Zhejiang University SCIENCE A*, 12(12), 885–894.
- Bian, Xuecheng, Jiang, H., Cheng, C., Chen, Y., Chen, R., & Jiang, J. (2014). Full-scale model testing on a ballastless high-speed railway under simulated train moving loads. *Soil Dynamics and Earthquake Engineering*, 66, 368–384.
- Bilow, D., & Randich, G. (2000). Slab track for the next 100 years. In Portland Cement Association (Ed.), *The American Railway Engineering and Maintenance-of-way Association - Proceedings of the 2000 Annual Conference* (pp. 1–20). Skokie, IL.
- Blanco-Lorenzo, J. (2011). Dynamic comparison of different types of slab track and ballasted track using a flexible track model. *Proc. IMechE Part F: Journal of Rail and Rapid Transit*, 225(6), 574–592.
- Bongini, E., Müller, R., Garburg, R., & Peringer, A. (2013). *Del 3.13: Design guide and technology assessment of the track mitigation measures*.
- Cachim, P. B. (1999). *Experimental and numerical analysis of the behaviour of structural concrete under fatigue loading with applications to concrete pavements*. Faculty of Engineering of the University of Porto.
- Cai, X. P., Luo, B. C., Zhong, Y. L., Zhang, Y. R., & Hou, B. W. (2019). Arching mechanism of the slab joints in CRTSII slab track under high temperature conditions. *Engineering Failure Analysis*, 98(January), 95–108.
- CEN. Eurocode 1: Actions on structures - Part 2: Traffic loads on bridges: EN 1991-2 (2004).

- CEN, C. E. de N. Eurocode 2: Design of concrete structures - Part 1-1: General rules and rules for buildings: EN 1992-1-1 (2004).
- Cervenka, V., Markova, J., Mloch, J., Caldentey, A. P., Sajdlova, T., & Sykora, M. (2018). Uncertainties of crack width models. *High Tech Concrete: Where Technology and Engineering Meet*, 1653–1661.
- Cervo, T. C. (2004). *Estudo da Resistência à Fadiga de Concretos de Cimento Portland para Pavimentação*. PhD Thesis. Universidade de São Paulo, São Paulo (In Portuguese).
- Chang, D. Il, & Chai, W. K. (1995). Flexural fracture and fatigue behavior of steel-fiber-reinforced concrete structures. *Nuclear Engineering and Design*, 156(1-2), 201–207.
- Chapeleau, X., Sedran, T., Cottineau, L. M., Cailliau, J., Taillade, F., Gueguen, I., & Henault, J. M. (2013). Study of ballastless track structure monitoring by distributed optical fiber sensors on a real-scale mockup in laboratory. *Engineering Structures*, 56, 1751–1757.
- Chiou, J. S., Lin, H. S., Yeh, F. Y., & Sung, Y. C. (2016). Plastic settlement evaluation of embedded railroads under repeated train loading. *Journal of GeoEngineering*, 11(2), 97–107.
- Cho, Y. K., Kim, S.-M., Chung, W., Kim, J. C., & Oh, H. J. (2014). Effect of steel ratio on behavior of Continuously Reinforced Concrete Railway Track under environmental loads. *KSCE Journal of Civil Engineering*, 18(6), 1688–1695.
- Chopra, A. (1995). *Dynamics of structures: Theory and applications to Earthquake Engineering*. New Jersey, USA: Prentice Hall.
- Choubane, B., & Tia, M. (1995). Analysis and Verification of Thermal-Gradient Effects on Concrete Pavement. *Journal of Transportation Engineering, ASCE*, 121, 75–81.
- Connolly, D. P., Kouroussis, G., Laghrouche, O., Ho, C. L., & Forde, M. C. (2015). Benchmarking railway vibrations - Track, vehicle, ground and building effects. *Construction and Building Materials*, 92, 64–81.
- Cooper, J., & Harrison, M. (2002). Development of an alternative design for the West Rail viaducts. In *Proceedings of Institution of Civil Engineers, Transport*, 153 (pp. 87–95).
- Cox, S. J., Wang, a., Morison, C., Carels, P., Kelly, R., & Bewes, O. G. (2006). A test rig to investigate slab track structures for controlling ground vibration. *Journal of Sound and Vibration*, 293(3–5), 901–909.
- Craig, R. R., & Bampton, M. D. D. (1968). Coupling of Substructures for Dynamic Analysis. *AIAA Journal*, 12, 1313–1319.
- Crail, S., Reichel, D., Schreiner, U., Lindner, E., Habel, W., Basedau, D. H. F., Brandes, K., & Barner, A. (2002). Strain Monitoring of a Newly Developed Precast Concrete Track for High Speed Railway Traffic Using Embedded Fiber-Optic Sensors. In *SPIE, Smart Structures and Materials 2002: Smart Sensor Technology and Measurement Systems* (Vol. 4694, pp. 259–264).
- Cross, R., Makeev, A., & Armanios, E. (2006). A Comparison of Predictions From Probabilistic Crack Growth Models Inferred From Virkler's Data. *Journal of ASTM International*, 3(10), 100574.
- Crozet, Y. (2013). High Speed Rail Performance in France: From Appraisal Methodologies to Ex-post Evaluation. *International Transport Forum*, (Discussion paper 2013-26).
- Cui, F., & Chew, C. H. (2000). The effectiveness of floating slab track system — Part I. Receptance methods. *Applied Acoustics*, 61(4), 441–453.

- Dai, F., Thompson, D. J., Zhu, Y., & Liu, X. (2016). Vibration properties of slab track installed on a viaduct. *Proceedings of the Institution of Mechanical Engineers, Part F: Journal of Rail and Rapid Transit*, 230(1), 235–252.
- Darr, E., & Fiebig, W. (2006). *Feste Fahrbahn: Konstruktion und Bauarten für Eisenbahn und Strassenbahn*. Berlin: Eurorail Press.
- De Vos, P. (2016). Railway Noise in Europe: State of the art report. *UIC Report*.
- Delaplace, M., & Dobruszkes, F. (2015). From low-cost airlines to low-cost high-speed rail? The French case. *Transport Policy*, 38, 73–85.
- Denneman, E., Wu, R., Kearsley, E. P., & Visser, A. T. (2009). Fracture mechanics in pavement design. In *Proceedings of the 28th Southern African Transport Conference (SATC 2009)*. Pretoria.
- Deutsche Bahn AG, & Terno, H.-J. (2011). *Del. 3.1: State of the art review of mitigation measures on track*.
- Diehl, R. J., Nowack, R., & Hödl, G. (2000). Solutions for Acoustical Problems With Ballastless Track. *Journal of Sound and Vibration*, 231(3), 899–906.
- Dieleman, L., Fumey, M., Robinet, A., & Martin, D. (2008). Experimentation of a track section without ballast on the new line of East European TGV. In *8th World Congress on Railway Research* (pp. 18–22).
- Do, M., Chaallal, O., & Aïtcin, P. (1993). Fatigue behaviour of high-performance concrete. *Journal of Materials in Civil Engineering*, 5(1), 96–111.
- Duan, X., Hu, J., Bian, X., & Jiang, J. (2018). Dynamic Interaction of Vehicle-Track Coupled System Under Different Patterns of Uneven Settlement. In *Environmental Vibrations and Transportation Geodynamics* (ISE 2016, pp. 565–573). Singapore.
- Esveld, C. (2001). *Modern Railway Track* (2nd Ed.).
- Esveld, C., & De Man, A. (2003). Use of Railway Track Vibration Behaviour for Design and Maintenance. *IABSE Symposium*, 87, 39–45.
- European Asphalt Pavement Association (EAPA). (2014). Asphalt in Railway Tracks. *Position Paper*. Brussels, Belgium.
- Fang, M., Qiu, Y., Rose, J., West, R., & Ai, C. (2011). Comparative analysis on dynamic behavior of two HMA railway substructures. *Journal of Modern Transportation*, 231(1), 26–34.
- Feng, Q., Chao, H., & Lei, X. (2017). Influence of the Seam between Slab and CA Mortar of CRTSII Ballastless Track on Vibration Characteristics of Vehicle-Track System. *Procedia Engineering*, 199, 2543–2548.
- Ferreira, P. A. (2010). *Modelling and Prediction of dynamic Behaviour of Railway Infrastructures at Very High-Speeds*. PhD Thesis. Instituto Superior Técnico. Lisbon.
- Ferreira, P. A., & López-Pita, A. (2015). Numerical modelling of high speed train/track system for the reduction of vibration levels and maintenance needs of railway tracks. *Construction and Building Materials*, 79, 14–21.
- Ferreira, T. M. (2015). *Design of railway track substructure modelling the long term thermo-hydro-mechanical behaviour due to traffic and environmental actions*. PhD Thesis. Instituto Superior Técnico, Portugal.
- Ferreira, T. M., & Teixeira, P. F. (2012). Rail track performance with different subballast solutions: Traffic and environmental effects on subgrade service life. *Journal of Transportation Engineering*, 138(12), 1541–1550.

- Ferreira, T. M., Teixeira, P. F., & Cardoso, R. (2011). Impact of Bituminous Subballast on Railroad Track Deformation Considering Atmospheric Actions. *Journal of Geotechnical and Geoenvironmental Engineering*, 137(3), 288–292.
- FIB. Model Code 2010, Vol. 1. Fédération Internationale du Béton § (2010). Lausanne.
- Freitas da Cunha, J. P. (2013). *Modelling of Ballasted Railway Tracks for High-Speed Trains. PhD Thesis*. University of Minho. Portugal.
- Fumey, M., Hofmann, C., Godart, P., Trevin, J., Simovic, T., Mißler, M., Klösters, F., Crail, S., Fila, R., Marvillet, D., Porta, L., & Zuber, P. (2002). Feasibility study ballastless track. *Infrastructure Commission - Civil Engineering Support Group. UIC Report*.
- Gaedicke, C., & Roesler, J. R. (2009). Fracture-based method to determine the flexural load capacity of concrete slabs. *FAA-05-CAT-UIUC, Department of Civil and Environmental Engineering, University of Illinois, Urbana, Illinois*.
- Galvín, P., Romero, A., & Domínguez, J. (2010a). Fully three-dimensional analysis of high-speed train-track-soil-structure dynamic interaction. *Journal of Sound and Vibration*, 329(24), 5147–5163.
- Galvín, P., Romero, A., & Domínguez, J. (2010b). Vibrations induced by HST passage on ballast and non-ballast tracks. *Soil Dynamics and Earthquake Engineering*, 30(9), 862–873.
- Gao, G. Y., Chen, Q. S., He, J. F., & Liu, F. (2012). Investigation of ground vibration due to trains moving on saturated multi-layered ground by 2.5D finite element method. *Soil Dynamics and Earthquake Engineering*, 40, 87–98.
- Gautier, P.-E. (2015). Slab track: Review of existing systems and optimization potentials including very high speed. *Construction and Building Materials*, 92, 9–15.
- Gautier, P.-E. (2017). *New slab track design and bench testing for dense traffic and high speed*. Madrid, Spain: C4R - Capacity for Rail (Dissemination Workshop).
- Giannakos, K., & Tsoukantas, S. (2009). Design methodology of slab track systems. *Advances in Transportation Geotechnics*, 585–592.
- Goicolea, J. (2014). *Simplified Mechanical Description of AVE S-103 - ICE3 Velaro E High Speed Train*. Madrid, Spain.
- Grassie, S. L. (2012). Squats and squat-type defects in rails: the understanding to date. *Proceedings of the Institution of Mechanical Engineers, Part F: Journal of Rail and Rapid Transit*, 226(3), 235–242.
- Grzybowski, M., & Meyer, C. (1993). Damage accumulation in concrete with and without fiber reinforcement. *ACI Materials Journals*, 95, 594–604.
- Guigou-Carter, C., Villot, M., Guillerme, B., & Petit, C. (2006). Analytical and experimental study of sleeper SAT S 312 in slab track Sateba system. *Journal of Sound and Vibration*, 293(3–5), 878–887.
- Gupta, S., & Degrande, G. (2010). Modelling of continuous and discontinuous floating slab tracks in a tunnel using a periodic approach. *Journal of Sound and Vibration*, 329(8), 1101–1125.
- Guyan, R. J. (1965). Reduction of Stiffness and Mass Matrices. *AIAA Journal*, 3(2).
- He, Q., Cai, C., Zhu, S., Zhang, J., & Zhai, W. (2018). Dynamic performance of low vibration slab track on shared high-speed passenger and freight railway. *Transport*, 33(3), 669–678.
- Hiller, J. E., & Roesler, J. R. (2005). Determination of Critical Concrete Pavement Fatigue Damage

- Locations Using Influence Lines. *Journal of Transportation Engineering*, 131(8), 599–607.
- Hornych, P. H., & Paute, J. L. (1998). Influence de l'eau sur la comportement mécanique des graves non traitées et des sols supports de chaussées. In *Simposio Internacional: Drenaje Interno de Firmes y Explanadas* (pp. 249–257). Granada, Spain.
- Houben, L. J. M. (1994). Finite-Elements Analysis of Plain Concrete Pavements Subjected to Temperature Gradients and Traffic LoadingsTitle. In *Proceedings of the 3rd International Workshop on the Design and Evaluation of concrete Pavements*. CROW - PIARC - CEMBUREAU (pp. 141–173). Krumbach.
- Hussein, M. F. M., & Hunt, H. E. M. (2006). Modelling of floating-slab tracks with continuous slabs under oscillating moving loads. *Journal of Sound and Vibration*, 297(1–2), 37–54.
- Hussein, M. F. M., & Hunt, H. E. M. (2009). A numerical model for calculating vibration due to a harmonic moving load on a floating-slab track with discontinuous slabs in an underground railway tunnel. *Journal of Sound and Vibration*, 321(1–2), 363–374.
- Ioannides, A. M. (2006). Concrete pavement analysis: the first eighty years. *International Journal of Pavement Engineering*, 7(4), 233–249.
- IRI, & LDEO. (2019). IRI/LDEO Climate Data Library.
- Jang, S. Y., Lee, H. S., Kim, Y. B., Kim, E., Lee, I. W., Kang, Y. S., Lee, S.-H., Kim, Y. B., Kim, E., Lee, I. W., & Kang, Y. S. (2008). Development of Prefabricated Concrete Slab Track Systems and Trial Installation on Revenue Line. *8th World Congress on Railway Research*.
- Johnston, C. D., & Zemp, R. W. (1991). Flexural fatigue performance of steelfiber reinforced concrete—Influence of fiber content, aspect ratio and type. *ACI Materials Journals*, 95(1), 58–67.
- Kaewunruen, S., & Remennikov, A. M. (2016). Current state of practice in railway track vibration isolation: an Australian overview. *Australian Journal of Civil Engineering*, 14(1), 63–71.
- Keerthana, K., & Kishen, J. M. C. (2019). Effect of Loading Frequency on Flexural Fatigue Behaviour of Concrete. In *10th International Conference on Fracture Mechanics of Concrete and Concrete Structures*. Bayonne, France.
- Khabbaz, H., & Fatahi, B. (2014). A Critical and Comparative Review of Ballasted and Slab Tracks: Where Are We Heading? In *Proceedings of the Second International Conference on Railway Technology: Research, Development and Maintenance* (pp. 1–19). Stirlingshire, Scotland.
- Konrad, M., & Wagg, B. T. (1993). Undrained cyclic loading of anisotropically consolidated clayey silts. *Journal of Geotechnical Engineering*, 119(5), 929–947.
- Korkiala-Tanttu, L. (2008). *Calculation method for permanent deformation of unbound pavement materials*. Helsinki University of Technology. Sweden. PhD.
- Kucharczyk, K., Głuchowski, A., Miturski, M., & Sas, W. (2018). Influence of load frequency on cohesive soil respond. *Geosciences (Switzerland)*, 8(12), 1–13.
- Kumar, S. S., Krishna, A. M., & Dey, A. (2018). Dynamic properties and liquefaction behaviour of cohesive soil in northeast India under staged cyclic loading. *Journal of Rock Mechanics and Geotechnical Engineering*, 10(5), 958–967.
- Kuo, C., Huang, C. H., & Chen, Y.-Y. (2008). Vibration characteristics of floating slab track. *Journal of Sound and Vibration*, 317(3–5), 1017–1034.
- Le, J. L., & Bažant, Z. P. (2011). Unified nano-mechanics based probabilistic theory of quasibrittle and brittle structures: II. Fatigue crack growth, lifetime and scaling. *Journal of the Mechanics and Physics of Solids*, 59(7), 1322–1337.

- Le, J. L., Bažant, Z. P., & Bazant, M. Z. (2011). Unified nano-mechanics based probabilistic theory of quasibrittle and brittle structures: I. Strength, static crack growth, lifetime and scaling. *Journal of the Mechanics and Physics of Solids*, 59(7), 1291–1321.
- Lee, M. K., & Barr, B. I. G. (2004). An overview of the fatigue behaviour of plain and fibre reinforced concrete. *Cement and Concrete Composites*, 26(4), 299–305.
- Lee, S.-H., Lee, J.-W., Park, D.-W., & Vo, H. V. (2014). Evaluation of asphalt concrete mixtures for railway track. *Construction and Building Materials*, 73, 13–18.
- Lei, X. (2017). *High Speed Railway Track Dynamics - Models, Algorithms and Applications*. (Springer, Ed.) (1st ed.). Beijing, China.: Science Press.
- Lei, X., Wu, S., & Zhang, B. (2016). Dynamic Analysis of the High Speed Train and Slab Track Nonlinear Coupling System with the Cross Iteration Algorithm. *Journal of Nonlinear Dynamics*, 2016, 17.
- Lei, X., & Zhang, B. (2011). Analysis of Dynamic Behavior for Slab Track of High-Speed Railway Based on Vehicle and Track Elements. *Journal of Transportation Engineering*, 137(4), 227–240.
- Li, D., Hyslip, J., Sussmann, T., & Chrismer, S. (2015). *Railway Geotechnics*. CRC Press.
- Li, D., Sussman, T. R., & Selig, E. T. (1996). *Procedure for railway track granular layer thickness determination*. Association of American Railroads, Transportation Technology Center.
- Li, Z. G., & Wu, T. X. (2008). Modelling and analysis of force transmission in floating-slab track for railways. *Proceedings of the Institution of Mechanical Engineers, Part F: Journal of Rail and Rapid Transit*, 222(1), 45–57.
- Li, Z., Zhao, X., Dollevoet, R., & Molodova, M. (2008). Differential wear and plastic deformation as causes of squat at track local stiffness change combined with other track short defects. *Vehicle System Dynamics*, 46(SUPPL.1), 237–246.
- Lichtberger, B. (2005). *Track Compendium* (1st Ed.). Eurorail Press.
- Liu, S., Yu, H., Wang, J., & Wanatowski, D. (2018). Shakedown for slab track substructures with stiffness variation. *Geotechnical Research*, 5.
- Liu, X., Zhao, P., & Dai, F. (2011). Advances in design theories of high-speed railway ballastless tracks. *Journal of Modern Transportation*, 19(3), 154–162.
- Lombaert, G., Degrande, G., Kogut, J., & François, S. (2006). The experimental validation of a numerical model for the prediction of railway induced vibrations. *Journal of Sound and Vibration*, 297(3–5), 512–535.
- Lombaert, G., Degrande, G., Vanhauwere, B., Vandeborgh, B., & François, S. (2006). The control of ground-borne vibrations from railway traffic by means of continuous floating slabs. *Journal of Sound and Vibration*, 297(3–5), 946–961.
- Madhkhan, M., Entezam, A., & Torki, M. E. (2013). Mechanical properties of steel fiber-reinforced concrete slab tracks on non-ballasted foundations. *Scientia Iranica*, 20(6), 1626–1636.
- Madshus, C., & Kaynia, A. M. (2000). High-speed railway lines on soft ground: dynamic behaviour at critical train speed. *Journal of Sound and Vibration*, 231(3), 689–701.
- Markine, V. L., De Man, A. P., & Esveld, C. (2000). Optimization of an embedded rail structure using a numerical technique. *Heron*, 45(1), 63–74.

- Matias, S. R. (2014). *Modelação Numérica e Dimensionamento de Vias-Férreas em Laje de Betão - Comparação com vias balastradas*. MSc Thesis. Instituto Superior Técnico. Portugal (In Portuguese).
- Matias, S. R., & Ferreira, P. A. (2020). Railway slab track systems : review and research potentials Railway slab track systems : review and research potentials. *Structure and Infrastructure Engineering*, 0(0), 1–19.
- Mazars, J. (1986). A description of micro- and macroscale damage of concrete structures. *Engineering Fracture Mechanics*, 25(5–6), 729–737.
- Michas, G. (2012). *Slab Track Systems for High-Speed Railways*. MSc Thesis. KTH, Sweden.
- Mohamed, R., & Hansen, W. (1997). Effect of nonlinear temperature gradients on curling stresses in concrete pavements. *Transportation Research Record*, 1568, 65–71.
- Musmar, M. (2013). Tensile strength of steel fiber reinforced concrete. *Contemporary Engineering Sciences*, 6(5–8), 225–237.
- Nielsen, J. C. O., & Ekberg, A. (2005). Influence of short-pitch wheel/rail corrugation on rolling contact fatigue of railway wheels. *Proceedings of the Institution of Mechanical Engineers, Part F: Journal of Rail and Rapid Transit*, 219, 177–188.
- Nielsen, J. C. O., Lundén, R., Johansson, A., & Vernersson, T. (2003). Train-Track Interaction and Mechanisms of Irregular Wear on Wheel and Rail Surfaces. *Vehicle System Dynamics*, 40(1–3), 3–54.
- Nsabimana, E., & Jung, Y.-H. (2015). Dynamic subsoil responses of a stiff concrete slab track subjected to various train speeds: A critical velocity perspective. *Computers and Geotechnics*, 69, 7–21.
- Oh, B. H. (1991). Fatigue- life distributions of concrete for various stress levels. *ACI Materials Journals*, 88, 122–127.
- Pacheco, J., De Brito, J., Chastre, C., & Evangelista, L. (2019). Scatter of constitutive models of the mechanical properties of concrete: Comparison of major international codes. *Journal of Advanced Concrete Technology*, 17(3), 102–125.
- Packard, G., & Tayabji, S. (1985). New PCA Thickness Design Procedure for Concrete Highway and Street Pavements. In *Concrete Pavement & Rehabilitation Conference*. Purdue, USA.
- Paskova, T., & Meyer, C. (1997). Low-cycle fatigue plain and fiber reinforced concrete. *ACI Materials Journals*, 94, 273–285.
- Paute, J. L., Jouve, P., Martinez, J., & Ragneau, E. (1988). *Modèle de calcul pour le dimensionnement des chaussées souples*.
- Pingrui, Z., Xueyi, L., & Guan, L. (2014). Experimental study of temperature gradient in track slab under outdoor conditions in Chengdu area. *Journal of Modern Transportation*, 22(3), 148–155.
- Pita, A. L., Teixeira, P. F., & Ferreira, P. A. (2012). High-speed rail modal split on routes with high air traffic density. *Proceedings of the Institution of Civil Engineers: Transport*, 165(2), 119–129.
- Poveda, E., Yu, R. C., Lancha, J. C., & Ruiz, G. (2015). A numerical study on the fatigue life design of concrete slabs for railway tracks. *Engineering Structures*, 100, 455–467.
- Professional Standard of the People's Republic of China. (2009). TB10621 - Code for Design of High-speed Railway.
- Rahardjo, H., Ong, T. H., Rezaur, R. B., & Leong, E. C. (2007). Factors controlling instability of

- homogeneous soil slopes under rainfall. *Journal of Geotechnical and Geoenvironmental Engineering*, 133(12), 1532–1543.
- Rahimi, A., Rahardjo, H., & Leong, E. C. (2011). Effect of antecedent rainfall patterns on rainfall-induced slope failure. *Journal of Geotechnical and Geoenvironmental Engineering*, 137(June), 1–8.
- Ren, J., Deng, S., Wei, K., Li, H., & Wang, J. (2019). Mechanical property deterioration of the prefabricated concrete slab in mixed passenger and freight railway tracks. *Construction and Building Materials*, 208(March), 622–637.
- Ren, J., Li, X., Yang, R., Wang, P., & Xie, P. (2016). Criteria for repairing damages of CA mortar for prefabricated framework-type slab track. *Construction and Building Materials*, 110(May), 300–311.
- Ripke, B. (2010). *Design and Performance of ballastless track - Success criteria and application ranges. (High-speed rail course)*. Instituto Superior Técnico, Portugal.
- Robertson, I., Masson, C., Sedran, T., Barresi, F., Cailliau, J., Keseljevic, C., & Vanzenberg, J. M. (2014). Advantages of a new ballastless trackform. *Construction and Building Materials*, 92, 16–22.
- Rodolfo, M., & Balbo, J. (2001). Modelagem de tensões em pavimentos de concreto submetidos a gradientes térmicos e cargas rodoviárias. *Escola Politécnica Da Universidade de São Paulo*.
- Russo, G., & Romano, F. (1992). Cracking response of rc members subjected to uniaxial tension. *Journal of Structural Engineering (United States)*, 118(5), 1172–1190.
- Sancho, J. M., Planas, J., Cendón, D. A., Reyes, E., & Gálvez, J. C. (2007). An embedded crack model for finite element analysis of concrete. *Engineering Fracture Mechanics*, 74, 270–277.
- Sañudo, R., Dell 'olio, L., Casado, J. A., Carrascal, I. A., & Diego, S. (2016). Track transitions in railways: A review. *Construction and Building Materials*, 112, 140–157.
- Sato, K., & Chen, Y. (2018). Analysis of high-speed rail and airline transport cooperation in presence of non-purchase option. *Journal of Modern Transportation*, 26(4), 231–254.
- Satoshi, A. (1989). Loading-deformation characteristics of slab track with temperature variation. *Railway Summary Report*, 10(3), 2–9.
- Selig, E. T., & Waters, J. M. (1994). *Track Geotechnology and Substructure Management*. (T. Telford, Ed.).
- Shahraki, M., Warnakulasooriya, C., & Witt, K. J. (2015). Numerical study of transition zone between ballasted and ballastless railway track. *Transportation Geotechnics*, 3, 58–67.
- Shan, Y., Zhou, S., Zhou, H., Wang, B., Zhao, Z., & Shu, Y. (2017). Iterative computation method of train-load-induced uneven settlement of high-speed railway transition zones. In *Transportation Research Board 96th annual meeting*. Washington.
- Shan, Z., & Yu, Z. (2015). A fiber bundle-plastic chain model for quasi-brittle materials under uniaxial loading. *Journal of Statistical Mechanics: Theory and Experiment*, 11, 0–38.
- Shanghai Railway Administration. (2017). The 14th China International Modern Railway Technology and Equipment Exhibition: Special subject.
- Sheng, X., Jones, C. J. C., & Thompson, D. J. (2006). Prediction of ground vibration from trains using the wavenumber finite and boundary element methods. *Journal of Sound and Vibration*, 293(3–5), 575–586.

- Sheng, X., Zhong, T., & Li, Y. (2017). Vibration and sound radiation of slab high-speed railway tracks subject to a moving harmonic load. *Journal of Sound and Vibration*, 395, 160–186.
- Shi, L., Cai, Y., Wang, P., & Sun, H. (2016). A theoretical investigation on influences of slab tracks on vertical dynamic responses of railway viaducts. *Journal of Sound and Vibration*, 374, 138–154.
- Shi, X. P., Fwa, T. F., & Tan, S. A. (1993). Flexural fatigue strength of plain concrete. *ACI Materials Journals*, 90(5), 435–440.
- Singh, S. P., & Khushik, S. K. (2002). Flexural fatigue strength and failure probability of steel fibrous concrete. *Journal of the Institution of Engineers (India): Civil Engineering Division*, 83(JUN.), 1–4.
- Smith, K. D., & Roesler, J. R. (2004). Review of fatigue models for concrete airfield pavement design. *Airfield Pavements*, 231–258.
- Song, X., Zhao, C., & Zhu, X. (2014). Temperature-induced deformation of CRTS II slab track and its effect on track dynamical properties. *Science China Technological Sciences*, 57(10), 1917–1924.
- Springenschmid, R. (1998). *Prevention of Thermal Cracking in Concrete at Early Ages*.
- SSF Ingenieure GmbH. (2010). Slab track systems on different substructures. Company brochure.
- STAIRRS. (2003). *STAIRRS - Strategies and Tools to Assess and Implement Noise Reducing Measures for Railway Systems - Final technical report*.
- Steenbergen, M., Metrikine, A. V., & Esveld, C. (2007). Assessment of design parameters of a slab track railway system from a dynamic viewpoint. *Journal of Sound and Vibration*, 306(1–2), 361–371.
- Stet, M., & Frénay, J. (1998). Fatigue properties of plain concrete. In *Proceedings of the 8th International Symposium on Concrete Roads, AIPCR-CEMBUREAU, Theme I* (pp. 129–136). Lisbon.
- Straub, D., & Faber, M. H. (2005). Risk based inspection planning for structural systems. *Structural Safety*, 27(4), 335–355.
- Sweere, G. T. H. (1990). *Unbound granular basis for roads*. University of Delft. Netherlands. PhD.
- Takai, H. (2007). 40 Years Experiences of the Slab Track on Japanese High Speed Lines. In Euskal Trenbide Sarea (Ed.), *1st International Conference*.
- Tan, R. (2019). *Consistent crack width calculation methods for reinforced concrete elements subjected to 1D and 2D stress states*. Faculty of Enginnering. Norwegian University of Science and Technology. Trondheim, Norway.
- Tan, R., Hendriks, M. A. N., Geiker, M., & Kanstad, T. (2018). A numerical investigation of the cracking behaviour of reinforced-concrete tie elements. *Magazine of Concrete Research*, 72(3), 109–121.
- Tarifa, M., Zhang, X., Ruiz, G., & Poveda, E. (2015). Full-scale fatigue tests of precast reinforced concrete slabs for railway tracks. *Engineering Structures*, 100, 610–621.
- Teixeira, P. F. (2004). *Contribución a la reducción de los costes de mantenimiento de vías de alta velocidad mediante la optimización de su rigidez vertical*. PhD Thesis. Universidad Politécnica de Catalunya. Barcelona (in Spanish).
- Teixeira, P. F., Ferreira, P. A., & Andrés Lopés-Pita. (2009). The use of bituminous subballast on future high-speed lines in Spain: structural design and economical impact. *International Journal of Railway*, 2(1), 1–7.

- Thompson, D. J. (2009). *Railway Noise and Vibration* (1st Editio). Southampton: Elsevier.
- Thompson, D. J., & Gautier, P.-E. (2006). Review of research into wheel/rail rolling noise reduction. *Proceedings of the Institution of Mechanical Engineers, Part F: Journal of Rail and Rapid Transit*, 220(4), 385–408.
- Thompson, D. J., Wu, T., & Armstrong, T. (2003). Wheel/rail rolling noise - the effects of nonlinearities in the contact zone. In *10th International Congress on Sound and Vibration ICSV2003*. Stockholm, Sweden.
- Timoshenko, S. (1926). Method of analysis of statical and dynamical stresses in rail. In *Second International Congress for Applied Mechanics*.
- Tsaparas, I., Rahardjo, H., Toll, D. G., & Leong, E. C. (2002). Controlling parameters for rainfall-induced landslides. *Computers and Geotechnics*, 29(1), 1–27.
- Tseng, K. H., & Lytton, R. L. (1989). *Prediction of permanent deformation in flexible pavement materials. ASTM STP 1016* (Implicatio). Philadelphia, P. A., P. A.
- Tzanakakis, K. (2013). *The Railway Track and Its Long Term Behaviour - A Handbook for a Railway Track of High Quality*. Springer.
- Van Lier, S. (2000). the Vibro-Acoustic Modelling of Slab Track With Embedded Rails. *Journal of Sound and Vibration*, 231(3), 805–817.
- Varandas, J. N. (2013). *Long-Term Behaviour of Railway Transitions Under Dynamic Loading. PhD Thesis*. New.
- Venhaus, H., & Petz, M. (2014). *Quiet Tracks for Sustainable Railway Infrastructures*.
- Verbraken, H., Lombaert, G., & Degrande, G. (2012). Experimental and numerical prediction of railway induced vibration. *Journal of Zhejiang University SCIENCE A*, 13(11), 802–813.
- Veverka, V. (1979). *Raming van de Spoordiepte bij Wegen met Cen Bitumineuze Verharding* (De Wegente).
- Vogt, L., Wolffersdorff, P.-A. von, & Rehfeld, E. (2005). Behaviour of slab track under extreme stress conditions. In *European Slab Track Symposium* (pp. 1–29). Belgium.
- Vossloh Fastening Systems GmbH. (2009). Design of Slab Track and Fastening Systems.
- Vucetic, M. (1988). Degradation of marine clays under cyclic loading. *Journal of Geotechnical Engineering*, 114(2), 133–149.
- Wan, Z., & Yang, R. (2018). Experimental Study on Temperature Characteristics of CRTS I Twin-Block Ballastless Track. In X. Bian, Y. Chen, & X. Ye (Eds.), *Environmental Vibrations and Transportion Geodynamics* (ISEV 2016, pp. 727–735). Singapore: Springer.
- Wang, J., Zhou, Y., Wu, T., & Wu, X. (2019). Performance of Cement Asphalt Mortar in Ballastless Slab Track over High-Speed Railway under Extreme Climate Conditions. *International Journal of Geomechanics*, 19(5), 1–11.
- Wang, M., Cai, C., Zhu, S., & Zhai, W. (2016). Experimental study on dynamic performance of typical nonballasted track systems using a full-scale test rig. *Proceedings of the Institution of Mechanical Engineers, Part F: Journal of Rail and Rapid Transit*, 0(0), 1–12.
- Westergaard, M. (1926). Analysis of stress in concrete pavements due to variations of temperature. *Proc., 6th Ann. Meeting, Highway Research Board, Washington D.C.*, 201–205.
- Williams, B. A., Holder, D., Edwards, J. R., Dersch, M. S., & Barkan, C. (2016). Quantification of the lateral forces in concrete sleeper fastening systems. *Proc. IMechE Part F: Journal of Rail*

- and Rapid Transit, 230(7), 1714–1721.
- Wu, J. Y., Li, J., & Faria, R. (2006). An energy release rate-based plastic-damage model for concrete. *International Journal of Solids and Structures*, 43(3–4), 583–612.
- Xiao, J., Li, H., & Yang, Z. (2013). Fatigue behavior of recycled aggregate concrete under compression and bending cyclic loadings. *Construction and Building Materials*, 38, 681–688.
- Xiao, J., Li, L., Tam, V. W. Y., & Li, H. (2014). The state of the art regarding the long-term properties of recycled aggregate concrete. *Structural Concrete*, 15(1), 3–12.
- Xin, T., & Gao, L. (2011). Reducing slab track vibration into bridge using elastic materials in high speed railway. *Journal of Sound and Vibration*, 330(10), 2237–2248.
- Yang, X., Gu, S., Zhou, S., Yang, J., Zhou, Y., & Lian, S. (2015). Effect of track irregularity on the dynamic response of a slab track under a high-speed train based on the composite track element method. *Applied Acoustics*, 99, 72–84.
- Yang, Y., Wu, G., Wu, Z.-S., Jiang, J.-B., & Wang, X.-B. (2015). Structural performance of ballastless track slabs reinforced with BFRP and SFCB. *Composites Part B: Engineering*, 71, 103–112.
- Yongjiang, X., Huajian, L., Zhongwei, F., & Ilwaha, L. (2009). Concrete Crack Case and its Damage in Ballastless Track Structure. *International Journal of Railway*, (1), 30–36.
- Yue, G., Xu, Z., Wang, L., Liu, C., & Zhou, W. (2017). Vibration analysis for slab track at different train speeds using Bayes wavelet denoising. *Proceedings of the Institution of Mechanical Engineers, Part F: Journal of Rail and Rapid Transit*, 231(8), 892–901.
- Zhai, W., Liu, P., Lin, J., & Wang, K. (2015). Experimental investigation on vibration behaviour of a CRH train at speed of 350 km/h. *International Journal of Rail Transportation*, 3(1), 1–16.
- Zhai, W., Wang, S., Zhang, N., & Gao, M. (2013). High-speed train – track – bridge dynamic interactions – Part II : experimental validation and engineering application. *International Journal of Rail Transportation*, 1–2, 25–41.
- Zhai, W., Wei, K., Song, X., & Shao, M. (2015). Experimental investigation into ground vibrations induced by very high speed trains on a non-ballasted track. *Soil Dynamics and Earthquake Engineering*, 72, 24–36.
- Zhang, B., Phillips, D. V., & Wu, K. (1996). Effects of loading frequency and stress reversal on fatigue life of plain concrete. *Magazine of Concrete Research*, 48(4), 361–375.
- Zhang, X., Burrow, M., & Zhou, S. (2015). An investigation of subgrade differential settlement on the dynamic response of the vehicle-track system. *Proceedings of the Institution of Mechanical Engineers, Part F: Journal of Rail and Rapid Transit*, 0(4800), 1–14.
- Zhou, M. (2011). *The influence of slab track and train operation safety on subgrade's uneven settlement*. MSc Thesis. Tongji University. People's Republic of China.
- Zhu, S., & Cai, C. (2011). Fatigue life prediciton of CRTS I ballastless slab track. In *ICTE 2011 - Proceedings of the Third International Conference on Transportation Engineering*, ASCE (pp. 1714–1719).
- Zhu, S., & Cai, C. (2014a). Interface damage and its effect on vibrations of slab track under temperature and vehicle dynamic loads. *International Journal of Non-Linear Mechanics*, 58, 222–232.
- Zhu, S., & Cai, C. (2014b). Stress intensity factors evaluation for through-transverse crack in slab track system under vehicle dynamic load. *Engineering Failure Analysis*, 46, 219–237.
- Zhu, S., Cai, C., & Spanos, P. D. (2015). A nonlinear and fractional derivative viscoelastic model

- for rail pads in the dynamic analysis of coupled vehicle–slab track systems. *Journal of Sound and Vibration*, 335, 304–320.
- Zhu, S., Wang, M., Zhai, W., Cai, C., Zhao, C., Zeng, D., & Zhang, J. (2018). Mechanical property and damage evolution of concrete interface of ballastless track in high-speed railway: Experiment and simulation. *Construction and Building Materials*, 187, 460–473.
- Zhu, S., Yang, J., Cai, C., Pan, Z., & Zhai, W. (2017). Application of dynamic vibration absorbers in designing a vibration isolation track at low-frequency domain. *Proceedings of the Institution of Mechanical Engineers, Part F: Journal of Rail and Rapid Transit*, 231(5), 546–557.
- Zhuang, Y., & Wang, K. (2017). Three-dimensional shakedown analysis of ballasted railway structures under moving surface loads with different load distributions. *Soil Dynamics and Earthquake Engineering*, 100(May), 296–300.
- Zongqi, B., Gong, Q., Zhuang, K., & Liushan, W. (2018). An Implicit-Explicit Transition Method for Settlement Prediction of High-Speed Railway Subgrade Under High-Cycle Load. In X. Bian, Y. Chen, & X. Ye (Eds.), *Environmental Vibrations and Transportation Geodynamics* (ISEV 2016, pp. 785–800). Singapore: Springer.

ANNEXES

LIST OF ANNEXES CONTENTS

A. ANNEX A	215
A.1 Performance scoring and comparison assessment.....	215
A.1.1 Train speed	215
A.1.2 Vehicle type.....	215
A.1.3 Weather events	216
A.1.4 Railpad stiffness	216
A.1.5 Reinforcement.....	217
A.1.6 Concrete type	217
A.1.7 HBL	218
A.1.8 Initial profile	218
A.1.9 Construction defects.....	219
A.1.10 Soft soil scenario	219
A.1.11 Transition scenario	220
A.2 Sensitivity analysis.....	220
A.2.1 Speed.....	221
A.2.2 Railpad.....	221
A.2.3 Concrete.....	222
A.2.4 HBL	222
A.2.5 Settlement amplitude.....	222
A.2.6 Settlement wavelength	223

A. ANNEX A

A.1 PERFORMANCE SCORING AND COMPARISON ASSESSMENT

This Annex presents the performance web plots of the several scenarios explained in Chapter 6.

A.1.1 TRAIN SPEED

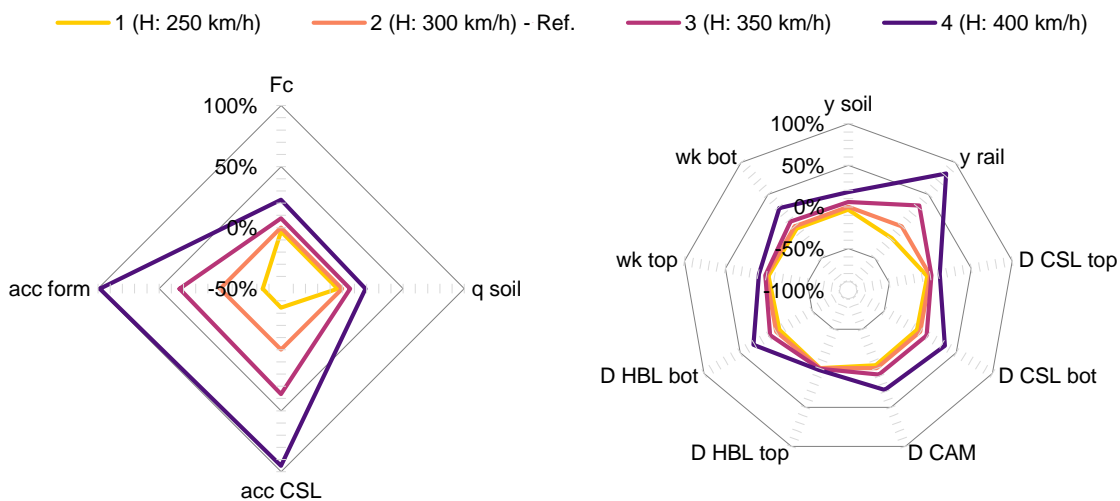


Figure A.1: Web plot of the train speed effect on the variation of slab track short-term behaviour

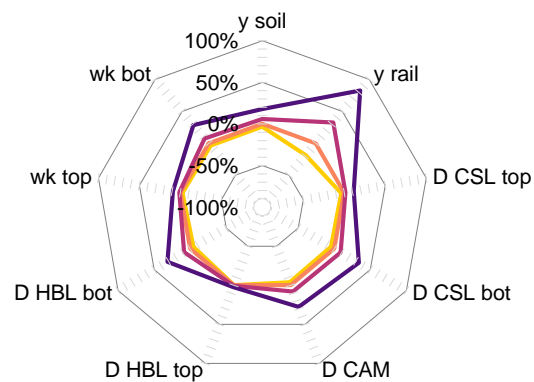


Figure A.2: Web plot of the train speed effect on the variation of slab track long-term behaviour

A.1.2 VEHICLE TYPE

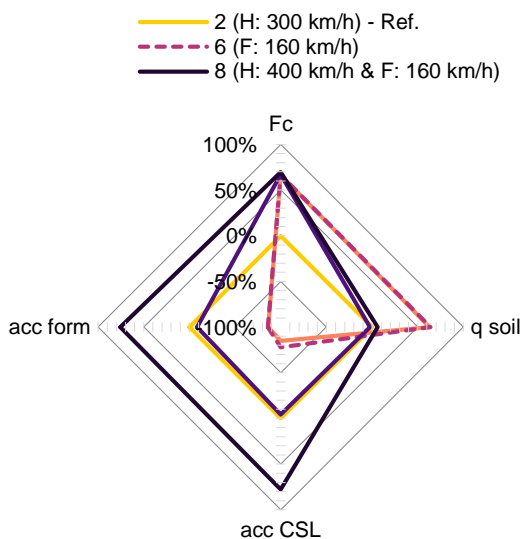


Figure A.3: Web plot of the vehicle type effect on the variation of slab track short-term behaviour

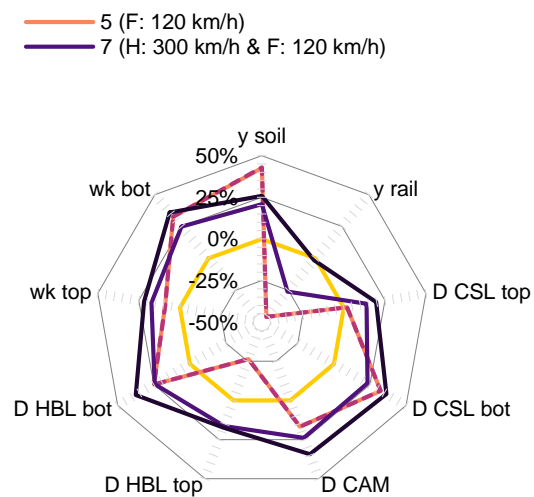


Figure A.4: Web plot of the vehicle type effect on the variation of slab track long-term behaviour

A.1.3 WEATHER EVENTS

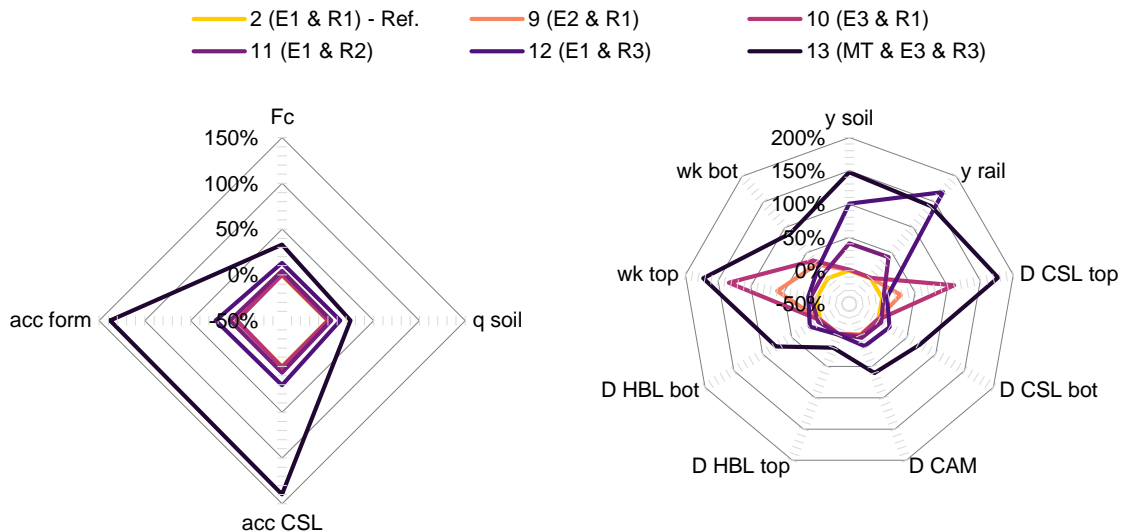


Figure A.5: Web plot of the weather effect on the variation of slab track short-term behaviour

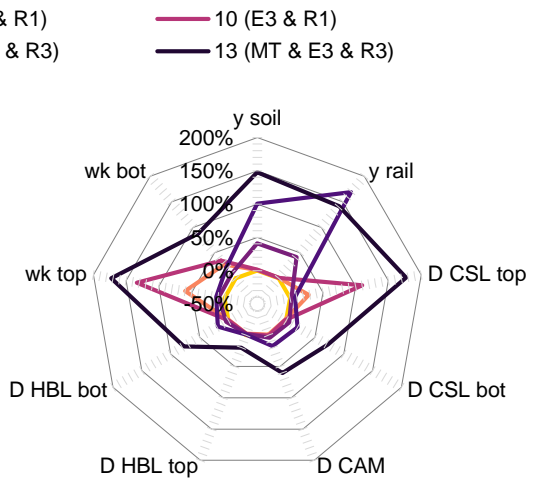


Figure A.6: Web plot of the weather effect on the variation of slab track long-term behaviour

A.1.4 RAILPAD STIFFNESS

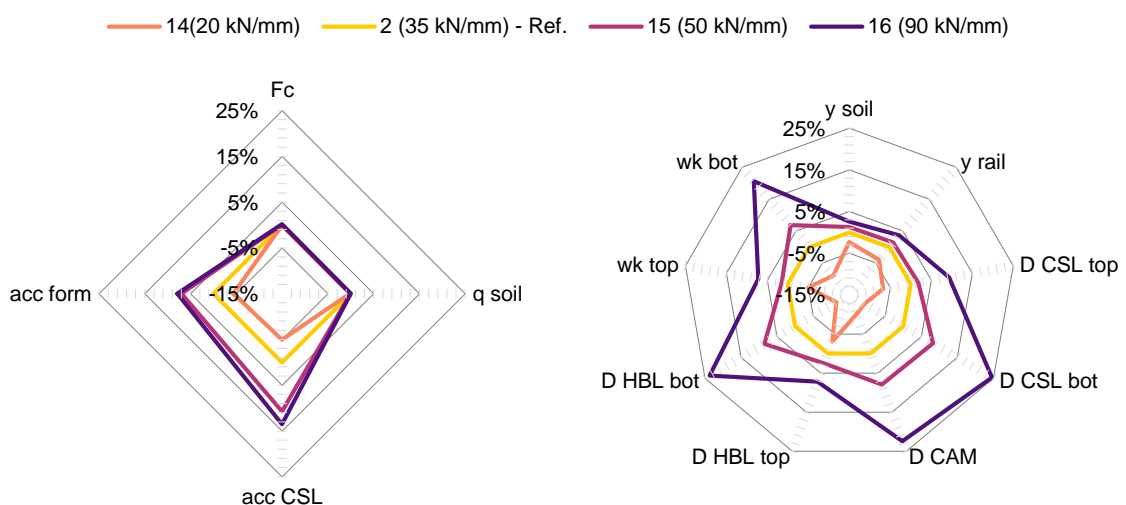


Figure A.7: Web plot of the railpad stiffness effect on the variation of slab track short-term behaviour

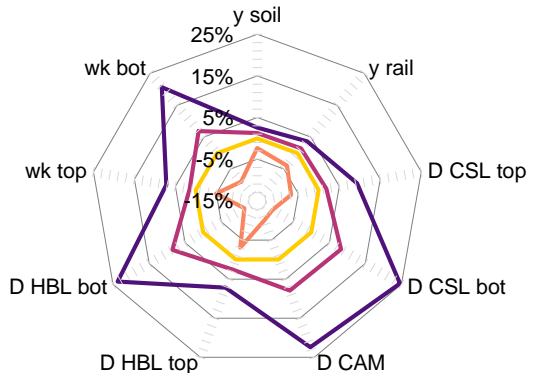


Figure A.8: Web plot of the railpad stiffness effect on the variation of slab track long-term behaviour

A.1.5 REINFORCEMENT

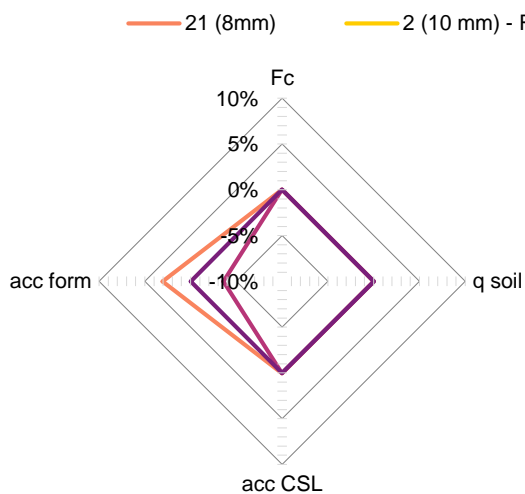


Figure A.9: Web plot of the effect of the longitudinal reinforcement rebar size on the variation of slab track short-term behaviour

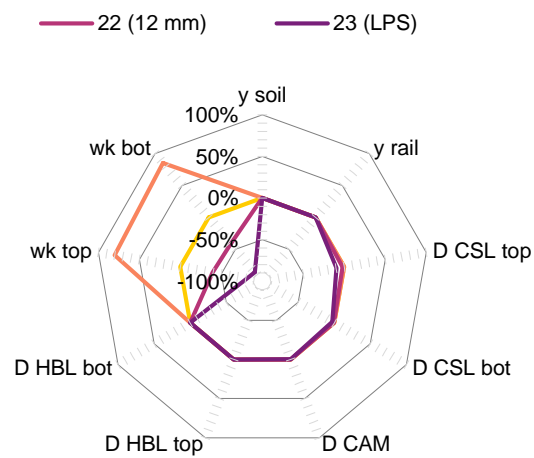


Figure A.10: Web plot of the effect of the longitudinal reinforcement rebar size on the variation of slab track long-term behaviour

A.1.6 CONCRETE TYPE

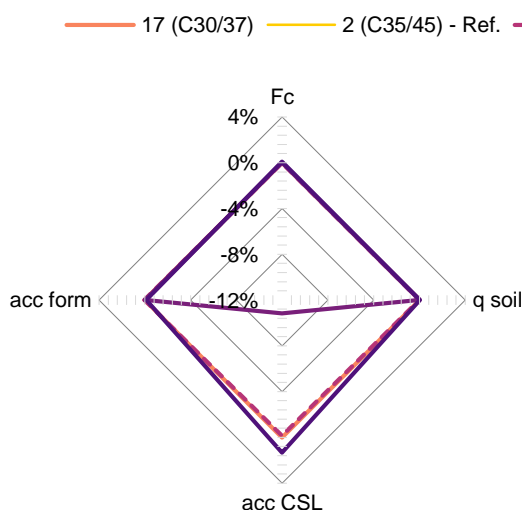


Figure A.11: Web plot of the concrete type effect on the variation of slab track short-term behaviour

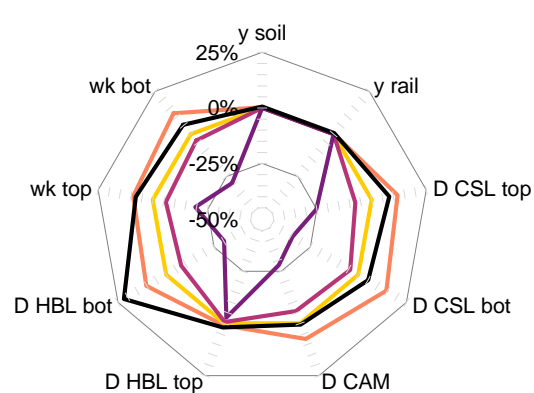


Figure A.12: Web plot of the concrete type effect on the variation of slab track long-term behaviour

A.1.7 HBL

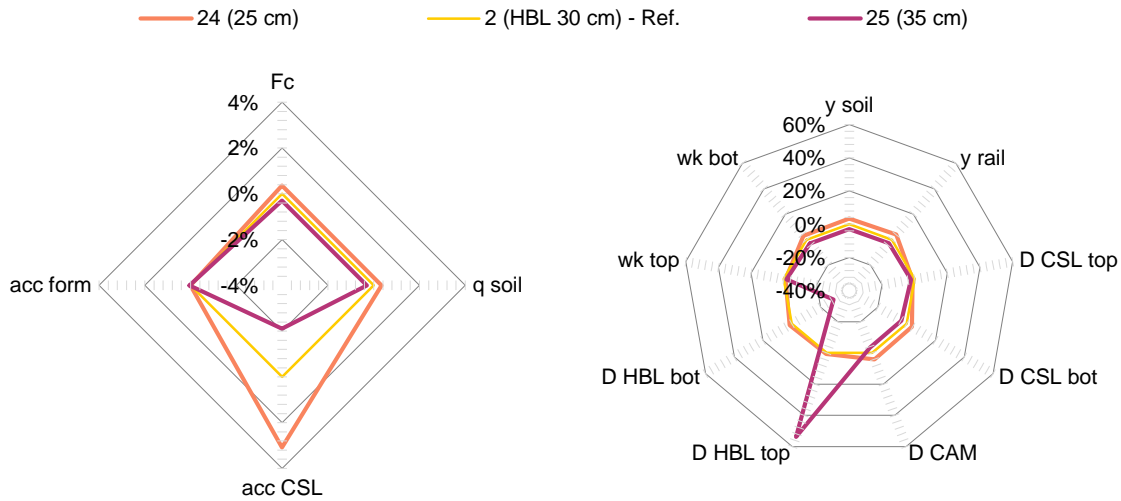


Figure A.13: Web plot of the HBL thickness effect on the variation of slab track short-term behaviour

Figure A.14: Web plot of the HBL thickness effect on the variation of slab track long-term behaviour

A.1.8 INITIAL PROFILE

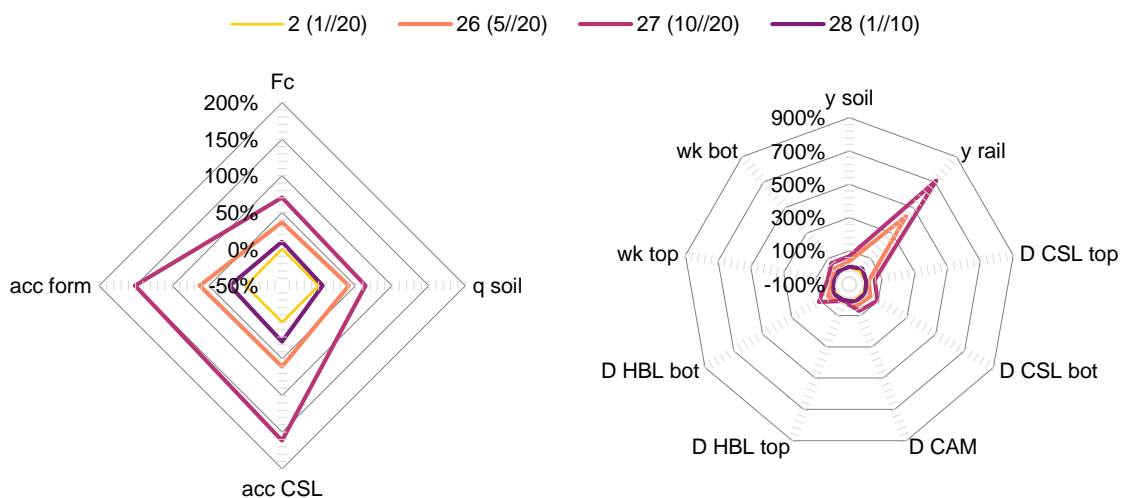


Figure A.15: Web plot of the initial profile effect on the variation of slab track short-term behaviour

Figure A.16: Web plot of the initial profile effect on the variation of slab track long-term behaviour

A.1.9 CONSTRUCTION DEFECTS

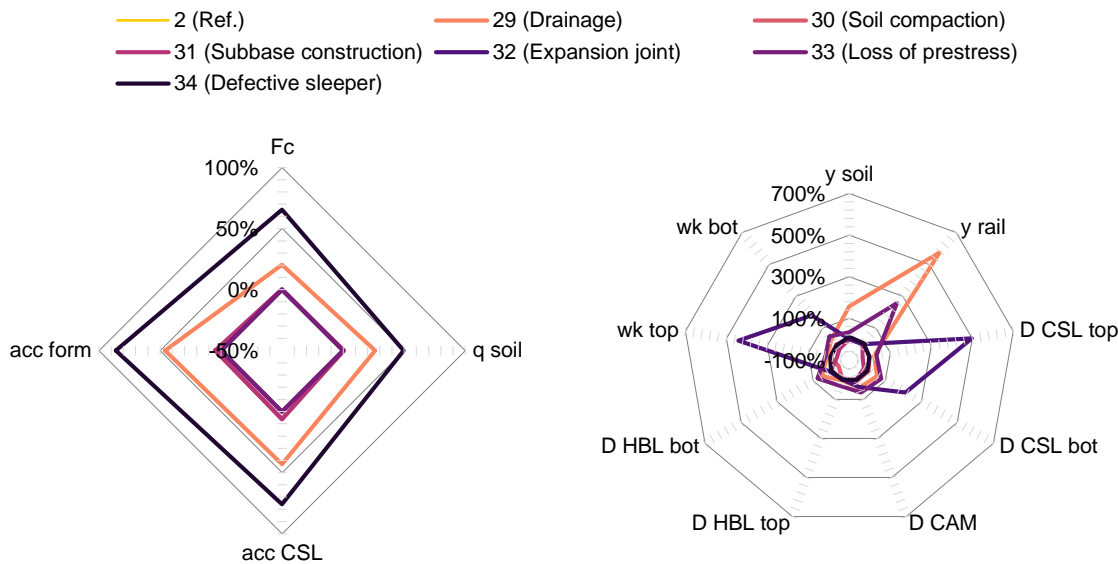


Figure A.17: Web plot of the construction defects effect on the variation of slab track short-term behaviour

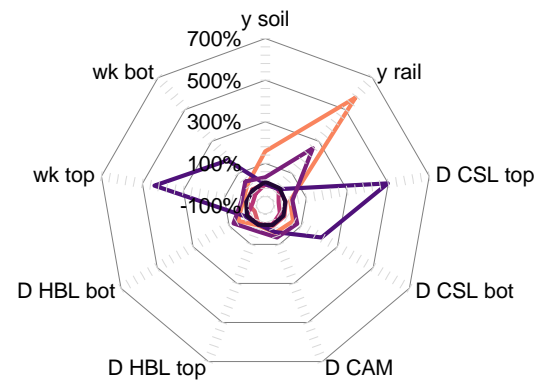


Figure A.18: Web plot of the construction defects effect on the variation of slab track long-term behaviour

A.1.10 SOFT SOIL SCENARIO

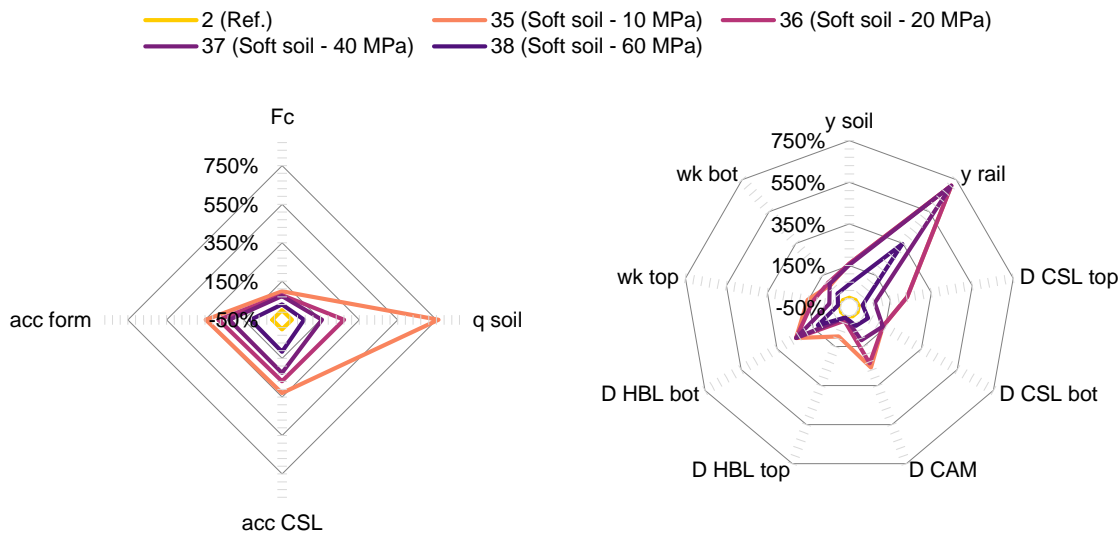


Figure A.19: Web plot of the soft soil effect on the variation of slab track short-term behaviour

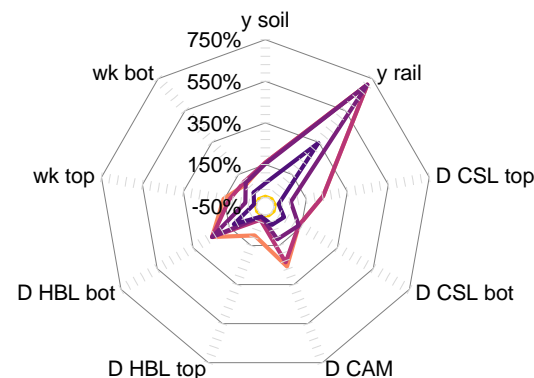


Figure A.20: Web plot of the soft soil effect on the variation of slab track long-term behaviour

A.1.11 TRANSITION SCENARIO

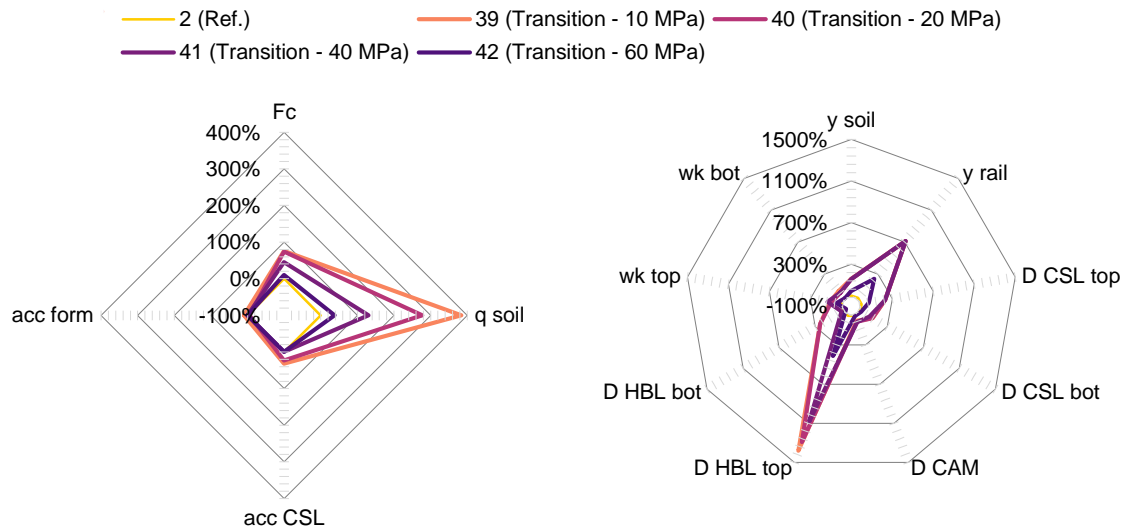


Figure A.21: Web plot of the transition effect on the variation of slab track short-term behaviour

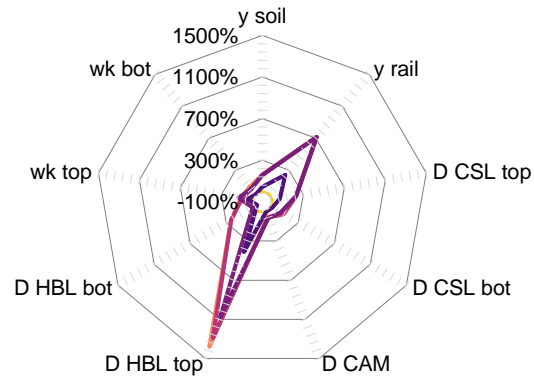


Figure A.22: Web plot of the transition effect on the variation of slab track long-term behaviour

A.2 SENSITIVITY ANALYSIS

Additional simulations were calculated to enhance the understanding of the slab track behaviour in short- and long-term. For this sensitivity analysis, temperature effects on the track (excepting for the settlement calculation of the soil) are neglected.

Table A.1: Sensitivity analysis scenarios

	#	High Speed	Freight	Temp.	Rainfall	Pad	CSL	HBL	Rail profile
Actions	S60	V250	-	-	R1	P35	C35/45	30	1/20
	S61	V300	-	-	R1	P35	C35/45	30	1/20
	S62	V350	-	-	R1	P35	C35/45	30	1/20
	S63	V400	-	-	R1	P35	C35/45	30	1/20
	S64	V450	-	-	R1	P35	C35/45	30	1/20
Vehicle speed	S65	V300	-	-	R1	P21	C35/45	30	1/21
	S66	V300	-	-	R1	P28	C35/45	30	1/22
	S67	V300	-	-	R1	P42	C35/45	30	1/24
	S68	V300	-	-	R1	P49	C35/45	30	1/25
Design	S69	V300	-	-	R1	P35	C25/30	30	1/20
	S70	V300	-	-	R1	P35	C30/37	30	1/20
	S71	V300	-	-	R1	P35	C40/50	30	1/20
	S72	V300	-	-	R1	P35	C45/55	30	1/20
HBL	S73	V300	-	-	R1	P35	C35/45	20	1/20
	S74	V300	-	-	R1	P35	C35/45	25	1/20
	S75	V300	-	-	R1	P35	C35/45	35	1/20
	S76	V300	-	-	R1	P35	C35/45	40	1/20
Track condition	S77	V300	-	-	R1	P35	C35/45	30	2//20
	S78	V300	-	-	R1	P35	C35/45	30	3//20
	S79	V300	-	-	R1	P35	C35/45	30	4//20
	S80	V300	-	-	R1	P35	C35/45	30	5//20
Settlement Amplitude	S81	V300	-	-	R1	P35	C35/45	30	1//10
	S82	V300	-	-	R1	P35	C35/45	30	1//15
	S83	V300	-	-	R1	P35	C35/45	30	1//25
	S84	V300	-	-	R1	P35	C35/45	30	1//30

A.2.1 SPEED

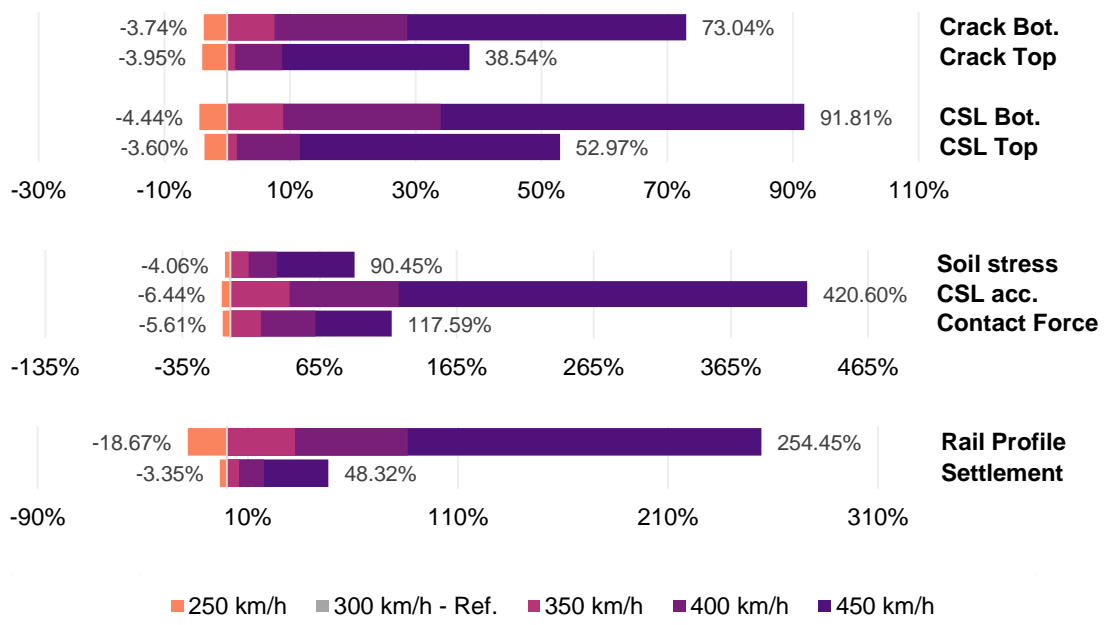


Figure A.23: Sensitivity analysis on the vehicle speed

A.2.2 RAILPAD

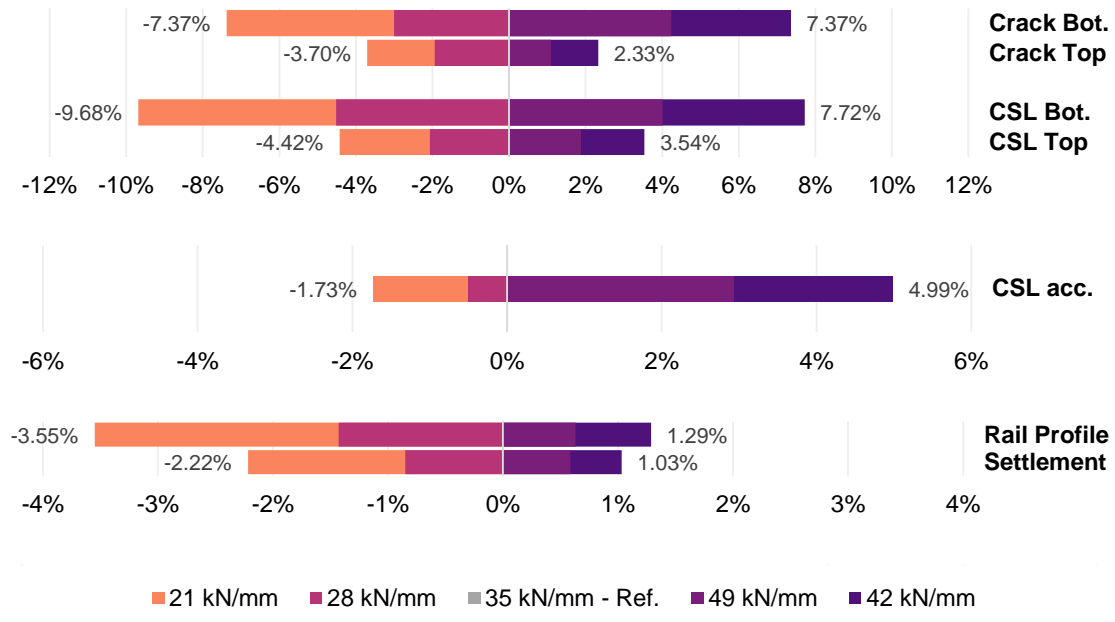


Figure A.24: Sensitivity analysis on the railpad stiffness

A.2.3 CONCRETE

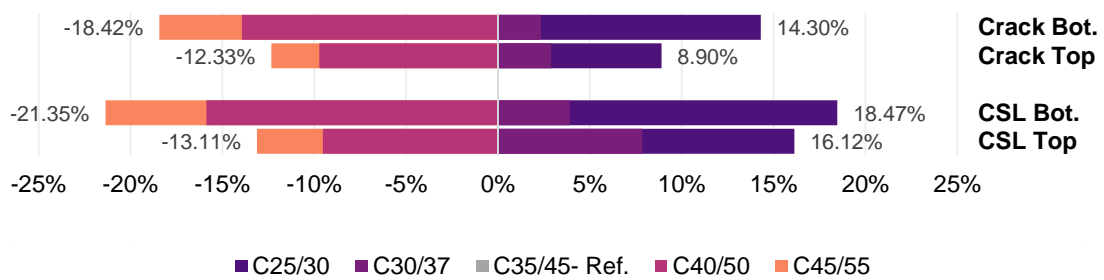


Figure A.25: Sensitivity analysis on the concrete strength class

A.2.4 HBL

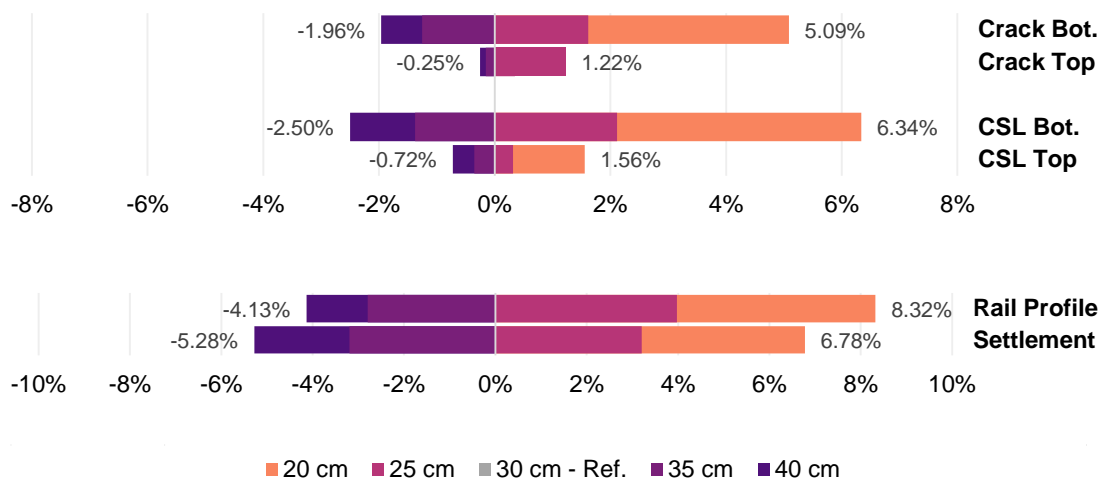


Figure A.26: Sensitivity analysis on the HBL thickness

A.2.5 SETTLEMENT AMPLITUDE

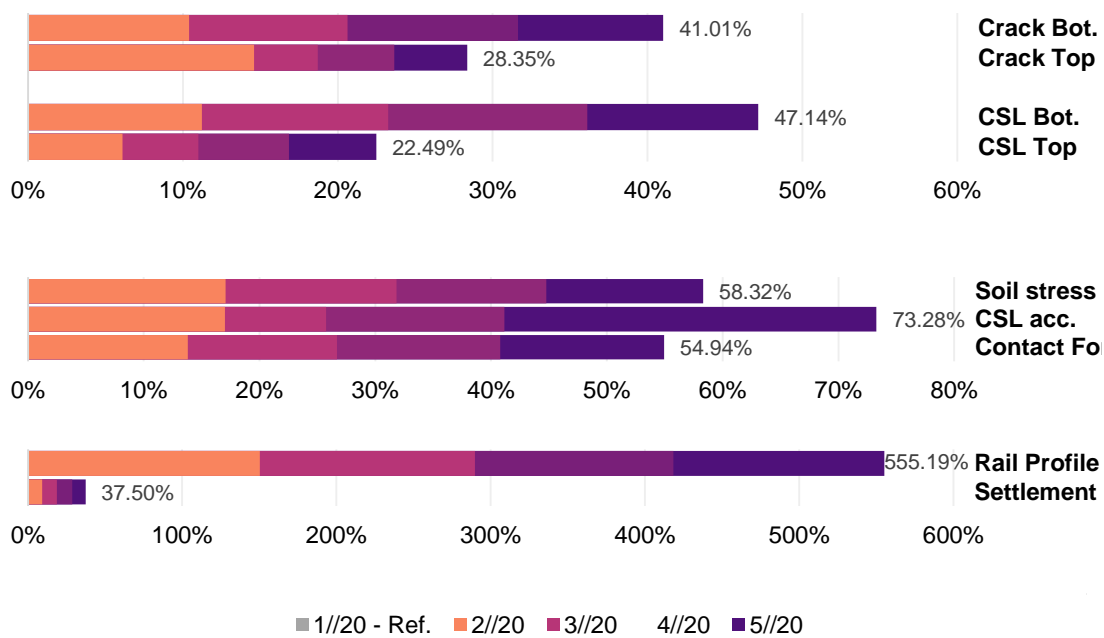


Figure A.27: Sensitivity analysis on the settlement amplitude

A.2.6 SETTLEMENT WAVELENGTH

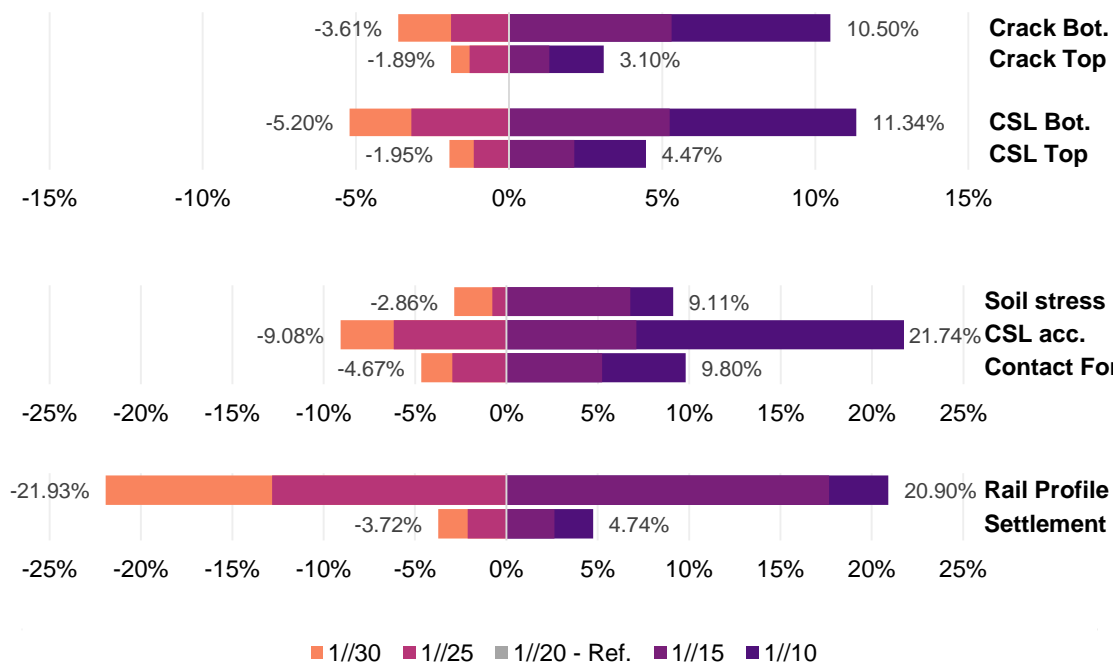


Figure A.28: Sensitivity analysis on the settlement wavelength